

## LIBRARY Michigan State University

## This is to certify that the dissertation entitled

## PREDICTION OF RHEOLOGICAL PROPERTIES OF STRUCTURED FLUIDS IN HOMOGENEOUS SHEAR BASED ON A REALIZABLE MODEL FOR THE ORIENTATION DYAD

presented by

YoChan Kim

has been accepted towards fulfillment of the requirements for the

Ph.D degree in Chemical Engineering and Materials Science

Major Professor's Signature

November 1<sup>st</sup>, 2006

Date

MSU is an Affirmative Action/Equal Opportunity Institution

# PLACE IN RETURN BOX to remove this checkout from your record. TO AVOID FINES return on or before date due. MAY BE RECALLED with earlier due date if requested.

DATE DUE	DATE DUE	DATE DUE
	<del> </del>	

2/05 p:/CIRC/DateDue.indd-p.1

# PREDICTION OF RHEOLOGICAL PROPERTIES OF STRUCTURED FLUIDS IN HOMOGENEOUS SHEAR BASED ON A REALIZABLE MODEL FOR THE ORIENTATION DYAD

By

YoChan Kim

## A DISSERTATION

Submitted to
Michigan State University
in partial fulfillment of the requirements
for the degree of

**DOCTOR OF PHILOSOPHY** 

Department of Chemical Engineering and Materials Science

2006

#### **ABSTRACT**

# PREDICTION OF RHEOLOGICAL PROPERTIES OF RIGID ROD FLUIDS IN SIMPLE HOMOGENEOUS SHEAR FLOWS BASED ON A REALIZABLE MODEL FOR THE ORIENTATION DYAD

## By YoChan Kim

Non-spherical particles dispersed in a fluid have a tendency to align in shear flows because of particle-fluid drag. This phenomenon is opposed by rotary diffusion. At high concentrations and in the absence of hydrodynamic couples, *self-alignment* can also occur because *excluded volume forces* prevent the return-to-isotropy of anisotropic states by rotary Brownian motion. The balance between microhydrodynamic and diffusive (i.e., Brownian and excluded volume) torques at the microscale has a direct impact on the rheological properties of rigid rod fluids (particulate suspensions and liquid crystalline polymers) at the continuum scale.

Over the past sixty years, important characteristics of the microstructure associated with the foregoing alignment phenomenon have been quantified in terms of the low order moments of the orientation density function governed by the rotary Smoluchowski equation. In this research, a closed model for the second order moment  $\langle \underline{p}\underline{p} \rangle$  (orientation dyad) has been identified based on the condition that in the absence of an external field all realizable anisotropic states must relax to stable equilibrium states. A key step in the development of the new closure is the use of an algebraic pre-closure for the orientation tetrad  $\langle \underline{p}\underline{p}\underline{p} \rangle$  in terms of the orientation dyad  $\langle \underline{p}\underline{p} \rangle$  that preserves the six-fold symmetry and contraction properties of the original orientation tetrad.

In the presence of a simple shear flow, the microstructure and the rheological characteristics predicted for rigid-rod fluids agree with previous theoretical and experimental results for a wide range of Péclet numbers. In addition to the Péclet number (i.e.,  $Pe = \|\nabla \underline{u}\|/(6D_R^o)$ ), the orientation director also depends on three other dimensionless groups: a tumbling parameter,  $\lambda$ ; an excluded volume coefficient, U; and, a dimensionless time  $t \equiv 6 D_R^0 \hat{t}$ . The rotary diffusion coefficient for dilute solutions,  $D_R^0$ , is used to scale time. Unlike other closure models, the approach developed hereinafter predicts that all two-dimensional and three-dimensional realizable anisotropic states relax to either a steady state (isotropic or anisotropic) or a periodic state, depending on Pe,  $\lambda$ , and U. The model predicts the existence of shear thinning and shear thickening phenomena, Newtonian plateau regions at low and high Péclet numbers, positive (and negative) first normal stress differences, and negative (and positive) second normal stress differences. For Pe = 0, multiple equilibrium states exist for  $4.72 \le U \le 5.00$ . For Pe > 0 and initial directors located in the flow-deformation plane, the predominant feature for U < 25 is the existence of a unique nematic-like microstructure with a steady alignment of the director that becomes completely aligned with the velocity as  $Pe \rightarrow \infty$ . For  $\lambda < 1$  and U > 25, tumbling and wagging of the director occur at low to moderate values of the Péclet number. If the initial director has a component in the direction of the vorticity, then director kayaking and director log-rolling may occur. The coexistence of stable anisotropic states (or texture) predicted by the model may provide an explanation of why micro defects occur during the processing of some structured fluids.

To My Family for Love, Support, and Patience

#### ACKNOWLEDGEMENT

First of all, I would like to thank Professor Charles A. Petty for his support and encouragement throughout my Ph.D. program. I truly believe that I would not have completed my program without him. He has not only inspired me in many aspects from an academic perspective, but has also given me personal guidance in my twenties. His suggestion to participate in two internships helped me greatly. The NSF summer program in Japan helped me broaden my world perspective. The summer internship at Bechtel National, Inc. inspired me to become a better engineer.

In addition, I want to acknowledge Professors Peter W. Bates, André Bénard, Krisnamurthy Jayaraman, and Michael E. Mackay for serving on my dissertation committee. I would also like to recognize Professor Jun-ichi Takimoto from Nagoya University (now at Yamaguchi University) for giving me guidance during my research. I also want to recognize my gradate school colleagues Dr. Steven Parks, Chinh Nguyen, Hemant Kini, and Dilip Mandal for the inspiration of this research. I thank also Jon Berkoe, Kelly Knight, Lin Lorraine, and Brigette Rosendall of Bechtel National, Inc for their wonderful support.

I gratefully acknowledge financial support of this work by the National Science Foundation and by Michigan State University.

Finally, I want to express a very special thanks to my wife Seiyoun Jung and my parents for unlimited love and moral support.

## TABLE OF CONTENTS

TABLE	OF CONTENTS	vi
LIST OF	TABLES	ix
LIST OF	FIGURES	x
NOTATI	ON	xvi
Chapter		
1. INTRO	DDUCTION	
1.1	Motivation	1
· 1.2	Background	4
1.3	Objective	14
1.4	Outline	16
2. SMOL	UCHOWSKI EQUATION FOR RIGID ROD SUSPENSIONS	
2.1	Introduction	17
2.2	Jeffery's Model for Rotary Convection: Tumbling Coefficient	18
2.3	Brownian Motion: Rotary Diffusivity	20
2.4	Excluded Volume Phenomena: Maier-Saupe Potential	
2.5	Discussion	23
3. <b>MOM</b>	ENTS OF THE ORIENTATION DISTRIBUTION	
3.1	Introduction	24
3.2	Orientation Dyad: Structure Tensor and the Order Parameter	26
3.3	Orientation Tetrad: Symmetry and Contraction Properties	28
3.4	Realizable Anisotropic States: Invariant Diagram	29
3.5	Discussion	32

4.	<b>EQU</b>	ATIONS FOR THE MICROSTRUCTURE AND THE STRESS	
	4.1	Introduction	33
	4.2	Dynamic Equation for the Orientation Dyad	33
	4.3	Dynamic Equations for the Structure Invariants for Pe = 0	34
	4.4	Algebraic Equation for the Stress	35
	4.5	Discussion	36
5.	CLOS	SURE FOR THE ORIENTATION TETRAD	
	5.1	Introduction	38
	5.2	Closure Models	40
	5.3	Discussion	44
6.	REAL	LIZABLE CLOSURE	
	6.1	Introduction	45
	6.2	Realizable Isotropic, Planar Isotropic, and Nematic States	46
	6.3	Realizable Prolate and Oblate States	50
	6.4	Realizable Planar Anisotropic Boundary	51
	6.5	Discussion	53
7.	MICE	ROSTRUCTURE IN THE ABSENCE OF AN EXTERNAL FIELD	
	7.1	Introduction	56
	7.2	Biphasic Phenomena	57
	7.3	Relaxation to Isotropic and Anisotropic Steady States	62
	7.4	Discussion	65
8.	MICE	ROSTRUCTURE INDUCED BY HOMOGENEOUS SHEAR	
	8.1	Introduction	72
	8.2	Relaxation of Planar Anisotropic States for L/d = ∞	73
	8.3	Relaxation of Planar Anisotropic States for L/d ≅ 12	76
	8.4	Relaxation of Planar Anisotropic States for $0 \le L/d < \infty$	93
	8.5	The Effect of Tube Dilation on the Relaxation of Planar Anisotropic States	96
	0.6	<b>D'</b>	100

9.	VISC	OSITY AND NORMAL STRESS DIFFERENCES	
	9.1	Introduction	102
	9.2	Rheological Properties: $L/d = \infty$	103
	9.3	Rheological Properties: L/d ≅ 12	117
	9.4	Rheological Properties: $0 \le L/d \le \infty$	129
	9.5	Rheological Properties: Effect of Tube Dilation	133
	9.6	Discussion	143
10.	CON	ICLUSIONS	145
11.	REC	COMMENDATIONS	154
ΑF	PEND	DICES	
ΑF	PEND	DIX A. Derivation of Moment Equations with Structure Tensor	161
ΑF	PEND	DIX B. Derivation of Moment Equations in Invariant Form	165
ΑF	PEND	DIX C. Normal Vectors in the Invariant Diagram	169
ΑF	PEND	DIX D. Derivation of Various Closure Analysis in the Invariant Form	172
ΑP	PEND	DIX E. Eigenvalues and Eigenvectors of the Orientation Dyad	182
ΑF	PEND	DIX F. Eigenvalues and Eigenvectors of the Orientation Dyad	189
ΑP	PEND	DIX G. Computational Code for Transient Calculations	189
LIS	ST OF	REFERENCES	199

## LIST OF TABLES

Table 7.1	Invariants and Order Parameter of the Equilibrium Structure Tensor on the Prolate Line	63
Table 7.2	Invariants and Order Parameter of the Equilibrium Structure Tensor on the Oblate Line	64
Table 8.1	Invariants of the Equilibrium Anisotropic Tensor for Different Tumbling Parameters (FSQ-model; $F_{TD} = 1$ ; $U = 0$ )	77
Table 8.2	Effect of $\lambda$ on the Tumbling Period (FSQ-model; $F_{TD} = 1$ ; $U = 27$ ; $Pe = 10$ )	98
Table 9.1	Viscous and Elastic Contributions to the Shear Viscosity and the First and Second Normal Stress Differences at Selected Values of U and Pe for $L/d=\infty$	113
Table 9.2	Viscous and Elastic Contributions to the Shear Viscosity and the First and Second Normal Stress Differences at Selected Values of U and Pe for $L/d \cong 12$ .	.124
Table 9.3	Legend for Figures 9.19 – 9.23	.135

## LIST OF FIGURES

Figure 1.1 A	Anisotropic Orientation States (Parks, 1997)
Figure 1.2 N	Molecular Structure of LPC (Larson, 1999)6
	Schematic of NMR Spectra for PBLG in DMF (Abe and Yamazaki, 1987a; Robinson, 1966)
_	nstantanous Orientation Vector Directed Along the Molecular Axis of a Rigid Rod25
Figure 3.2 T	Three Orientation States for the Orientation Dyad27
Figure 6.1 C	Closure Coefficient C <sub>2</sub> (III <sub>b</sub> ) for the Realizable FSQ-model54
	The Excluded Volume Potential for the Decoupling Approximation and the FSQ-model
_	Multiple Equilibrium States Predicted by the FSQ-model for C <sub>2</sub> = constant
Figure 7.2 M	Multiple Equilibrium States Predicted by the FSQ-model for C <sub>2</sub> = C <sub>2</sub> (III <sub>b</sub> )61
_	Relaxation of the Microstructure due to Rotary Brownian Diffusion $(U = 0; \hat{t} = 1/(6D_R^0))$ 66
	Effect of Excluded Volume on the Relaxation of the Microstructure (FSQ-model; $F_{TD} = 1$ )
_	The Effect of Tube Dilation on the Relaxation of the Microstructure (FSQ-model; $U = 3$ ; initial conditions: $II_b(0) = 2/9$ ; $III_b(0) = 0$ )68

Figure 7.6	The Effect of U and Tube Dilation on the Characteristic Relaxation Time $t_c$	
	(FSQ-model; $\alpha(0) = 0.9$ )	.69
Figure 8.1	The Effect of U and Pe on the Steady State Director Angle for $L/d = \infty$	
	(FSQ-model; $F_{TD} = 1$ ; $\lambda = 1$ )	.74
Figure 8.2	The Effect of U and Pe on the Steady State Microstructure for $L/d = \infty$	
	(FSQ-model; $F_{TD} = 1$ ; $\lambda = 1$ )	.75
Figure 8.3	Instantaneous Microstructure for Director Tumbling for L/d $\cong$ 12	
	(FSQ-model; $F_{TD} = 1$ ; $\lambda = 0.987$ ; $U = 27$ , $Pe = 10$ ;	
	$2 < \underline{p}\underline{p} > (0) = \underline{e}_{y}\underline{e}_{y} + \underline{e}_{z}\underline{e}_{z})$	.78
Figure 8.4	Microstructure for Director Tumbling in the Phase Plane for $L/d \cong 12$	
	(FSQ-model; $F_{TD} = 1$ ; $\lambda = 0.987$ ; $U = 27$ , $Pe = 10$ ;	
	$2 < \underline{p}\underline{p} > (0) = \underline{e}_{y}\underline{e}_{y} + \underline{e}_{z}\underline{e}_{z})$	.79
Figure 8.5	Instantaneous Microstructure for Director Wagging for L/d ≅ 12	
	(FSQ-model; $F_{TD} = 1$ ; $\lambda = 0.987$ ; $U = 27$ , $Pe = 24$ ;	
	$2 < \underline{p}\underline{p} > (0) = \underline{e}_{y}\underline{e}_{y} + \underline{e}_{z}\underline{e}_{z})$	.81
Figure 8.6	Microstructure for Director Wagging in the Phase Plane for $L/d \cong 12$	
	(FSQ-model; $F_{TD} = 1$ ; $\lambda = 0.987$ ; $U = 27$ , $Pe = 24$ ;	
	$2 < \underline{pp} > (0) = \underline{e}_{y} \underline{e}_{y} + \underline{e}_{z} \underline{e}_{z})$	
	- \ <u>P</u> \ (*) = y \ = z \ = z \	82
Figure 8.7	Instantaneous Microstructure for Director Steady Alignment for $L/d\cong 12$	
	(FSQ-model; $F_{TD} = 1$ ; $\lambda = 0.987$ ; $U = 27$ , $Pe = 95$ ;	
	$2 < pp > (0) = e_v e_v + e_z e_z$ )	84

_	ructure for Director Steady Alignment in the Phase Plane for L/c nodel; $F_{TD} = 1$ ; $\lambda = 0.987$ ; $U = 27$ , $Pe = 95$ ;	d ≅ 12
2 < <u>p p</u> >	$>(0) = \underline{\mathbf{e}}_{\mathbf{y}} \underline{\mathbf{e}}_{\mathbf{y}} + \underline{\mathbf{e}}_{\mathbf{z}} \underline{\mathbf{e}}_{\mathbf{z}})$	85
Figure 8.9 Phase D	riagram of U and Pe for L/d ≅ 12	
(FSQ-m	nodel; $F_{TD} = 1$ ; $\lambda = 0.987$ ; $2 < \underline{p}\underline{p} > (0) = \underline{e}_y \underline{e}_y + \underline{e}_z \underline{e}_z$ )	86
	aneous Director Log-rolling for L/d ≅ 12	
(FSQ-m	nodel; U = 27; Pe = 95; $F_{TD}$ = 1; $\lambda$ = 0.987;	
2 < <u>pp</u> >	$>(0) = \underline{\mathbf{e}}_{\mathbf{x}} \underline{\mathbf{e}}_{\mathbf{x}} + \underline{\mathbf{e}}_{\mathbf{z}} \underline{\mathbf{e}}_{\mathbf{z}})$	87
•	or Log-rolling in the Phase Plane L/d ≅ 12	
(FSQ-n	model; $U = 27$ ; $Pe = 95$ ; $F_{TD} = 1$ ; $\lambda = 0.987$ ;	
2 < <u>pp</u> ?	$>(0) = \underline{\mathbf{e}}_{\mathbf{x}} \underline{\mathbf{e}}_{\mathbf{x}} + \underline{\mathbf{e}}_{\mathbf{z}} \underline{\mathbf{e}}_{\mathbf{z}})$	88
Figure 8.12 Phase I	Diagram of Shear-voriticity Plane Initial Condition L/d ≅ 12	
(FSQ-n	model; $F_{TD} = 1$ ; $\lambda = 0.987$ ; $2 < \underline{p}\underline{p} > (0) = \underline{e}_{x}\underline{e}_{x} + \underline{e}_{z}\underline{e}_{z})$	90
Figure 8.13 Instant	aneous Director Kayaking L/d ≅ 12	
(FSQ-n	model; U = 27; Pe = 95; $F_{TD}$ = 1; $\lambda$ = 0.987)	92
Figure 8.14 Micros Phase P	structures for Director Tumbling and Steady State Alignment in	the
(FSQ-m	nodel; $F_{TD} = 1$ ; $\lambda = 0.5$ ; $U = 27$ , $Pe = 95$ ;	
2 < <u>pp</u>	$> (0) = \underline{\mathbf{e}}_{\mathbf{y}} \underline{\mathbf{e}}_{\mathbf{y}} + \underline{\mathbf{e}}_{\mathbf{z}} \underline{\mathbf{e}}_{\mathbf{z}})$	94
Phase P		the
	nodel; $F_{TD} = 1$ ; $\lambda = 0$ ; $U = 27$ , $Pe = 95$ ;	
2 < pp:	$>(0) = \underline{\mathbf{e}}_{\mathbf{y}}\underline{\mathbf{e}}_{\mathbf{y}} + \underline{\mathbf{e}}_{\mathbf{z}}\underline{\mathbf{e}}_{\mathbf{z}})$	95

_	Microstructure for Director Tumbling and Steady State Alignment in the Phase Plane
	(FSQ-model; $F_{TD} = 1$ ; $\lambda = 0$ ; $U = 0$ , $Pe = 95$ ;
	$2 < \underline{p}\underline{p} > (0) = \underline{e}_{y}\underline{e}_{y} + \underline{e}_{z}\underline{e}_{z})$
-	The Effect of Tube Dilation on the Phase Diagram (FSQ-model; $F_{TD} = 1$ ; $\lambda = 0.987$ ; $2 < \underline{p}\underline{p} > (0) = \underline{e}_y\underline{e}_y + \underline{e}_z\underline{e}_z$ )99
_	The Effect of U and Pe on the Shear Viscosity for $L/d = \infty$ (FSQ-model; $F_{TD} = 1$ ; $\lambda = 1$ )
•	The Effect of U and Pe on the Viscous and Elastic Components of the Shear Viscosity for $L/d = \infty$ (FSQ-model; $F_{TD} = 1$ ; $\lambda = 1$ )
1	The Effect of U and Pe on the Brownian and Excluded Volume Contributions to the Shear Elastic Component of Viscosity for $L/d = \infty$ (FSQ-model; $F_{TD} = 1$ ; $\lambda = 1$ )
	Elastic Contributions to the Shear Stress (FSQ-model; $\lambda = 1$ ; $F_{TD} = 1$ )
_	The Effect of U and Pe on the First Normal Stress Difference for L/d = $\infty$ (FSQ-model; $F_{TD} = 1$ ; $\lambda = 1$ )
	The Effect of U and Pe on the Second Normal Stress Difference for $L/d = \infty$ (FSQ-model; $F_{TD} = 1$ ; $\lambda = 1$ )
_	The Contributions of Stress on the Time Averaged Normal Stress Differences (FSQ-model; $F_{TD} = 1$ ; $\lambda = 1$ ; $U = 27$ )
•	The Effect of Tumbling Parameter on the Shear Viscosity for U = 0 (FSQ-model; F <sub>TD</sub> = 1)118

Figure 9.9 The Instantaneous Shear Viscosity for Director Tumbling (FSQ-model; $F_{TD} = 1$ ; $\lambda = 0.987$ ; $U = 27$ , $Pe = 10$ )
Figure 9.10 The Effect of U and Pe on the Time Averaged Shear Viscosity for L/d $\cong$ 12 (FSQ-model; $F_{TD} = 1$ ; $\lambda = 0.987$ )
Figure 9.11 The Contributions of Viscous and Elastic Stresses on the Time Averaged Shear Viscosity for $L/d \cong 12$ (FSQ-model; $F_{TD} = 1$ ; $\lambda = 0.987$ ; $U = 27$ )
Figure 9.12 The Instantaneous First Normal Stress Difference for Director Tumbling (FSQ-model; $F_{TD} = 1$ ; $\lambda = 0.987$ ; $U = 27$ , $Pe = 10$ )
Figure 9.13 The Effect of U and Pe on the Time Averaged First Normal Stress Difference for L/d $\cong$ 12 (FSQ-model; $F_{TD} = 1$ ; $\lambda = 0.987$ )
Figure 9.14 The Instantaneous Second Normal Stress Difference for Director Tumbling with L/d $\cong$ 12 (FSQ-model; $F_{TD} = 1$ ; $\lambda = 0.987$ ; $U = 27$ , $Pe = 10$ )
Figure 9.15 The Effect of U and Pe on the Time Averaged Second Normal Stress Difference for $L/d \cong 12$ (FSQ-model; $F_{TD} = 1$ ; $\lambda = 0.987$ )
Figure 9.16 The Effect of Tumbling Parameter on the Time Averaged Shear Viscosity (FSQ-model; $F_{TD} = 1$ ; $U = 27$ , $Pe = 10$ )
Figure 9.17 The Effect of Tumbling Parameter on the Time Averaged First Normal Stress Difference (FSQ-model; F <sub>TD</sub> = 1; U = 27, Pe = 10)
Figure 9.18 The Effect of Tumbling Parameter on the Time Averaged Second Normal Stress Difference (FSQ-model; F <sub>TD</sub> = 1; U = 27, Pe = 10)134

Figure 9.19 The Effect of Tube Dilation on the Time Averaged Shear Viscosity	
(FSQ-model; $\lambda = 0.987$ ; U = 27 see Table 9.3 for legend)	37
Figure 9.20 The Contributions of Stress on the Time Averaged Shear Viscosity	
(FSQ-model; $F_{TD}^{Doi}$ in Eqs.(4.1) and (4.6); $\lambda = 0.987$ ; $U = 27$ )	38
Figure 9.21 The Effect of Tube Dilation on the Time Averaged First Normal Stress Difference	
(FSQ-model; $\lambda = 0.987$ ; U = 27 see Table 9.3 for legend)	39
Figure 9.22 The Effect of Tube Dilation on the Time Averaged Second Normal Stress Difference	
(FSQ-model; $\lambda = 0.987$ ; U = 27 see Table 9.3 for legend)	41
Figure 9.23 The Contributions of Stress on the Time Averaged Normal Stress Differenc	
(FSQ-model; $F_{TD}^{Doi}$ ; $\lambda = 0.987$ ; $U = 27$ )	42
Figure 10.1 Validation of the FSQ-closure14	47
Figure 11.1 The Effect of Particle Aspect Ratio on the Dimensionless Friction  Coefficient	56
Figure 11.2 Multiple Stable Steady States for Various Initial Orientation Dyads $(U = 27, Pe = 95, \lambda = 0.987)$	58

#### **NOTATION**

<u>A</u> Second order tensor, or dyadic-valued operator  $\mathbf{B}$ Second order tensor, or dyadic-valued operator  $A_{ij}B_{k\ell}$ Index notation for tetradic-valued operator for dyadic valued operators  $\underline{A}$  and  $\underline{B}$ , equivalent to  $a_i b_j c_d d_\ell$ Diameter of tube in tube dilation effect Anisotropic structure tenser b Closure coefficient for FSQ-model  $C_2$ С Number of rigid rods in unit volume  $D_{R}$ Rotary diffusion coefficient (units: 1/time)  $D_{R}^{o}$ Rotary diffusion coefficient in dilute solution d Diameter of rigid rod Unit vector in II<sub>b</sub> and III<sub>b</sub> direction  $\underline{e}_{II},\underline{e}_{III}$ Unit vector in the radius direction <u>e</u>r Unit vector in the vorticity direction <u>e</u>x Unit vector in the cross-flow direction <u>e</u>y Unit vector in flow direction  $\underline{\mathbf{e}}_{\mathbf{z}}$  $F_{TD}$ Tube dilation effect F<sub>TD</sub>oi Tube dilation effect in Doi's model **FSQ** Fully symmetric quadratic <u>f</u> Invariant form of dynamic moment vector in the invariant space

$\hat{\mathbf{f}}_{t}$	Dimensional tumbling frequency
$\mathbf{f_t}$	Dimensionless tumbling frequency
$\boldsymbol{\hat{f}_w}$	Dimensional wagging frequency
$f_w$	Dimensionless wagging frequency
HL1	Hinch and Leal 1 closure
HL2	Hinch and Leal 2 closure
Ī	Unit dyadic tensor
$I_b$	First invariant of $\underline{\underline{b}}$
$I_{\alpha\beta}$	Index notation of unit dyadic tensor
$II_b$	Second invariant of <u>b</u>
$\mathrm{III}_{\mathbf{b}}$	Third invariant of $\underline{b}$
$k_{\mathbf{B}}$	Boltzmann constant
L	Length of rigid rod
N	Number of species
$N_1$	Dimensionless first normal stress
$\mathbf{\hat{N}_{l}}$	Dimensional first normal stress
N <sub>2</sub>	Dimensionless second normal stress
$\hat{N}_2$	Dimensional second normal stress
NP	Newtonian plateau
<u>n</u>	Normal vector

<u>p</u>	Unit vector direct along rigid rod axis						
$\dot{\underline{\mathbf{p}}}$	Unit vector in rigid rod rotation						
<u>p</u> '	Neighboring rigid rod vector respect to <u>p</u>						
$\dot{\underline{p}}_{\mathbf{C}}$	Convective flux of rigid rod rotation						
< <u>p</u> >	The first order moment						
$p_x, p_y, p_z$	Components of unit vector direct along rigid rod axis						
$\hat{p}_x, \hat{p}_y, \hat{p}_z$	Component of unit vector direct along rigid rod axis, respect to eigenvector $\underline{x}_1$ , $\underline{x}_2$ , and $\underline{x}_3$						
<u>pp</u>	Orientation dyad						
< <u>p p</u> >	The second order moment						
ΡαΡβ	Index notation of orientation dyad						
<u>pppp</u>	Orientation tetrad						
< <u>pppp</u> >	The fourth order moment						
Pe	Péclet number						
r, θ, φ	Three spherical coordinate axes						
	Timee spherical coordinate axes						
<u>ŝ</u>	Dimensional strain rate tensor						
<u>\$</u> <u>\$</u>							
	Dimensional strain rate tensor						
<u>s</u>	Dimensional strain rate tensor  Dimensionless strain rate tensor						

t	Dimensionless time					
ît	Dimensional tumbling period					
t <sub>t</sub>	Dimensionless tumbling period					
U	Nematic potential coefficient					
U	Critical nematic potential coefficient of the phase transition					
$U_1$	Upper critical nematic potential coefficient for biphasic region					
U <sub>2</sub>	Lower critical nematic potential coefficient for biphasic region					
<u>û</u>	Fluid velocity					
$u_z$	Scalar valued fluid velocity in flow direction					
<u>w</u>	Dimensionless vorticity tensor					
$\underline{\mathbf{X}}_1, \underline{\mathbf{X}}_2, \underline{\mathbf{X}}_3$	Eigenvectors associated with $\lambda_{p1}$ , $\lambda_{p2}$ , $\lambda_{p3}$ , respectively.					
x, y, z	Three Cartesian coordinate axes					
<u>z</u>	Arbitrary vector					

## Other Symbols

α	Degree of orientation order parameter, structure parameter
â	Motion of the suspension with velocity
δ	Jaumann derivative
Δη	Polymer contribution shear viscosity
$\Delta\eta_{0}$	Zero-shear rate viscosity
Δt	Change of time step
$\Delta U_{MS}$	Maier-Saupe excluded volume potential

$\Delta U_{O}$	Onsager nematic potential					
$\Delta U_{MS}$	Maier-Saupe nematic potential					
Φ	Excluded volume potential					
ф	Angle between the projection of molecular axis on the plane $[x_1, x_3]$ and $x_1$ axis					
Ϋ́	Strain rate					
η̂	Total shear viscosity					
$\eta_{ m E}$	Elastic contribution of shear viscosity					
$\eta_{\mathrm{S}}$	Solvent contribution of shear viscosity					
$\eta_V$	Solvent contribution of shear viscosity					
λ	Tumbling parameter					
$\lambda_{p1}, \lambda_{p2}, \lambda_{p3}$	Three eigenvalues of $\langle \underline{p} \underline{p} \rangle$					
$\lambda_{b1}, \lambda_{b2}, \lambda_{b3},$	Three eigenvalues of <u>b</u>					
θ	Angle between rigid rod and y-direction					
<u>τ</u>	Total stress tensor					
$ au_{23}^{E}$	Elastic contribution of shear stress					
τ <sup>E</sup>	Elastic contribution of stress tensor					
τ S	Solvent contribution of stress tensor					
Ţ <sup>V</sup>	Viscous contribution of stress tensor					
Ψ	Orientation density function					

Viscous drag coefficient  $\zeta_{\mathbf{R}}$  $\nabla$ Gradient Ŷû dimensional velocity gradient  $\nabla \underline{\mathbf{u}}$ dimensionless velocity gradient <.> Ensemble average 3 Function of symmetry operator  $\mathfrak{I}_1$ Hand's first order closure  $\mathfrak{I}_2$ Second order quadratic closure Dimensional quantity • Subscript Structure tensor component b C Convective contribution Ε Elastic contribution i, j, k, ℓ Vector indices MS Maier-Saupe R Body rotation r, θ, φ Three spherical coordinate axes S Solvent contribution TD **Tube Dilation** V Viscous contribution Three Cartesian coordinate axes x, y, z

<u>X</u>

Material frame of reference

 $\alpha, \beta, \gamma$  Vector indices

Superscript

E Elastic contribution

S Solvent contribution

V Viscous contribution

#### CHAPTER 1

#### INTRODUCTION

#### 1.1 Motivation

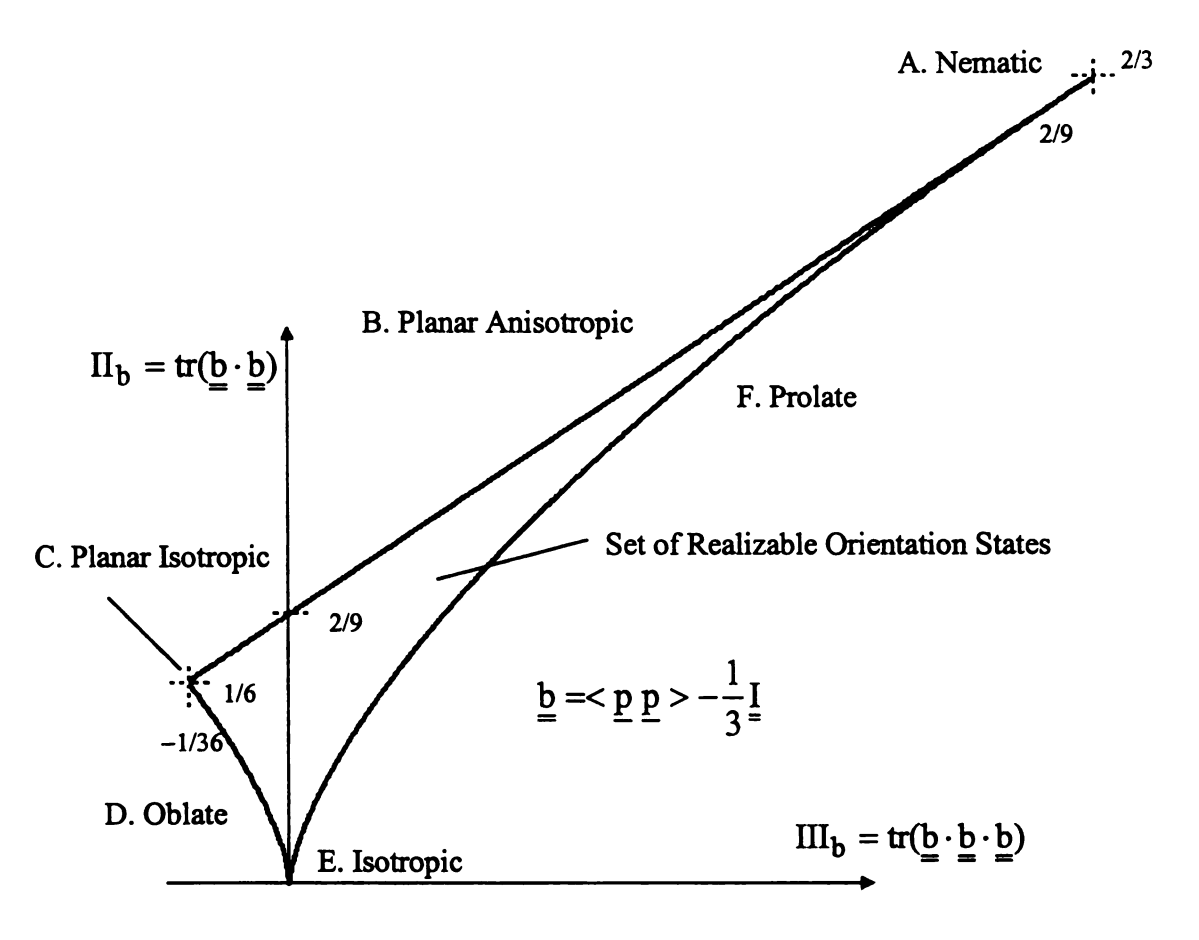
The statistical theory of rigid rod suspensions provides a means for understanding the microstructure and rheology of structured fluids (Doi and Edwards, 1978a, 1978b; Doi, 1981). The microstructure may be either isotropic or anisotropic. Under extreme conditions, a *nematic phase* may occur wherein the long axis of rod-like particles (or molecules) align in the same direction. The tendency for some fluids to develop nematic-like microstructures either spontaneously or under the influence of an external force field has a significant and practical impact on the rheological, optical, and material properties of structured fluids.

Particle suspensions and liquid crystalline polymers may be either isotropic or anisotropic, depending on the local environment. The microstructure is often characterized statistically by low-order moments of the orientation distribution function, referred to hereinafter as the orientation dyad (second order tensor) and the orientation tetrad (fourth order tensor). The orientation dyad,  $\langle pp \rangle$ , is symmetric and nonnegative (i.e., realizable). The orientation vector  $\underline{p}$  has unit length and is aligned with the principal axis of an axisymmetric ellipsoidal particle, cylindrical rod, or disk-like particle. The eigenvalues of  $\langle pp \rangle$  are real and non-negative (i.e.,  $0 < \lambda_{p1} < \lambda_{p2} < \lambda_{p3} < 1$ ). The "director" of the microstructure is defined as the eigenvector associated with the largest eigenvalue of the orientation dyad. For an

isotropic material, the director has no preferred direction inasmuch as all the eigenvalues of  $\langle pp \rangle$  are the same ( $\lambda_{p1} = \lambda_{p2} = \lambda_{p3} = 1/3$ ).

Figure 1.1 illustrates the type of possible anisotropic states that can occur for axisymmetric ellipsoidal suspensions (see Kini et al., 2003; Nguyen et al., 2001a; Parks et al., 1998; Petty et al., 1999; Weispfennig et al., 1999). Each orientation state is parameterized by two nontrivial invariants of the structure tensor  $\underline{b}$  ( $\Pi_b = \text{tr}(\underline{b} \cdot \underline{b})$ ) and  $\Pi_b = \text{tr}(\underline{b} \cdot \underline{b} \cdot \underline{b})$ ). The b-operator is defined as the anisotropic component of the orientation dyad ( $\underline{b} = (\langle \underline{p} \underline{p} \rangle - \frac{1}{3} \underline{I})$ ). As noted on Figure 1.1, three-dimensional anisotropic states for which  $0 < \lambda_{p1} = \lambda_{p2} < \lambda_{p3} < 1$  have quadratic forms with prolate surfaces (F-boundary) whereas three-dimensional anisotropic states for which  $0 < \lambda_{p1} < \lambda_{p2} = \lambda_{p3} < 1$  have quadratic forms with oblate surfaces (D-boundary). In the absence of external hydrodynamic forces, all stable and unstable equilibrium states are either on the prolate boundary or on the oblate boundary of the invariant diagram (Doi and Edwards, 1986; Kini, 2003).

Two-dimensional planar anisotropic states are located on the B-boundary of Figure 1.1. These states are associated with structure tensors with one eigenvalue equal to zero and two unequal positive eigenvalues ( $\lambda_{p1}=0$ ,  $\lambda_{p2}\neq\lambda_{p3}$ ,  $\lambda_{p2}+\lambda_{p3}=1$ ). Two-dimensional planar isotropic states (Point C on Figure 1.1) have one zero eigenvalue and two equal eigenvalues ( $\lambda_{p1}=0$ ,  $\lambda_{p2}=\lambda_{p3}=1/2$ ). A fully-aligned microstructure forms an ideal nematic phase with  $\lambda_1=0$ ,  $\lambda_2=0$ , and  $\lambda_3=1$  (Point A on Figure 1.1).



Orientation State	Invarinats of <u>b</u>		Eigenvalues of < pp>>			
	Пь	Шь	$\lambda_{p1}$	$\lambda_{p2}$	λ <sub>p3</sub>	Notes
A. Nematic	2/3	2/9	0	0	1	
B. Planar Anisotropic	$\Pi_b = 2/9 + 2\Pi \Pi_b$		0	$\lambda_{p2}$	$1-\lambda_{p2}$	$\lambda_{p2} = [0, 1/2]$
C. Planar Isotropic	1/6	-1/36	0	1/2	1/2	
D. Oblate	$II_b = 6(-III_b/6)^{2/3}$		1-2λ <sub>p2</sub>	$\lambda_{p2}$	$\lambda_{p2}$	$\lambda_{p2} = [1/3, 1/2]$
E. Isotropic	0	0	1/3	1/3	1/3	
F. Prolate	$II_b = 6(III_b/6)^{2/3}$		$\lambda_{p1}$	$\lambda_{p1}$	1-2λ <sub>p1</sub>	$\lambda_{p1} = [0, 1/3]$

Figure 1.1 Anisotropic Orientation States (Parks, 1997)

Microstructures associated with axisymmetric suspensions must fall either on the boundaries or within the bounded region of the (II<sub>b</sub>, III<sub>b</sub>)-plane identified by Figure 1.1. Microstructures outside this domain are unphysical because at least one of the eigenvalues of the orientation dyad is negative.

The realizability domain defined by Figure 1.1 stems directly from the algebraic properties of real, symmetric, non-negative operators and is a fundamental characteristic of any second-order moment of a distribution function. Appendix A shows how the boundaries depend on the invariants of the structure tensor. This model-independent result places an important theoretical constraint on allowable models for the orientation dyad. A practical consequence of Figure 1.1 is that it provides a means to identify a closure model for the orientation tetrad in terms of the orientation dyad, i.e.,  $\langle pppp \rangle = \Im(\langle pp \rangle)$ . This closure is developed in CHAPTER 5 and 6 below.

## 1.2 Background

The primary objective of this research is to examine the influence of the low-order moments of the orientation distribution (microstructure) on the equilibrium and rheological properties of rigid-rod suspensions. Liquid crystalline polymers (LCPs), such as poly (g-benzyl-L-glutamate) in m-cresol and hydroxypropylcellulose in water are often represented as rigid-rod suspensions with a characteristic length  $L \sim 110$  nm and a characteristic diameter  $d \sim 1.16$ -1.75 nm (Bibbo and Armstrong, 1988; Larson, 1999; Walker and Wagner, 1994; Yousefi et al., 2003). The stiffness of LCPs stems from the presence of aromatic rings in the backbone of the polymer or from the  $\alpha$ -helix structure

due to hydrogen bonding (see Figure 1.2). The significant decrease in the shear viscosity of thermotropic and lyotropic liquid crystalline polymers (LCPs) during processing makes these materials commercially attractive. Specific end uses of LCPs exploit their low elongation resistance to cutting, favorable thermal properties, high resistance to wear, and high-strength, low-weight, and high-impact resistance (Collyer, 1992). The tensile moduli of LCPs in the solid phase may vary between 1-100 GPa, depending on the molecular orientation of the constituent polymers (Donald and Windle, 1992). Applications of LCPs are numerous and range from reinforced bulletproof vest to optical components in electrical devices (Collyer, 1992).

Liquid crystalline polymers are generally manufactured by a stepwise polycondensation reaction in either a batch or a continuous process (Jansson, 1992). The polymer is mixed with various additives and extruded as a filament. Over half of the LCPs sold are reinforced with 30% – 40% glass fillers having polymeric sizing to produce a strong interface between the fiber and the matrix material (Clarke et al., 1997). Some LCPs are injection molded for special applications.

#### Equilibrium Microstructure

In the absence of an external field, a rigid rod suspension has an isotropic microstructure (i.e.,  $\Pi_b = 0$  and  $\Pi_b = 0$ ) at low concentration. As the concentration increases to a critical value, the microstructure undergoes a spontaneous transition to an anisotropic nematic-like state. Several methods have been developed to study this transition experimentally. For example, Robinson (1966) developed a birefringence

Figure 1.2 Molecular Structure of LCP (Larson, 1999)

technique to study biphasic phenomena (i.e., coexistence of isotropic states and anisotropic states at the same concentration) for poly-γ-benzyl-L-glutamate (PBLG) in dioxane solutions. This phenomenon was observed for PBLG aspect ratios from 10 to 100 and has been reported by other investigators using other methods (see Abe and Yamazaki, 1989b; Kubo and Ogino, 1979; Murthy et al., 1976; Sartirana et al., 1987).

Abe and Yamazaki (1989a) developed a NMR technique to correlate the relative orientation of the α-helical backbone of PBLG rigid-rod molecules by exploiting a quadrupolar splitting phenomena related to the pendant side chain containing C-D and N-D bonds. If the PBLG solution is isotropic, the NMR spectrum has only one resonance peak. As the concentration increases and the microstructure approaches the biphasic region, quadrupolar splitting occurs. The split increases as the fluid becomes more anisotropic. In the biphasic region, the central peak corresponds to an isotropic microstructure and the split signal corresponds to a nematic-like microstructure. As the concentration increases further, the isotropic peak disappears while the peak-to-peak distance in the split increases. Figure 1.3 illustrates the observations reported by Abe and Yamazaki for PBLG in DMF (dimethylformamide) and in 1, 4-dioxane with aspect ratios of 32, 121, and 185.

#### Non-Equilibrium Microstructure

In a time independent external field, director tumbling of LCP solutions may occur at low shear rates, but direct measurements using optical methods are difficult. However, optical measurements of this phenomenon for lower molecular weight liquid crystal (LC) suspensions have been reported extensively (Bedford and Burghardt, 1996;

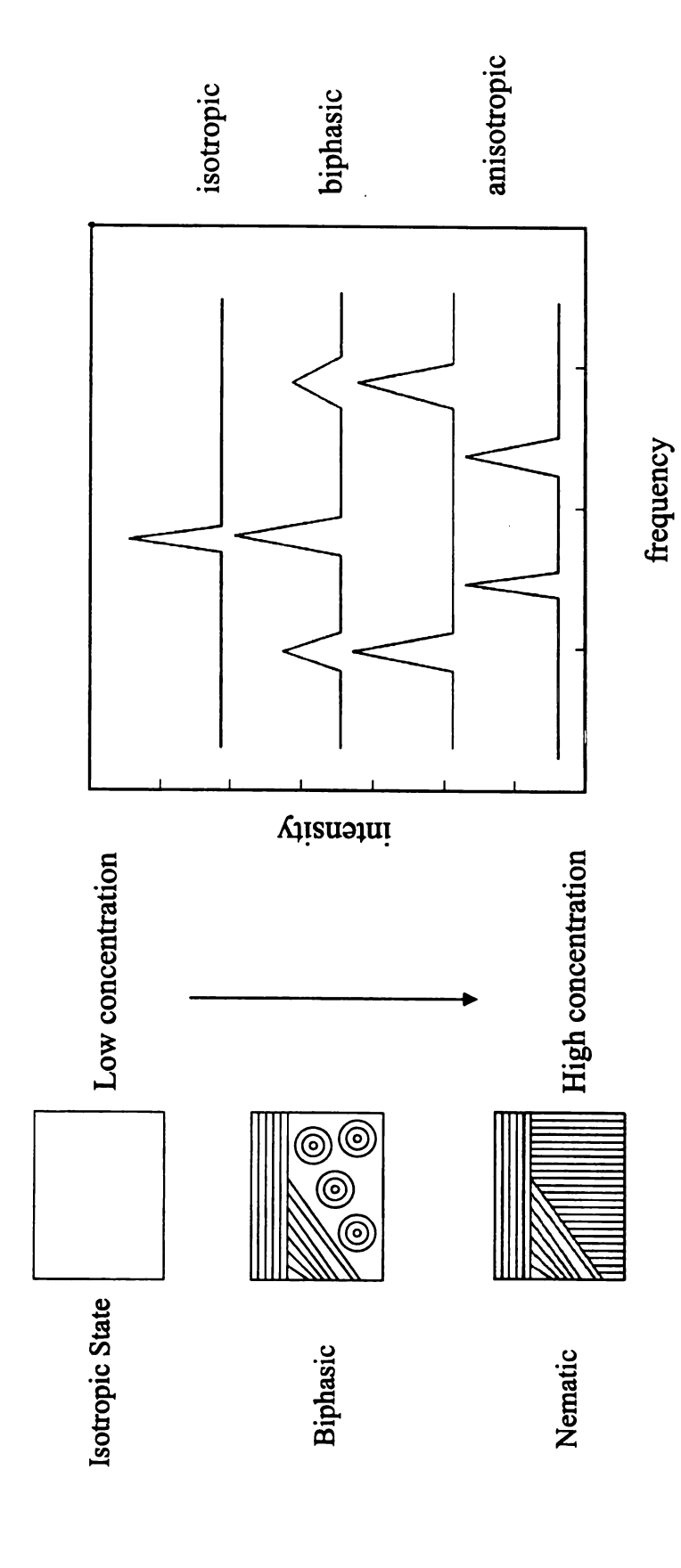


Figure 1.3 Schematic of NMR Spectra for PBLG in DMF (Abe and Yamazaki, 1987a; Robinson, 1966)

Burghardt and Fuller, 1991; Fuller, 1995; Larson, 1999). Rheological measurements on LCP solutions and melts have been used to study director tumbling. Erickson and others (see p. 453-456 in Larson, 1999) related this phenomenon to a phenomenological tumbling parameter  $\lambda$  that couples the angular motion of the rigid rod to the strain rate of the flow field (see Eq.(10-3) p. 448 in Larson, 1999). For homogeneous shear flows and  $|\lambda| > 1$ , the director attains a steady alignment relative to the flow direction in the shear (or deformation) plane (i.e., flow/cross-flow plane). On the other hand, if  $|\lambda| < 1$ , the director rotates continuously in the shear plane (see p. 454 in Larson, 1999; Carlsson, 1982; Carlsson and Skarp, 1986). Because  $\lambda$  is related to rheological Leslie-Ericksen coefficients, tumbling phenomenon has been studied indirectly for more than thirty years by measuring fluid properties of the suspensions (see Cladis and Torza, 1975; Gähwiller, 1973; Pieranski and Guyon, 1974; Skarp et al., 1981).

Skarp et al. (1981) (also see Carlsson and Skarp, 1986; Clark et al., 1981) measured the Leslie-Ericksen coefficients for 4-n-octyl-4'-cyano-biphenyl (a thermotropic liquid crystal) over a range of temperatures (35 – 40 °C). They used an electromagnetic field to initially align the orientation director parallel and perpendicular to the flow direction. After removing the magnetic field, the anisotropic microstructure relaxes and the LE-coefficients were measured. The rheological data indicated that the magnitude of the tumbling parameter was less than unity, which implies director tumbling according to Ericson's theory. This approach has also been applied to infer director tumbling in LCP solutions subjected to homogeneous shear flows with limited success (see Burghardt and Fuller, 1990; Larson, 1988).

### Rheological Properties

The rheological characteristics of LCPs are important indicators of molecular orientation because time-dependent molecular conformation is strongly coupled with the flow (Walker et al., 1995). Some LCPs in simple shear flows show shear viscosity with strain rate (or stress) response curves with three distinct characteristics: 1) a shear thinning region at low strain rates (Region I); 2) a Newtonian plateau (Region II); and, 3) an additional shear thinning region at high strain rates (Region III) (Walker and Wagner, 1994; Walker et al., 1995; Larson, 1999). Region II occurs for a wide range of strain rates because the molecular orientation and the conformation of the rigid-rod polymer solution are maintained. Shear thinning occurs at higher strain rates because the flow field distorts the microstructure by flow alignment. Clearly, flow alignment enhances the relative motion between phases (i.e. translational diffusion) with the result that the shear viscosity decreases (i.e., shear thinning).

An anomalous shear-thinning region at low strain rates has only been observed for LCPs. However, not all LCPs show a Region I behavior. Walker and Wagner (1994) have shown that (1,4-phenylene-2,6-benzobisthiazole) (PBZT) has a Region I response only at relatively high concentrations. This phenomenon has not been fully characterized experimentally because of inaccurate shear stress measurements at low strain rates (see Doraiswamy and Metzner, 1986; Larson, 1999; Walker et al., 1995). In addition, no clear theoretical explanation for this phenomenon has been identified.

Another interesting characteristic of LCP solutions is the occurrence of a negative first normal stress difference (N<sub>1</sub>) at intermediate strain rates (see Back et al., 1993; Chono et al., 1996; Kiss and Porter, 1980; Larson, 1999; Magda et al., 1991). At low

strain rates,  $N_1$  is positive; however, as the strain rate increases,  $N_1$  attains a maximum value and then decreases to zero and becomes negative. At higher shear rates, the first normal stress difference becomes positive again. This observation suggests that  $N_1$  is sensitive to changes in the microstructure as the strain rate increases. Beck et al. (1993) have suggested that the transition from positive to negative values of  $N_1$  was associated with the orientation director changing from a stable periodic tumbling state to a stable periodic wagging state. This is consistent with the Leslie-Ericksen theory, which requires director tumbling for negative first normal stress differences (also, see p. 449 in Larson, 1999; Burghardt and Fuller, 1990).

In addition to the negative first normal stress difference, direct oscillatory response of the viscosity also indicates molecular tumbling phenomenon. When the rate of shear is suddenly changed, the shear stress component of the deviatoric molecular stress shows an oscillatory response including a reversal in the strain rate (Burghardt and Fuller, 1991; Picken et al., 1991; Vermant et al., 1994; Walker et al., 1995). This relaxation response has multiple overshoots and undershoots that can be imposed with various shear rates before the steady state is reached against strain. Since this type of response is independent of strain rate, it must be due to changes in the microstructure rather than the flow properties. In addition, there is only one overshoot when the microstructure relaxes to a steady flow alignment state. These experimental observations support the hypothesis that multiple stress oscillations and director tumbling are correlated (Burghardt and Fuller, 1991; Larson, 1999).

#### Theoretical Studies

Liquid crystalline polymers have stiffness characteristics that are different from other polymers. LCPs have been studied for many years. Although "industrial" LCPs are not as rigid as "laboratory" LCPs, understanding the behavior of rigid rod suspensions would nevertheless provide valuable information and insight related to processing LCPs.

Theoretical studies of LCP orientation phenomenon are primarily related to the Smoluchowski's (S-) equation. The S-equation governs the distribution of orientation states. It is a partial differential equation that balances the accumulation of states subject to rotary convection and rotary diffusion in orientation space (see CHAPTER 2 below). The diffusive flow has two contributions: Brownian motion and the excluded volume phenomenon. Brownian motion tends to mix the LCP molecules randomly whereas the excluded volume effect tends to align the LCP molecules. The convective flux arises due to the torque on the LCP molecules in a shear field.

There are several ways to study the S-equation. One approach is to develop a solution using spherical harmonics (Chaubal and Leal, 1997, 1999; Larson, 1990). Another approach is based on the method-of-moments. Developing an explicit expansion for the density function is a complicated process and requires significant computational resources. On the other hand, developing a solution based on low order moments of the density function requires a closure approximation (Marrucci, 1996).

Doi (1981) developed a second order moment equation by integrating the S-equation with Maier-Saupe potential for the excluded volume. Doi used a quadratic closure approximation for the orientation tetrad (i.e.,  $\langle \underline{p} \, \underline{p} \, \underline{p} \, \underline{p} \rangle = \langle \underline{p} \, \underline{p} \rangle \langle \underline{p} \, \underline{p} \rangle$ ). Unfortunately, these approaches do not retain the six-fold symmetry and six-fold

contraction properties of the fourth order moment (see CHAPTER 3 and the development in CHAPTER 5).

Hand (1962) used a first order closure approximation for  $\langle \underline{p} \ \underline{p}$ 

Later, Cintra and Tucker (1995) developed a new closure for the orientation tetrad based on an orthotropic operator. The approach assumes that the symmetry directions of the tetrad coincide with the orientation dyad. The closure coefficients of the tetrad are obtained by fitting the moment equation with the "exact" solution based on a spherical harmonic expansion of the orientation density function. The orthotropic closure is applicable to simple geometries and can provide valuable bench mark information.

There are other closures that combine previous approximations (Tucker, 1988; Larson, 1999). For example, Tucker (1988) has combined Hand's closure approximation at the isotropic state and the decoupling approximation at the nematic state. This superposition of two asymptotic closures is similar to the strategy employed by Hinch and Leak and is an example of a hybrid closure approximation. Larson (1990) used the decoupling closure for the excluded volume potential and the HL-closure for the convective flux in the same model. None of the foregoing closure approximations satisfy the symmetry properties of the orientation tetrad and the realizable condition on the

second order moment. In addition, none have fully predicted the microstructure and rheological properties of LCPs.

Recent research at Michigan State University has developed a representation of the orientation tetradic in terms of the orientation dyad that satisfies the six-fold symmetry and the six-fold contraction properties associated with  $\langle \underline{p} \underline{p} \underline{p} \underline{p} \rangle$  (see Parks et al., 1999; Parks and Petty, 1999a, 1999b; Petty et al., 1999; Imhoff, 2000; Nguyen, 2001; Kini, 2003; Mandal, 2004). This closure is incomplete and needs an appropriate closure coefficient  $C_2$  ( $\Pi_b$ ,  $\Pi_b$ ) so that the orientation dyad is realizable for all conditions. Previous studies assumed that  $C_2 = 1/3$  for all anisotropic states within the invariant diagram (Figure 1.1). This condition must be true at the nematic state, but it is not required elsewhere. However, it is noteworthy that  $C_2 = 1/3$  predicts biphasic phenomena (Kini, 2003; Nguyen, 2001) and tumbling phenomena (Nguyen, 2001). However, a "universal" value of  $C_2 = 1/3$  causes unrealizable behavior for some physically allowable initial conditions. This is unacceptable and a resolution of the problem is developed in CHAPTER 6 below. Imhoff (2000) and Mandal (2004) identified a value for C<sub>2</sub> by using solutions of the S-equation. Their best fitted C<sub>2</sub> value was 0.37, but this choice of C<sub>2</sub> is also unacceptable because it yields unrealizable results orientation dyad for certain initial conditions.

## 1.3 Objective

This research addresses a long-standing fundamental problem related to the self-alignment and flow alignment of structured fluids. The approach, which builds on

the statistical theory developed earlier by Doi and many others (see, esp., Doi and Edwards, 1986; Bird et al., 1987a,b; Larson, 1999) provides new insights and understanding of the relationship between the microstructure and the phenomenological properties of structured fluids at the continuum scale.

The objective of the research is to develop a closure for the orientation tetrad that yields a realizable model for the orientation dyad. The new approach is used to predict the microstructure and the rheological response of rigid rod suspensions to simple shear flows. By using the S-equation based on Doi's theory (1981), an equation for the second order moment of the orientation density function can be developed that depends on the fourth order moment (i.e., the orientation tetrad). Although the method-of-moments has been employed for more than thirty years as a mean to study the microstructure of rigid rod suspensions, understanding the equation has been limited by the absence of a satisfactory closure model for the orientation tetrad. This is a significant theoretical deficiency that hinders the interpretation of rheological anomalies associated with the response of microstructure fluids to simple shear fields. To address this issue, this research presumes that the orientation tetrad can be approximated by using an algebraic closure,  $\langle pppp \rangle = \Im(\langle pp \rangle)$ . The efficacy of this hypothesis will be evaluated for a class of microstructured fluids (i.e., rigid rod suspensions) in homogeneous shear flows. The aim of the research is to develop a realizable dynamic model for the orientation dyad for a wide class of complex engineering flows.

#### 1.4 Outline

The equilibrium relaxation of the orientation dyad in the absence of an external field (CHAPTER 7) and the non-equilibrium relaxation of the orientation dyad in the presence of an external field (CHAPTER 8) are addressed in this research. The Sequation in orientation space (CHAPTER 2) is used to develop an ordinary differential equation for the orientation dyad,  $\langle \underline{p}\,\underline{p} \rangle$  (CHAPTER 4). The moment equation has three physical contributions: rotary Brownian motion, excluded volume phenomenon, and hydrodynamic interactions through particle/fluid torque. A Maier-Saupe potential is used for the excluded volume effect and Jeffery's model is used for the hydrodynamic interactions (CHAPTER 2). In addition, the effect of tube dilation on the diffusive flux is examined. Doi's stress model is used to predict the viscosity and the normal stress differences (CHAPTER 9).

Once the realizable closure approximation is obtained, the ordinary differential equation is solved for the orientation dyad by using a fourth order Runge-Kutta algorithm with a dimensionless time step less than 0.0003 (see APPENDIX G). The moment equation has three independent dimensionless variables: U, Pe, and  $\lambda$  (see CHAPTER 2). For  $\lambda \leq 1$ , the model is used to study the microstructure and rheology of rigid rod suspensions for a wide range of U and Pe (CHAPTER 7 and CHAPTER 8). Various initial value problems are examined with and without homogeneous shear. In CHAPTER 3, two metrics of the microstructure are defined to evaluate the results: 1) the order parameter  $\alpha$ ; and, the deviation of the director from the flow direction,  $\underline{x}_3 \cdot \underline{e}_z$ .

### **CHAPTER 2**

## SMOLUCHOWSKI EQUATION FOR RIGID ROD SUSPENSIONS

### 2.1 Introduction

Smoluchowski's equation (S-equation) governs the evolution of the orientation density function  $\Psi(\underline{p}, \hat{t}; \hat{\underline{\chi}}(\hat{\underline{X}}, \hat{t}))$  for a suspension of rigid rod particles (see p.50 in Doi and Edwards, 1986). The fraction of particles with orientation vectors with angular coordinates between  $(\theta, \phi)$  and  $(\theta + \Delta\theta, \phi + \Delta\phi)$  is given by  $\Psi(\underline{p}, \hat{t}; \hat{\underline{\chi}}(\hat{\underline{X}}, \hat{t}))\sin\theta\Delta\theta\Delta\phi$ . In a frame of reference moving with the local velocity of the suspension, the S-equation is a balance equation for orientation states and can be written as:

$$\left(\frac{\partial \Psi}{\partial \hat{\mathbf{t}}}\right)_{\underline{\hat{\mathbf{X}}}} = -\frac{\partial}{\partial p} \cdot \left(\underline{\dot{\mathbf{p}}}\Psi\right). \tag{2.1}$$

In the above equation,  $\frac{\partial}{\partial \underline{p}}$  is a surface gradient operator on a sphere in orientation space and the vector  $\underline{\dot{p}}$  is the angular velocity of the particle about its center of mass. The vector  $\underline{\hat{X}}$  represents the spatial position of a material fluid element at some arbitrary reference time; the spatial position of the material fluid element at time  $\hat{t}$  is  $\underline{\hat{x}} = \underline{\hat{\chi}}(\underline{\hat{X}}, \hat{t})$ . The vector  $\underline{\hat{\chi}}(\underline{\hat{X}}, \hat{t})$  is the motion of the suspension with velocity  $\underline{\hat{u}}(\hat{x}, \hat{t})$  defined by

$$\underline{\hat{\mathbf{u}}}(\underline{\hat{\mathbf{x}}}, \, \hat{\mathbf{t}}) = \left(\frac{\partial \, \underline{\hat{\mathbf{x}}}}{\partial \, \hat{\mathbf{t}}}\right)_{\underline{\hat{\mathbf{X}}}}.$$
(2.2)

The operator on the left-hand-side of Eq.(2.1) represents the substantial (or material) derivative of the orientation density function:

$$\left(\frac{\partial \hat{\mathbf{\chi}}}{\partial \hat{\mathbf{t}}}\right)_{\hat{\mathbf{X}}} = \left(\frac{\partial \mathbf{\Psi}}{\partial \hat{\mathbf{t}}}\right)_{\hat{\mathbf{X}}} + \left(\frac{\partial \hat{\mathbf{\chi}}}{\partial \hat{\mathbf{t}}}\right)_{\hat{\mathbf{X}}} \cdot \hat{\nabla}.$$
(2.3)

The rotary flux of orientation states relative to a material frame of reference,  $\underline{\dot{p}}\Psi$ , can be separated into a rotary convective flux  $\underline{\dot{p}}_C\Psi$  and a rotary diffusive flux  $(\underline{\dot{p}}-\underline{\dot{p}}_C)\Psi$ :

$$\dot{p}\Psi \equiv \dot{p}_C \Psi + \left(\dot{p} - \dot{p}_C\right)\Psi. \tag{2.4}$$

In this research, the rotary convective flux developed by Jeffery (1922) for ellipsoidal particles suspended in a homogenous shear field will be used for  $\dot{\underline{p}}_C\Psi$  (see Section 2.2 below). Doi's model for the rotary diffusive flux (see Section 2.3 below) will be used for  $(\dot{\underline{p}}-\dot{\underline{p}}_C)\Psi$ . The rigid rods have the same density as the suspending fluid so gravity is unimportant. The S-equation given by Eq.(2.1) above assumes that spatial diffusion of the particles relative to the translational velocity is also unimportant.

# 2.2 Jeffery's Model for Rotary Convection: Tumbling Coefficient

Jeffery's model is used for the rotary convective flux (Jeffery, 1922). Hydrodynamic drag causes the rotary motion of the suspended particles (Batchelor, 1976, 1982; Bibbo et al., 1985). A balance of angular momentum on an axisymmetric rigid rod yields the following equation for  $\dot{p}_{C}$  (see Jeffery, 1922; Parks et al., 1999):

$$\underline{\dot{\mathbf{p}}}_{\mathbf{C}} \equiv \left(\frac{\partial \underline{\mathbf{p}}_{\mathbf{C}}}{\partial \hat{\mathbf{t}}}\right)_{\underline{\mathbf{X}}} = -\underline{\hat{\mathbf{W}}} \cdot \underline{\mathbf{p}} + \lambda \left[\underline{\mathbf{I}} - \underline{\mathbf{p}}\underline{\mathbf{p}}\right] \cdot \left[\underline{\hat{\mathbf{S}}} \cdot \underline{\mathbf{p}}\right], \tag{2.5}$$

where  $\lambda$  is a dimensionless tumbling parameter.  $\hat{\underline{S}}$  and  $\hat{\underline{W}}$  are the rate-of-strain and vorticity tensors, respectively:

$$\hat{\underline{S}} = \frac{1}{2} \left[ \hat{\nabla} \hat{\underline{u}} + (\hat{\nabla} \hat{\underline{u}})^{T} \right] = \frac{\dot{\gamma}}{2} \left[ \nabla \underline{u} + (\nabla \underline{u})^{T} \right]; \qquad (2.6a)$$

$$\underline{\underline{\hat{\mathbf{W}}}} = \frac{1}{2} \left[ \hat{\nabla} \underline{\hat{\mathbf{u}}} - (\hat{\nabla} \underline{\hat{\mathbf{u}}})^{\mathrm{T}} \right] = \frac{\dot{\gamma}}{2} \left[ \nabla \underline{\mathbf{u}} - (\nabla \underline{\mathbf{u}})^{\mathrm{T}} \right]. \tag{2.6b}$$

For homogeneous shear,  $\hat{\nabla} \hat{\underline{u}} = \dot{\gamma} \underline{e}_{v} \underline{e}_{z}$  where

$$\dot{\gamma} = \sqrt{(\hat{\nabla}\underline{\hat{\mathbf{u}}}) : (\hat{\nabla}\underline{\hat{\mathbf{u}}})^{\mathrm{T}}} = \sqrt{2\underline{\hat{\mathbf{S}}} : \underline{\hat{\mathbf{S}}}^{\mathrm{T}}} = \sqrt{2\underline{\hat{\mathbf{W}}} : \underline{\hat{\mathbf{W}}}^{\mathrm{T}}} = \text{constant}.$$
 (2.7)

In this research,  $\lambda$  is only a function of the particle aspect ratio, L/d. For axisymmetric particles (see Jeffery, 1922)

$$-1 \le \lambda = \frac{(\frac{L}{d})^2 - 1}{(\frac{L}{d})^2 + 1} \le +1. \tag{2.2}$$

For large aspect ratio particles  $\lambda = 1$ . For disk-like particles  $\lambda = 1$ . A typical tumbling parameter for slender rod-like particles is about 0.7, which is equivalent to L/d  $\cong$  2.38 (see p.280 Larson, 1999; Bretherton, 1962; Trevelyn and Mason, 1951). The rotational period of a rigid rod can be related to the tumbling parameter (Jeffery, 1922; p.280 Larson, 1999). For  $\lambda = \pm 1$ , a prolate spheroidal particle and a disk-like oblate particle have infinite rotation periods (i.e., they are not rotating). Experimental evidence for particle rotation (or tumbling) in rigid rod suspensions has been given by Larson and many others (see p.280 Larson, 1999; Anczurowski and Mason, 1967a, 1967b; Frattini and Fuller, 1986).

### 2.3 Brownian Motion: Rotary Diffusivity

Rotary Brownian motion is an important phenomenon in particle/fluid suspensions. This phenomenon has a direct impact on models for viscoelasticity, diffusion, birefringence and dynamic light scattering.

The theory of rotary diffusion in concentrated suspensions is well described by the following hypothesis (see p.294, Doi and Edwards, 1986; Parks et al., 1999):

$$\underline{\dot{p}} - \underline{\dot{p}}_{C} = -\langle D_{R} \rangle \left( \frac{\partial \Psi}{\partial \underline{p}} - \Psi \frac{\partial}{\partial \underline{p}} (\frac{\Delta \hat{U}}{k_{B}T}) \right). \tag{2.3}$$

In the above equation,  $\Delta \hat{U}$  is an excluded volume potential and  $\langle D_R \rangle$  represents an average rotary diffusion coefficient. In general,  $\langle D_R \rangle$  depends on the phenomenon of tube dilation (see p.360 in Doi and Edwards, 1986; Kuzuu and Doi, 1993, 1994; p.520 in Larson, 1999), the particle aspect ratio L/d, the volume fraction of particles, and the temperature. In this research, the influence of tube dilation on the microstructure and rheology will be examined (see CHAPTER 8 and CHAPTER 9), but most of the applications will assume that  $\langle D_R \rangle$  is given by

$$\langle D_R \rangle \doteq D_R^o \equiv \frac{3k_B T}{\pi \eta_S L^3}. \tag{2.9}$$

In the above equation,  $k_B$  and  $\eta_S$  represent, respectively, the Boltzmann constant and the solvent viscosity; T is the temperature.  $D_R^o$  has units of 1/(time) and represents the rotary diffusion coefficient for dilute suspensions of rigid rods (see p.334 in Doi and Edwards, 1986; p.281 in Larson, 1999). For semi-dilute and concentrated suspensions, Eq.(2.9) is multiplied by a tube dilation factor  $F_{TD}$  ( $P_R > F_{TD}$   $P_R^o$ ), which depends

on the invariants of the microstructure (see Figure 1.1). In this research,  $F_{TD} = 1$  for most of the applications. For the tube dilation examples (see Sections 8.5 and 9.5), Doi's theory for  $F_{TD}$  is used (see p.360 in Doi and Edwards, 1986):

$$F_{TD}^{Doi} = \frac{1}{(1 - \frac{3}{2} \Pi_b)^2} . \tag{2.10}$$

Note that Eq.(2.10) implies that  $< D_R > \to \infty$  as the microstructure approaches a nematic state (see Point A on Figure 1.1).

### 2.4 Excluded Volume Phenomena: Maier-Saupe Potential

The excluded volume potential introduced by Eq.(2.6) above accounts for the interaction of a rigid rod particle with neighboring particles. The main physical idea is that particles cannot occupy the same space at the same time. This phenomenon has important consequences that partly explain the self-alignment and the flow-induced alignment of particles. Doi (1981) and others have developed models for the instantaneous excluded volume potential by minimizing the Onsager free energy for rigid rod suspensions (Ilg et al., 1999; Onsager, 1949) with the result that (see p.359, Doi and Edwards, 1986):

$$\frac{\Delta \hat{U}}{k_B T} = -U \,\underline{p}\,\underline{p} :< \underline{p}\,\underline{p} > + \{\text{higher order terms}\}. \tag{2.11}$$

The above equation stems from an expansion of the second virial coefficient of the Onsager nematic potential. The lead term is the so-called Maier-Saupe potential:

$$\frac{\Delta \hat{\mathbf{U}}_{MS}}{\mathbf{k}_{B}T} = -\mathbf{U}\,\underline{\mathbf{p}}\,\underline{\mathbf{p}} < \underline{\mathbf{p}}\,\underline{\mathbf{p}} > . \tag{2.12}$$

This model is used in the Doi theory for rigid rod suspensions and is also used hereinafter. The average of Eq.(2.12) shows that  $<\Delta\hat{U}_{MS}>$  is proportional to the second invariant of the orientation dyad:  $<\Delta\hat{U}_{MS}>=-Uk_BT<\underline{p}p>:<\underline{p}p>$ . With  $<\underline{p}p>=\frac{1}{3}\underline{I}+\underline{b}$ , the average excluded volume potential can be expressed as

$$<\Delta \hat{U}_{MS}> = -Uk_BT\left(\frac{1}{3} + II_b\right).$$
 (2.13)

Thus, at the isotropic state (i.e., Point E on Figure 1.1),  $<\Delta \hat{U}_{MS}>=-\frac{1}{3}Uk_BT$ ; and, at the nematic state (i.e., Point A on Figure 1.1),  $<\Delta \hat{U}_{MS}>=-Uk_BT$ .

The nematic coefficient U is dimensionless and, as indicated above, compares the average excluded volume potential with  $k_BT$ . For rigid rod suspensions (see p.66 in Larson, 1999), U is proportional to the concentration of particles and the excluded volume  $V_E = a^0L$ . The parameter  $a^0$  is the diameter of a tube of length L that contains a single rigid rod. In this research,  $a^0$  is assumed to be independent of the local microstructure (i.e.,  $\Pi_b$  and  $\Pi_b$ ). Tube dilation affects the nematic potential (and rotary Brownian diffusion) through the  $F_{TD}$ -factor introduced by Eq.(2.10).

## 2.5 Discussion

The S-equation with Jeffery's model for rotary convection (see, Eq.(2.5)) and Doi's model for the excluded volume potential (see, Eq.(2.12)) can be written as

$$\frac{\partial \Psi}{\partial \underline{t}} \underbrace{\sum_{\underline{\underline{Y}}} + \operatorname{Pe} \frac{\partial}{\partial \underline{p}} \cdot \left[ \left( -\underline{\underline{W}} \cdot \underline{p} + \lambda \left[ \underline{\underline{I}} - \underline{p} \underline{p} \right] \cdot \left[ \underline{\underline{S}} \cdot \underline{p} \right] \right] \Psi \right] =} + F_{TD} \frac{\partial}{\partial \underline{p}} \cdot \left[ \frac{\partial \Psi}{\partial \underline{p}} + U \Psi \frac{\partial}{\partial \underline{p}} \left( \underline{p} \underline{p} : < \underline{p} \underline{p} > \right) \right] }$$
(2.14)

where t is a dimensionless time and Pe is Péclet number:

$$t = 6D_{R}^{o} \hat{t}$$
,  $Pe = \frac{1}{6D_{R}^{o}} \frac{d\hat{u}_{z}}{d\hat{y}}$ . (2.15)

The S-equation determines how the orientation density function changes with time over the surface of a sphere in orientation (phase) space (see Edwards and Beris, 1989). The relaxation of  $\Psi(\underline{p},t)$  from an initial state is controlled by four physical factors: 1) a rotational torque due to the antisymmetric component of the velocity gradient; 2) a rotational torque due to the symmetric component of the velocity gradient; 3) a rotational torque due to Brownian motion; and, 4) a rotational torque due to the excluded volume phenomenon. A direct numerical (or analytical) analysis of Eq.(2.14) subject to arbitrary, but realizable, an initial condition has not been done. Some limited results have been reported for isotropic initial conditions (see Doi, 1981; Hand, 1962; Hinch and Leal, 1976; Petty et al.,1999; Tucker, 1988), but an understanding of Eq.(2.14) has primarily resulted from a study of the low order moments of  $\Psi(\underline{p},t)$ . The moment method (see CHAPTER 3) will be used in this research.

### **CHAPTER 3**

### MOMENTS OF THE ORIENTATION DISTRIBUTION

### 3.1 Introduction

In this research, a rigid rod is approximated as an axisymmetric ellipsoid. A single orientation vector  $\underline{\mathbf{p}}$  defines the instantaneous orientation state of the rod in terms of the angular variable  $\theta$  and  $\phi$  (see Figure 3.1):

$$\underline{\mathbf{p}} = \underline{\mathbf{e}}_{\mathbf{r}} = \sin(\theta)\cos(\phi)\underline{\mathbf{e}}_{\mathbf{x}} + \sin(\theta)\sin(\phi)\underline{\mathbf{e}}_{\mathbf{y}} + \cos(\theta)\underline{\mathbf{e}}_{\mathbf{z}}. \tag{3.1}$$

There is no distinction between the head and the tail of the rod. Therefore, the orientation density function satisfies the symmetry condition  $\Psi(\underline{p},t) = \Psi(-\underline{p},t)$ . The vorticity direction is  $\underline{e}_x$ ; the cross-flow direction is  $\underline{e}_y$ ; and, the flow direction is  $\underline{e}_z$ . The plane that contains the flow direction and the cross-flow direction is called the shear plane (or the deformation plane); the plane that contains the cross-flow direction and the vorticity direction is called the cross-flow/vorticity plane; and, the plane that contains the vorticity direction and the flow direction is called the vorticity/flow plane (see Figure 3.1).

Measuring the orientation of individual rigid rods in a suspension is not practical. However, low-order moments of the density function  $\Psi(\underline{p}, t)$  can be measured. These moments provide an objective means to understand the complex behavior of rigid rod suspensions. For a suspension of axisymmetric particles, the first moment  $\langle \underline{p} \rangle$  is zero because of symmetry:

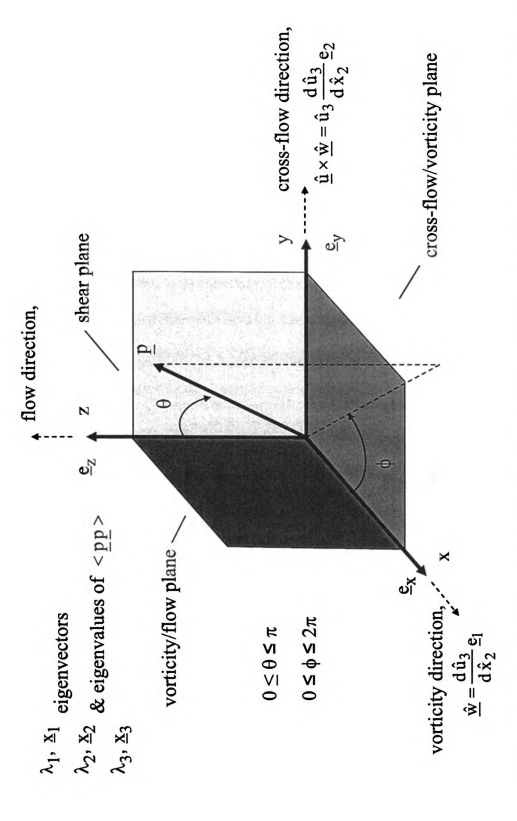


Figure 3.1 Instantaneous Orientation Vector Directed Along the Molecular Axis of a Rigid Rod

$$\langle \underline{p} \rangle \equiv \int_{0}^{2\pi} \int_{0}^{\pi} \underline{p} \ \Psi(\theta, \phi, t) \sin(\theta) d\theta d\phi = \underline{0}.$$
 (3.2)

All of the odd moments are zero. The zeroth moment (i.e., integration of the density function over the sphere) is unity because the total number of particles is a constant.

## 3.2 Orientation Dyad: Structure Tensor and the Order Parameter

The second moment of the orientation density function is

$$\langle \underline{p}\underline{p} \rangle \equiv \int_{0}^{2\pi} \int_{0}^{\pi} \underline{p}\underline{p} \, \Psi(\theta, \phi, t) \sin(\theta) d\theta d\phi$$
 (3.3)

The second moment  $\langle \underline{p} \underline{p} \rangle$  is also called the orientation dyad.  $\langle \underline{p} \underline{p} \rangle$  is a symmetric, non-negative operator, and its trace is unity because

$$tr(\langle pp \rangle) \equiv \langle p \cdot p \rangle = 1. \tag{3.4}$$

This dyadic-valued operator defines the microstructure of rigid rod suspensions. Figure 3.2 illustrates an isotropic (or three-dimensional random) orientation state for which

$$\langle \underline{p}\,\underline{p} \rangle = \frac{1}{3} (\underline{e}_x\,\underline{e}_x + \underline{e}_y\,\underline{e}_y + \underline{e}_z\,\underline{e}_z),$$
 isotropic state.

When the rigid rod particles are randomly distributed in a two-dimensional plane (see Figure 3.2 and Figure 1.1), then

$$\langle \underline{p}\,\underline{p} \rangle = \frac{1}{2} (\underline{e}_{y}\,\underline{e}_{y} + \underline{e}_{z}\,\underline{e}_{z}),$$
 planar isotropic state.

When all of the rigid rods are pointing in one direction (see Figure 3.2), then

$$\langle \underline{p} \, \underline{p} \rangle = \underline{e}_z \, \underline{e}_z$$
, nematic state.

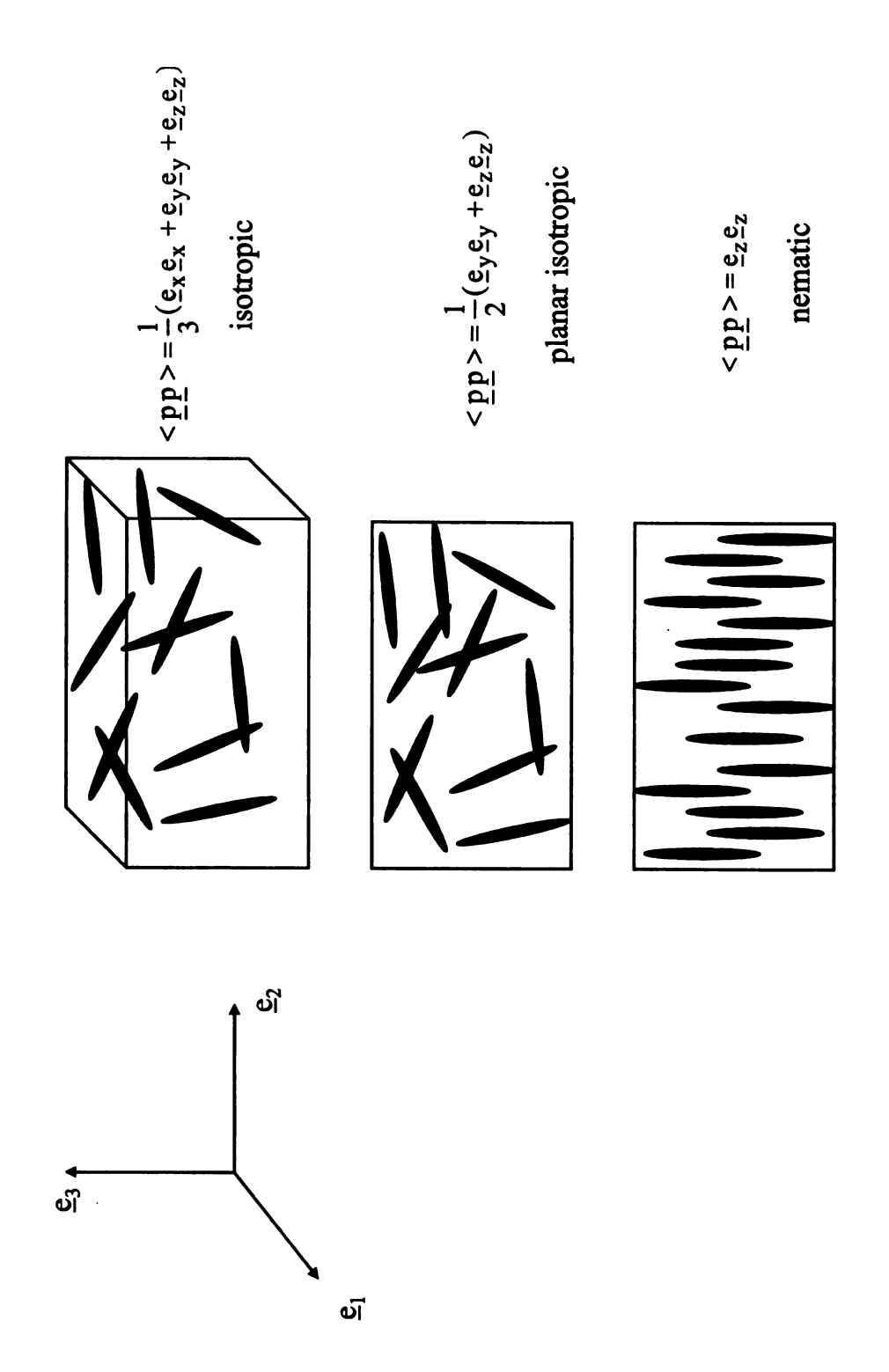


Figure 3.2 Three Orientation States for the Orientation Dyad

The orientation dyad can be represented as the sum of an isotropic operator and an anisotropic operator:

$$\langle \underline{p}\,\underline{p} \rangle = \frac{1}{3}\underline{I} + \underline{b}.$$
 (3.5)

A scalar-valued order parameter  $\alpha$  is often used to define the orientation state or the prolate (and oblate) boundary of Figure 1.1. This parameter defined in terms of the second invariant of the structure tensor  $\underline{b}$ :

$$\alpha = \left(\frac{3}{2} \operatorname{II}_{\mathbf{b}}\right)^{1/2}.\tag{3.6}$$

Note that:

 $\alpha = 1$  at the nematic state;  $\alpha = 0$  at the isotropic state; and,  $\alpha = -1/2$  at the planar isotropic state (see Figure 1.1).

# 3.3 Orientation Tetrad: Symmetry and Contraction Properties

The fourth order moment of the orientation density function is:

$$\langle \underline{p}\underline{p}\underline{p}\underline{p} \rangle \equiv \int_{0}^{2\pi} \int_{0}^{\pi} \underline{p}\underline{p}\underline{p}\underline{p} \Psi(\theta,\phi,t)\sin(\theta)d\theta d\phi.$$
 (3.7)

This statistical property is called the orientation tetrad. Previous studies have used the following closure hypothesis for the orientation tetrad (Hand, 1962; Hinch and Leal, 1976; Doi, 1981; Tucker, 1988; Petty et al., 1999):

$$\langle \underline{pppp} \rangle = \Im(\langle \underline{pp} \rangle) \tag{3.8}$$

Eq.(3.8) is also used to support this research (see CHAPTER 5). Clearly, the orientation tetrad has six-fold symmetry. For example, with  $\underline{p} = \underline{a} = \underline{b} = \underline{c} = \underline{d}$ , it follows that

$$\langle \underline{p}\,\underline{p}\,\underline{p}\,\underline{p}\rangle \equiv \langle \underline{a}\,\underline{b}\,\underline{c}\,\underline{d}\rangle$$

$$\equiv \langle \underline{b}\,\underline{a}\,\underline{c}\,\underline{d}\rangle \equiv \langle \underline{c}\,\underline{b}\,\underline{a}\,\underline{d}\rangle \equiv \langle \underline{d}\,\underline{b}\,\underline{c}\,\underline{a}\rangle$$

$$\equiv \langle \underline{a}\,\underline{c}\,\underline{b}\,\underline{d}\rangle \equiv \langle \underline{a}\,\underline{d}\,\underline{c}\,\underline{b}\rangle \equiv \langle \underline{a}\,\underline{b}\,\underline{d}\,\underline{c}\rangle.$$
(3.9)

The orientation tetrad also has the following contraction property,  $tr(pppp) \equiv p>$ .

$$tr(\langle \underline{p}\,\underline{p}\,\underline{p}\,\underline{p}\,\rangle) \equiv tr(\langle \underline{a}\,\underline{b}\,\underline{c}\,\underline{d}\,\rangle)$$

$$\equiv \langle (\underline{a}\cdot\underline{b})\,\underline{c}\,\underline{d}\,\rangle \equiv \langle (\underline{a}\cdot\underline{c})\,\underline{b}\,\underline{d}\,\rangle \equiv \langle (\underline{a}\cdot\underline{d})\,\underline{b}\,\underline{c}\,\rangle$$

$$\equiv \langle (\underline{b}\cdot\underline{c})\,\underline{a}\,\underline{d}\,\rangle \equiv \langle (\underline{b}\cdot\underline{d})\,\underline{a}\,\underline{c}\,\rangle \equiv \langle (\underline{c}\cdot\underline{d})\,\underline{a}\,\underline{b}\,\rangle$$

$$\equiv \langle \underline{p}\,\underline{p}\,\rangle.$$
(3.10)

Eqs.(3.9) and (3.10) are important properties that should be retained by any closure based on Eq.(3.8) above.

## 3.4 Realizable Anisotropic States: Invariant Diagram

The orientation dyad is a symmetric and non-negative operator (see Parks et al., 1999). The eigenvectors  $\underline{x}_i$  and the eigenvalues  $\lambda_{pi}$  of the orientation dyad  $\langle \underline{p}\underline{p} \rangle$  are defined by:

$$\langle p \, p \rangle \cdot \underline{x}_i = \lambda_{pi} \, \underline{x}_i \ .$$
 (3.11)

The eigenvalues of  $\langle \underline{p}\underline{p} \rangle$  are real and non-negative:  $0 \le \lambda_{p1} \le \lambda_{p2} \le \lambda_{p3} \le 1$ . The eigenvectors of  $\langle \underline{p}\underline{p} \rangle$  are:

$$\lambda_{1}$$
 ,  $\underline{x}_{1} = x_{x1}\underline{e}_{x} + x_{y1}\underline{e}_{y} + x_{z1}\underline{e}_{z}$ 

$$\lambda_{2}$$
 ,  $\underline{x}_{2} = x_{x2}\underline{e}_{x} + x_{y2}\underline{e}_{y} + x_{z2}\underline{e}_{z}$ 

$$\lambda_{3}$$
 ,  $\underline{x}_{3} = x_{x3}\underline{e}_{x} + x_{y3}\underline{e}_{y} + x_{z3}\underline{e}_{z}$ 

$$(3.12)$$

The three invariants of  $\langle \underline{p} \underline{p} \rangle$  are

$$I_{p} = tr(\langle \underline{p}\underline{p} \rangle) = \lambda_{p1} + \lambda_{p2} + \lambda_{p3}$$

$$II_{p} = tr(\langle \underline{p}\underline{p} \rangle \cdot \langle \underline{p}\underline{p} \rangle) = \lambda_{p1}^{2} + \lambda_{p2}^{2} + \lambda_{p3}^{2}$$

$$III_{p} = tr(\langle \underline{p}\underline{p} \rangle \cdot \langle \underline{p}\underline{p} \rangle) = \lambda_{p1}^{3} + \lambda_{p2}^{3} + \lambda_{p3}^{3}.$$

$$(3.13)$$

The orientation director is defined as the eigenvector associated with the largest eigenvalue of  $\langle \underline{p}\underline{p} \rangle$  (i.e.,  $\underline{x}_3$ ).

The structure tensor  $\underline{b}$ , defined by Eq.(3.5), has three eigenvalues:  $\lambda_{b1}$ ,  $\lambda_{b2}$ , and  $\lambda_{b3}$ . The invariants of  $\underline{b}$  are

$$I_{b} = tr(\underline{b}) = \lambda_{b1} + \lambda_{b2} + \lambda_{b3} = 0$$

$$II_{b} = tr(\underline{b} \cdot \underline{b}) = \lambda_{b2}^{2} + \lambda_{b2}^{2} + \lambda_{b3}^{2}$$

$$III_{b} = tr(\underline{b} \cdot \underline{b} \cdot \underline{b}) = \lambda_{b1}^{3} + \lambda_{b2}^{3} + \lambda_{b3}^{3}.$$

$$(3.14)$$

The second and third invariants of  $\underline{b}$  are non-zero. Figure 1.1 uses these invariants of the microstructure to identify all possible realizable orientation (see Parks et al., 1999; esp., Lumley, 1978). The orientation states within this designated region are realizable inasmuch as the eigenvalues of  $\langle pp \rangle$  are real and non-negative.

The eigenvectors of  $\langle \underline{p}\underline{p} \rangle$  and  $\underline{b}$  are the same. The eigenvalues are related by

$$\lambda_{bi} = \lambda_{pi} - \frac{1}{3}$$
 ,  $i = 1, 2, 3$ . (3.15)

For uniaxial alignment states (see point A of Figure 1.1),

$$\lambda_{p1} = 0$$
,  $\lambda_{p2} = 0$ , and  $\lambda_{p3} = 1$  ( $\lambda_{b1} = -\frac{1}{3}$ ,  $\lambda_{b2} = -\frac{1}{3}$ ,  $\lambda_{b3} = \frac{2}{3}$ ). (3.16a)

For planar isotropic states (see Point C of Figure 1.1),

$$\lambda_{p1} = 0$$
,  $\lambda_{p2} = 1/2$ , and  $\lambda_{p3} = 1/2$   $(\lambda_{b1} = -\frac{1}{3}, \lambda_{b2} = \frac{1}{6}, \lambda_{b3} = \frac{1}{6})$ . (3.16b)

For isotropic states (see Point E of Figure 1.1),

$$\lambda_{p1}=1/3,\ \lambda_{p2}=1/3,\ and\ \lambda_{p3}=1/3\ (\lambda_{b1}=0,\ \lambda_{b2}=0,\ \lambda_{b3}=0)$$
 . (3.16c)

For planar anisotropic states (see Line B of Figure 1.1),

$$\lambda_{p1} = 0$$
,  $\lambda_{p2} = 1 - \lambda_{p3}$ , and  $\lambda_{p3}$   $(\lambda_{b1} = -\frac{1}{3}, \lambda_{b2} = \lambda_{p2} - \frac{1}{3}, \lambda_{b3} = \frac{3}{2} - \lambda_{p2})$  (3.16d)

For axisymmetric oblate states (see Line D of Figure 1.1),

$$\lambda_{p1}=1-2\lambda_{p2}\,,\;\;\lambda_{p2}\,,\;\text{and}\;\;\lambda_{p3}=\lambda_{p2}\quad(\frac{1}{3}\!\leq\!\lambda_{p2}\!\leq\!\frac{1}{2})$$

$$(\lambda_{b1} = \frac{4}{3} - 2\lambda_{p2}, \ \lambda_{b2} = \lambda_{p2} - \frac{1}{3}, \ \lambda_{b3} = \lambda_{p2} - \frac{1}{3})$$

(3.16e)

For axisymmetric oblate states (see Line D of Figure 1.1),

$$\lambda_{p1}$$
,  $\lambda_{p2} = \lambda_{p1}$ , and  $\lambda_{p3} = 1 - 2\lambda_{p1}$   $(0 \le \lambda_{p1} \le \frac{1}{3})$ 

$$(\lambda_{b1} = \lambda_{p1} - \frac{1}{3}, \ \lambda_{b2} = \lambda_{p1} - \frac{1}{3}, \ \lambda_{b3} = \frac{4}{3} - 2\lambda_{p1})$$
 (3.16f)

The planar anisotropic boundary of Figure 1.1 follows by substituting the planar anisotropic eigenvalues of  $\underline{b}$  into Eq.(3.14):

$$II_b = 2/9 + 2 III_b$$
 (3.17)

The prolate boundary of Figure 1.1 follows by substituting the axisymmetric prolate eigenvalues of  $\underline{b}$  into Eq.(3.14):

$$II_b = 6\left(\frac{III_b}{6}\right)^{2/3}.$$
(3.18)

The oblate boundary of Figure 1.1 follows by substituting the axisymmetric oblate eigenvalues of  $\underline{b}$  into Eq.(3.14):

$$II_b = 6\left(\frac{-III_b}{6}\right)^{2/3}. (3.19)$$

# 3.5 Discussion

This research proposes to examine a longstanding moment closure problem related to the orientation tetrad of rigid rod suspensions, such as liquid crystalline polymer (LCP). The proposed approach is based on an analysis of the low order moments of the S-equation for the orientation density function. The moment equation for  $\langle \underline{p}\underline{p} \rangle$  is unclosed inasmuch as it depends explicitly on  $\langle \underline{p}\underline{p}\underline{p}\underline{p} \rangle$ . In CHAPTER 4, the moment equation for  $\langle \underline{p}\underline{p} \rangle$  is presented. In CHAPTER 5 and CHAPTER 6, a realizable closure for  $\langle \underline{p}\underline{p}\underline{p}\underline{p} \rangle$  based on the hypothesis expressed by Eq.(3.8) is developed that satisfies all the symmetry and contraction properties defined by Eq.(3.9) and Eq.(3.10).

# **CHAPTER 4**

# EQUATIONS FOR THE MICROSTRUCTURE AND THE STRESS

### 4.1 Introduction

In principle, the S-equation given by Eq.(2.14) can be solved numerically for any initial condition,  $\Psi(\underline{p},0)$ . The resulting solution can be used a posteriori to calculate the low-order moments that appear explicitly in the stress equation. This approach does not require an a priori closure model for moments. Although a direct numerical simulation of the S-equation for relatively simple flows and initial conditions provides useful predictions of statistical properties, this approach is not practical for complex flows or complex initial conditions. The method-of-moments provides an alternative means to study Eq.(2.14). Unfortunately, this approach is unclosed inasmuch as the dynamic equation for  $\langle \underline{p}\underline{p} \rangle$  depends explicitly on  $\langle \underline{p}\underline{p}\underline{p}\underline{p} \rangle$ . However, once an appropriate closure has been identified (and validated) the moment equation for  $\langle \underline{p}\underline{p} \rangle$  can be used to study the relaxation of the microstructure of rigid rod suspensions from arbitrary anisotropic states. Thus, the main objective of this research is to develop an algebraic closure for the orientation tetrad in terms of the orientation dyad.

# 4.2 Dynamic Equation for the Orientation Dyad

An equation for  $\langle \underline{p}\underline{p} \rangle$  follows directly from Eq.(2.14) by first multiplying the equation by pp and then integrating over the unit sphere:

$$\left(\frac{\partial <\underline{p}\,\underline{p}>}{\partial t}\right)_{\underline{X}} + \operatorname{Pe}\left[\underline{\underline{W}}^{T} \cdot <\underline{p}\,\underline{p}> + <\underline{p}\,\underline{p}>\underline{\underline{W}}\right] = \\
-F_{TD}\left[\left(<\underline{p}\,\underline{p}> -\frac{1}{3}\,\underline{\underline{I}}\right) - U\left(<\underline{p}\,\underline{p}> \cdot <\underline{p}\,\underline{p}> - <\underline{p}\,\underline{p}\,\underline{p}\,\underline{p}> :<\underline{p}\,\underline{p}>\right)\right] \\
+\lambda \operatorname{Pe}\left[\underline{\underline{S}}^{T} \cdot <\underline{p}\,\underline{p}> + <\underline{p}\,\underline{p}> \cdot \underline{\underline{S}} - 2 <\underline{p}\,\underline{p}\,\underline{p}> :\underline{\underline{S}}\right] \tag{4.1}$$

The terms on the left-hand-side of Eq.(4.1) is the Jaumann derivative of  $\langle \underline{p}\underline{p} \rangle$ , which represents the rate of change of  $\langle \underline{p}\underline{p} \rangle$  relative to a frame rotating with an angular velocity proportional to the vorticity (see Bird et al., 1987b). The first bracket on the right-hand-side represents rotary diffusion due to Brownian motion and excluded volume phenomenon. The second bracket on the right-hand-side accounts for rotary convection due to fluid/particle drag. Clearly, Eq.(4.1) is unclosed due to the explicit appearance of the orientation tetrad  $\langle \underline{p}\underline{p}\underline{p}\underline{p} \rangle$ . Note that both of the bracket terms, which represents different physical phenomena, depend on  $\langle \underline{p}\underline{p}\underline{p}\underline{p} \rangle$ .

# 4.3 Dynamic Equations for the Structure Invariants for Pe = 0

For Pe = 0, Eq.(4.1) can be reduced to two coupled scalar equations for the structure tensor invariants  $II_b$  and  $III_b$  (see Figure 1.1). The following equations for Pe = 0 are derived in APPENDIX A and B:

$$\frac{d \Pi_b}{d t} = -2\Pi_b + 2 F_{TD} U \left[ \frac{1}{3} \Pi_b + \Pi_b - \underline{b} : \langle \underline{p} \, \underline{p} \, \underline{p} \, \underline{p} \rangle : \underline{b} \right]$$
(4.2)

$$\frac{d \operatorname{III}_{b}}{d t} = -3 \operatorname{III}_{b} + 3 \operatorname{F}_{TD} \operatorname{U} \left[ \frac{1}{3} \operatorname{III}_{b} + \frac{1}{2} \operatorname{II}_{b}^{2} - \underline{b} : \langle \underline{p} \, \underline{p} \, \underline{p} \, \underline{p} \, \underline{p} \rangle : \left( \underline{\underline{b}} \cdot \underline{\underline{b}} \right) \right]$$
(4.3)

The structure tensor  $\underline{b}$  ( $\equiv < \underline{p}\,\underline{p} > -\frac{1}{3}\underline{I}$ ) appears explicitly in Eqs.(4.2) and (4.3). Once closed, the above coupled nonlinear autonomous (i.e., the independent variable does not appear explicitly in the differential equation) first-order, ordinary differential equations can be integrated from any orientation state in the realizable region defined by Figure 1.1. If U = 0, then the equations are closed and linear and can be integrated analytically (see Section 7.3).

# 4.4 Algebraic Equation for the Stress

The deviatoric component of the total stress for a rigid rod suspension consists of three contributions:

$$\hat{\underline{\hat{\mathbf{I}}}} = \hat{\underline{\hat{\mathbf{I}}}}^{\mathbf{S}} + \hat{\underline{\hat{\mathbf{I}}}}^{\mathbf{V}} + \hat{\underline{\hat{\mathbf{I}}}}^{\mathbf{E}} \tag{4.4}$$

where  $\hat{\underline{\tau}}^S$  is the *solvent* contribution;  $\hat{\underline{\tau}}^V$  is the *viscous* contribution; and,  $\hat{\underline{\tau}}^E$  is the *elastic* contribution (Back and Magda, 1994).  $\hat{\underline{\tau}}^S$  depends on the solvent viscosity  $\eta_S$  and the strain rate of the flow (Newtonian fluid):

$$\hat{\underline{\tau}}^{S} = 2 \eta_{S} \hat{\underline{S}} . \tag{4.5}$$

The microstructure of the suspension couples with the strain rate to produce an additional viscous contribution to  $\hat{\underline{\tau}}$ :

$$\underline{\hat{\mathbf{z}}}^{\mathbf{V}} = c\zeta_{\mathbf{R}} < \underline{\mathbf{p}}\underline{\mathbf{p}}\underline{\mathbf{p}}\underline{\mathbf{p}} > : \underline{\hat{\mathbf{S}}} . \tag{4.6}$$

The viscosity coefficient  $c\zeta_R$  is given by

$$c\zeta_{R} = \frac{3ck_{B}T}{6D_{R}^{o}F_{TD}}$$
(4.7)

The viscous stress is due to the drag of the solvent on the rigid rod (see p.521 Larson, 1999).

Doi (1981) developed an elastic stress based on the Onsager free energy with the result that (see Han and Kim, 1993; Larson, 1988):

$$\underline{\hat{\mathbf{r}}}^{E} = 3ck_{B}T\left[\left(\langle \underline{p}\underline{p}\rangle - \frac{1}{3}\underline{\mathbf{I}}\right) - U(\langle \underline{p}\underline{p}\rangle \cdot \langle \underline{p}\underline{p}\rangle - \langle \underline{p}\underline{p}\underline{p}\underline{p}\rangle : \langle \underline{p}\underline{p}\rangle\right]. \tag{4.8}$$

The first term on the right-hand-side of Eq.(4.8) represents the stress induced by rotary Brownian motion. The second term is the stress caused by the excluded volume phenomenon. For homogeneous shear flows, the viscosity of the suspension is given by

$$\hat{\eta} = \frac{\underline{\mathbf{e}}_{\mathbf{y}} \cdot \underline{\hat{\mathbf{r}}} \cdot \underline{\mathbf{e}}_{\mathbf{z}}}{\dot{\mathbf{y}}}.$$
(4.9)

The first and second normal stress differences are defined as follows

$$\hat{N}_1 = \underline{\mathbf{e}}_z \cdot \hat{\underline{\mathbf{t}}} \cdot \underline{\mathbf{e}}_z - \underline{\mathbf{e}}_y \cdot \hat{\underline{\mathbf{t}}} \cdot \underline{\mathbf{e}}_y. \tag{4.10}$$

$$\hat{N}_2 = \underline{\mathbf{e}}_{\mathbf{v}} \cdot \hat{\underline{\mathbf{\tau}}} \cdot \underline{\mathbf{e}}_{\mathbf{v}} - \underline{\mathbf{e}}_{\mathbf{x}} \cdot \hat{\underline{\mathbf{\tau}}} \cdot \underline{\mathbf{e}}_{\mathbf{x}}. \tag{4.11}$$

In a cone-and-plate viscometer, a positive  $N_1$  represents a force that pushes on the cone. A negative  $N_1$  represents a force that causes the cone to push on the fluid.

## 4.5 Discussion

Eq.(4.1) provides the relaxation of the dyad. The solution governs depends on three dimensionless groups: Pe, U, and  $\lambda$ . These groups are independent and account for different physical phenomena. A closure approximation for the orientation tetrad

 $\langle \underline{p}\,\underline{p}\,\underline{p}\,\underline{p}\rangle$  in Eq.(4.1) is developed based on six-fold symmetry and six-fold contraction properties (CHAPTER 5). In CHAPTER 6, Eqs.(4.2) and (4.3) are used to develop a realizable closure for Eq.(4.1).

Doi's elastic stress model defined by Eq.(4.8), is similar to but not as complete as Ericksen, Leslie, and Parodi's (ELP) stress. Doi (1981) noted that the ELP stress has a limitation for predicting nonlinear viscoelasticity, which is important in rigid rod suspensions (Doi, 1981). The Doi stress, even if it is not as general as the ELP stress, separates the elastic and viscous contributions of the stress in both isotropic and nematic phase transition. However, Doi emphasizes that his model is incomplete because of physical and mathematical assumptions. The influence of the microstructure (i.e.,  $\langle pp \rangle$  and  $\langle pppp \rangle$ ) on Eqs.(4.6) and (4.8) is the focus of CHAPTER 9.

### CHAPTER 5

### CLOSURE FOR THE ORIENTATION TETRAD

## 5.1 Introduction

In this chapter, a closure strategy for the orientation tetrad is introduced based on the hypothesis that

$$\langle \underline{p}\underline{p}\underline{p}\underline{p} \rangle = \Im(\langle \underline{p}\underline{p} \rangle)$$
 (5.1)

Parks et al. (1999) used the Cayley-Hamilton theorem of linear algebra (Frazer et al., 1960) and developed a representation for  $\Im(\langle \underline{p}\underline{p} \rangle)$  in terms of the following six independent tetradic operators:

They proposed that  $\Im(\langle \underline{p}\underline{p} \rangle)$  could be written as a linear combination of two tetradic operators with six-fold symmetry and six-fold contraction (see Eqs.(3.9) and (3.10)):

$$\langle \underline{p}\,\underline{p}\,\underline{p}\,\underline{p}\rangle = C_1\,\Im_1(\langle \underline{p}\,\underline{p}\rangle) + C_2\,\Im_2(\langle \underline{p}\,\underline{p}\rangle). \tag{5.2}$$

In the above representation,  $\Im_1(\langle \underline{p}\,\underline{p} \rangle)$  is first-order in  $\langle \underline{p}\,\underline{p} \rangle$  and  $\Im_2(\langle \underline{p}\,\underline{p} \rangle)$  is second-order in  $\langle \underline{p}\,\underline{p} \rangle$ . The scalar coefficients  $C_1$  and  $C_2$  are functions of the eigenvalues of  $\langle \underline{p}\,\underline{p} \rangle$  or, equivalently, the eigenvalues of the structure tensor  $\underline{b} = \langle \underline{p}\,\underline{p} \rangle - \frac{1}{3}\,\underline{I}$ . The closure coefficients  $C_1$  and  $C_2$  are not independent because

Eq.(5.2) must satisfy the six-fold contraction conditions (see Eq.(3.10):

$$tr < \underline{p} \ \underline{p} \ \underline{p} \ \underline{p} > = tr \Big[ \Im(\langle \underline{p} \ \underline{p} \rangle) \Big]$$

$$= C_1 tr \Big[ \Im_1(\langle \underline{p} \ \underline{p} \rangle) \Big] + C_2 tr \Big[ \Im_2(\langle \underline{p} \ \underline{p} \rangle) \Big]$$

$$= (C_1 + C_2) \langle p \ p \rangle .$$

The above result implies that  $C_1 + C_2 = 1$ .

Parks, Petty, and Shao (see Parks et al., 1999) developed explicit expressions for  $\Im_1(\langle \underline{p}\,\underline{p}\rangle)$  and  $\Im_2(\langle \underline{p}\,\underline{p}\rangle)$  by using the following two six-fold symmetric tetradic operators:

$$S[\underline{\underline{A}}\underline{\underline{A}}] = A_{ij}A_{k\ell} + A_{ik}A_{j\ell} + A_{i\ell}A_{jk}$$
(5.3)

and

$$S[\underline{A} \ \underline{B}] = A_{ij}B_{k\ell} + A_{ik}B_{j\ell} + A_{i\ell}B_{jk} + B_{ij}A_{k\ell} + B_{ik}A_{j\ell} + B_{i\ell}A_{jk}$$
 (5.4)

In the above equations, the operators  $\underline{\underline{A}}$  and  $\underline{\underline{B}}$  are symmetric and may be  $\underline{\underline{I}}$ ,  $\langle \underline{p}\underline{p} \rangle$ ,

or  $<\underline{p}\,\underline{p}>\cdot<\underline{p}\,\underline{p}>$ . The operators  $\mathfrak{I}_1(<\underline{p}\,\underline{p}>)$  and  $\mathfrak{I}_2(<\underline{p}\,\underline{p}>)$  are defined as follows:

$$\Im_{1}(\langle \underline{p}\,\underline{p}\,\rangle) = -\frac{1}{35}S[\underline{I}\,\underline{I}] + \frac{5}{35}S[\langle \underline{p}\,\underline{p}\,\rangle\,\underline{I}] \tag{5.5}$$

$$\mathfrak{I}_{2}(\langle \underline{p}\underline{p} \rangle) = \frac{2}{35} \langle \underline{p}\underline{p} \rangle \langle \underline{p}\underline{p} \rangle S[\underline{\underline{I}}\underline{\underline{I}}]$$

$$+S[\langle \underline{p}\underline{p} \rangle \langle \underline{p}\underline{p} \rangle]$$

$$-\frac{10}{35}[\langle \underline{p}\underline{p} \rangle \langle \underline{p}\underline{p} \rangle \underline{\underline{I}}] . \qquad (5.6)$$

Eqs.(5.2), (5.5), and (5.6) define a *preclosure* for the orientation tetrad  $\langle p p p p \rangle$ :

$$\langle \underline{p} \, \underline{p} \, \underline{p} \, \underline{p} \rangle = \left[ 1 - C_2(II_b, III_b) \right] \Im_1(\langle \underline{p} \, \underline{p} \rangle) + C_2(II_b, III_b) \Im_2(\langle \underline{p} \, \underline{p} \rangle). \tag{5.7}$$

This representation satisfies all six-fold symmetry and six-fold contraction properties of the exact orientation tetrad. A closure for the second-order coefficient  $C_2(II_b,III_b)$  will be identified in CHAPTER 6 based on the idea that solutions to Eq.(4.1) must be realizable (i.e.,  $\langle pp \rangle : \underline{z}\,\underline{z} \geq 0$ ,  $\underline{z}$  arbitrary) for all initial conditions  $\langle pp \rangle (0)$  with invariants  $II_b(0)$  and  $III_b(0)$  on the invariant diagram defined by Figure 1.1. Realizable solutions (unsteady, steady, or periodic) must be produced for any combination of the physical property groups of  $\lambda$ , U, and Pe:  $-1 \leq \lambda \leq 1$ ;  $0 \leq U < \infty$ ;  $0 \leq Pe < \infty$ . The development of  $C_2(II_b, III_b)$  in CHAPTER 6 is the primary accomplishment of this research.

#### 5.2 Closure Models

### Hand's Closure

Hand (1962) studied the microstructure and rheology of rigid-rod suspensions near the isotropic state (see Figure 1.1) and assumed that Eq.(5.1) could be approximated as

$$\langle p p p p \rangle_{\text{Hand}} = \mathfrak{I}_1(\langle \underline{p} \underline{p} \rangle),$$
 (5.8)

Which is Eq.(5.7) with  $C_2 = 0$ . As demonstrated in CHAPTER 7 (Pe = 0), this yields unrealizable orientation dyads for finite values of U and, thereby does not provide a basis for understanding the self-alignment phenomenon of rigid-rod suspensions.

### Doi's Closure (Decoupling Approximation)

Doi (1981) studied the microstructure and rheology of rigid rod suspensions near the nematic state (see Figure 1.1) and assumed that Eq.(5.1) could be approximated as

$$\langle \underline{p} \ \underline{p} \ \underline{p} \ \underline{p} \rangle_{\text{Doi}} = \langle \underline{p} \ \underline{p} \rangle \langle \underline{p} \ \underline{p} \rangle.$$
 (5.9)

Unfortunately, this closure does not satisfy the six-fold symmetry and six-fold contraction properties of the orientation tetrad. Although Eq.(5.9) has been widely used by many researches for more than fifty years, it misrepresents the fundamental symmetry characteristics of the orientation tetrad and, thereby, the symmetry characteristics of the orientation density function for rigid suspensions of ellipsoidal particles. This unphysical property occurs for all realizable orientation states, including the nematic-like states near Point A of Figure 1.1. Eq.(5.9) is not a good approximation for  $\langle p p p p p \rangle$ , comments to the contrary in the current literature notwithstanding (Doi and Edwards, 1986; Chaubal, 1997; Larson, 1999).

### Tucker's Hybrid Closure

Tucker (see Tucker, 1988) used the following hybrid closure for  $\langle \underline{p} \ \underline{p} \ \underline{p} \ \underline{p} \rangle$  to study the flow-induced alignment of rigid rod suspensions:

$$\langle \underline{p} \ \underline{p} \ \underline{p} \ \underline{p} \ \rangle_{\text{Tuc ker}} = 27(\det \langle \underline{p} \ \underline{p} \rangle) \Im_{1}(\langle \underline{p} \ \underline{p} \rangle) + \left[1 - 27(\det \langle p \ p \rangle)\right] \langle p \ p \rangle \langle p \ p \rangle .$$
(5.10)

For isotropic states,  $\lambda_{p1} = \lambda_{p2} = \lambda_{p3} = 1/3$ ; therefore,  $27(\det < \underline{p} \, \underline{p} >) = 1$  and Eq.(5.10) asymptotically approaches Hand's closure for orientation states near the isotropic state (see Point E, Figure 1.1). For the nematic state,  $\lambda_{p1} = \lambda_{p2} = 0$  and  $\lambda_{p3} = 1$ ; therefore,  $27(\det ) = 0$  and Eq.(5.10) asymptotically approaches Doi's closure. For the

reason cited above, the hybrid closure also misrepresents the fundamental symmetry characteristics of the orientation density function and, thereby, does not provide an appropriate closure for the moment equation governing the behavior of .

### Hinch and Leal's Closure

Hinch and Leal (1976) developed the following closure for  $\langle \underline{p} \ \underline{p} \ \underline{p} \ \underline{p} \ \underline{p} \rangle : \langle \underline{p} \ \underline{p} \rangle$ , which appears in the moment equation for  $\langle \underline{p} \ \underline{p} \rangle$  (see Eq.(4.1)):

$$\langle \underline{p} \, \underline{p} \, \underline{p} \, \underline{p} \rangle_{HL} : \langle \underline{p} \, \underline{p} \rangle = c_1 \underline{\underline{I}} + c_2 \langle \underline{p} \, \underline{p} \rangle + c_3 \langle \underline{p} \, \underline{p} \rangle \cdot \langle \underline{p} \, \underline{p} \rangle + c_4 \langle p \, p \rangle \cdot \langle p \, p \rangle \cdot \langle p \, p \rangle$$
(5.11)

where

$$c_{1} = -\frac{2}{15} + \frac{8}{15} \operatorname{tr} \left[ \langle \underline{p} \, \underline{p} \rangle \cdot \langle \underline{p} \, \underline{p} \rangle \right] - \frac{6}{15} \operatorname{tr} \left[ \langle \underline{p} \, \underline{p} \rangle \cdot \langle \underline{p} \, \underline{p} \rangle \right]$$

$$c_{2} = \frac{2}{5} - \frac{1}{5} \operatorname{tr} \left[ \langle \underline{p} \, \underline{p} \rangle \cdot \langle \underline{p} \, \underline{p} \rangle \right]$$

$$c_{3} = -\frac{2}{5}$$

$$c_{4} = \frac{6}{5}$$

Note that the above result is symmetric and that  $tr[\langle \underline{p} \underline{p} \underline{p} \underline{p} \rangle : \langle \underline{p} \underline{p} \rangle] = \langle \underline{p} \underline{p} \rangle : \langle \underline{p} \underline{p} \rangle$ , as required by Eq.(4.1). The foregoing closure stems from the idea that for Pe = 0 and U  $\rightarrow$  0 ('weak' nematic strength), the microstructure asymptotically approached the isotropic state. And, for Pe = 0 and U  $\rightarrow \infty$  ('strong' nematic strength), the microstructure asymptotically approaches the nematic state. Unfortunately, as shown in CHAPTER 7, the Hinch and Leal closure yields unrealizable predictions for Pe = 0 and

finite values of U and, thereby, does not provide a physically acceptable closure for Eq.(4.1) (see APPENDIX D).

### Fully Symmetric Quadratic (FSQ-) and Orthotropic Closure

Petty and Bénard together with their students (see Imhoff, 2000; Imhoff et al., 2000; Kim et al., 2001, 2002, 2003, 2004, 2005; Kini 2003; Kini et al., 2003, 2004; Mandal et al., 2003, 2004; Nguyen, 2001; Nguyen et al., 2001a, 2001b; Parks et al., 1999; Parks and Petty, 1999a, 1990b; Petty et al., 1999) have used Eq.(5.7) as a closure for the orientation tetrad by assuming that  $C_2$  is a *universal constant*. However, realizability at the nematic state (Point A or Figure 1.1) and at the planar isotropic state (Point C or Figure 1.1) requires  $C_2 = 1/3$  and  $C_2 = 1/2$ , respectively (see CHAPTER 6). Clearly,  $C_2$  must depend or the local orientation state characterized by  $II_b$  and  $III_b$ . Therefore, as demonstrated in CHAPTER 7, Eq.(5.7) with  $C_2$  = constant may yield unrealizable predictions for  $P_0 = 0$  and  $P_0 < \infty$  and, thereby, does not provide a physically acceptable closure for Eq.(4.1).

Cintra and Tucker (1995) also developed a closure for  $\langle \underline{p} \underline{p} \underline{p} \underline{p} \rangle$  that satisfies all six-fold symmetry and six-fold contraction properties of the exact orientation tetrad. They related their closure coefficients to the local properties of the microstructure by "fitting" model predictions with results based on a direct numerical simulation of the S-equation for homogeneous shear flows and for homogeneous extensional flows. The general realizability of the resulting *orthotropic* closure has not been determined.

# 5.3 Discussion

Hand's closure satisfies six-fold symmetry and six-fold contraction properties, but it is not realizable for finite values of U. Doi's (decoupling) closure predicts realizable solutions to Eq.(4.1) (see APPENDIX D), but does not satisfy six-fold symmetry and six-fold contraction properties. Fully symmetric quadratic (FSQ) closure and the *orthotropic* closure satisfy six-fold symmetry, and six-fold contraction. In CHAPTER 6, the FSQ-closure coefficient  $C_2$  is related to the local microstructure so that  $\langle pp \rangle$  is also realizable for all rigid rod suspensions subject to simple homogeneous shear.

### **CHAPTER 6**

### REALIZABLE CLOSURE

### 6.1 Introduction

In this chapter, a realizable closure model for the orientation dyad  $\langle \underline{p}\underline{p} \rangle$  is identified for the relaxation of anisotropic microstructures in the absence of an external field (i.e., Pe = 0). A closure for the orientation tetrad  $\langle \underline{p}\underline{p}\underline{p}\underline{p} \rangle$ , defined by Eq.(5.7), will be completed by developing an equation for  $C_2(II_b, III_b)$  based on the condition that all initial orientation states on the boundary of the realizable region (see Figure 1.1) must remain either on the boundary or be attracted by states within the realizable region. Clearly, this condition requires

$$\underline{\mathbf{n}} \cdot \frac{d\underline{\mathbf{F}}}{dt} \bigg|_{\text{all boundaries of Figure 1.1}} \le 0. \tag{6.1}$$

In the above inequality, the vector  $\underline{\mathbf{n}}$  is an outward pointing unit vector perpendicular to the local tangent of the realizable boundary. The components of the vector  $\underline{\mathbf{F}}$  are the invariants of the structure tensor:

$$\underline{F} = \frac{dII_b}{dt} \underline{e}_{II} + \frac{dIII_b}{dt} \underline{e}_{III}$$
 (6.2a)

The vectors  $\underline{e}_{II}$  and  $\underline{e}_{III}$  are orthogonal unit vectors on the two-dimensional invariant plane (i.e.,  $\underline{e}_{II} \cdot \underline{e}_{III} = 0$ ). For Pe = 0,  $F_{TD} = 1$ , and  $\langle \underline{p} \underline{p} \underline{p} \underline{p} \rangle$  defined by Eq.(5.7), it follows directly from Eq.(4.1) that (see Appendix D):

$$\frac{d II_b}{d t} = -2II_b + 2U \left[ \frac{7}{35}II_b + \frac{3}{7}III_b - \frac{54}{35}II_b^2C_2 \right]$$
 (6.2b)

$$\frac{d III_b}{d t} = -3III_b + 3U \left[ \frac{7}{35}III_b + \frac{1}{14}II_b^2 - \frac{54}{35}II_bIII_bC_2 \right] . \tag{6.2c}$$

Eqs.(6.2b) and (6.2c) govern the relaxation of all orientation states. The objective of this chapter is to relate the second-order closure coefficient  $C_2$  to the local invariants  $II_b$  and  $III_b$  by using Ineq.(6.1).

## 6.2 Realizable Isotropic, Planar Isotropic, and Nematic States

The excluded volume term in Eq.(4.1) is zero at the isotropic, the planar isotropic, and the nematic states. This can be seen by evaluating  $\langle \underline{p}\underline{p}\underline{p}\underline{p} \rangle :\langle \underline{p}\underline{p} \rangle$  at these three states.

An eigenvector representation for the orientation dyad < pp > is

$$<\underline{p}\,\underline{p}>(t)=\sum_{i=1}^{3}\lambda_{pi}(t)\,\underline{x}_{i}(t)\,\underline{x}_{i}(t)=\sum_{i=1}^{3}\sum_{j=1}^{3}< p_{i}p_{j}>(t)\,\underline{e}_{i}\,\underline{e}_{j}$$
 (6.3)

Eq.(6.3) is a representation of  $\langle \underline{p}\underline{p} \rangle$  using the fixed mutually orthogonal base vectors  $\underline{e}_1, \underline{e}_2$ , and  $\underline{e}_3$ . The *instantaneous* orientation vector  $\underline{p}$  can be expressed as

$$\underline{p} = \sum_{i=1}^{3} p_i(t) \underline{e}_i = \sum_{k=1}^{3} \widetilde{p}_k(t) \underline{x}_k(t), \qquad (6.4)$$

which implies that

$$\underline{p}\,\underline{p} = \sum_{i=1}^{3} \sum_{j=1}^{3} p_i(t) p_j(t) \underline{e}_i \underline{e}_j = \sum_{k=1}^{3} \sum_{\ell=1}^{3} \widetilde{p}_k(t) \widetilde{p}_\ell(t) \underline{x}_k(t) \underline{x}_\ell(t). \tag{6.5}$$

Therefore, the average of Eq.(6.5) shows that

$$\langle \widetilde{p}_{k}(t)\widetilde{p}_{\ell}(t) \rangle = \begin{cases} 0, & \text{if } k \neq \ell \\ \lambda_{k}, & \text{if } k = \ell \end{cases}$$
 (6.6)

Note that  $\langle \underline{p} \rangle = \underline{0}$  implies that  $\langle \underline{p}_1 \rangle = 0$  and  $\langle \widetilde{p}_k \rangle = 0$ . Also,

$$\operatorname{tr} \langle \underline{p}\,\underline{p} \rangle = \sum_{i} \langle p_{i}p_{i} \rangle = \sum_{k} \langle \widetilde{p}_{k}\,\widetilde{p}_{\ell} \rangle = \sum_{k} \lambda_{k} = 1 \tag{6.7}$$

Eqs.(6.3) and (6.5) can be used to represent the components of  $\langle \underline{p}\underline{p}\underline{p}\underline{p} \rangle : \langle \underline{p}\underline{p} \rangle$  in terms of the eigenvectors of  $\langle pp \rangle$  with the result that

$$\langle \underline{p}\underline{p}\underline{p}\underline{p} \rangle : \langle \underline{p}\underline{p} \rangle \equiv \langle \underline{p}\underline{p}\underline{p}\underline{p} : \langle \underline{p}\underline{p} \rangle \rangle =$$

$$\langle (\sum \sum \widetilde{p}_{i} \widetilde{p}_{j} \underline{x}_{i}\underline{x}_{j}) (\sum \sum \widetilde{p}_{k} \widetilde{p}_{\ell} \underline{x}_{k}\underline{x}_{\ell}) : (\sum_{m} \lambda_{pm} \underline{x}_{m}\underline{x}_{m}) \rangle$$
(6.8)

Eq.(6.8) holds for all orientation states (see Figure 1.1).

Isotropic States

For an isotropic state, 
$$\langle \underline{p}\,\underline{p} \rangle = \frac{1}{3} (\underline{x}_1^{\,0}\,\underline{x}_1^{\,0} + \underline{x}_2^{\,0}\,\underline{x}_2^{\,0} + \underline{x}_3^{\,0}\,\underline{x}_3^{\,0})$$
 and

$$\lambda_1^0 + \lambda_2^0 + \lambda_3^0 = \frac{1}{3}$$
. Thus, Eq.(6.8) reduces to

$$\begin{aligned}
&\left[\langle \underline{p}\,\underline{p}\,\underline{p}\,\underline{p}\,\underline{p}\rangle : \langle \underline{p}\,\underline{p}\rangle\right]_{\text{isotropic}} \\
&= \frac{1}{3}\sum_{m}\sum_{i}\sum_{j}\langle \widetilde{p}_{i}\,\widetilde{p}_{j}\widetilde{p}_{m}\,\widetilde{p}_{m} \rangle \underline{x}_{i}^{o}\,\underline{x}_{j}^{o} \\
&= \frac{1}{3}\sum_{i}\sum_{j}\langle \widetilde{p}_{i}\,\widetilde{p}_{j}(\sum_{m}\widetilde{p}_{m}\,\widetilde{p}_{m}) > \underline{x}_{i}^{o}\,\underline{x}_{j}^{o} \\
&= \frac{1}{3}\sum_{i}\sum_{j}\langle \widetilde{p}_{i}\,\widetilde{p}_{j} > \underline{x}_{i}^{o}\,\underline{x}_{j}^{o} \\
&= \frac{1}{3}\langle \underline{p}\,\underline{p} \rangle \bigg|_{\text{isotropic}} = \frac{1}{9}\underline{I}.
\end{aligned} \tag{6.9}$$

Eq.(6.9) implies that the excluded volume effect in Eq.(4.1) is zero at the isotropic state. This conclusion holds for the FSQ-closure for any value of  $C_2(0, 0)$ . Thus, the isotropic state is a fixed point (i.e., steady state) of Eq.(4.1) for Pe = 0 and  $U \ge 0$ .

#### Nematic States

For a nematic state,  $\langle \underline{p}\,\underline{p} \rangle = \underline{x}_3^o\,\underline{x}_3^o$  and  $\lambda_1^o = \lambda_2^o = 0$ ,  $\lambda_3^o = 1$  (see Figure 1.1). Thus, Eq.(6.9) reduces to

$$\begin{aligned}
&\left[\langle \underline{p}\,\underline{p}\,\underline{p}\,\underline{p}\,\rangle : \langle \underline{p}\,\underline{p}\,\rangle\right]_{\text{nematic}} \\
&=\langle \underline{p}\,\underline{p}\,\underline{p}\,\underline{p}\,\rangle : \underline{x}_{3}^{\,0}\,\underline{x}_{3}^{\,0} \\
&=\langle \underline{p}\,\underline{p}\,\widetilde{p}_{3}\,\widetilde{p}_{3}\,\rangle \\
&=\sum_{i}\sum_{i}\langle \widetilde{p}_{i}\,\widetilde{p}_{j}\,\widetilde{p}_{3}\,\widetilde{p}_{3}\,\rangle \underline{x}_{i}^{\,0}\,\underline{x}_{j}^{\,0} .
\end{aligned} (6.10)$$

At the nematic state,

$$\langle \widetilde{p}_{i}\widetilde{p}_{j}\widetilde{p}_{3}\widetilde{p}_{3} \rangle = \begin{cases} 1, & \text{if } i = j = 3 \\ 0, & \text{otherwise} \end{cases}$$
 (6.11)

Therefore,

$$\left[ \langle \underline{p}\,\underline{p}\,\underline{p}\,\underline{p}\,\rangle : \langle \underline{p}\,\underline{p}\,\rangle \right]_{\text{nematic}} = \underline{x}_{3}^{0}\,\underline{x}_{3}^{0}, \tag{6.12}$$

which shows that the excluded volume effect in Eq.(4.1) is zero at the nematic state:

$$\left[ \langle \underline{p}\,\underline{p} \rangle \cdot \langle \underline{p}\,\underline{p} \rangle - \langle \underline{p}\,\underline{p}\,\underline{p}\,\underline{p} \rangle : \langle \underline{p}\,\underline{p} \rangle \right]_{\text{nematic}} = (\underline{x}_3^{\,0}\,\underline{x}_3^{\,0}) \cdot (\underline{x}_3^{\,0}\,\underline{x}_3^{\,0}) - (\underline{x}_3^{\,0}\,\underline{x}_3^{\,0}) = \underline{0}. \tag{6.13}$$

This conclusion holds for the FSQ-closure provided  $C_2(2/9, 2/3) = 1/3$ . Unlike the isotropic state, the nematic state is not a fixed point (i.e., steady state) of Eq.(4.1) inasmuch as the Brownian motion term is non-zero:

$$\left[ < \underline{p}\,\underline{p} > -\frac{1}{3}\,\underline{I} \right]_{\text{nematic}} = \frac{2}{3}\,\underline{x}_{3}^{\,0}\,\underline{x}_{3}^{\,0} - \frac{1}{3}(\underline{x}_{1}^{\,0}\,\underline{x}_{1}^{\,0} + \underline{x}_{2}^{\,0}\,\underline{x}_{2}^{\,0}) \tag{6.14}$$

Planar Isotropic States

For a planar isotropic state,  $\langle \underline{p}\,\underline{p} \rangle = \frac{1}{2} (\underline{x}_{2}^{o}\,\underline{x}_{2}^{o} + \underline{x}_{3}^{o}\,\underline{x}_{3}^{o})$  and  $\lambda_{1}^{o} = 0, \lambda_{2}^{o} = \lambda_{3}^{o} = \frac{1}{2}$ 

(see Figure 1.1). Thus, Eq.(6.9) reduces to

$$\begin{aligned}
&\left[\langle \underline{p}\,\underline{p}\,\underline{p}\,\underline{p}\,\rangle > \langle \underline{p}\,\underline{p}\,\rangle\right]_{\text{planar isotropic}} \\
&= \frac{1}{2} \sum_{m} \sum_{i} \sum_{j} \langle \widetilde{p}_{i}\,\widetilde{p}_{j}\widetilde{p}_{m}\,\widetilde{p}_{m} \rangle \underline{x}_{i}^{o}\,\underline{x}_{j}^{o} \\
&= \frac{1}{2} \sum_{i} \sum_{j} \langle \widetilde{p}_{i}\,\widetilde{p}_{j}(\sum_{m}\widetilde{p}_{m}\,\widetilde{p}_{m}) > \underline{x}_{i}^{o}\,\underline{x}_{j}^{o} \\
&= \frac{1}{2} \sum_{i} \sum_{j} \langle \widetilde{p}_{i}\,\widetilde{p}_{j} > \underline{x}_{i}^{o}\,\underline{x}_{j}^{o} \\
&= \frac{1}{2} \langle \underline{p}\,\underline{p} \rangle \Big|_{\text{planar isotropic}} = \frac{1}{4} (\underline{x}_{2}^{o}\,\underline{x}_{2}^{o} + \underline{x}_{3}^{o}\,\underline{x}_{3}^{o}) .
\end{aligned} \tag{6.15}$$

Eq.(6.15) implies that the excluded volume effect in Eq.(4.1) is zero at the planar isotropic state:

$$\left[ \langle \underline{p}\,\underline{p} \rangle \cdot \langle \underline{p}\,\underline{p} \rangle - \langle \underline{p}\,\underline{p}\,\underline{p}\,\underline{p} \rangle : \langle \underline{p}\,\underline{p} \rangle \right] \Big|_{\text{planar isotropic}} \\
= \frac{1}{4} (\underline{x}_{2}^{\circ}\underline{x}_{2}^{\circ} + \underline{x}_{3}^{\circ}\underline{x}_{3}^{\circ}) \cdot (\underline{x}_{2}^{\circ}\underline{x}_{2}^{\circ} + \underline{x}_{3}^{\circ}\underline{x}_{3}^{\circ}) - \frac{1}{4} (\underline{x}_{2}^{\circ}\underline{x}_{2}^{\circ} + \underline{x}_{3}^{\circ}\underline{x}_{3}^{\circ}) = \underline{0} \tag{6.16}$$

This conclusion holds for the FSQ-closure provided  $C_2(1/6, -1/36) = 1/2$ . This result shows that the planar isotropic state is not a fixed point of Eq.(4.1) because the Brownian motion term is not zero

$$\left[ \langle \underline{p}\,\underline{p} \rangle - \frac{1}{3}\,\underline{I} \right]_{\text{planar isotropic}} = -\frac{1}{3}\,\underline{x}_1^{\,0}\,\underline{x}_1^{\,0} + \frac{1}{6}(\underline{x}_2^{\,0}\,\underline{x}_2^{\,0} + \underline{x}_3^{\,0}\,\underline{x}_3^{\,0}). \tag{6.17}$$

### 6.3 Realizable Prolate and Oblate States

The prolate boundary is defined by (see Figure 1.1):

$$II_b = 6 \left(\frac{III_b}{6}\right)^{2/3}, \quad 0 \le III_b \le 2/9.$$
 (6.18)

The outward pointing normal vector on the prolate boundary is given by

$$\underline{\mathbf{n}}_{\mathbf{p}} = +\mathbf{n}_{\mathbf{H}}^{\mathbf{p}} \underline{\mathbf{e}}_{\mathbf{H}} + +\mathbf{n}_{\mathbf{H}}^{\mathbf{p}} \underline{\mathbf{e}}_{\mathbf{H}} \tag{6.19a}$$

where

$$n_{II}^{p} \equiv -\frac{1}{\sqrt{1 + \frac{4}{9} \left(\frac{6}{III_{b}}\right)^{2/3}}}$$
 (6.19b)

$$n_{\text{III}}^{p} = + \frac{\frac{2}{3} \left(\frac{6}{\text{III}_{b}}\right)^{1/3}}{\sqrt{1 + \frac{4}{9} \left(\frac{6}{\text{III}_{b}}\right)^{2/3}}}$$
(6.19c)

Note that  $\underline{n}_p \cdot \underline{n}_p = (n_{II}^p)^2 + (n_{III}^p)^2 = 1$ . On the prolate boundary, the components of  $\underline{dF}/\underline{dt}$  are defined by Eqs.(6.2b) and (6.2c) with  $II_b$  and  $III_b$  related by Eq.(6.18). It is noteworthy that Ineq.(6.1) on the prolate boundary (F-line on Figure 1.1) reduces to

$$\left[\underline{\underline{n}} \cdot \frac{d\underline{F}}{dt}\right] \bigg|_{\text{prolate boundary}} = 0, \qquad (6.20)$$

which implies that initial orientation states on the prolate boundary remain on the prolate boundary for all time without any additional conditions on  $C_2(II_b, III_b)$ .

A similar result holds for the oblate boundary (see Figure 1.1):

$$\left[\underline{n} \cdot \frac{d\underline{F}}{dt}\right]_{\text{oblate boundary}} = 0. \tag{6.21}$$

The analog of Eq. (6.18) for the oblate boundary (see Figure 1.1) is

$$II_b = 6\left(\frac{-III_b}{6}\right)^{2/3}, -\frac{1}{36} \le III_b \le 0$$
 (6.22)

The outward pointing normal vector on the oblate boundary is

$$\underline{\mathbf{n}}_{0} = +\mathbf{n}_{II}^{0} \underline{\mathbf{e}}_{II} + +\mathbf{n}_{III}^{0} \underline{\mathbf{e}}_{III} \tag{6.23a}$$

where

$$n_{II}^{o} = -\frac{1}{\sqrt{1 + \frac{4}{9} \left(-\frac{6}{III_{b}}\right)^{2/3}}}$$
 (6.23b)

$$n_{\text{III}}^{0} = -\frac{\frac{2}{3} \left(-\frac{6}{\text{III}_{b}}\right)^{1/3}}{\sqrt{1 + \frac{4}{9} \left(-\frac{6}{\text{III}_{b}}\right)^{2/3}}}$$
(6.23c)

Note that  $\underline{n}_o \cdot \underline{n}_o = (n_{II}^o)^2 + (n_{III}^o)^2 = 1$ . Eq.(6.21) implies that initial orientation states on the oblate boundary remain on the oblate boundary for all time without any additional conditions on  $C_2(II_b, III_b)$ .

# 6.4 Realizable Planar Anisotropic Boundary

The planar anisotropic boundary is defined by (see Figure 1.1):

$$II_b = 2III_b + \frac{2}{9}, \quad -\frac{1}{36} \le III_b \le \frac{2}{9}.$$
 (6.24)

The outward pointing normal vector on the planar anisotropic boundary is given by

$$\underline{\mathbf{n}}_{pa} = +\mathbf{n}_{II}^{pa} \underline{\mathbf{e}}_{II} + +\mathbf{n}_{III}^{pa} \underline{\mathbf{e}}_{III}$$
 (6.25a)

where

$$n_{II}^{pa} = \frac{1}{\sqrt{5}}$$
 (6.25b)

$$n_{\text{III}}^{\text{pa}} = -\frac{2}{\sqrt{5}}$$
 (6.25c)

Note that  $\underline{n}_{pa} \cdot \underline{n}_{pa} = (n_{II}^{pa})^2 + (n_{III}^{pa})^2 = 1$ . On the planar anisotropic boundary, the components of  $d\underline{F}/dt$  are defined by Eqs.(6.2.b) and (6.2c) with II<sub>b</sub> and III<sub>b</sub> related by Eq.(6.24) above. Ineq.(6.1) on the planar anisotropic boundary has two contributions (see APPENDIX F):

$$\left[\underline{n} \cdot \frac{d\underline{f}}{dt}\right]_{\text{planar anisotropic}} = n_{\text{II}}^{\text{pa}} \left(\frac{d \Pi_{b}}{dt}\right)_{\text{pa}} + n_{\text{III}}^{\text{pa}} \left(\frac{d \Pi_{b}}{dt}\right)_{\text{pa}}$$

$$= \frac{2(-2 + 9\Pi_{b})\left\{105 + 2U\left[-8 - 45\Pi_{b} + 18C_{2}(1 + \Pi_{b})\right]\right\}}{945\sqrt{5}} \le 0, \quad 0 \le U < \infty. \quad (6.26)$$

Note that  $(-2 + 9 \text{ III}_b) \le 0$  for  $-1/36 \le \text{III}_b \le 8/36$ . Clearly, a necessary condition for Ineq.(6.26) to be satisfied for all  $U \ge 0$  is

$$C_2 \ge \frac{8 + 45III_b}{18(1 + 9III_b)}. (6.27)$$

Ineq.(6.27) is a significant finding and represents one of the primary results of this research. The conclusion here is that Eq.(4.1) and the FSQ-closure (see Eq.(5.7)) produces realizable microstructures for  $0 \le U < \infty$  and Pe = 0. This theory will be tested in CHAPTERS 7, 8, and 9 for a wide range of conditions.

#### 6.5 Discussion

In this research,

$$C_2 = \frac{8 + 45III_b}{18(1 + 9III_b)} \tag{6.28}$$

for  $-1 \le \lambda \le +1$ ,  $0 \le U < \infty$ , and  $0 \le Pe < \infty$  for all realizable state defined by Figure 1.1. The analysis in this chapter shows that Eq.(6.28) is consistent with the idea that planar anisotropic states are attracted to 3D anisotropic states (see Figure 1.1). The results of CHAPTER 8 (Pe > 0) show that this important feature of the FSQ-closure is satisfied by a wide class of planar anisotropic states. Figure 6.1 illustrates the behavior of  $C_2(III_b)$  for  $-1/36 \le III_b \le 8/36$ . A major hypothesis for the theoretical results developed in CHAPTER 7, 8, and 9 is that the FSQ-closure coefficient defined by Eq.(6.28) above applies for all anisotropic states.

Although the Doi-closure (see Eq.(5.9)) does not satisfy all the six-fold symmetry and six-fold contraction properties of  $\langle pppp \rangle$ , Eq.(4.1) nevertheless yields a realizable orientation dyad for Pe = 0 and  $\langle pppp \rangle = \langle pp \rangle \langle pp \rangle$ . Figure 6.2 shows that how the excluded volume (EV) terms that appear in Eqs.(6.2b) and (6.2c) vary over the planar anisotropic boundary of Figure 6.1. Note that the EV-terms are zero for the Doi-closure and the FSQ-closure at the planar isotropic state and the nematic state. The Doi EV-term in Eq.(6.2b) is significantly larger than the FSQ EV-term in Eq.(6.2b). This indicates that the Doi-closure has a higher tendency for self-alignment. This conjecture is confirmed by the equilibrium calculations presented in CHAPTER 7 inasmuch as the Doi theory predicts biphasic phenomenon at smaller values of U.

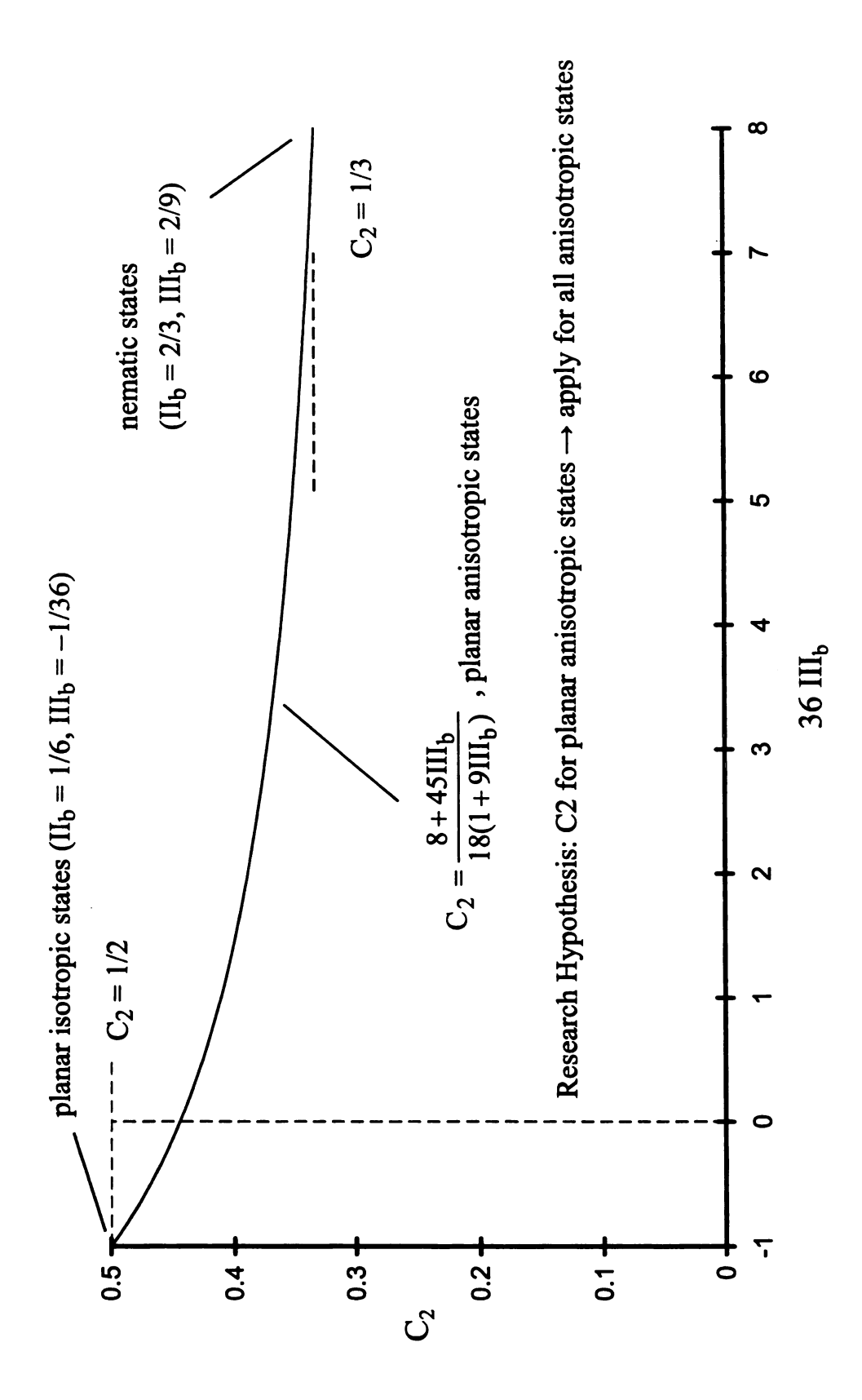


Figure 6.1 Clousre Coefficient C<sub>2</sub> (III<sub>b</sub>) for the FSQ-model

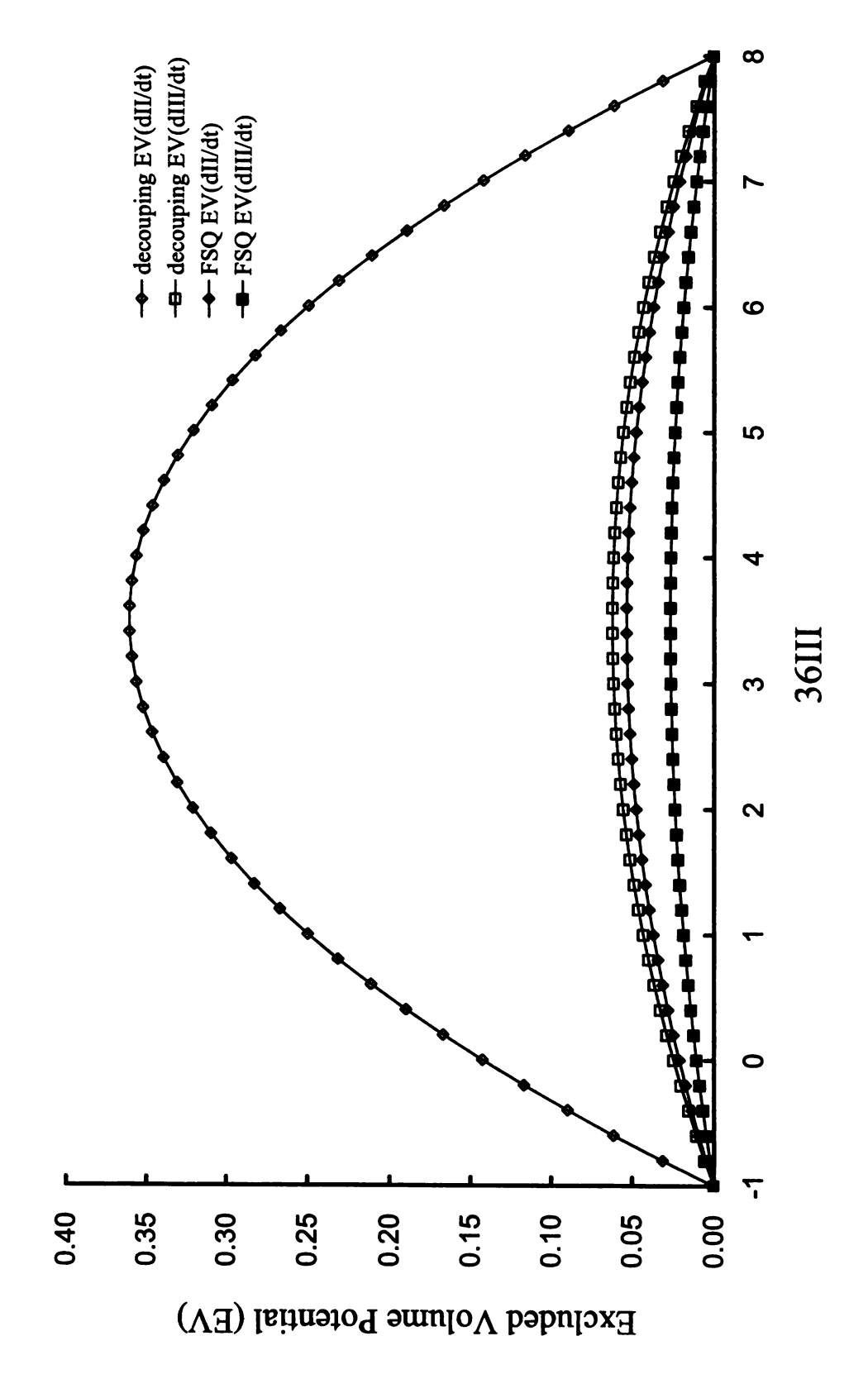


Figure 6.2 The Excluded Volume Potential for the Decoupling Approximation and the FSQ-model

### CHAPTER 7

#### MICROSTURCTURE IN THE ABSENCE OF AN EXTERNAL FIELD

## 7.1 Introduction

In the absence of an external field, the relaxation of  $\langle \underline{p} \, \underline{p} \rangle$  is governed Eq.(4.1) with Pe = 0:

$$\frac{d < \underline{p} \, \underline{p} >}{d \, t} = F_{TD} \left( -(< \underline{p} \, \underline{p} > -\frac{1}{3} \underline{\underline{I}}) + U(< \underline{p} \, \underline{p} > \cdot < \underline{p} \, \underline{p} > - < \underline{p} \, \underline{p} > : < \underline{p} \, \underline{p} \, \underline{p} \, \underline{p} >) \right). \tag{7.1}$$

The  $F_{TD}$ -factor in the above equation accounts for the tube dilation phenomenon (see Eq. (2.6)). The first term on the right-hand-side of Eq.(7.1) represents rotary Brownian diffusion. The second term accounts for the excluded volume phenomenon. The dimensionless group U measures the relative importance of self-alignment and rotary Brownian motion.

Experimental studies for rigid rod suspensions, such as lyotropic liquid crystalline polymers, show that a transition from an isotropic state to an anisotropic state occurs at some critical concentration (Abe and Yamazaki 1989a, 1989b; Farhoudi and Rey, 1993; Kubo and Ogino, 1979; Murthy et al.,1976; Orwoll and Vold, 1971; Robinson, 1966; Sartirana et al., 1987; Srinivasarao and Barry, 1991). The equilibrium orientation state is isotropic for dilute solutions ( $U \ll U_c$ ) and anisotropic for concentrated solutions ( $U \gg U_c$ ).  $U_c$  is a critical value of the nematic coefficient that depends on the concentration of the dispersed phase. The objective of this chapter is to determine the effect of U on the steady state solutions of Eq. (7.1) for the FSQ-closure developed in CHAPTER 5 and CHAPTER 6.

## 7.2 Biphasic Phenomena

The asymptotic solutions of Eq.(7.1) are steady equilibrium states for all U. Clearly, the  $F_{TD}$ -factor does not affect the steady state solutions. In APPENDIX B and APPENDIX D, the following equations for the second and third invariants of the structure tensor  $\underline{b}$  are derived from Eq.(7.1):

$$\frac{d \Pi_b}{d t} = -2F_{TD}II_b + 2F_{TD}U \left[ \frac{7}{35}II_b + \frac{3}{7}III_b - \frac{54}{35}II_b^2C_2 \right]$$
 (7.2a)

$$\frac{d III_b}{d t} = -3F_{TD}III_b + 3F_{TD}U \left[ \frac{7}{35}III_b + \frac{1}{14}II_b^2 - \frac{54}{35}II_bIII_bC_2 \right]. \tag{7.2b}$$

The steady state solutions to Eq. (7.1) have two equal eigenvalues (see APPENDIX D). This means that the equilibrium states in the absence of an external field are either prolate states or oblate states (see Figure 1.1). Thus, application of Eq.(3.6) implies that the steady state solutions to Eqs.(7.2a) and (7.2b) can be represented in terms of the order parameter  $\alpha$  defined by  $II_b = \frac{2}{3}(\alpha)^2$ . Since the equilibrium solutions of Eq.(7.2a) and Eq.(7.2b) are either prolate or oblate states, Eq.(3.6) can be represented in terms of  $\alpha$  and  $III_b$ :  $III_b = \frac{2}{9}(\pm \alpha)^3$ . The positive sign is for prolate states and the negative sign is for oblate states (see Figure 1.1). It follows directly from Eq. (7.2a) that the order parameter is determined by the following algebraic equation:

$$0 = \alpha \left[ 1 - U \left( \frac{7}{35} + \frac{1}{7} \alpha - \frac{36}{35} \alpha^2 C_2 \right) \right]. \tag{7.3}$$

Eq. (7.3) has three solutions:

$$\alpha = 0$$

$$\alpha = \frac{1/7 \pm \sqrt{(1/7)^2 - (144/35) C_2 \left(\frac{1}{U} - \frac{1}{5}\right)}}{(72/35) C_2}.$$
(7.4)

The solution  $\alpha=0$  corresponds to the isotropic state. This steady state may be stable or unstable, depending on the value of U. If the steady state is on the prolate boundary of Figure 1.1, then the positive sign of Eq.(7.4) applies. For oblate steady states, the negative sign applies. Previous application of the FSQ-closure assumed that  $C_2$  was constant and independent of the microstructure (Imhoff, 2000; Imhoff et al., 2000; Kim et al., 2001, 2002, 2003, 2004, 2005; Kini 2003; Kini et al., 2003, 2004; Mandal et al., 2003, 2004; Nguyen, 2001; Nguyen et al., 2001a, 2001b; Parks et al., 1999; Parks and Petty, 1999a, 1990b; Petty et al., 1999).

Figure 7.1 shows how U influences the steady state order parameter  $\alpha$  for  $C_2$  = constant. For  $U < U_1$ , all steady states are isotropic ( $\alpha$  = 0). For  $U_1 < U < U_2$ , three steady states exist: two stable and one unstable. The unstable state is on the prolate boundary. The region  $U_1 < U < U_2$  is called the biphasic region. Regardless of the  $C_2$  value,  $U_2$  = 5 for the FSQ-closure, but the value of  $U_1$  depends on  $C_2$  (see Figure 7.1). For  $C_2 < 1/2$ , the oblate solutions become unrealizable for large finite value of U. For  $C_2 < 1/3$ , the prolate solutions become unrealizable for finite values of U. The orientation state is always realizable if  $C_2 > 1/2$ , but it can not cover all possible orientation states inasmuch as the order parameter  $\alpha \le 0.78$  for  $C_2 \le 1/2$ . Nevertheless, this result provides the possibility that the FSQ-closure coefficient  $C_2$  can be fitted to the

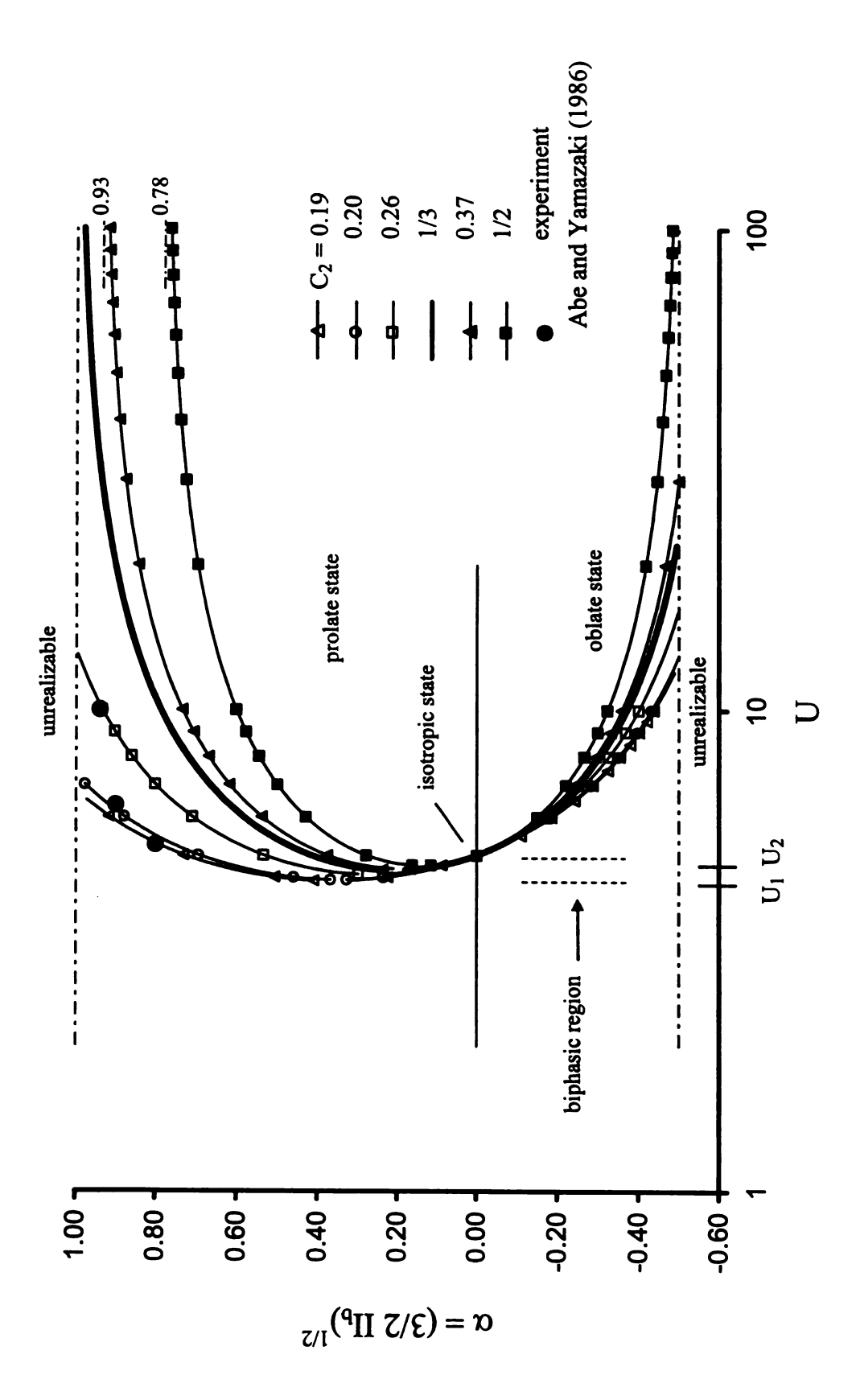


Figure 7.1 Multiple Equilibrium States Predicted by the FSQ-model for  $C_2$  = constant.

experimental results with  $C_2 = C_2$  ( $II_b$ ,  $III_b$ ) (see Abe and Yamazaki, 1986 for the experimental data and CHAPTER 6 for the FSQ-closure coefficient).

Analogous to Eq. (7.4), the order parameters for the decoupling-closure and the HL1-closure are (Chaubal et al., 1995):

$$\alpha = 0, \ \frac{1}{4} \pm \frac{3}{4} \sqrt{1 - \frac{8}{3U}}$$
 for decoupling-closure (7.5a)

$$\alpha = 0, \ \frac{1}{8} \pm \frac{1}{8} \sqrt{49 - \frac{240}{U}}$$
 for HL1-closure. (7.5b)

Figure 7.2 shows the comparison between decoupling-closure, HL1-closure, and the FSQ-closure developed in CHAPTER 6. The phase transition from the isotropic state to the anisotropic state appears in both closure approximations. The figure also shows the biphasic region for the decoupling-closure, HL1-closure, and FSQ-closure. The biphasic region has two stable states and one unstable state that can coexist for the same U. The isotropic state is a steady state solution to Eq. (7.1) for all three closures. The equilibrium orientation state is the anisotropic state if the initial condition on  $\alpha$  is above the unstable state. When the initial condition on  $\alpha$  is below the unstable state, the orientation state relaxes to the isotropic state. The locations of the unstable states were determined by solving Eq.(7.1) as an initial value problem.

Although the qualitative trends of each closure are similar, the quantitative differences are significant. The decoupling approximation predicts the existence of prolate states for which  $\alpha(U) \to \frac{1}{2}$  as  $U \to \infty$  (see Figure 7.2). However, the biphasic transition point is lower than the other models ( $U_2 = 3$ ). The HL1-closure, however, has

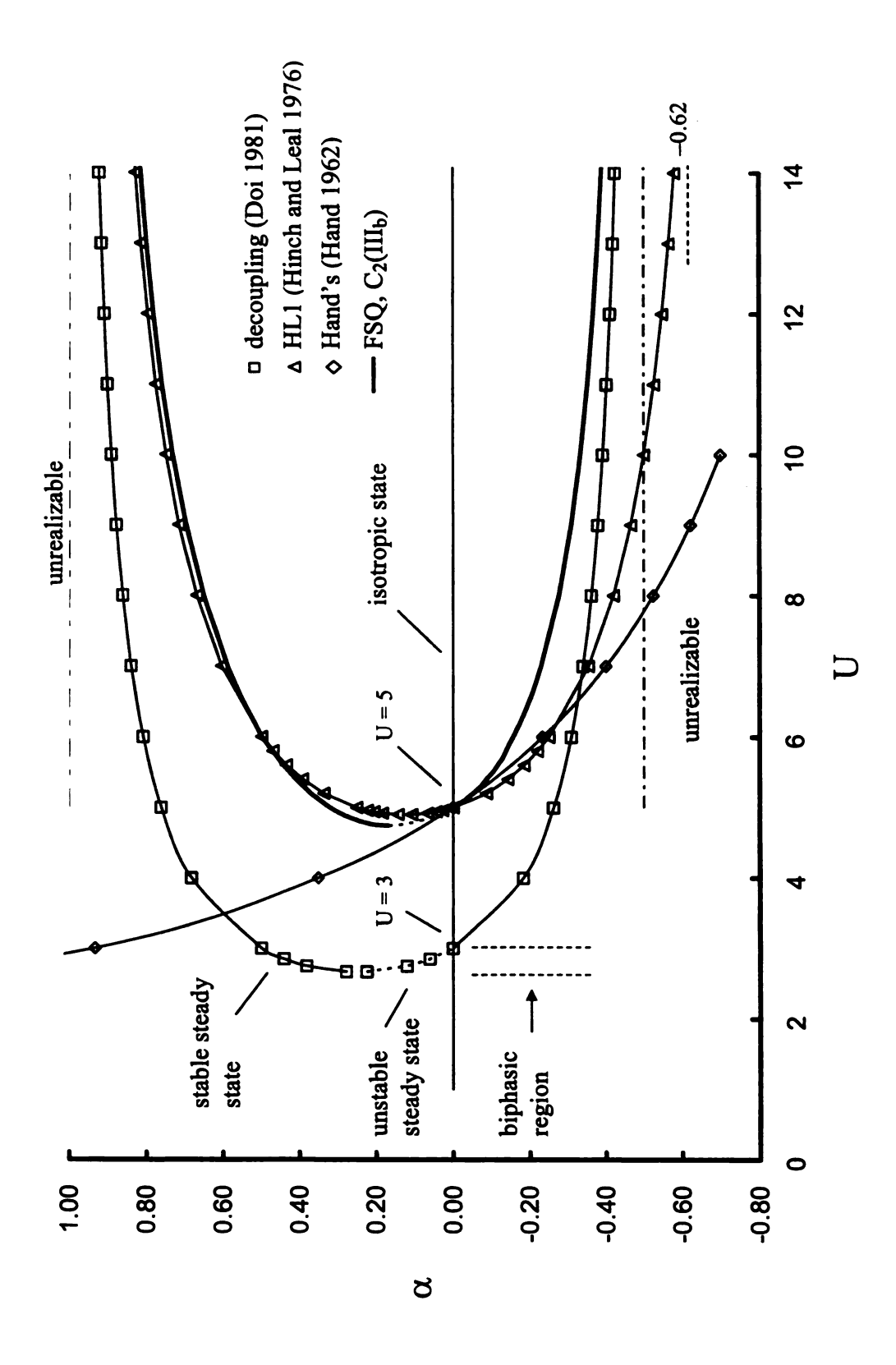


Figure 7.2 Multiple Equilibrium States Predicted by the FSQ-model for  $C_2 = C_2$  (III<sub>b</sub>).

the same  $U_2$  as the FSQ-closure, but the HL1-closure predicts unrealizable oblate states for  $U < \infty$ . The FSQ-closure with  $C_2$  (III<sub>b</sub>) defined by (6.12) satisfies both prolate and oblate realizability conditions. Therefore, the decoupling approximation and the FSQ-closure are realizable for all equilibrium steady states. Tables 7.1 and 7.2 show how U influences the order parameter and the invariants for the equilibrium states.

## 7.3 Relaxation to Isotropic and Anisotropic Steady States

When U and Pe are zero and  $F_{TD} = 1$ , Eq.(4.1) reduces to

$$\frac{d < \underline{p} \, \underline{p} >}{d \, t} = \frac{1}{3} \, \underline{I} - \langle \underline{p} \, \underline{p} > \tag{7.6a}$$

Nguyen (2001) discussed various aspects of this equation. An analytical solution to Eq.(7.6a) is

$$\langle \underline{p}\,\underline{p} \rangle (t) = \frac{1}{3}\underline{\underline{I}} + \left(\langle \underline{p}\,\underline{p} \rangle (0) - \frac{1}{3}\underline{\underline{I}}\right) \exp(-t).$$
 (7.6)

Eq. (7.6a) becomes an isotropic state  $(\langle \underline{p}\underline{p} \rangle = \underline{I}/3)$  as  $t \to \infty$ . The structure tensor corresponding to  $\langle p p \rangle$  (t), defined by Eq.(7.6b), is

$$\underline{\underline{b}}(t) = \underline{\underline{b}}(0) \exp(-t) \tag{7.7}$$

The two invariants,  $II_b$  and  $III_b$  of  $\underline{b}$  are

$$II_b = tr(\underline{\underline{b}} \cdot \underline{\underline{b}}) = II_b (0) \exp(-2t)$$
, and (7.8a)

$$III_{b} = tr(\underline{\underline{b}} \cdot \underline{\underline{b}} \cdot \underline{\underline{b}}) = III_{b} (0) \exp(-3t). \tag{7.8b}$$

Eqs.(7.8a) and (7.8b) imply that

Table 7.1: Invariants and Order Parameter of the Equilibrium Structure Tensor on the Prolate Line

U	$\Pi_{b}$	Шь	α		
$U_1 = 4.73$	0.0221	0.0013	0.1670		
$U_2 = 5$	0.0682	0.0073	0.3205		
6	0.1640	0.0271	0.5513		
7	0.2311	0.0454	0.6110		
8	0.2828	0.0614	0.6604		
9	0.3239	0.0752	0.7008		
10	0.3572	0.0872	0.7335		
27	0.5511	0.1670	0.9092		
$\alpha_{\rm p} = \left(3/2  \mathrm{II_b}\right)^{1/2}$					

Table 7.2: Invariants and Order Parameter of the Equilibrium Structure Tensor on the Oblate Line

U	$II_b$	$\mathrm{III}_{b}$	α		
$U_2 = 5$	0.0000	0.0000	0.0000		
6	-0.2744	0.0162	-0.0008		
7	-0.3200	0.0352	-0.0027		
8	-0.3510	0.0509	-0.0047		
9	-0.3728	0.0637	-0.0066		
10	-0.3890	0.0741	-0.0082		
$\alpha_{\rm o} = -\left(3/2\Pi_{\rm b}\right)^{1/2}$					

$$III_{b}(t) = III_{b}(0) \left(\frac{II_{b}(t)}{II_{b}(0)}\right)^{3/2}$$
(7.9)

Figure 7.3 shows that all planar anisotropic states relax to isotropic states on a time scale of order  $4t_c$  if U = 0 and Pe = 0. If U > 0, the relaxation trajectories in the invariant plane depend on the closure approximation and the excluded volume potential model. When the initial state is planar isotropic (see Figure 1.1), solutions to Eqs. (7.2a) and (7.2b) remain on the oblate line. All other initial conditions relax to the prolate boundary.

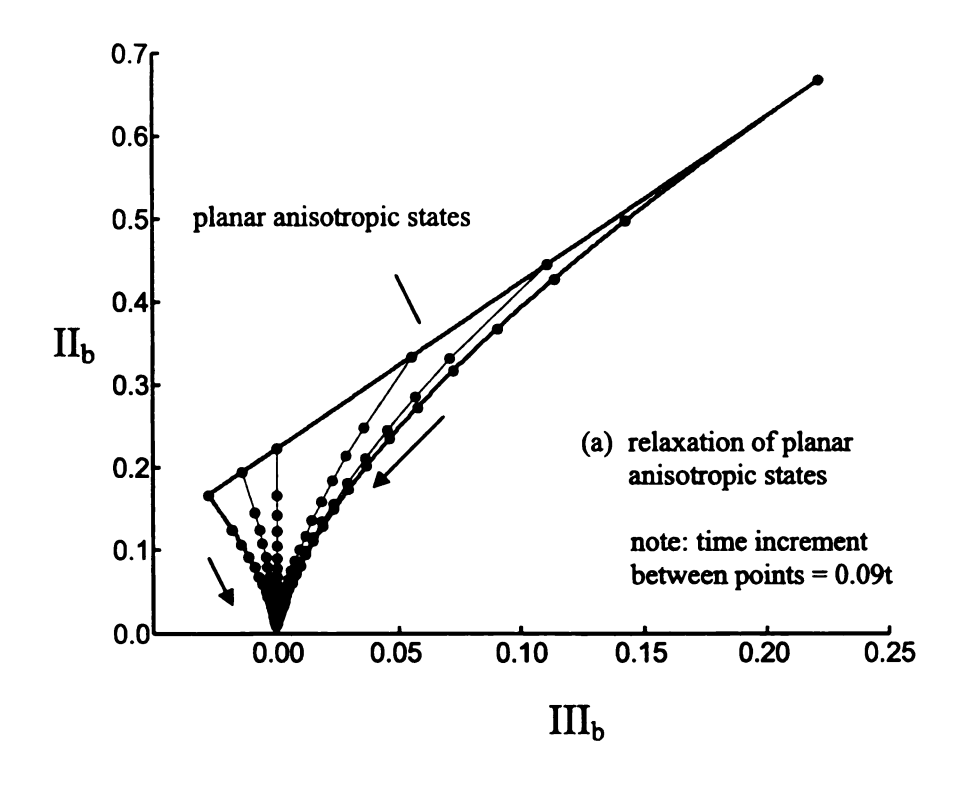
Figure 7.4 shows that transient solutions for U = 0 and U = 3. Both solutions relax to the isotropic state. However, the transient solution for U = 3 is attracted towards the nematic state before it reaches the isotropic steady state. When the rigid rod suspension is concentrated, the orientation state is anisotropic state ( $U > U_2 = 5$ ).

Tube dilation does not affect the steady state solutions. However, as illustrated by Figures 7.5 and 7.6, tube dilation makes the orientation state relax faster to the equilibrium state. In addition, the relaxation time increases as the orientation state is closer to  $U_1$ , and it decreases for higher U (see Figures 7.5 and 7.6).

## 7.4 Discussion

The microstructures of rigid-rod particle suspensions predicted by the FSQ-closure are realizable for all values of U. For  $U > U_1$ , the orientation structure parameter  $\alpha$  increases as U increases. For  $U \to \infty$ ,  $\alpha \to 1$ , which is the nematic state (see Figure 1.1). These predictions are consistent with other closure approximations and experimental observations.

The decoupling approximation with the Maier-Saupe potential has  $U_1 = 8/3$  with



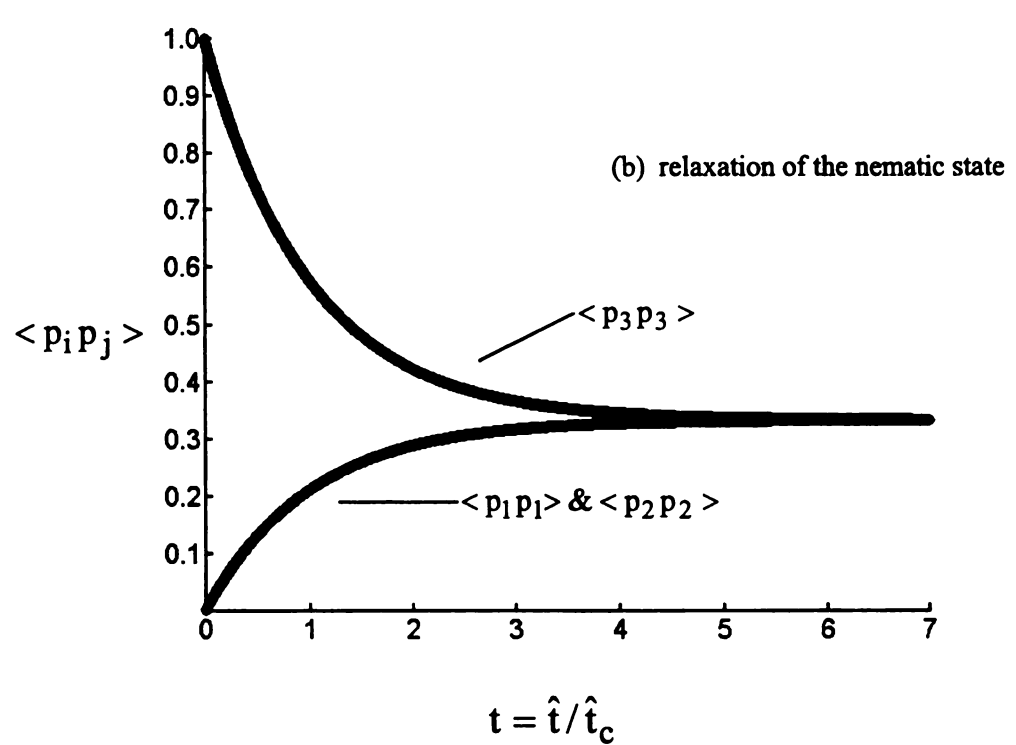


Figure 7.3 Relaxation of the Microstructure due to Rotary Brownian Diffusion (U = 0;  $\hat{t} = 1/(6D_R^0)$ ).

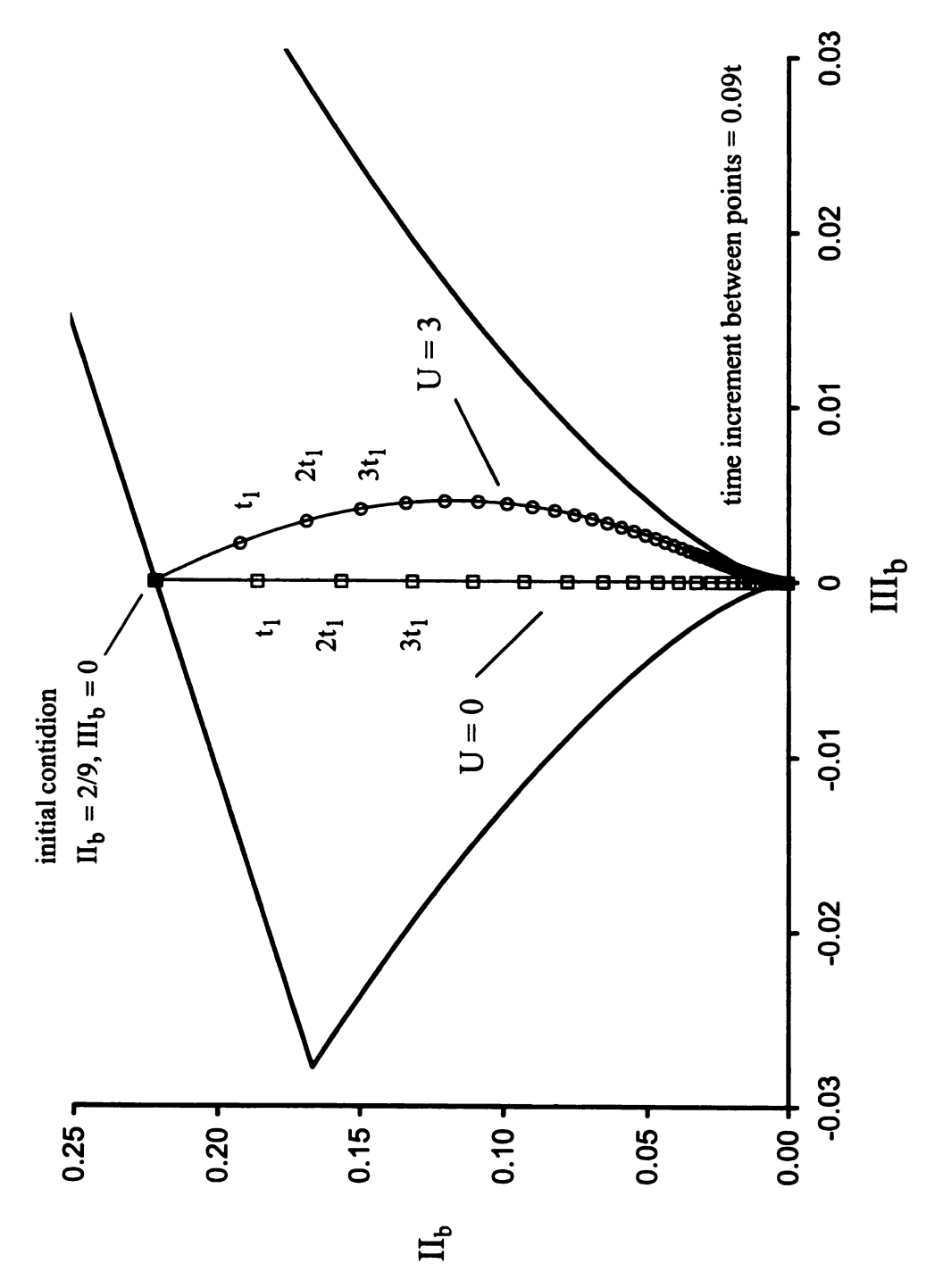


Figure 7.4 Effect of Excluded Volume on the Relaxation of the Microstructure (FSQ-model;  $F_{TD} = 1$ ).

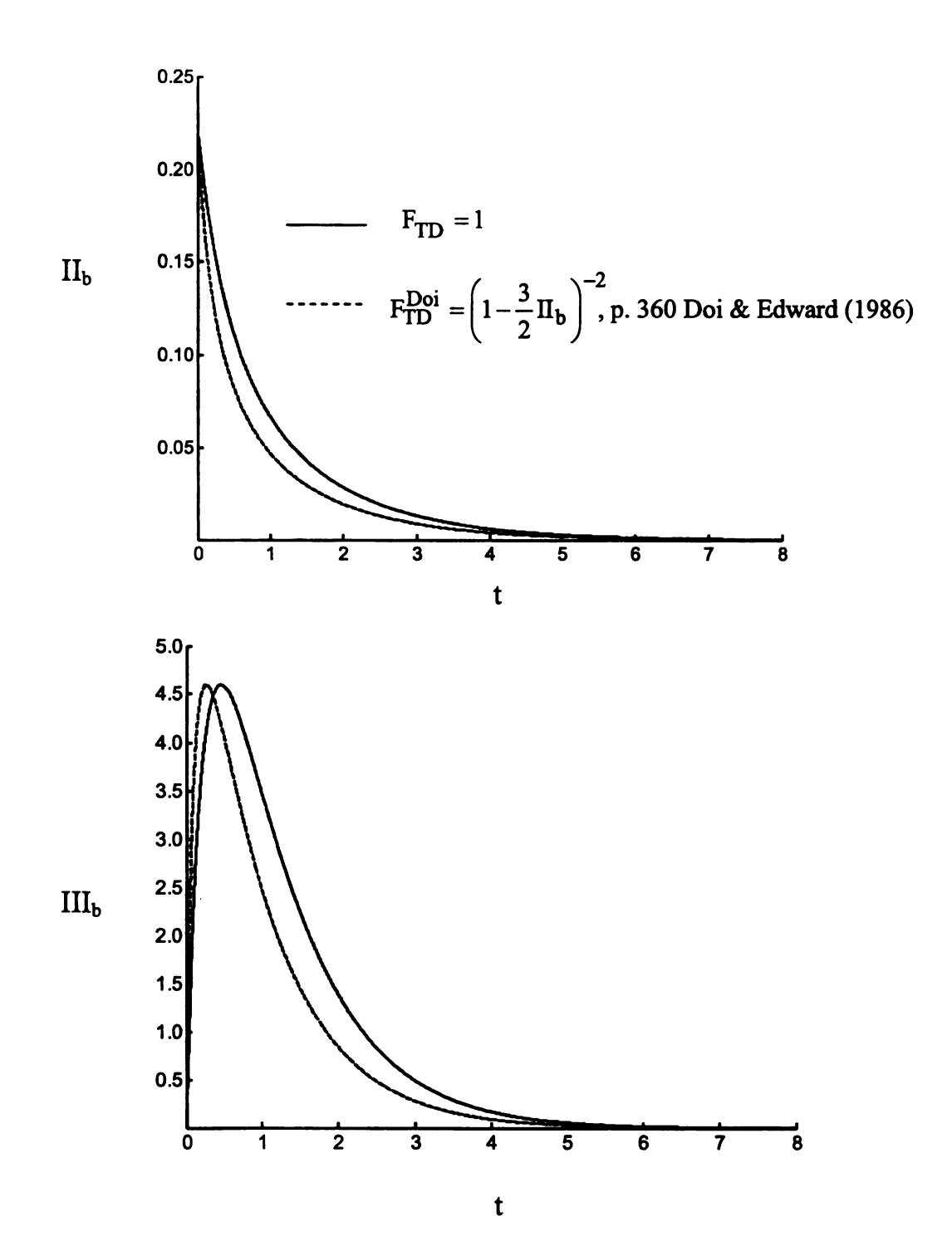


Figure 7.5 The Effect of Tube Dilation on the Relaxation of the Microstructure (FSQ-model; U = 3; initial conditions:  $II_b(0) = 2/9$ ;  $III_b(0) = 0$ ).

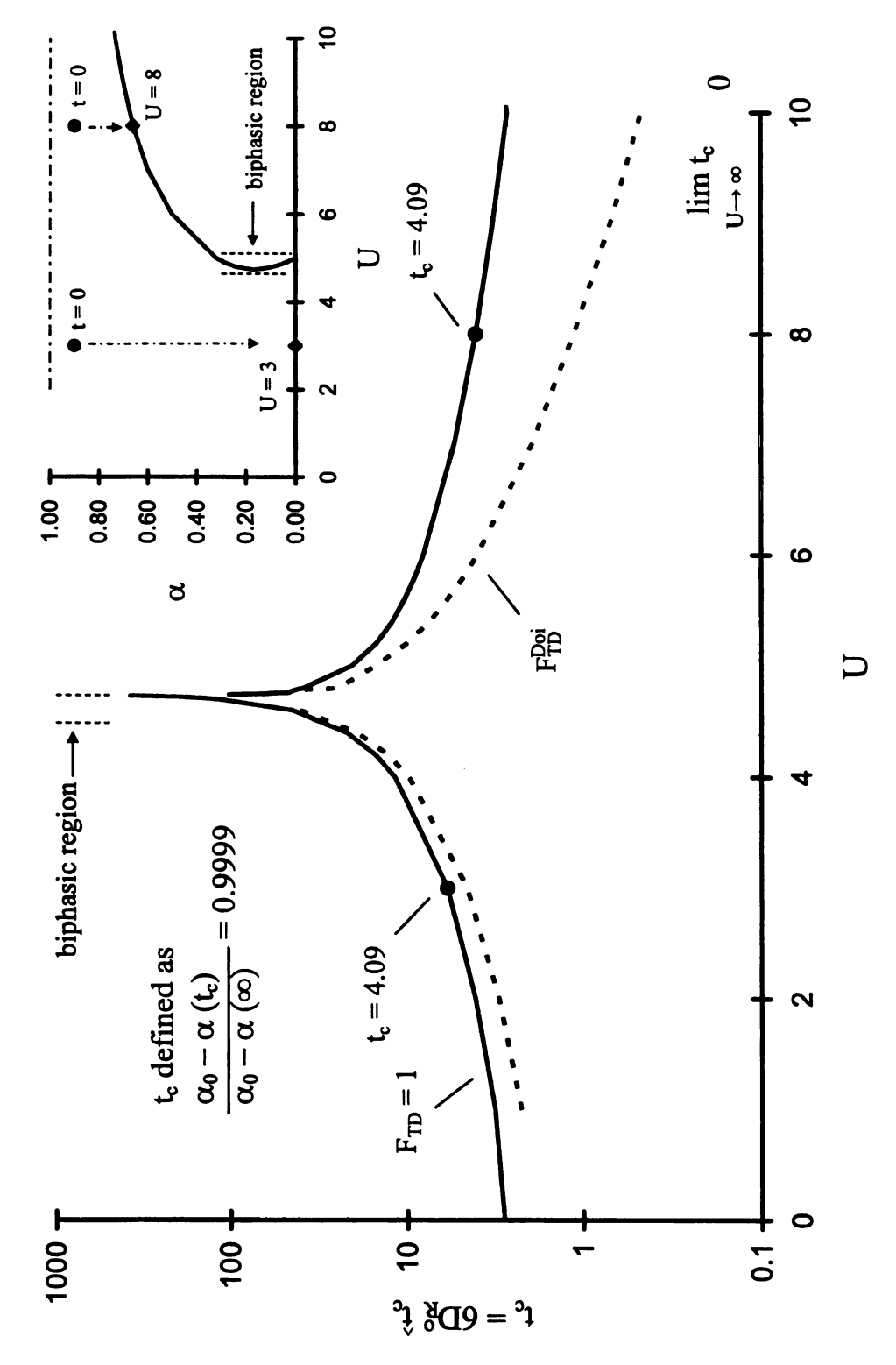


Figure 7.6 The Effect of U and Tube Dilation on the Characteristic Relaxation Time t<sub>c</sub> (FSQ-model;  $\alpha(0) = 0.9$ ).

 $\alpha$  = 1/4. The second critical U for the decoupling approximation is  $U_2$  = 3 with  $\alpha$  = 0 and 1/2. The HL1-closure predicts that  $U_1$  = 240/49 with  $\alpha$  = 1/8, and  $U_2$  = 5 with  $\alpha$  = 0 and 1/4. The FSQ-closure predicts that  $U_1$  = 4.73 with  $\alpha$  = 0.167, and  $U_2$  = 5 with  $\alpha$  = 0 and 0.321 (see Table 7.1). de Genne (1974) estimated a value for  $U_2$  ( $\cong$  4.55) from the orientation density function. Chaubal et al. (1995) also calculated the order parameter curve based on the density function.

The HL1- and FSQ-closures agree better with the transition point than the decoupling approximation. However, the anisotropic transition fits the decoupling approximation better (i.e., the curve is much steeper in both the exact and Chaubal et al. solutions). The HL1-closure becomes unrealizable on the oblate boundary. Using other types of excluded volume potential model, qualitative difference with Chaubal et al. can be modified, but U<sub>2</sub> is much higher than other approximations (see Ilg et al., 1999).

The computational results are based on initial condition for  $\langle \underline{p}\,\underline{p} \rangle$  with only diagonal components in the planar anisotropic state. When U=0 and Pe=0, Brownian motion is the only driving force that makes the orientation state random. The nematic potential coefficient U influences the anisotropic orientation state as well as the equilibrium isotropic state. For  $U>U_2$ , all the steady states are either on the prolate or on the oblate boundaries (see Figure 1.1). In addition, relaxation experiments provide a means to determine the rotary diffusion coefficient  $D_R$ . Previous studies have estimated  $D_R$  values by fitting the first normal stress difference  $N_1$  with computational results. Beak and Magda (1993) have reported that the  $D_R$  coefficient for PBLG solutions is about 2 s<sup>-1</sup>. With  $D_R \sim 2 \, \text{s}^{-1}$ , the time scale for relaxation to an equilibrium state in the

biphasic region may be as long as 10-100s inasmuch as  $t_c \cong 10$  to 100 (see Figure 7.6). Figure 7.6 may be used to design an experiment to estimate the rotary diffusion coefficient by measuring the relaxation time of rigid rod suspensions are a wide range of concentrations inasmuch as  $\hat{t}_c \sim 1/(6D_R^o)$ .

### **CHAPTER 8**

### MICROSTUCTURE INDUCED BY HOMOGENOUS SHEAR

## 8.1 Introduction

The relaxation of  $\langle \underline{p}\,\underline{p} \rangle$  (t) in the presence of a homogeneous shear field  $(\dot{\gamma} = \text{constant})$  will be examined in this chapter by solving Eq.(4.1) for Pe > 0. The velocity gradient for the rigid rod suspension is

$$\hat{\nabla}\,\underline{\hat{\mathbf{u}}} = \dot{\gamma}\,\underline{\mathbf{e}}_{\mathbf{y}}\,\underline{\mathbf{e}}_{\mathbf{z}}.\tag{8.1}$$

The strain rate dyadic and the vorticity dyadic are defined as

$$\underline{\underline{S}} = \underline{\hat{S}} / \dot{\gamma} = \frac{1}{2} (\underline{e}_{y} \underline{e}_{z} + \underline{e}_{z} \underline{e}_{y})$$
 (8.2)

$$\underline{\underline{\mathbf{W}}} = \underline{\hat{\mathbf{W}}} / \dot{\gamma} = \frac{1}{2} (\underline{\mathbf{e}}_{\mathbf{y}} \underline{\mathbf{e}}_{\mathbf{z}} - \underline{\mathbf{e}}_{\mathbf{z}} \underline{\mathbf{e}}_{\mathbf{y}}). \tag{8.3}$$

The objective of the chapter is to explore the effect of the tumbling parameter  $\lambda$  on the microstructure for a wide range of U and Pe. Appendix E shows how the director of  $\langle \underline{p}\,\underline{p} \rangle$  can be calculated in terms of the components of  $\langle \underline{p}\,\underline{p} \rangle$ . The motion of the director relative to the fixed flow direction  $(\underline{u}=u_z\underline{e}_z)$  will be examined for L/d =  $\infty$  (Section 8.2), L/d =12 (Section 8.3), and  $0 \leq L/d < \infty$  (Section 8.4). In Section 8.5, the influence of tube dilation on the microstructure will be discussed. The results of this chapter are based on the FSQ-closure for  $\langle \underline{p}\,\underline{p}\,\underline{p}\,\underline{p} \rangle$  defined by Eqs. (5.11) and (6.12). Eq. (4.1) is integrated by using a fourth-order Runge-Kutta algorithm (see APPENDIX G).

## 8.2 Relaxation of Planar Anisotropic States for $L/d = \infty$

For  $L/d=\infty$ ,  $\lambda=1$  (see Eq.(2.4)). For this case, Eq. (4.1) with  $\Xi=1$ ,  $F_{TD}=1$ , and  $\hat{\nabla} \hat{\underline{u}}$  defined by Eq.(8.1) above predicts that all realizable orientation states (see Figure 1.1) relax to steady states for  $U\geq 0$  and Pe>0 (see CHAPTER 7 for Pe=0). If the initial condition for the director (i.e., the eigenvector associated with the largest eigenvalue of < pp>) is in the deformation plane, then the steady state is unique.

Figure 8.1 shows the effect of U and Pe on the steady state angle between the flow direction ( $\underline{u} = u_z \underline{e}_z$ ) and the director ( $\cos\theta = \underline{x}_3 \cdot \underline{e}_z$ ). The director angle decreases monotonically as U increases for fixed Pe, and as Pe increases for fixed U. The results show that hydrodynamic coupling ( $\lambda$ -parameter) and the excluded volume phenomenon (U-parameter) cause anisotropic steady states.

For  $U \le 3$  and  $Pe \to 0$ , Figure 8.2 indicates that the microstructure is isotropic (i.e.,  $II_b = 0$  and  $III_b = 0$ ). As Pe increases, anisotropic steady states occur. For fixed values of Pe, the microstructure becomes more nematic-like as U increases. This occurs because the excluded volume term in Eq.(4.1) mitigates the return-to-isotropy due to rotary Brownian motion. Thus, the flow-induced alignment mechanism and the excluded-volume effect simultaneously promote nematic-like microstructures. The excluded volume mechanism makes the microstructure more prolate axisymmetric (see CHAPTER 7) whereas the hydrodynamic coupling of  $\langle \underline{p}\,\underline{p} \rangle$  with  $\underline{S}$  tends to make the microstructure more isotropic.

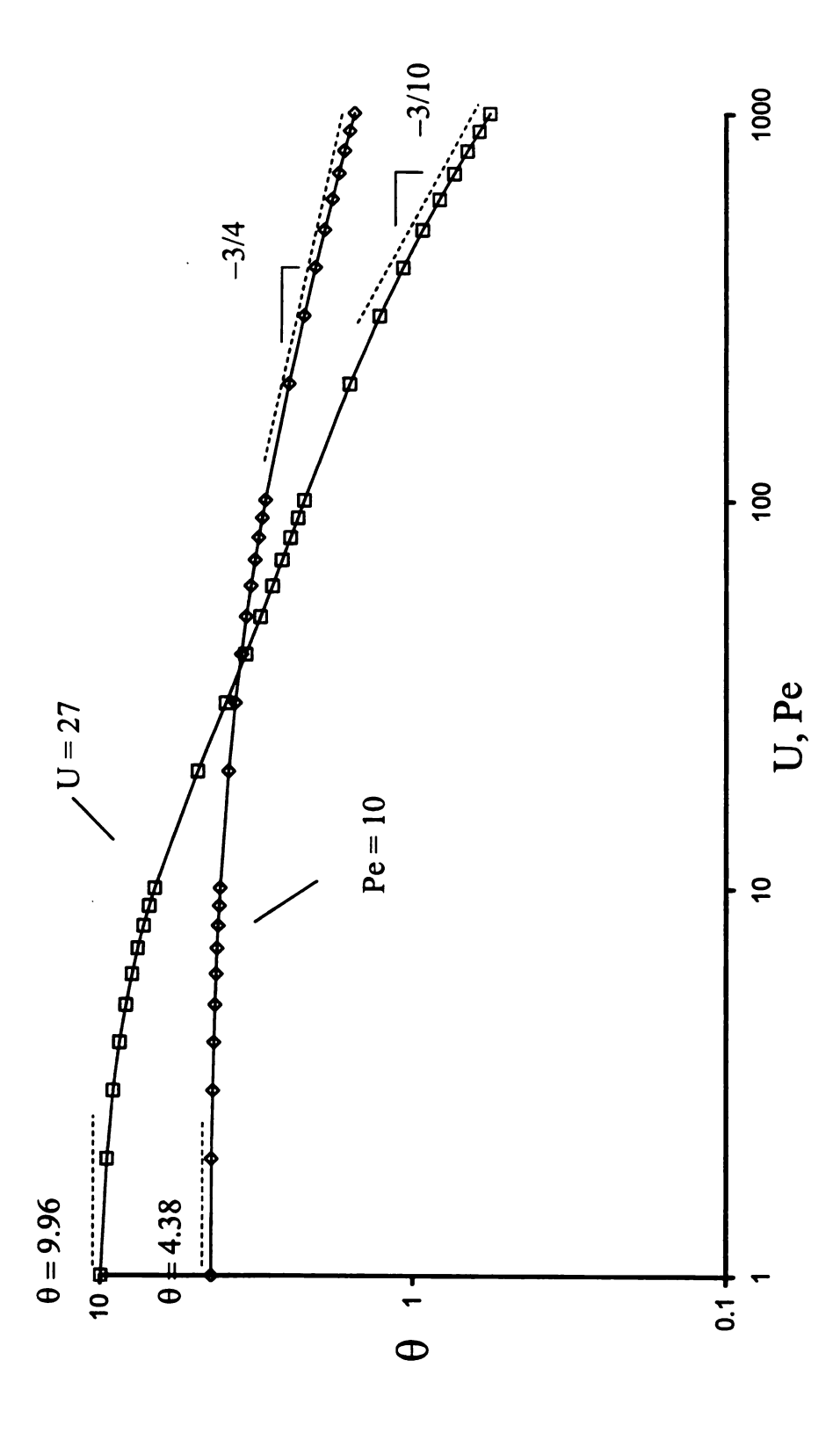


Figure 8.1 The Effect of U and Pe on the Steady State Director Angle for L/d =  $\infty$ (FSQ-model;  $F_{TD} = 1$ ;  $\lambda = 1$ ).

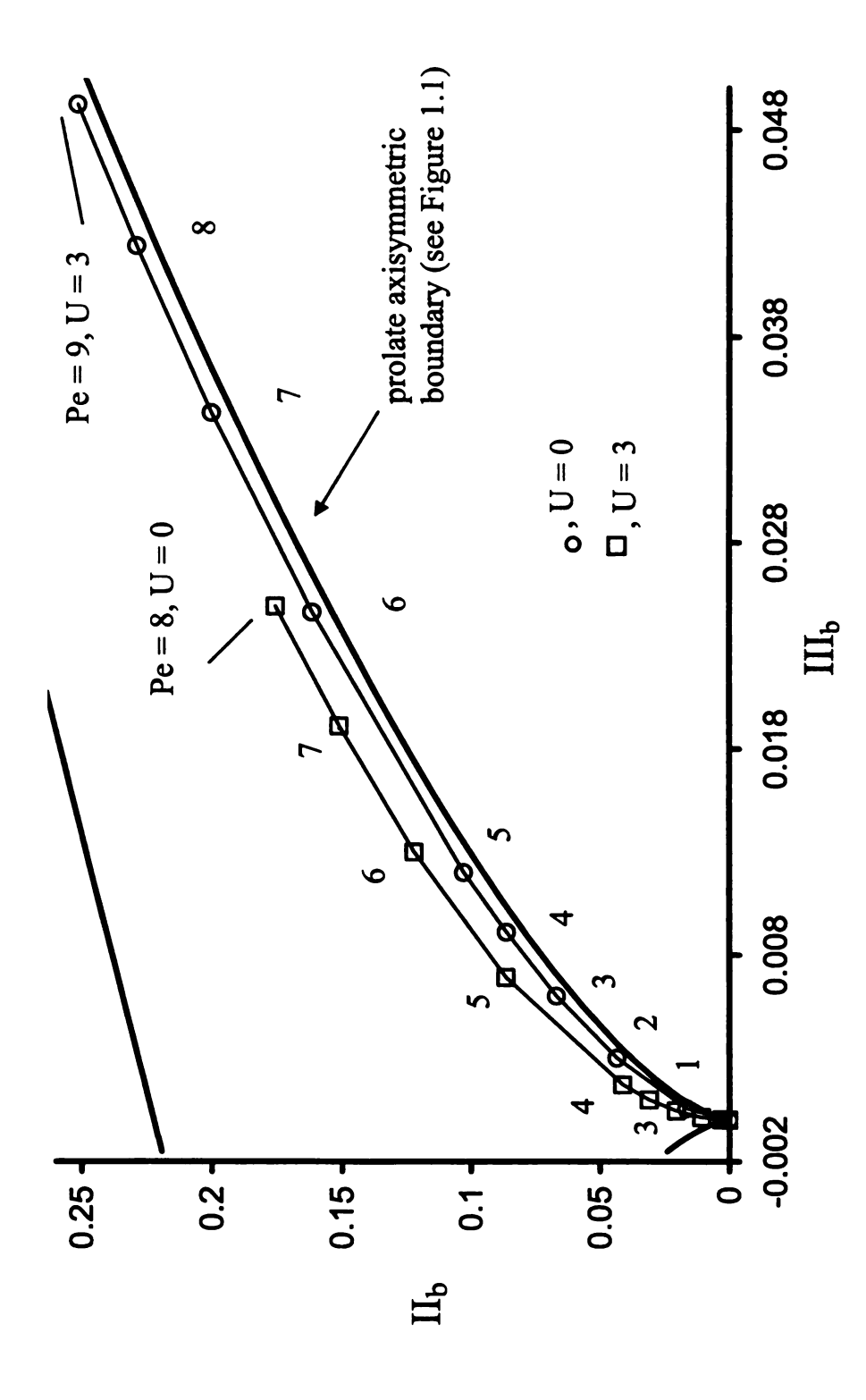


Figure 8.2 The Effect of U and Pe on the Steady State Microstructure for L/d =  $\infty$ (FSQ-model;  $F_{TD} = 1$ ;  $\lambda = 1$ ).

## 8.3 Relaxation of Planar Anisotropic States for $L/d \approx 12$

The tumbling parameter  $\lambda$  in Eq.(4.1) plays a significant role in the relaxation of the microstructure. This is anticipated by Eq.(2.2), which predicts that a single rigid rod in a steady shear flow will tumble continuously if  $|\lambda| < 1$  (see p.449, Larson 1999). For U = 0 and  $1 \le Pe \le 1,000$ , Table 8.1 compares the invariants of the structure tensor for L/d  $= \infty$  ( $\lambda = 1$ ) and L/d = 12 ( $\lambda = 0.987$ ). For  $\lambda = 1$ , the steady state invariants approach the nematic state (see Figure 1.1) for large values of Pe. However, for Pe = 1,000 and  $\lambda = 0.987$ , the microstructure of the suspension is less nematic (II<sub>b</sub> = 0.48, III<sub>b</sub> = 0.13).

For  $\lambda=0.987$  and U>27, Eq.(4.1) predicts director tumbling for Pe  $\cong 10$ . For this case, Figures 8.3 and 8.4 show that an initial planar isotropic state (see Figure 1.1) relaxes to a periodic state characterized by *director tumbling* with a frequency of  $\hat{f}_t\cong 6D_R^o\pi/15$ . The initial condition for  $<\underline{p}\,\underline{p}>(0)$  is planar isotropic:

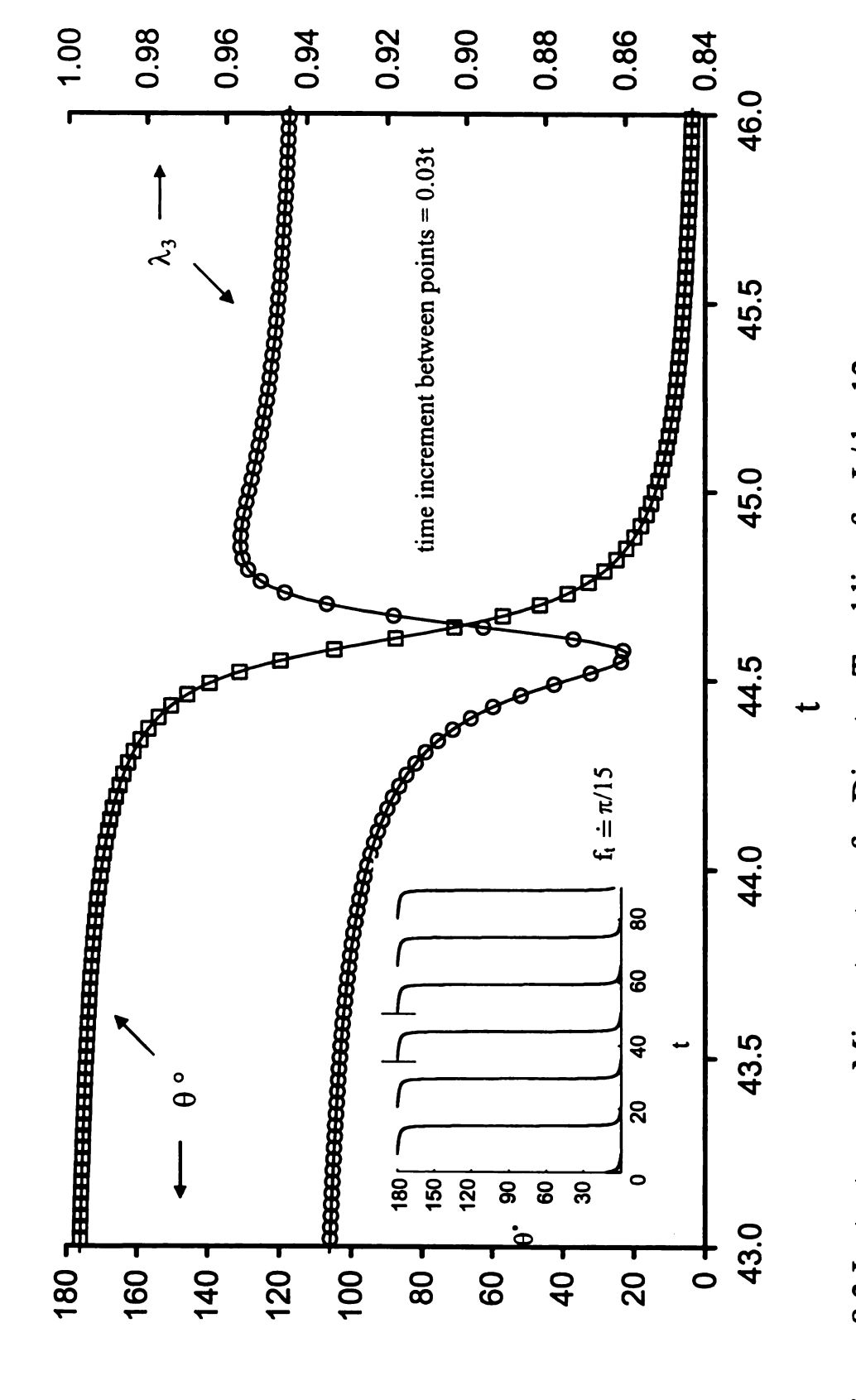
$$2 < pp > (0) = (\underline{e}_{y}\underline{e}_{y} + \underline{e}_{z}\underline{e}_{z}). \tag{8.4}$$

The eigenvectors of  $\langle \underline{p} \underline{p} \rangle$  (0) are in the deformation (or shear) plane (see Figure 3.1). The director tumbles  $180^{\circ}$  because there is no distinction between the head and the tail of a rigid rod.

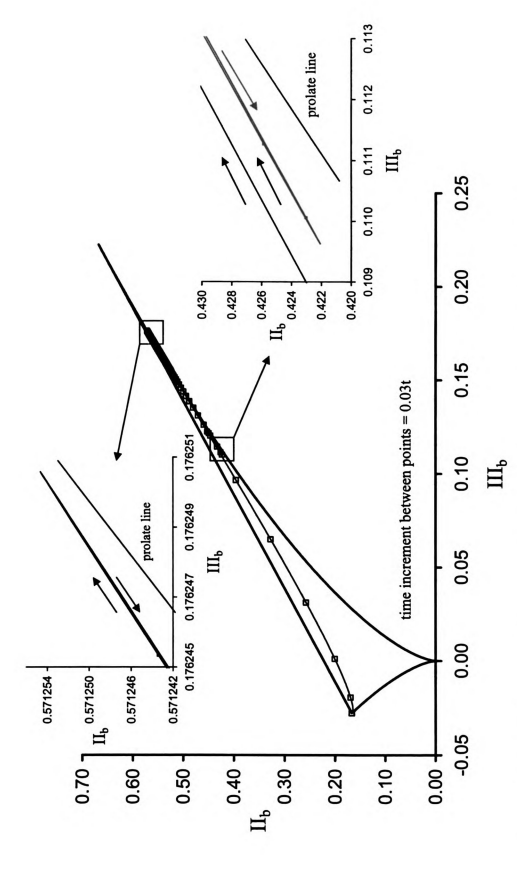
Director tumbling occurs for two reason: 1) the excluded volume phenomenon mitigates rotary Brownian motion and, thereby, reduces the intrinsic diffusive torque on the microstructure; and, 2) the torque on the microstructure due to particle coupling with the shear rate is weakened by a reduced tumbling parameter (i.e.,  $\lambda = 0.987 < 1$ ). As a consequence, the torque due to the antisymmetric component of the velocity gradient can

Table 8.1 Invariants of the Equilibrium Anisotropic Tensor for Different Tumbling Parameters (FSQ-model;  $F_{TD} = 1$ ; U = 0)

Pe	$\lambda = 1$		$\lambda = 0.987$	
	$\Pi_{b}$	$\mathrm{III}_{\mathrm{b}}$	$\Pi_{b}$	$\mathrm{III}_{\mathrm{b}}$
1	0.0412	0.0017	0.0402	0.0016
5	0.1754	0.0249	0.1686	0.0232
10	0.2588	0.0488	0.2458	0.0447
50	0.4477	0.1202	0.4062	0.1029
100	0.5099	0.1475	0.4475	0.1201
500	0.6020	0.1905	0.4785	0.1335
1000	0.6240	0.2011	0.4801	0.1342
∞	0.6667	0.2222	0.4805	0.1344



(FSQ-model;  $F_{TD} = 1$ ;  $\lambda = 0.987$ ; U = 27,  $P_{e} = 10$ ;  $2 < \underline{p} \, \underline{p} > (0) = \underline{e}_{y} \, \underline{e}_{y} + \underline{e}_{z} \, \underline{e}_{z}$ ). Figure 8.3 Instantaneous Microstructure for Director Tumbling for L/d ≈ 12

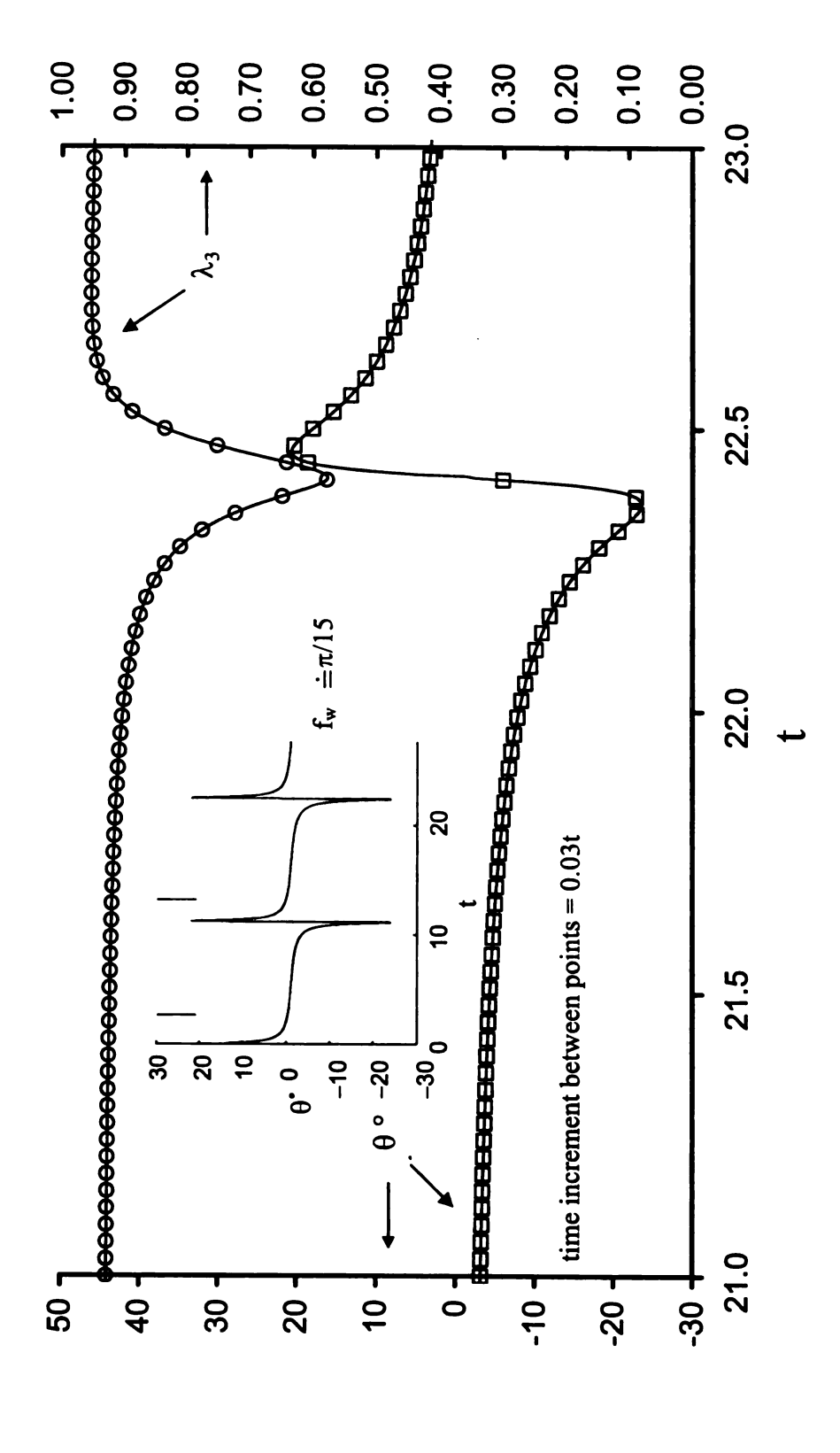


(FSQ-model;  $F_{TD} = 1$ ;  $\lambda = 0.987$ ; U = 27,  $P_{e} = 10$ ;  $2 < \underline{p} \, \underline{p} > (0) = \underline{e}_{y} \, \underline{e}_{y} + \underline{e}_{z} \, \underline{e}_{z}$ ). Figure 8.4 Microstructure for Director Tumbling in the Phase Plane for L/d  $\approx 12$ 

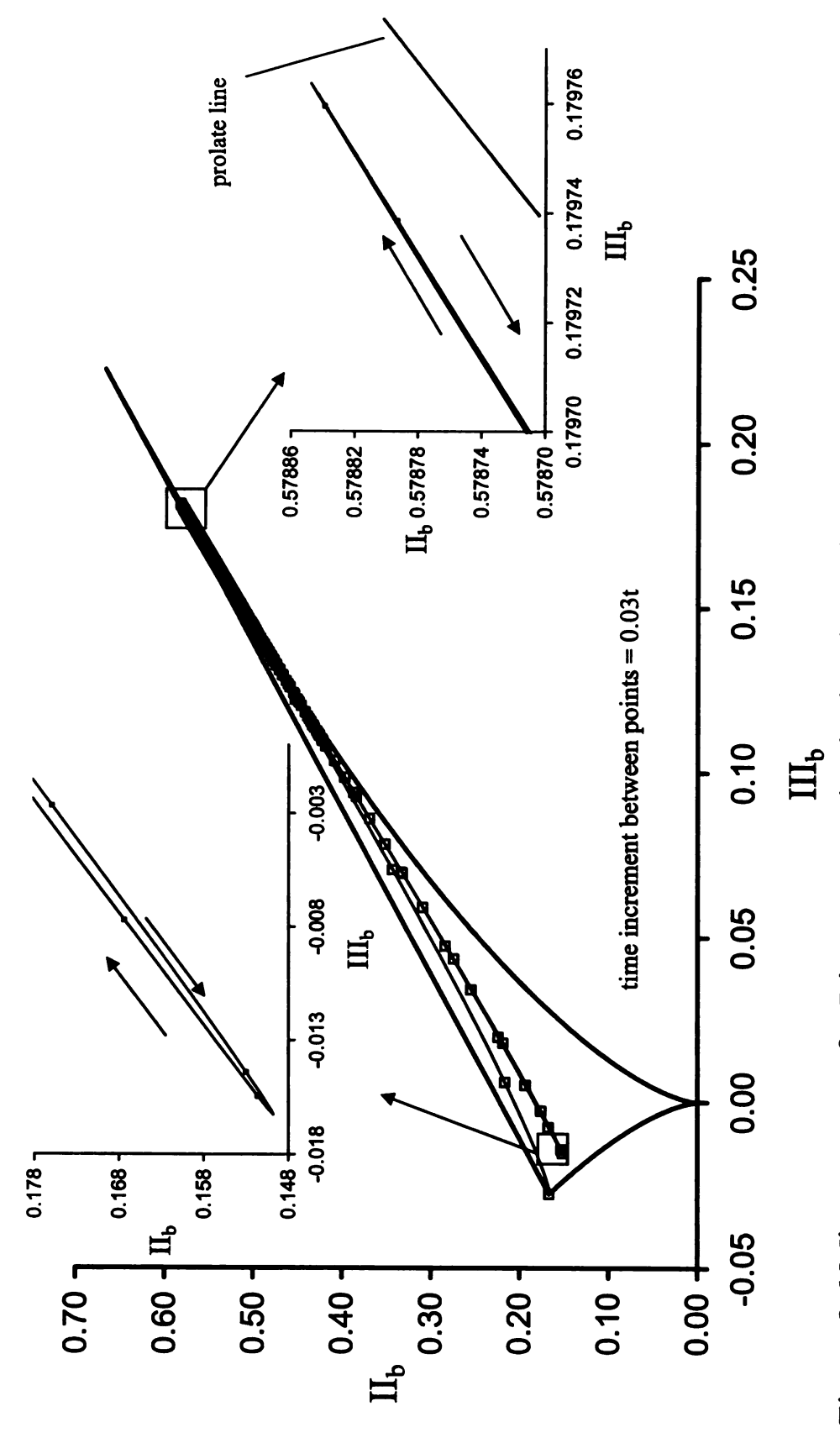
sustain the phenomenon of director tumbling (see Eq.(4.1)). The dimensionless tumbling frequency  $f_t = \hat{f}_t/6D_R^o$  depends on U and Pe. For U > 27, Eq.(4.1) predicts that  $f_t$  increases as Pe increases. This conclusion is consistent with previous theoretical and experimental studies related to director tumbling (see p.280 and p. 463, Larson, 1999).

Figure 8.3 shows that the director rotates slowly when it is nearly aligned with the flow direction and rapidly rotates as it crosses the vorticity/cross-flow plane (see Figure 3.1). The temporal response of the eigenvalue associated with the director is also shown in Figure 8.3. It is noteworthy that  $\lambda_3$  (t) is a minimum during the rapid tumbling phase of the motion. The invariants of the structure tensor for this example are shown on the invariant diagram, Figure 8.4. Clearly, Eq.(4.1) together with the FSQ-closure yields a realizable orientation dyad for director tumbling. Note also that the initial planar isotropic orientation state rapidly locks onto the tumbling orbit for  $\hat{t} \cong 0.09/6D_R^0$ .

For  $\lambda=0.987$  and U=27, Eq.(4.1) predicts that director wagging will occur for Pe=24. This phenomenon is illustrated by Figure 8.5, which shows the angle between the fixed flow direction and the director. For this case, the wagging frequency  $\hat{f}_{\mathbf{w}}\cong 6D_{\mathbf{R}}^{\mathbf{o}}\pi/11$ . Note that the director eigenvalue  $\lambda_3$  is a minimum as the director wags about the flow director. A planar isotropic initial condition is also specified for this calculation and, as illustrated by Figure 8.6, the orientation state locks onto the periodic wagging state within  $\hat{t}\cong 0.09/6D_{\mathbf{R}}^{\mathbf{o}}$ . Eq.(4.1) predicts that  $f_{\mathbf{w}}\equiv \hat{f}_{\mathbf{w}}/6D_{\mathbf{R}}^{\mathbf{o}}\to\infty$  for  $Pe\cong 30$  and  $U\cong 27$ . As the Péclet number increases, the microstructure approaches the fully aligned state (Point A, Figure 1.1). The coupling between the strain rate dyadic and the



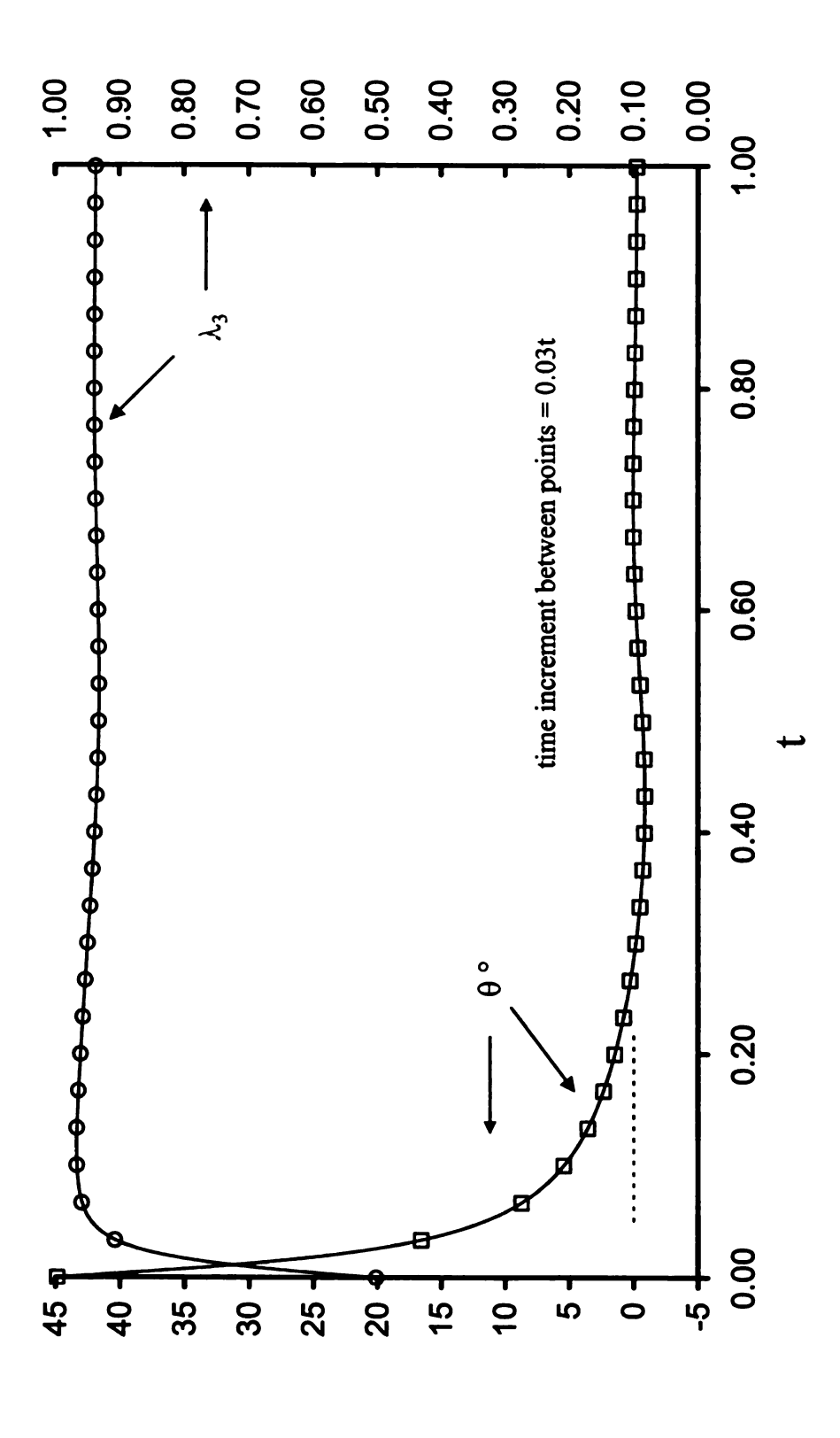
(FSQ-model;  $F_{TD} = 1$ ;  $\lambda = 0.987$ ; U = 27,  $P_{e} = 24$ ;  $2 < \underline{p} \, \underline{p} > (0) = \underline{e}_{y} \, \underline{e}_{y} + \underline{e}_{z} \, \underline{e}_{z}$ ). Figure 8.5 Instantaneous Microstructure for Director Wagging for  $L/d \cong 12$ 



(FSQ-model;  $F_{TD} = 1$ ;  $\lambda = 0.987$ ; U = 27, Pe = 24;  $2 < \underline{p}\,\underline{p} > (0) = \underline{e}_{y}\,\underline{e}_{y} + \underline{e}_{z}\,\underline{e}_{z}$ ). Figure 8.6 Microstructure for Director Wagging in the Phase Plane for  $L/d \approx 12$ 

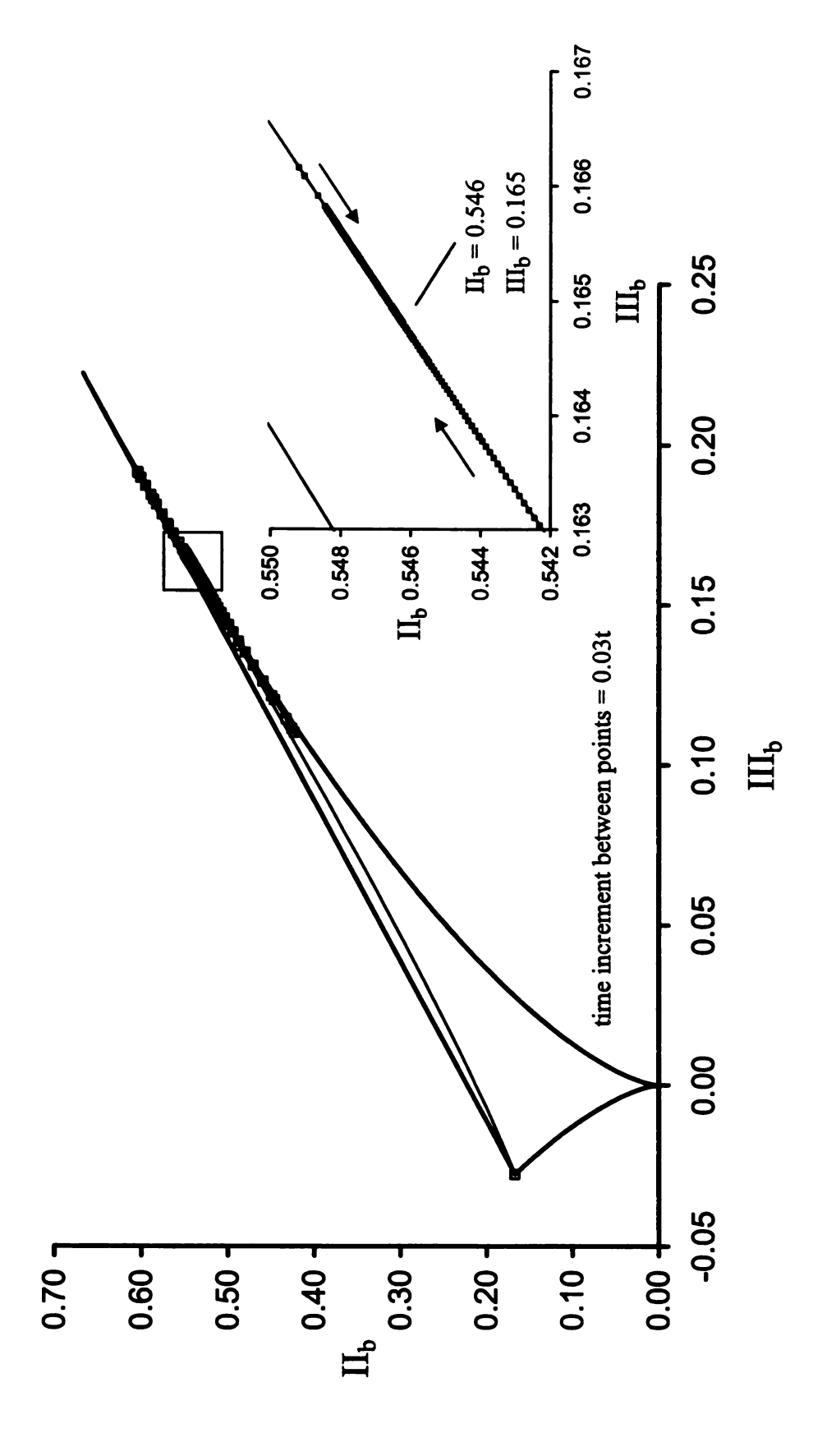
orientation dyad weakens as  $(II_b, III_b) \rightarrow Point A$ . Thus, for U = 27 and Pe > 30, the diffusive torque balances the hydrodynamic torque to produce a steady state microstructure. Figures 8.7 and 8.8 illustrate this phenomenon for  $\lambda = 0.987$ , U = 27, and Pe = 95. A planar isotropic initial condition with the director in the shear plane was also specified for the calculation  $(2 < \underline{p}\underline{p} > (0) = \underline{e}_y\underline{e}_y + \underline{e}_z\underline{e}_z)$ . The director angle relaxes rapidly from its initial condition of 45° and fluctuates around the flow director. Eventually the director attains a steady state with a small *negative* offset from the flow direction. Figure 8.8 shows that the invariants of the structure tensor are close to the prolate axisymmetric boundary. It is noteworthy that for U = 27, Pe = 95, and  $\lambda = 1$  (rather than 0.987), the director also attains a steady state, but with a small *positive* offset from the flow direction (see results on Figure 8.1).

Figure 8.9 gives a phase diagram for  $\lambda=0.987$ . The diagram was constructed by integrating Eq.(4.1),  $F_{TD}=1$ , and the FSQ-closure from a planar isotropic initial condition  $(2 < \underline{p}\,\underline{p} > (0) = \underline{e}_y\,\underline{e}_y + \underline{e}_z\,\underline{e}_z)$ . The asymptotic state depends on U and Pe. Three possible states were found: 1) steady states; 2) periodic tumbling states; and 3) periodic wagging states. The boundaries shown on Figure 8.9 were determined within  $(\Delta Pe, \Delta U) = (1, 1)$ . For example, at Pe = 10, steady alignment occurs for U = 25 and director tumbling occurs for U = 26. For U = 27, Pe = 95, and  $\lambda = 0.987$ , Figures 8.10 and 8.11 show how a planar isotropic state with an initial director colinear with the vorticity (see Figure 3.1) relaxes to its steady state. The initial condition for the orientation dyad is  $2 < \underline{p}\,\underline{p} > (0) = \underline{e}_x\,\underline{e}_x + \underline{e}_z\,\underline{e}_z$ . The eigenvalues and eigenvectors for this initial condition are

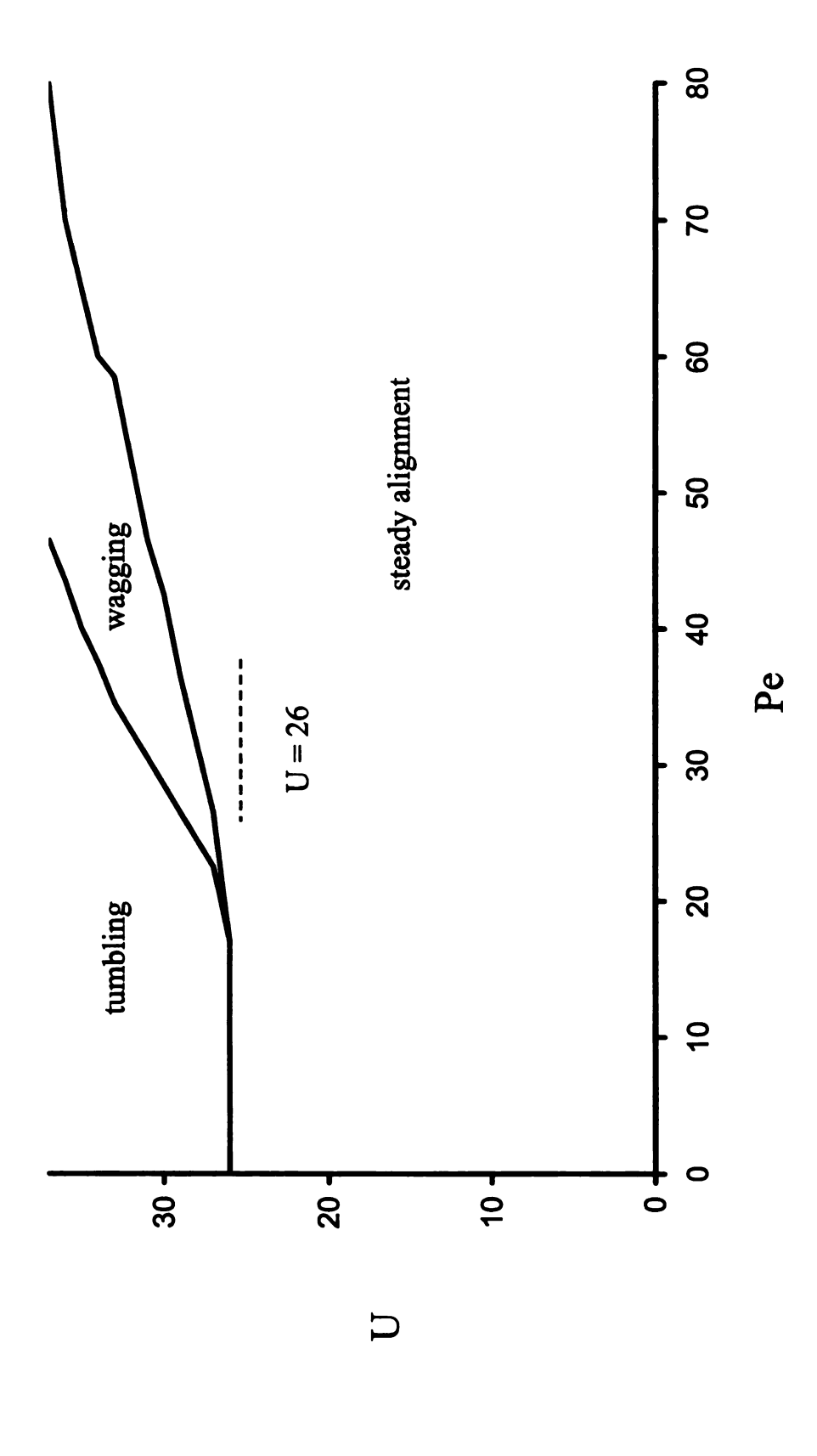


(FSQ-model;  $F_{TD} = 1$ ;  $\lambda = 0.987$ ; U = 27,  $P_{e} = 95$ ;  $2 < \underline{p}\,\underline{p} > (0) = \underline{e}_{y}\,\underline{e}_{y} + \underline{e}_{z}\,\underline{e}_{z}$ ). Figure 8.7 Instantaneous Microstructure for Director Steady Alignment for L/d 

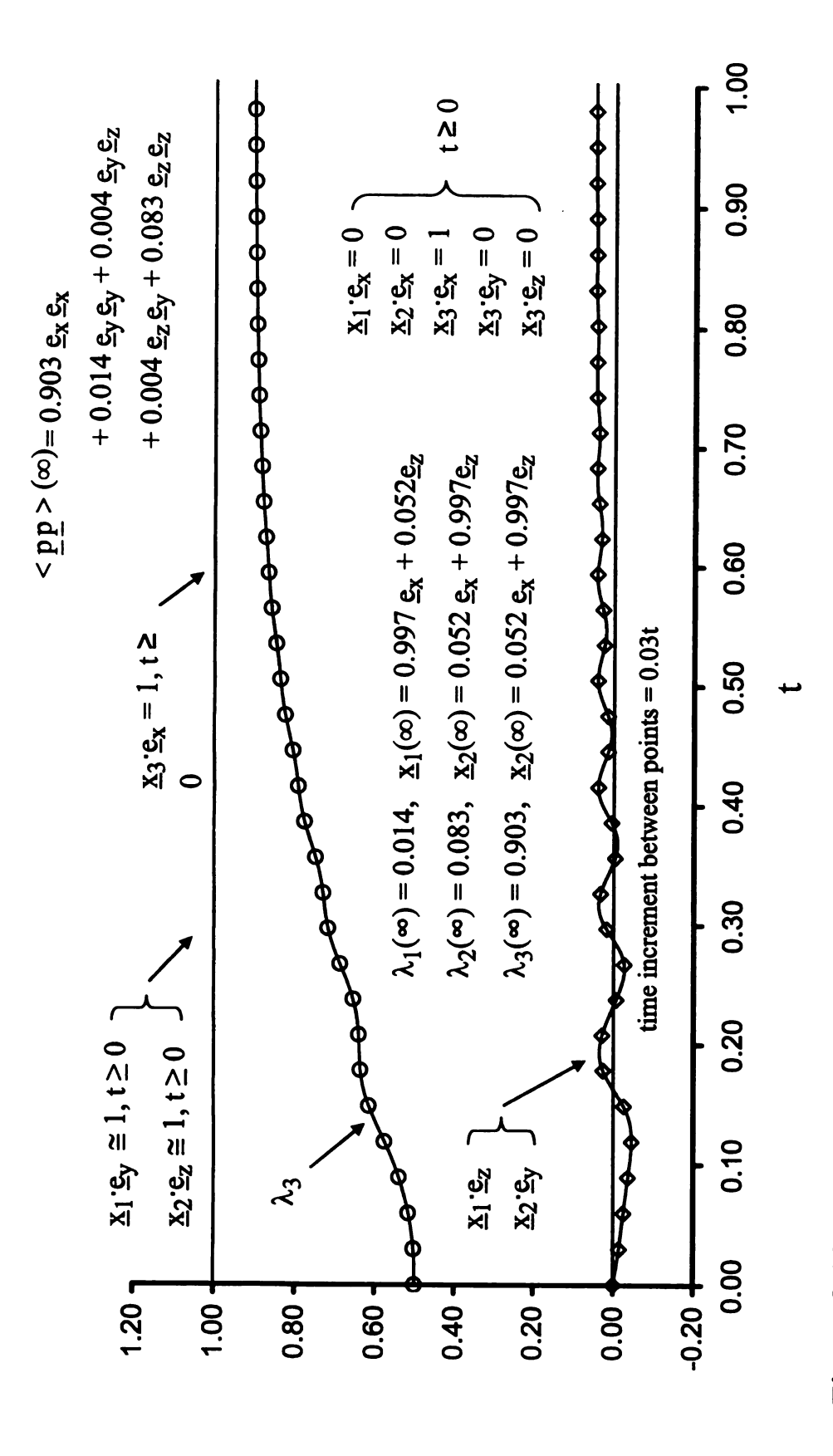
≡ 12



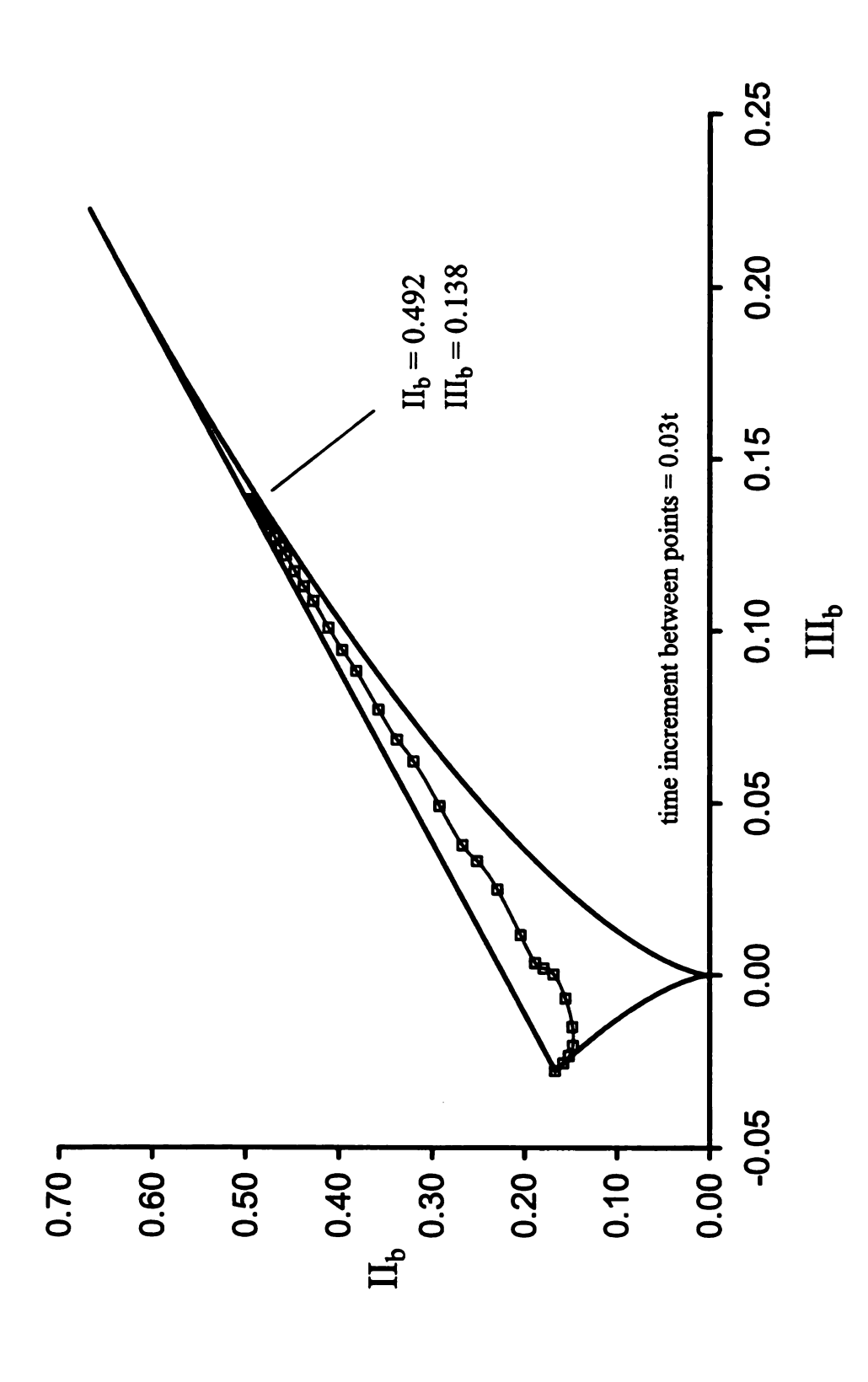
(FSQ-model;  $F_{TD} = 1$ ;  $\lambda = 0.987$ ; U = 27,  $P_{e} = 95$ ;  $2 < \underline{p}\,\underline{p} > (0) = \underline{e}_{y}\,\underline{e}_{y} + \underline{e}_{z}\,\underline{e}_{z}$ ). Figure 8.8 Microstructure for Director Steady Alignment in the Phase Plane for L/d  $\approx 12$ 



(FSQ-model;  $F_{TD} = 1$ ;  $\lambda = 0.987$ ;  $2 < \underline{p}\,\underline{p} > (0) = \underline{e}_y\,\underline{e}_y + \underline{e}_z\,\underline{e}_z$ ). Figure 8.9 Phase Diagram of U and Pe for L/d  $\approx 12$ 



(FSQ-model; U = 27; Pe = 95;  $F_{TD} = 1$ ;  $\lambda = 0.987$ ;  $2 < \underline{p} \, \underline{p} > (0) = \underline{e}_x \, \underline{e}_x + \underline{e}_z \, \underline{e}_z$ ). Figure 8.10 Instantaneous Director Log-rolling for  $L/d \approx 12$ 



(FSQ-model; U = 27; Pe = 95;  $F_{TD} = 1$ ;  $\lambda = 0.987$ ;  $2 < \underline{p} \, \underline{p} > (0) = \underline{e}_x \, \underline{e}_x + \underline{e}_z \, \underline{e}_z$ ). Figure 8.11 Director Log-rolling in the Phase Plane for L/d  $\approx 12$ 

$$\lambda_1 (0) = 0, \qquad \underline{x}_1 (0) = \underline{e}_y,$$

$$\lambda_2 (0) = 1/2 \qquad \underline{x}_2 (0) = \underline{e}_z$$

$$\lambda_3 (0) = 1/2 \qquad \underline{x}_3 (0) = \underline{e}_x.$$
(8.5)

The director  $\underline{x}_3$  is initially aligned with the vorticity  $\nabla \times \underline{u} = \underline{w} = w_x \, \underline{e}_x$  and as indicated by Figure 8.10, remains colinear with  $\underline{w}$  for the entire relaxation process. The steady state invariants of the structure tensor are  $II_b(\infty) = 0.492$  and  $III_b(\infty) = 0.138$  (see Figure 8.11). It is noteworthy that this steady state is different from the one that develops from a planar isotropic state with an initial director in the shear plane (see Figure 8.7 and 8.8). Thus, if U = 27, Pe = 95, and  $\lambda = 0.987$ , Eq.(4.1) predicts the existence of two steady states:

- 1)  $II_b(\infty) = 0.546$ ,  $III_b(\infty) = 0.165$  (see Figure 8.8); and,
- 2)  $II_b(\infty) = 0.492$ ,  $III_b(\infty) = 0.138$  (see Figure 8.10).

Figure 8.10 shows that  $\underline{x}_1 \cdot \underline{e}_z = \underline{x}_2 \cdot \underline{e}_y = 0.052$  for  $t \to \infty$ . The rocking motion of the two eigenvectors  $\underline{x}_1$  and  $\underline{x}_2$  around the director  $\underline{x}_3$  (see Figure 8.10) has been termed log-rolling (see p.450 Larson, 1999). The three eigenvalues associated with the steady state orientation dyad  $\langle \underline{p}\underline{p} \rangle (\infty)$  are  $\lambda_1(\infty) = 0.014$ ,  $\lambda_2(\infty) = 0.083$ , and  $\lambda_3(\infty) = 0.903$ . Thus, a relaxation process with the initial director colinear with the vorticity (i.e.,  $\underline{x}_3(0) \sim \underline{w}$ ) produces a final microstructure which is less nematic than a process with the initial director colinear with the cross flow direction (i.e.,  $\underline{x}_3(0) \sim \underline{u} \times \underline{w}$ ). Figure 8.12 gives a phase diagram for  $\lambda = 0.987$  for a planar isotropic initial condition with the director in colinear with the vorticity (see Figure 3.1):  $2 \langle \underline{p}\underline{p} \rangle (0) = \underline{e}_{\underline{x}}\underline{e}_{\underline{x}} + \underline{e}_{\underline{z}}\underline{e}_{\underline{z}}$ . The

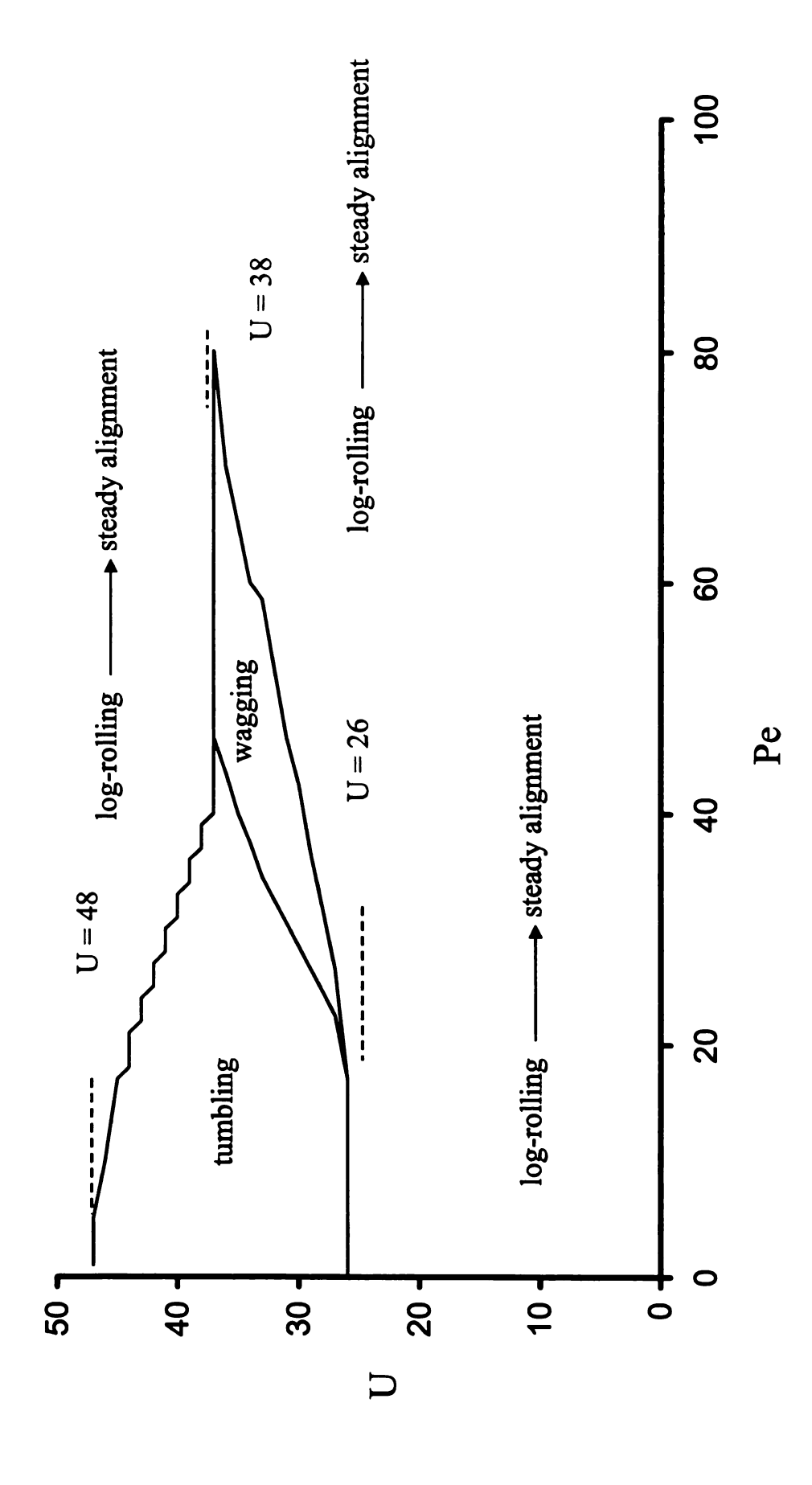


Figure 8.12 Phase Diagram of Shear-vorticity Plane Initial Condition for  $L/d \approx 12$ (FSQ-model;  $F_{TD} = 1$ ;  $\lambda = 0.987$ ;  $2 < \underline{p}\,\underline{p} > (0) = \underline{e}_x\,\underline{e}_x + \underline{e}_z\,\underline{e}_z$ ).

asymptotic states depend on U and Pe. Three possible states were found: 1) log-rolling/steady alignment; 2) periodic tumbling; and, 3) periodic wagging.

Figure 8.13 shows the relaxation of an anisotropic microstructure with the initial director located in the vorticity/flow plane. The initial condition for the orientation dyad is

$$<\underline{p}\underline{p}>(0) = \frac{5}{12}\underline{e}_{x}\underline{e}_{x} + \frac{2}{12}\underline{e}_{y}\underline{e}_{y} + \frac{5}{12}\underline{e}_{z}\underline{e}_{z} + \frac{1}{12}(\underline{e}_{x}\underline{e}_{z} + \underline{e}_{z}\underline{e}_{x})$$
 (8.6)

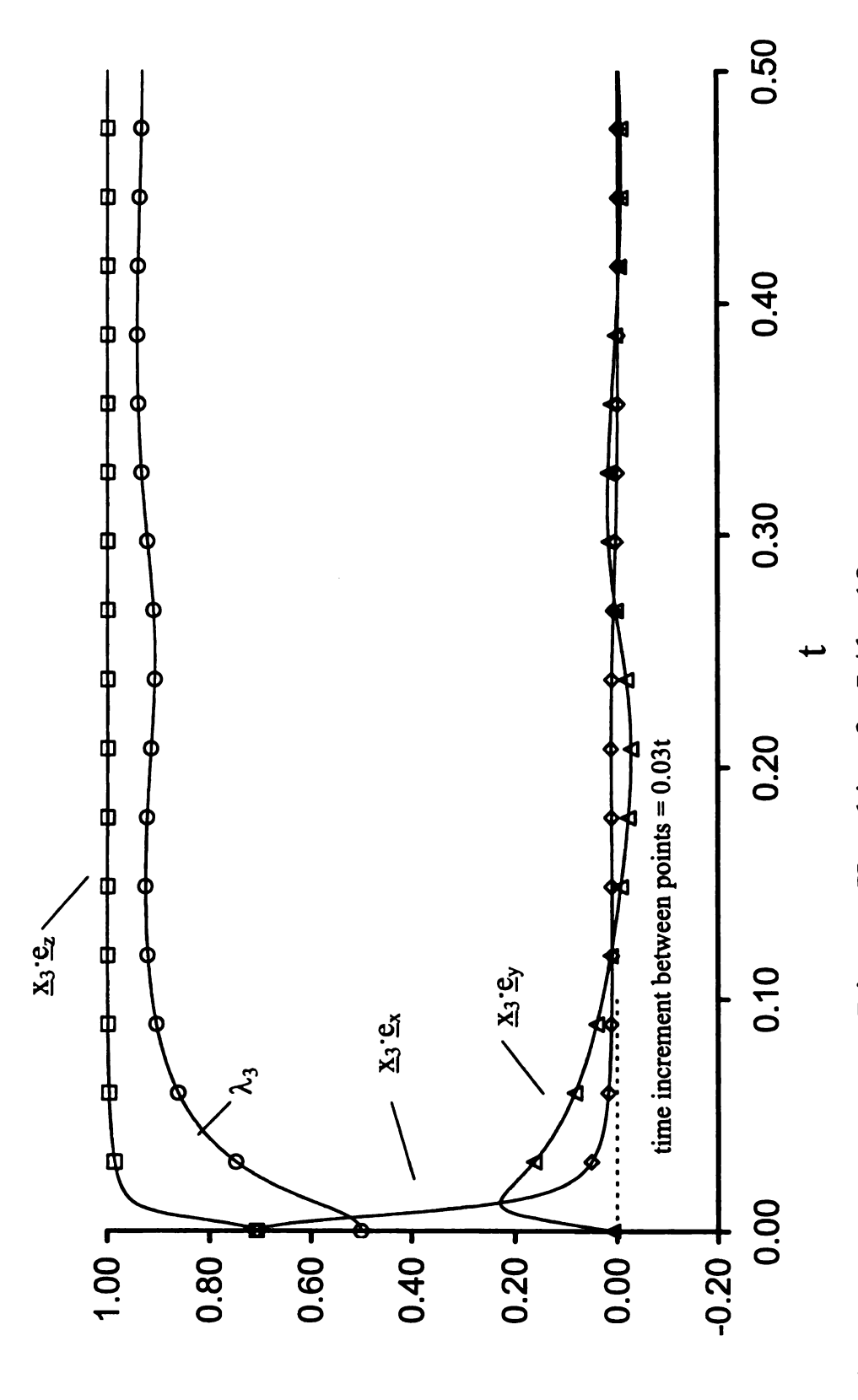
The dimensionless groups U, Pe, and  $\lambda$  are the same as the relaxation process illustrated by Figures 8.8 and 8.10 (i.e., U = 27, Pe = 95, and  $\lambda$  = 0.987). The initial condition for the eigenvalues and eigenvectors for  $\langle pp \rangle$  (0) are

$$\lambda_1(0) = 1/6, \quad \underline{\mathbf{x}}_1(0) = -\underline{\mathbf{e}}_{\mathbf{y}},$$

$$\lambda_2(0) = 2/6, \quad \underline{\mathbf{x}}_2(0) = \sqrt{2} (\underline{\mathbf{e}}_{\mathbf{x}} - \underline{\mathbf{e}}_{\mathbf{z}})$$

$$\lambda_3(0) = 3/6, \quad \underline{\mathbf{x}}_3(0) = \sqrt{2} (\underline{\mathbf{e}}_{\mathbf{x}} + \underline{\mathbf{e}}_{\mathbf{z}}).$$
(8.7)

As indicated by Figure 8.13, the director  $\underline{x}_3$  relaxes to a final steady state  $(\underline{x}_3(\infty) = \underline{e}_z)$  by executing a complex three dimensional motion wherein the "cross-flow" component of  $\underline{x}_3$  (i.e.,  $\underline{x}_3 \cdot \underline{e}_y$ ) first increases to a maximum and then decreases to a steady state (i.e.,  $\underline{x}_3(\infty) \cdot \underline{e}_y = 0$ ) by a damped oscillation through the vorticity/cross-flow plane. The "vorticity" component of  $\underline{x}_3$  (i.e.,  $\underline{x}_3 \cdot \underline{e}_x$ ) shows a monotonic decrease from its initial condition ( $\underline{x}_3(0) \cdot \underline{e}_x = \sqrt{2}$ ) to its final steady state ( $\underline{x}_3(\infty) \cdot \underline{e}_x < 0$ ). This relaxation process, which has been termed director kayaking, produces a microstructure with invariants  $II_b(\infty) = 0.546$ , and  $III_b(\infty) = 0.165$  (see p537, in Larson, 1999). Steady state component of  $< pp > (\infty)$  are



(FSQ-model; U = 27; Pe = 95;  $F_{TD} = 1$ ;  $\lambda = 0.987$ ). Figure 8.13 Instantaneous Director Kayaking for  $L/d \approx 12$ 

$$\langle \underline{p}\,\underline{p} \rangle (\infty) = 0.031 e_x e_x - 0.001 e_x e_y - 0.001 e_x e_z - 0.001 e_y e_x + 0.032 e_y e_y - 0.004 e_y e_z.$$

$$-0.001 e_z e_x - 0.004 e_z e_y - 0.937 e_z e_z$$
(8.8)

The eigenvalues and eigenvectors associated with  $\langle \underline{p} \underline{p} \rangle (\infty)$  are

$$\lambda_{1}(\infty) = 0.031, \ \underline{x}_{1}(\infty) = 0.998 \, \underline{e}_{x} + 0.065 \, \underline{e}_{y} + 0.052 \, \underline{e}_{z}$$

$$\lambda_{2}(\infty) = 0.032, \ \underline{x}_{2}(\infty) = 0.065 \, \underline{e}_{x} - 0.098 \, \underline{e}_{y} - 0.004 \, \underline{e}_{z}$$

$$\lambda_{3}(\infty) = 0.937, \ \underline{x}_{3}(\infty) = -0.001 \, \underline{e}_{x} - 0.004 \, \underline{e}_{y} + 0.997 \, \underline{e}_{z}$$
(8.9)

# 8.4 Relaxation of Planar Anisotropic States for $0 \le L/d < \infty$

Figure 8.14 shows relaxation of a planar anisotropic state with  $(\langle \underline{p}\,\underline{p}\rangle(0) = \frac{1}{3}\,\underline{e}_y\,\underline{e}_y + \frac{2}{3}\,\underline{e}_z\,\underline{e}_z)$  for  $\lambda = 0.5$ , U = 27, Pe = 95, and  $F_{TD} = 1$ . The director and its eigenvalue are periodic. One eigenvalue relaxes to a steady state. The other two eigenvalues fluctuate and the director tumbles in the deformation plane with a period  $\hat{t}_t \doteq 0.08/6D_R^o$ .

Figure 8.15 shows director tumbling for  $\lambda=0$ , U=27,  $F_{TD}=1$ , and Pe=95. The director tumbles 180° with period of  $\hat{t}_t \doteq 0.07/6D_R^0$ . However, for this case the invariants of the structure tensor and the eigenvalues of  $\langle \underline{p}\,\underline{p} \rangle$  relax to steady state values with a microstructure on the prolate boundary ( $\Pi_b(\infty)=0.551$ ,  $\Pi_b(\infty)=0.167$ ). For this case ( $\lambda=0$ ), asymptotic solutions to Eq.(4.1) split into two contributions: 1) solid body rotation; and, 2) a steady state microstructure that exactly balances the Brownian torque and the torque due to the excluded volume potential. It is noteworthy that  $\Pi_b(\infty)$ 

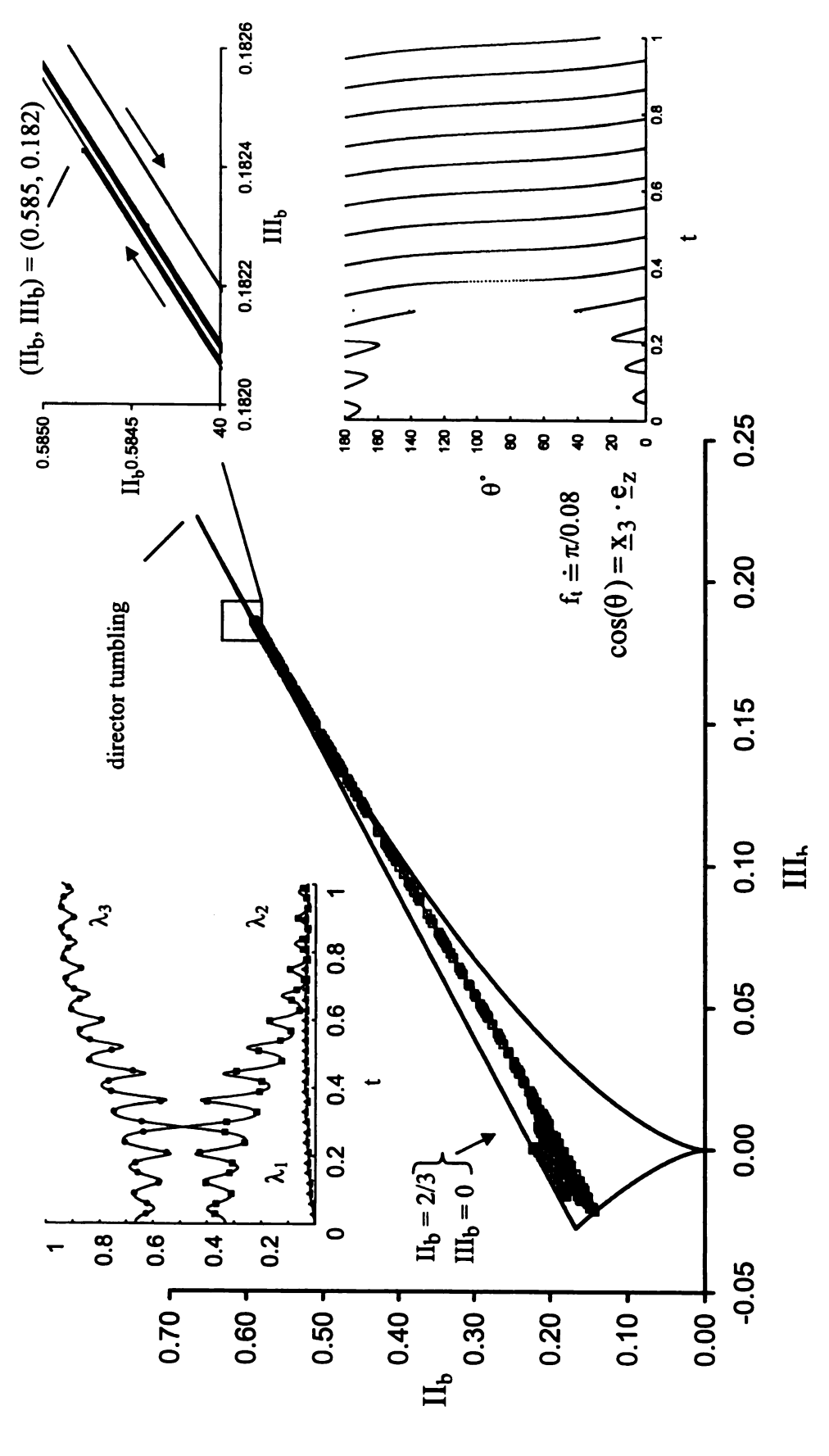


Figure 8.14 Microstructures for Director Tumbling and Steady State Alignment in the Phase Plane (FSQ-model;  $F_{TD} = 1$ ;  $\lambda = 0.5$ ; U = 27, Pe = 95;  $2 < \underline{p}\,\underline{p} > (0) = \underline{e}_y\,\underline{e}_y + \underline{e}_z\,\underline{e}_z$  ).

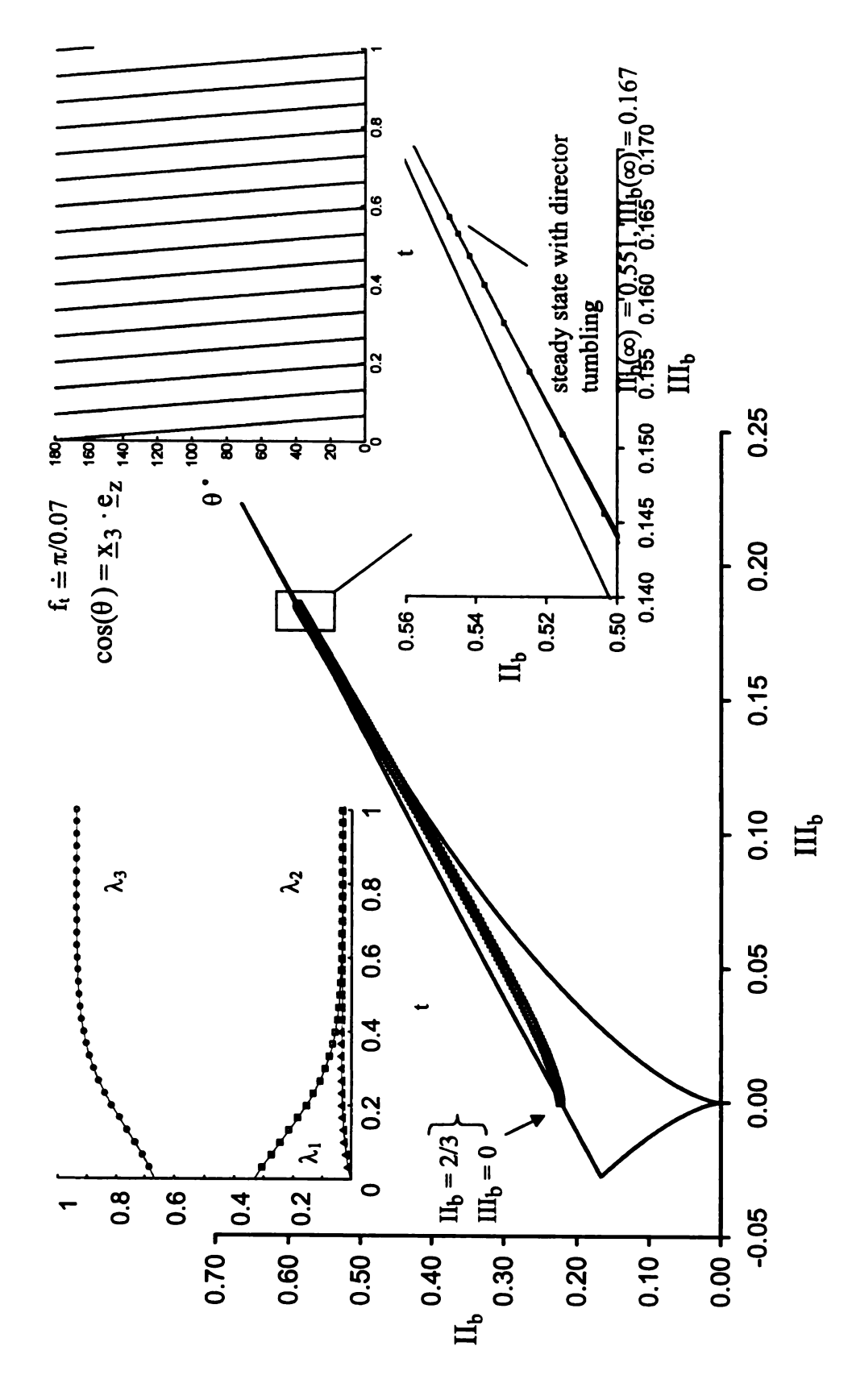


Figure 8.15 Microstructures for Director Tumbling and Steady State Alignment in the Phase Plane (FSQ-model;  $F_{TD} = 1$ ;  $\lambda = 0$ ; U = 27, Pe = 95;  $2 < \underline{p} \, \underline{p} > (0) = \underline{e}_y \, \underline{e}_y + \underline{e}_z \, \underline{e}_z$ 

and III<sub>b</sub> ( $\infty$ ) are the same as shown in Table 7.1, for U = 27, Pe = 95, and  $\lambda$  = 0 and for as well as U = 27, Pe = 0,  $\lambda$  = 1. For  $\lambda$  = 0, U = 0, and F<sub>TD</sub> = 1, Eq.(4.1) reduces to

$$\frac{\partial \langle \underline{p}\underline{p} \rangle}{\partial t} \bigg|_{\underline{X}} + \text{Pe} \left[ \underline{\underline{W}}^{\text{T}} \cdot \langle \underline{p}\underline{p} \rangle + \langle \underline{p}\underline{p} \rangle \cdot \underline{\underline{W}} \right] = \frac{1}{3} \underline{\underline{I}} - \langle \underline{p}\underline{p} \rangle. \tag{8.10}$$

For Pe = 95, Figure 8.16 shows the relaxation of the invariants of the structure tensor  $\frac{b}{b} (\equiv -\frac{1}{3} I)$  to the isotropic state. The director tumbles with a period  $\hat{t}_t = 0.07/6D_R^0$ , which is the same dynamic response as  $\lambda = 0$ , U = 27, and Pe = 95 (see Figure 8.15). Figures 8.15 and 8.16 support the idea that the asymptotic solutions to Eq.(4.1) for  $\lambda = 0$  splits into a solid body rotation and a steady state axisymmetric prolate microstructure on the F-boundary of Figure 1.1.

For U=27, Pe=10, and  $F_{TD}=1$ , Table 8.2 shows that the dimensionless tumbling period decreases as  $\lambda$  decreases. Larson noted that the tumbling period  $t_t \sim L/d$ . Table 8.2 shows the relation of  $t_t \sim (L/d)^{2/3}$  for  $0 < \lambda < 0.91$ , but as  $\lambda \to 1$ ,  $t_t \to \infty$ .

# 8.5 The Effect of Tube Dilation on the Relaxation of Planar Anisotropic States

Figure 8.17 shows the effect of tube dilation on the microstructure for  $\lambda = 0.987$ . The phase transition between steady alignment and tumbling for fixed Pe is the same as Figure 8.9 (i.e., U = 26), but the tumbling and wagging regions are extended to larger values of Pe. This occurs because the diffusive flux becomes larger inasmuch as  $F_{TD}^{Doi} \rightarrow \infty$  as  $II_b \rightarrow 3/2$ .

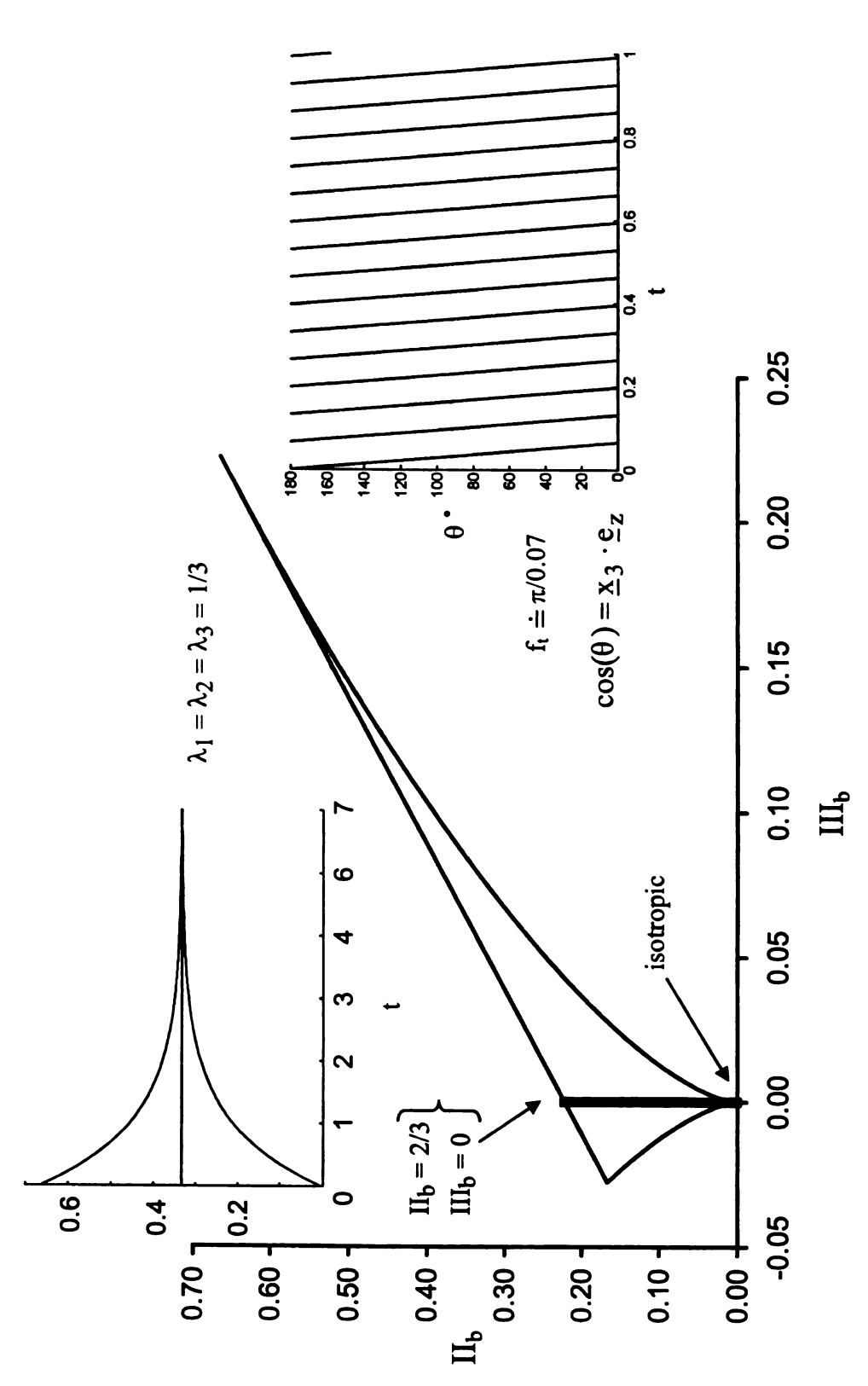
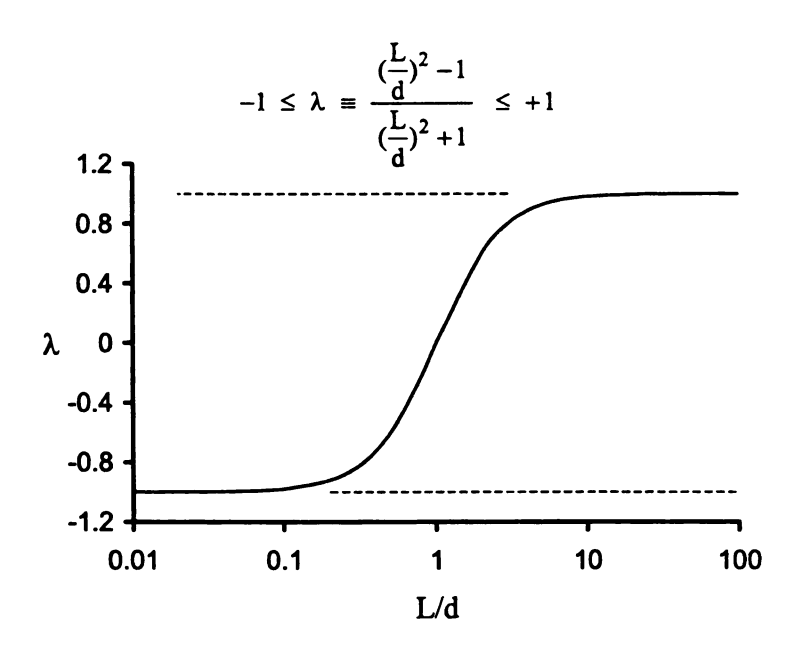
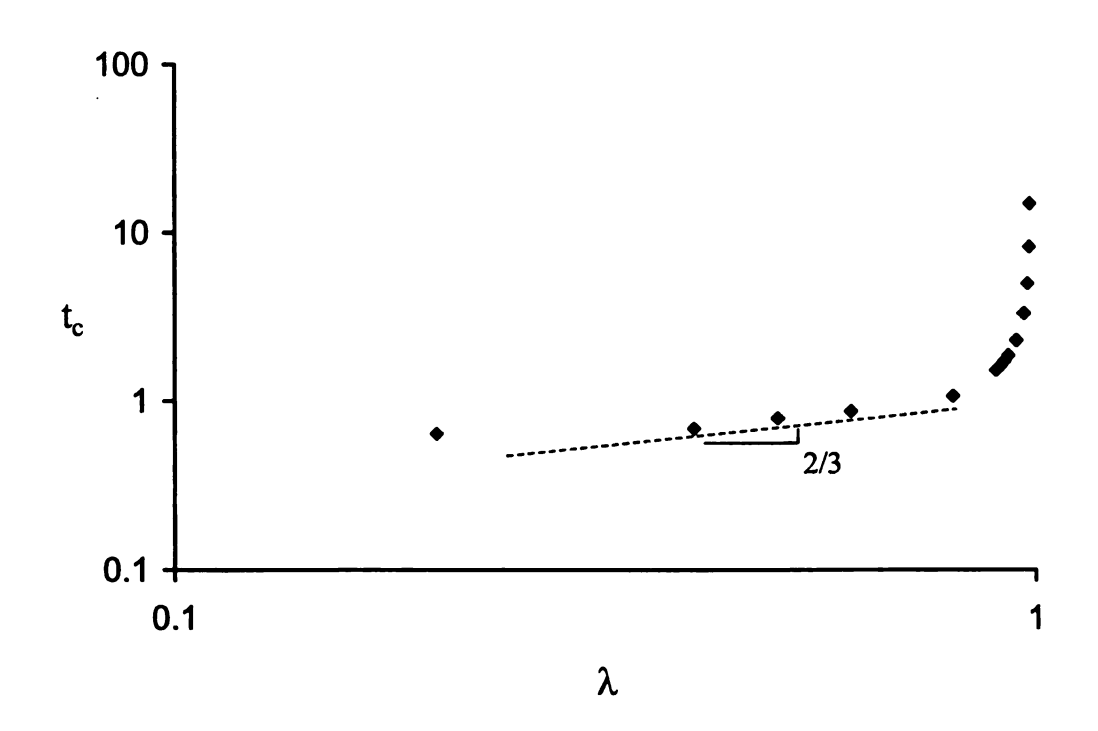


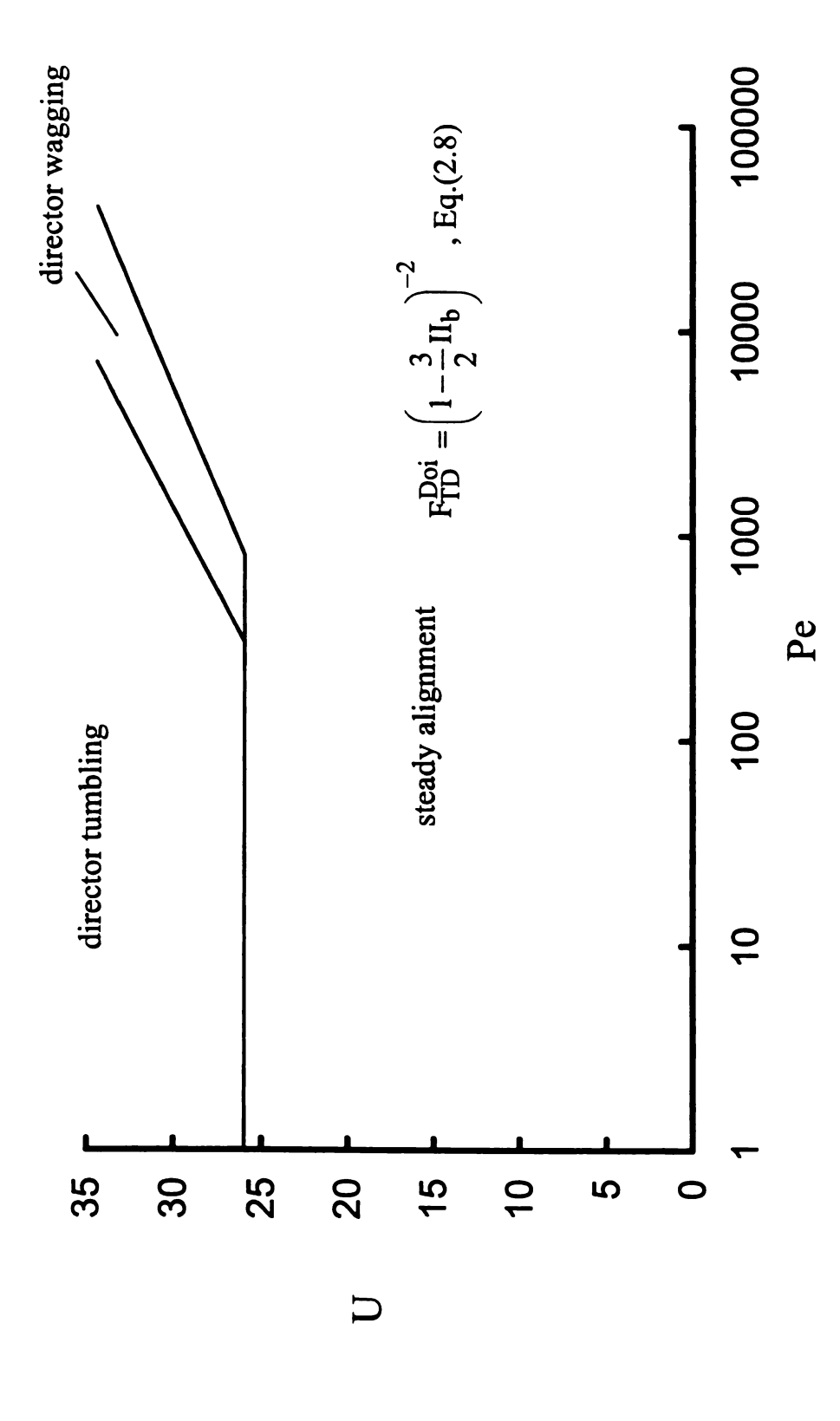
Figure 8.16 Microstructures for Director Tumbling and Steady State Alignment in the Phase Plane (FSQ-model;  $F_{TD} = 1$ ;  $\lambda = 0$ ; U = 0, Pe = 95;  $2 < \underline{p}\,\underline{p} > (0) = \underline{e}_y\,\underline{e}_y + \underline{e}_z\,\underline{e}_z$ ).

Table 8.2 The Effect of  $\lambda$  on the Tumbling Period (FSQ-model;  $F_{TD} = 1$ ; U = 27; Pe = 10)

λ	$t_t \equiv 6D_R^{\circ} \hat{t}_t$		
1	∞		
0.987	14.883		
0.985	8.232		
0.980	4.983		
0.970	3.312		
0.950	2.286		
0.930	1.858		
0.920	1.720		
0.910	1.610		
0.900	1.520		
0.800	1.068		
0.500	0.913		
0.600	0.790		
0.400	0.687		
0.200	0.641		
0.000	0.628		







(FSQ-model;  $F_{TD}^{Doi} = 1$ ;  $\lambda = 0.987$ ;  $2 < \underline{p} \, \underline{p} > (0) = \underline{e}_y \, \underline{e}_y + \underline{e}_z \, \underline{e}_z$ Figure 8.17 The Effective of Tube Dilation on the Phase Diagram

#### 8.6 Discussion

The microstructure of the orientation dyad, which is induced by a homogeneous shear, has four independent variables: U; Pe;  $\lambda$ ; and, the initial state of the orientation dyad. Figures 8.2 and 8.15 show that the nematic potential U influences the axisymmetric orientation state (the prolate state) regardless of director tumbling. For Pe > 0 and  $\lambda = 1$ , the microstructure is anisotropic and inside the invariant diagram. For large values of U and Pe, the orientation states are near the nematic state.

The tumbling parameter  $\lambda$  influences the periodic orientation state and its period. For  $\lambda=1$ , the orientation states are steady states. For  $\lambda<1$ , periodic orientation states occur. Table 8.2 shows that reducing  $\lambda$  reduces the tumbling period. Eq.(4.1) has four physical features that determine the orientation state: vorticity, Brownian motion, nematic, and strain contributions. The vorticity contribution tends to have periodic rotation, but the strain contribution hinders its motion. For U < 26, the nematic contribution is not large enough to reduce the strain contribution (steady alignment). For U > 26 with  $\lambda<1$ , the director tumbling occurs at low value of Pe because the vorticity contribution becomes larger than the strain rate term. However, for large values of Pe, the strain rate contribution regains its strength (steady alignment) (see Figure 8.9). If the strain rate contribution is reduced by  $\lambda$  (Figure 8.14 and 8.15), director tumbling occurs for even larger values of Pe.

The HL1-closure approximation predicts tumbling phenomenon with  $\lambda = 1$ . According to Chaubal (1995), the decoupling approximation used by Doi and others can also predict tumbling phenomenon (Chaubal and Leal, 1997, 1998; Chaubal et al. 1995) provided the flow field is modified. The results developed in this chapter shows that

Doi's theory predicts director tumbling for homogenous shear provided  $\lambda < 1$  (see Figure 11.3).

The log-rolling and kayaking phenomena have been predicted by other closure models (Chaubal et al. 1995; Faraoni et al. 1999; Larson and Öttinger 1991). FSQ-closure also predicts director tumbling, log-rolling, and kayaking. As demonstrated in this chapter, the *realizable* FSQ-closure also predicts log-rolling, and kayaking by the director as well as the existence of multiple steady states for Pe > 0.

## **CHAPTER 9**

## VISCOSITY AND NORMAL STRESS DIFFERENCES

## 9.1 Introduction

For homogenous shear flow, the deviatoric stress has three nontrivial normal components and two non trivial shear components:  $\hat{\underline{\tau}} : \underline{e}_x \underline{e}_x$ ,  $\hat{\underline{\tau}} : \underline{e}_y \underline{e}_y$ ,  $\hat{\underline{\tau}} : \underline{e}_z \underline{e}_z$ ,  $\hat{\underline{\tau}} : \underline{e}_y \underline{e}_z$  =  $\hat{\underline{\tau}} : \underline{e}_z \underline{e}_y$ . In this chapter, the effect of the tumbling parameter  $\lambda$ , the excluded volume coefficient U, and the Péclet number Pe on the viscosity, the first normal stress difference, and the second normal stress difference will be developed by using Doi's theory for the stress (see Eqs.(4.8)) and the FSQ-closure for the orientation tetrad (see Eqs.(5.8) and (6.12)). The dimensional rheological properties are defined as follows: *viscosity* 

$$\hat{\eta} \equiv \frac{\hat{\mathbf{r}} : \mathbf{e}_z \mathbf{e}_y}{\dot{\gamma}}, \tag{9.1}$$

first normal stress difference

$$\hat{N}_1 = \hat{\tau} : (\underline{e}_z \underline{e}_z - \underline{e}_y \underline{e}_y), \tag{9.2}$$

second normal stress difference

$$\hat{N}_2 = \hat{\underline{\tau}} : (\underline{e}_{\mathbf{v}} \underline{e}_{\mathbf{v}} - \underline{e}_{\mathbf{z}} \underline{e}_{\mathbf{z}}). \tag{9.3}$$

The objective is to access the impact of the realizable FSQ-closure on the rheological properties of rigid rod suspensions.

# 9.2 Rheological Properties: $L/d = \infty$

## Shear Viscosity

Figure 9.1 shows the effect of the excluded volume coefficient U and the Péclet number,  $Pe = \dot{\gamma}/(6D_R)$ , on the steady state shear viscosity due to the viscous and elastic components of Doi's stress for the realizable FSQ-closure (see Eq.(4.8)):

$$\eta - \eta_S \equiv (\hat{\eta} - \hat{\eta}_S) \frac{6D_R}{3ck_BT} = F(U, Pe) , \quad 0 \le U < \infty , \quad 0 \le Pe < \infty.$$
 (9.4)

The theory predicts the existence of a Newtonian plateau for low shear rates (i.e.,  $\dot{\gamma} < 60 \, D_R$ ) and a shear-thinning region for high strain rates (i.e.,  $\dot{\gamma} > 600 \, D_R$ ). For large Pe, Figure 9.1 shows that the shear viscosity becomes independent of U for large Pe:

$$\eta - \eta_s \equiv F(U, Pe) \xrightarrow{Pe \to \infty} 0.18 \, Pe^{-3/5}. \tag{9.5}$$

PBLG in m-cresol solution and PBZT in methane sulfonic acid solution, which are lyotropic LCPs, also show shear thinning phenomena at large strain rates with  $n \cong -1/3$  and  $n \cong -3/4$ , resp. (see, p.286 and p.510 in Larson, 1999).

For low values of Pe, the shear viscosity becomes independent of Pe (i.e., Newtonian plateau) but still depends on U. Figure 9.1 shows that

$$\lim_{Pe \to 0} F(U, Pe) = 0.01 + \frac{0.25}{1 + 1.17 U}.$$
 (9.6)

For dilute suspensions,  $D_R$  is independent of concentration (i.e.,  $D_R \to D_R^0$ ) and  $U \ll 1$ . Therefore, Eq.(9.4) and Eq.(9.6) predict that  $\Delta \hat{\eta}_o \propto c$ , which is consistent with experiments and other theoretical predictions for rigid rod suspensions and LCPs (see p.281 in Larson, 1999).

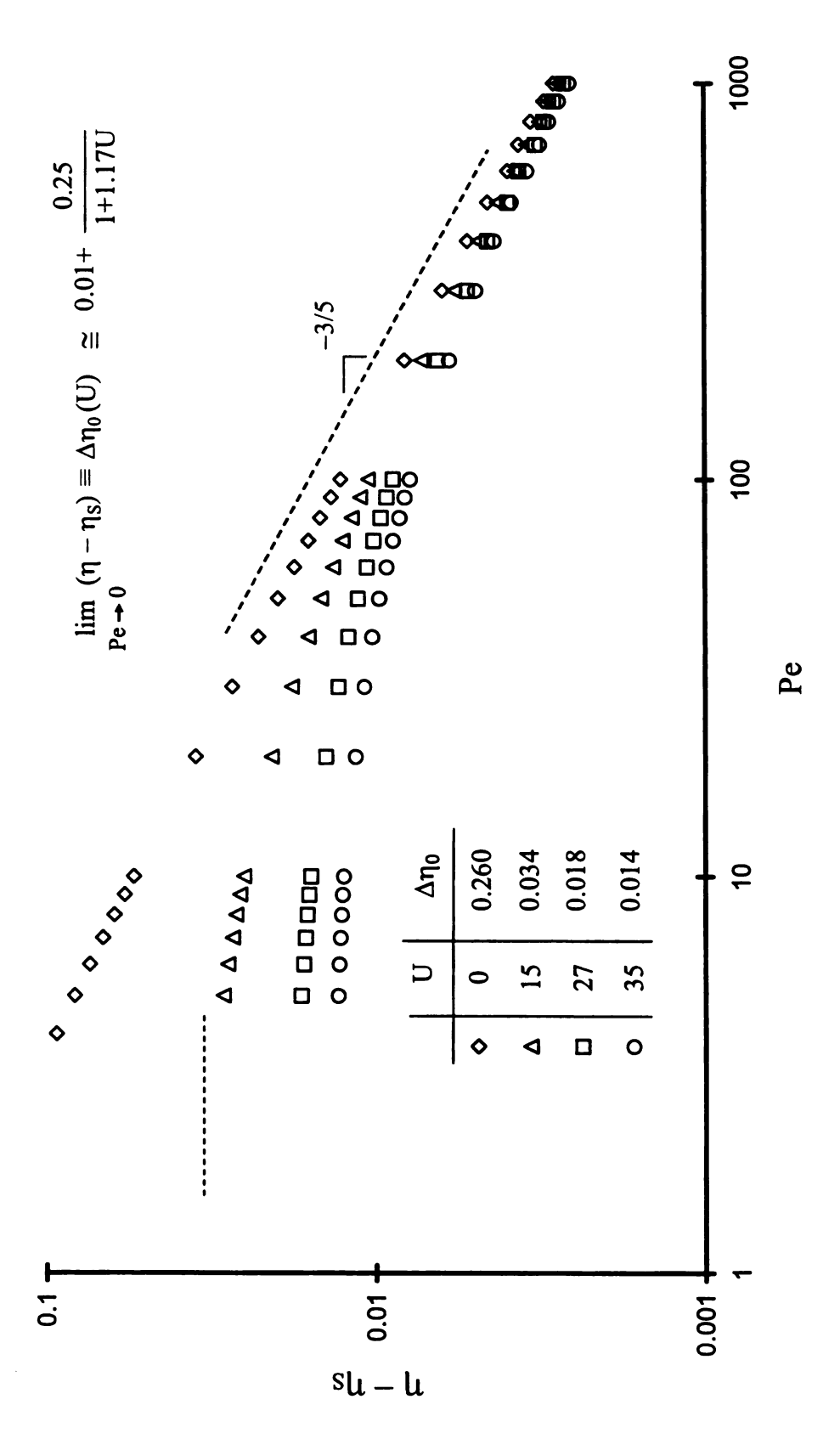


Figure 9.1 The Effect of U and Pe on the Shear Viscosity for L/d =  $\infty$ (FSQ-model;  $F_{TD} = 1$ ;  $\lambda = 1$ ).

As the concentration increases, U becomes large and  $D_R \propto c^{-2}$  (see p.287 and p. 520 in Larson, 1999). Under these conditions, Eq.(9.4) indicates that  $\Delta \hat{\eta}_o \propto c^3 / U$  for "concentrated" suspensions. For "high" concentrations of PBLG in m-cresol (i.e., > 0.5 wt%), Mead and Larson (see p. 290 in Larson, 1999) observed that the zero-shear rate viscosity increases with concentration as  $\Delta \hat{\eta}_o \propto c^3$ . Thus, Eq.(9.6) and the foregoing experimental observation imply that U becomes independent of concentration for semi-dilute and concentrated suspensions. For dilute suspensions, U \pi c (see p.66 in Larson, 1999).

Figure 9.2 shows how the viscous and elastic contributions to the shear viscosity (i.e.,  $\Delta \hat{\eta} \equiv \hat{\eta} - \hat{\eta}_S = \hat{\eta}_V + \hat{\eta}_E$ ) depend on Pe for U = 0 and U = 27. For the stress model used herein (see Eqs.(4.6) and (4.8)),  $\hat{\eta}_V$  and  $\hat{\eta}_E$  are defined as follows:

$$\hat{\eta}_{V} = \frac{\hat{\tau}_{yz}^{V}}{\dot{\gamma}} = \frac{c\zeta_{R} < p_{y}p_{z}\underline{p}\underline{p} >: \underline{\underline{S}}}{\|\underline{S}\|}$$

$$(9.7)$$

and

$$\hat{\eta}_{E} \equiv \frac{\hat{\tau}_{yz}^{E}}{\dot{\gamma}} = \frac{3c k_{B} T \left[ \langle p_{y} p_{z} \rangle - U \left( \langle p_{y} \underline{p} \rangle \cdot \langle \underline{p} p_{z} \rangle - \langle p_{y} p_{z} \underline{p} \underline{p} \rangle \cdot \langle \underline{p} p_{z} \rangle \right]}{\left\| \underline{\underline{S}} \right\|}.$$
 (9.8)

In the above equations,  $c\zeta_R$  represents the viscous drag coefficient between the rod and the suspending fluid per unit volume of mixture and has units of viscosity (force-time/area). The parameter  $3ck_BT$  has units of energy per unit volume of mixture, and  $c\zeta_R$  is related to  $3ck_BT$  and the rotary diffusion coefficient  $D_R$  as follows

$$c\zeta_{R} = \frac{3ck_{B}T}{6D_{R}}.$$
(9.9)

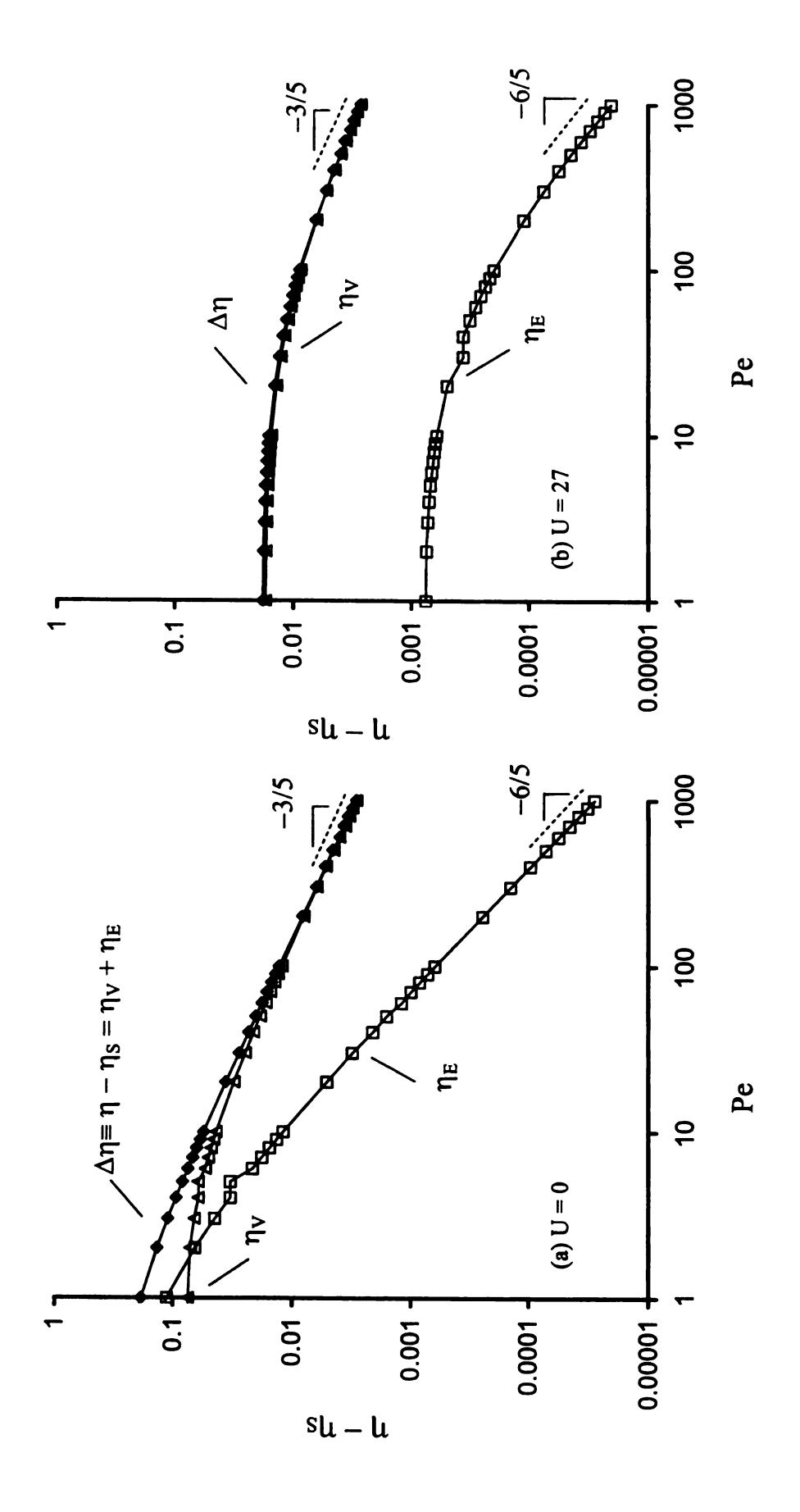


Figure 9.2 The Effect of U and Pe on the Viscous and Elastic Components of the Shear Viscosity for L/d =  $\infty$  (FSQ-model;  $F_{TD} = 1$ ;  $\lambda = 1$ ).

Bachelor developed Eq.(9.9) for dilute suspensions of slender rods (see p. 284 in Larson, 1999). This parameter is used to scale the viscosity coefficients:  $\eta_V = \hat{\eta}_V/c\zeta_R$  and  $\eta_E = \hat{\eta}_E/c\zeta_R$ . For Pe > 50, Figure 9.2a and 9.2b show that the shear viscosity is primarily due to the viscous stress; however, for Pe << 5, the elastic stress becomes more important although the viscous contribution remains significant ( $\eta_V$  is approximately 25% of  $\Delta\eta$  at Pe = 0.1).

For U = 0, the elastic stress is due to Brownian motion. For U > 0, the excluded volume phenomenon mitigates rotary Brownian motion. With U = 27, Figure 9.3 shows that the elastic stress does not contribute significantly to the viscosity because rotary Brownian motion is balanced by counter diffusion due to the excluded volume potential.

For low values of Pe, both the viscous and the elastic components of the viscosity are approximately independent of the strain rate (i.e., Newtonian plateau, NP); therefore, Eqs.(9.7) and (9.8) imply that in this region

$$\langle p_{y}^{2} p_{z}^{2} \rangle \Big|_{NP} = \frac{\hat{\eta}_{V}|_{NP}}{c \zeta_{R}} \neq f(\|\underline{\underline{S}}\|)$$

$$(9.10)$$

$$\left[ \langle p_{y}p_{z} \rangle - U \left( \langle p_{y}\underline{p} \rangle \cdot \langle \underline{p}p_{z} \rangle - \langle p_{y}p_{z}\underline{p}\underline{p} \rangle : \langle \underline{p}\underline{p} \rangle \right) \right]_{NP} \propto \left\| \underline{\underline{S}} \right\|. \tag{9.11}$$

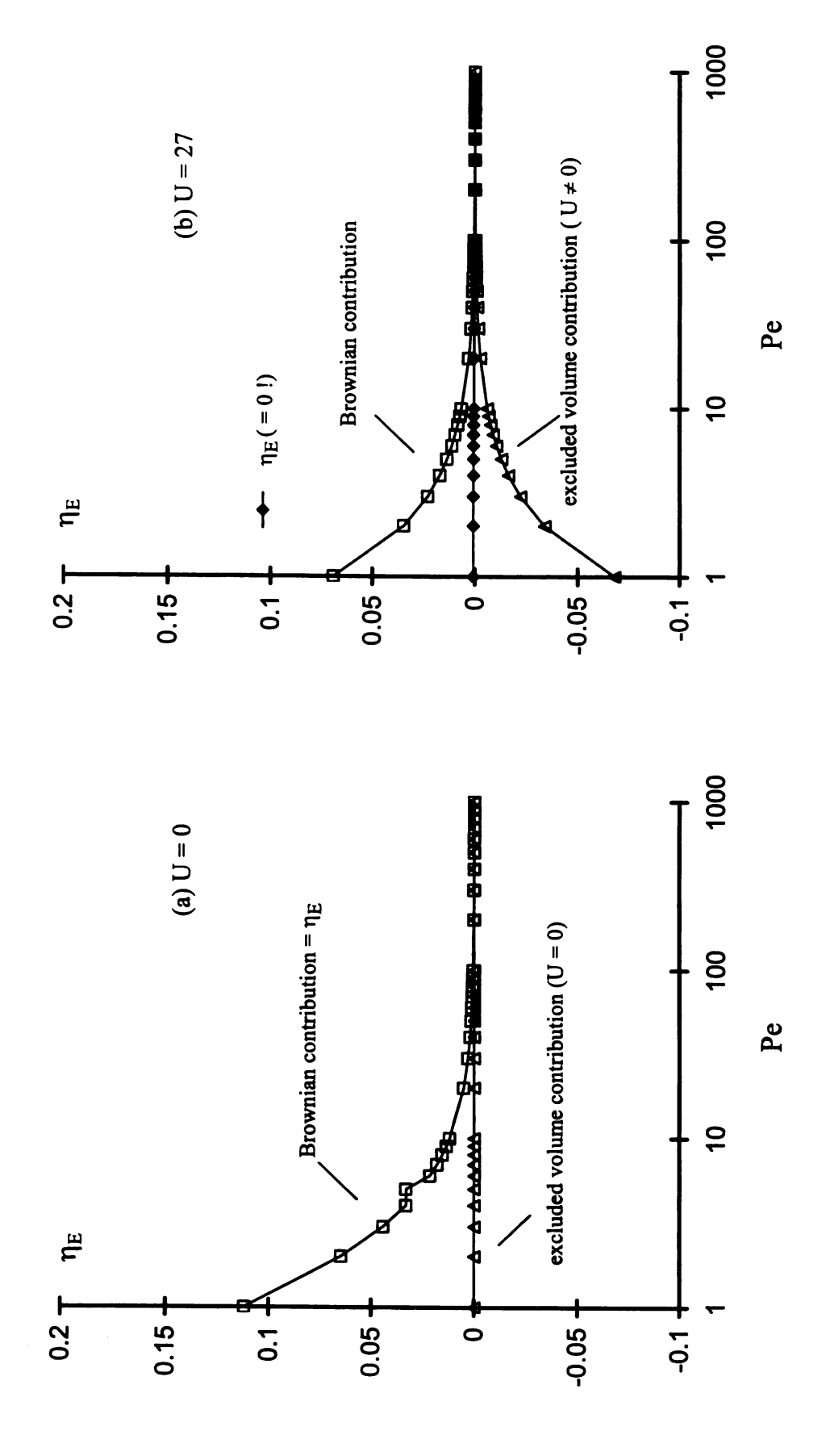
For U = 0 and large Pe, Eq.(9.7), Eq.(9.8), and Figure 9.2a imply that

$$\lim_{Pe \to \infty} \langle p_y^2 p_z^2 \rangle \propto \|\underline{S}\|^{-3/5}$$
 (9.12)

$$\lim_{\mathsf{Pe}\to\infty} \langle \mathsf{p}_{\mathsf{y}}\mathsf{p}_{\mathsf{z}} \rangle \propto \|\underline{\mathsf{S}}\|^{-1/5}. \tag{9.13}$$

For U = 27 and large Pe, Eq.(9.7) and Figure 9.2b imply that

$$\lim_{Pe \to \infty} \langle p_y^2 p_z^2 \rangle \propto \|\underline{S}\|^{-3/5}, \tag{9.14}$$



the Shear Elastic Component of the Viscosity for L/d =  $\infty$  (FSQ-model;  $F_{TD} = 1$ ;  $\lambda = 1$ ). Figure 9.3 The Effect of U and Pe on the Brownian and Excluded Volume Contributions to

which is the same as Eq.(9.12). It also follows from Figure 9.2b and Eq.(9.5) that

$$\lim_{\mathrm{Pe}\to\infty} \left[ \langle p_{y}p_{z} \rangle - U(\langle p_{y}\underline{p} \rangle \cdot \langle \underline{p}p_{z} \rangle - \langle p_{y}p_{z}\underline{p}\underline{p} \rangle : \langle \underline{p}\underline{p} \rangle) \right] \propto \|\underline{\underline{S}}\|^{-1/5}. \tag{9.15}$$

The effect of U and Pe on the elastic contribution of  $\hat{\underline{t}} : \underline{e}_z \underline{e}_y$  is shown in Figure 9.4. If  $U \cong 0$  for dilute and semi-dilute solution, then Doi's shear stress for the elastic contribution can be approximated by the Brownian motion contribution of stress (see p.308 and p.338, Doi and Edward, 1986; and, Smyth et al., 1995). Thus, with U = 0, Eq.(9.8) implies that

$$\hat{\tau}_{yz}^{E} \mid_{U=0} = 3nk_{B}T < p_{y}p_{z} > \tag{9.16}$$

Figure 9.4 shows that the general trend of total elastic contribution, predicted by Doi's shear stress depends on U and Pe. Smyth et al. (1995) used a birefringence method to estimate the elastic contribution to the shear stress for semi-dilute solutions of xanthan gum (L = 1440 nm and L/d 660) in fructose solvent ( $\eta_S$  = 0.483 Pa-s). They used Eq.(9.16) to relate the stress to the microstructure. For limited range of shear rates, their experimental data indicated that  $\hat{\tau}^E_{yz} \propto (\hat{\gamma})^{1/3}$ . Figure 9.4 shows that these experiments are consistent with the Doi theory with a realizable FSQ-closure provided U = 5 and 0.2 < Pe < 2 (i.e.,  $1.2\,D_R^o < \hat{\gamma} < 12\,D_R^o$ ). The strain rates in the Smyth/Mackay experiments covered the range  $1s^{-1} < \hat{\gamma} < 20s^{-1}$ . Therefore a combination of Doi's theory and the experimental observations gives the following estimate  $D_R^o \cong 1.3\,s^{-1}$ . For U = 0, the elastic stress makes a significant contribution to the total stress for Pe < 100.

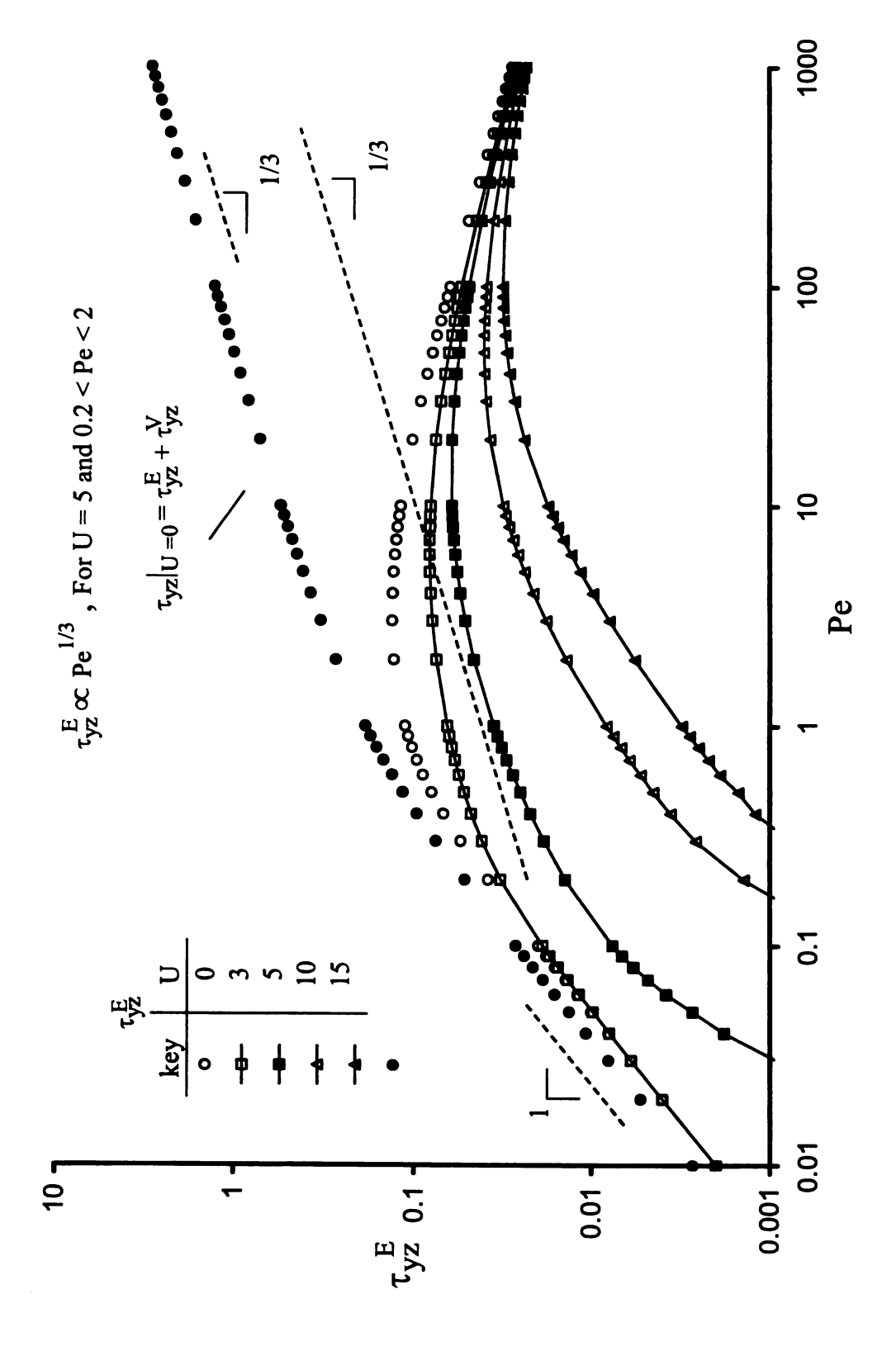


Figure 9.4 Elastic Contributions to the Shear Stress (FSQ-model;  $\lambda = 1$ ;  $F_{TD} = 1$ )

#### Normal Stress Differences

Figure 9.5 shows that  $N_1$  is positive for  $10^{-1} \le Pe \le 10^3$  and  $0 \le U \le 35$ . For large values of Pe,  $N_1 \propto Pe^{3/5}$ . For small values of Pe,  $N_1 \propto Pe$ . These results are consistent with the experimental measurements of Zirnsak et al. (see p. 295 in Larson, 1999) for glass fibers suspended in Newtonian fluids and with experimental measurements of Kim and Han (see p. 513 in Larson, 1999) for thermotropic polyesters, OQO (phenylsulfonyl) 10. By contrast, at low Péclet numbers,  $N_1 \propto Pe^2$  for isotropic viscoelastic fluids (see p. 450 in Larson, 1999).

For a fixed value of Pe, Figure 9.5 also shows that the first normal stress difference decreases as the excluded volume coefficient U increases. This occurs because counter diffusion due to the excluded volume effect balances rotary Brownian motion for sufficiently large values of U (see Table 9.1). For  $U \rightarrow \infty$  at low Pe,  $N_1$  is primarily determined by the viscous stress. This prediction is qualitatively supported by the thermotropic polyester experiments mentioned of Kim and Han (1993) above inasmuch as  $N_1$  increases with an increase in molecular weight. In an earlier study of PBLG solutions (lyotropic LCP), Robinson (1965) observed that the critical concentration corresponding to a transition from an isotropic to a nematic state decreases with an increase in molecular weight. Therefore, if U decreases as the molecular weight increases, it follows that Figure 9.5 is qualitatively consistent with trends observed for both thermotropic and lyotropic LCPs.

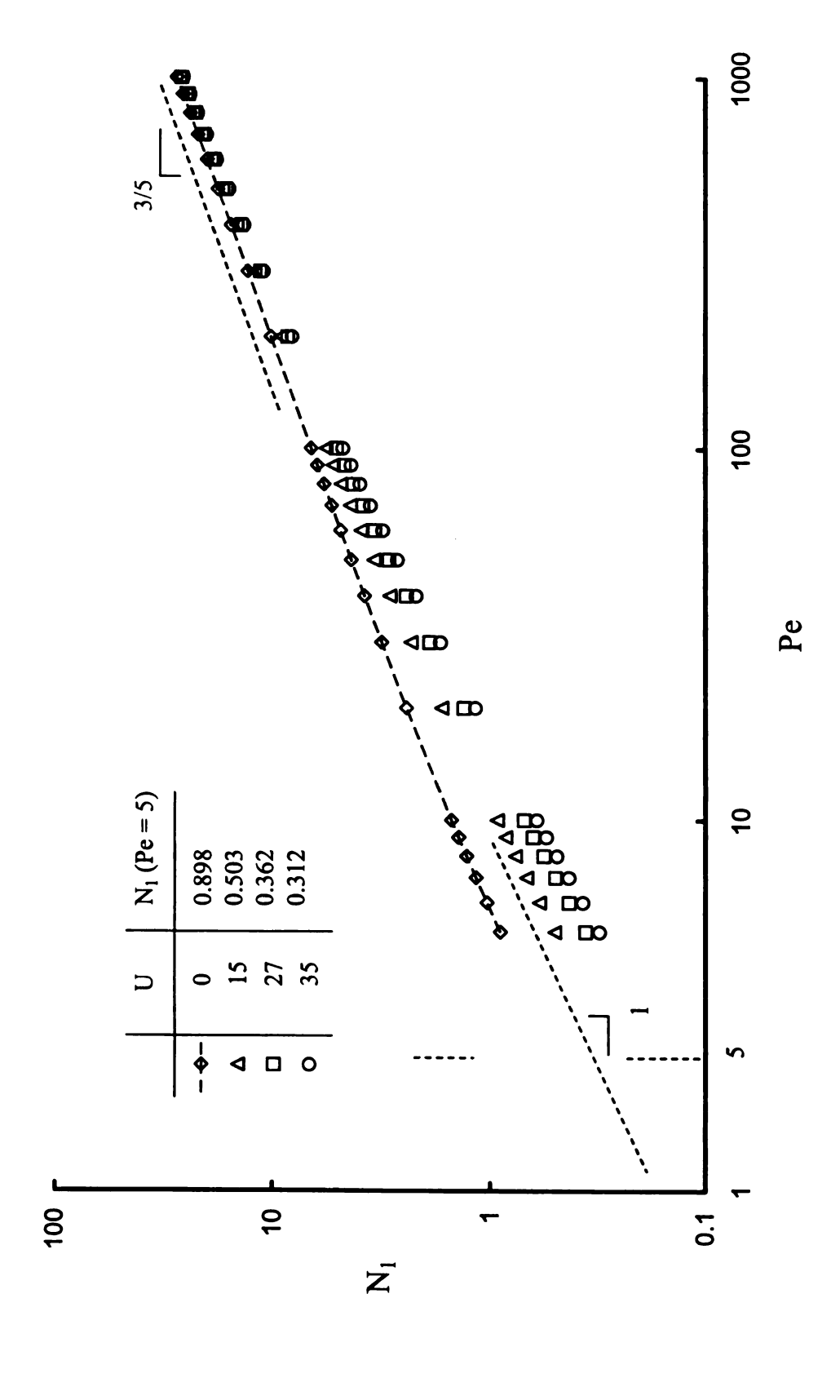


Figure 9.5 The Effect of U and Pe on the First Normal Stress Difference for L/d =  $\infty$ (FSQ-model;  $F_{TD} = 1$ ;  $\lambda = 1$ ).

Table 9.1 Viscous and Elastic Contributions to the Shear Viscosity and the First and Second Normal Stress Differences at Selected Values of U and Pe for  $L/d = \infty$ 

Property	Pe	U	Total	Viscous	Elastic		
					Total	Brownian	Excluded Volume
η-η <sub>s</sub>	5	0	0.0761	0.0374	0.0387	0.0387	0
		15	0.0295	0.0272	0.0023	0.0180	-0.0157
		27	0.0122	0.0109	0.0013	0.0208	-0.0195
	1,000	0	0.0019	0.0019	0.0000+	0.0000+	0
		15	0.0028	0.0028	0.0000+	0.0000+	0.0000+
		27	0.0017	0.0017	0.0000+	0.0000+	0.0000+
N <sub>1</sub>	5	0	0.8928	0.4011	0.4972	0.4972	0
		15	0.5027	0.3965	0.1062	0.8337	-0.7274
		27	0.3619	0.3160	0.0459	0.9040	-0.8581
	1,000	0	28.487	27.515	0.9717	0.9717	0
		15	27.675	26.840	0.8351	0.9756	-0.1405
		27	27.016	26.267	0.7488	0.9780	-0.2292
N <sub>2</sub>	5	0	-0.0420	0.0420	-0.0840	-0.0840	0
		15	-0.0159	0.0159	-0.0318	0.0037	-0.0355
		27	-0.0071	0.0071	-0.0142	0.0037	-0.0179
	1,000	0	-0.0055	0.0055	-0.0110	-0.0110	0
		15	-0.0294	0.0294	-0.0588	-0.0076	-0.0512
		27	-0.0394	0.0394	-0.0788	-0.0059	-0.0729

Unlike  $N_1$ , Figure 9.6 shows that  $N_2 < 0$  for  $10^{-1} \le Pe \le 10^3$  and  $0 \le U \le 35$ . As expected, the magnitude of the second normal stress difference is significantly smaller than the first normal stress difference ( $|N_2| \le |N_1|/200$ ). The calculations support the conclusion that  $|N_2|/|N_1| \to 0$  for  $Pe \to 0$  and  $Pe \to \infty$ . Note that for  $Pe \cong 100$ ,  $|N_2| \le |N_1|/100$  for U = 35 and decreases to  $|N_2| \le |N_1|/250$  for U = 0. For a fixed value of U, the second normal stress difference increases in magnitude as Pe increases, but reaches a maximum for an intermediate value of Pe. For large values of U (i.e., U > 15),  $|N_2|$  occurs at  $Pe \cong 200$ . For  $Pe \cong 10$  and  $Pe \cong 10$  and  $Pe \cong 10$  and  $Pe \cong 10$  increases as U increases; however, for  $Pe \cong 500$ ,  $|N_2|$  increases as U increases. Coincidently, for  $Pe \cong 500$  and  $Pe \cong$ 

Figure 9.7 shows the contribution of normal stress differences with  $F_{TD} = 1$ ,  $\lambda = 0.987$ , and U = 27. For Pe > 10, the viscous contribution to  $N_1$  becomes dominant, though the elastic contribution is increasing (see Table 9.1). On the other hand, the elastic contribution to  $N_2$  is more important than the viscous contribution. Table 9.1 shows that the elastic contribution of  $N_2$  is nearly twice as larger as the viscous contribution

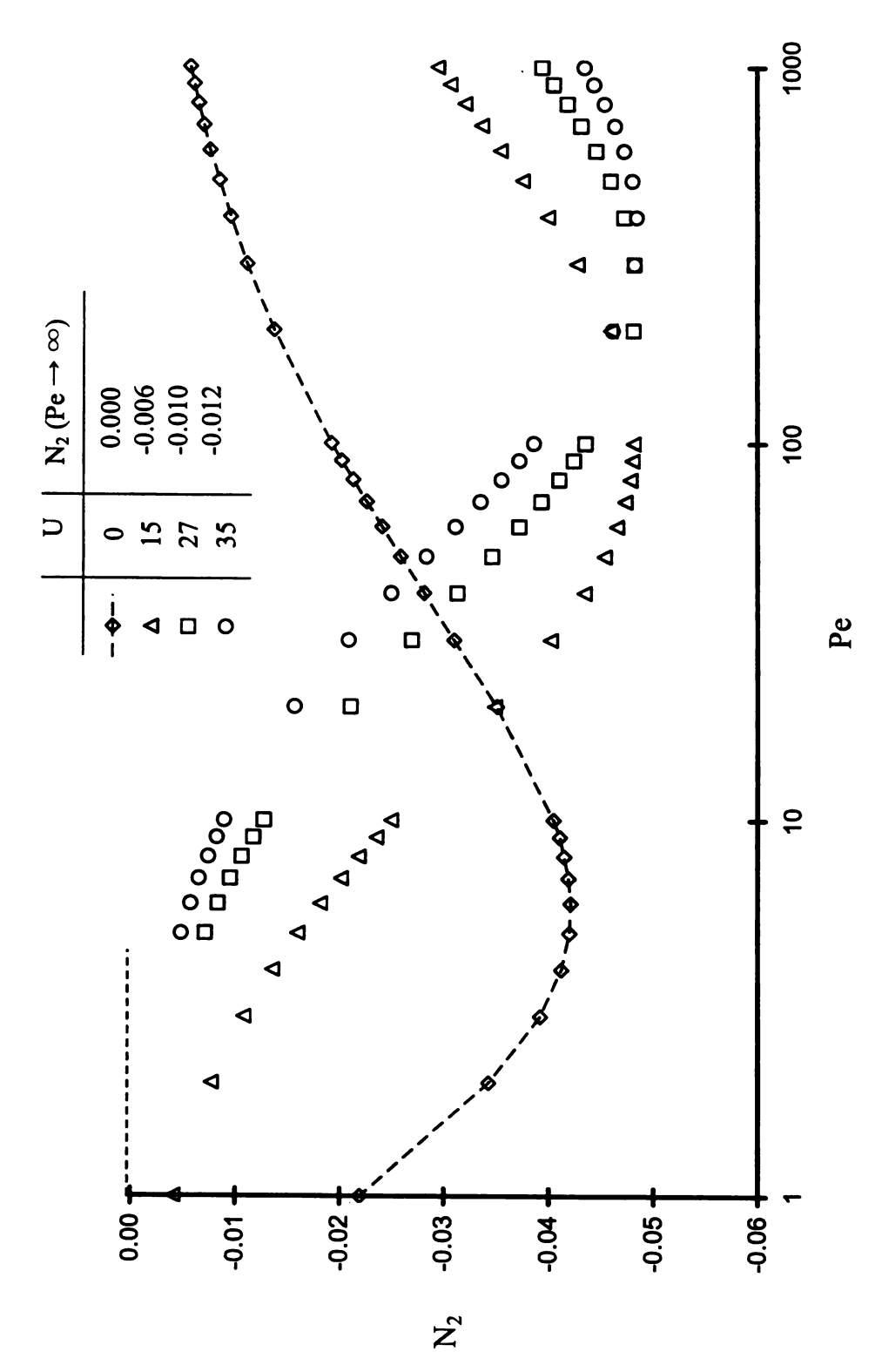


Figure 9.6 The Effect of U and Pe on the Second Normal Stress Difference for L/d =  $\infty$ (FSQ-model;  $F_{TD} = 1$ ;  $\lambda = 1$ ).

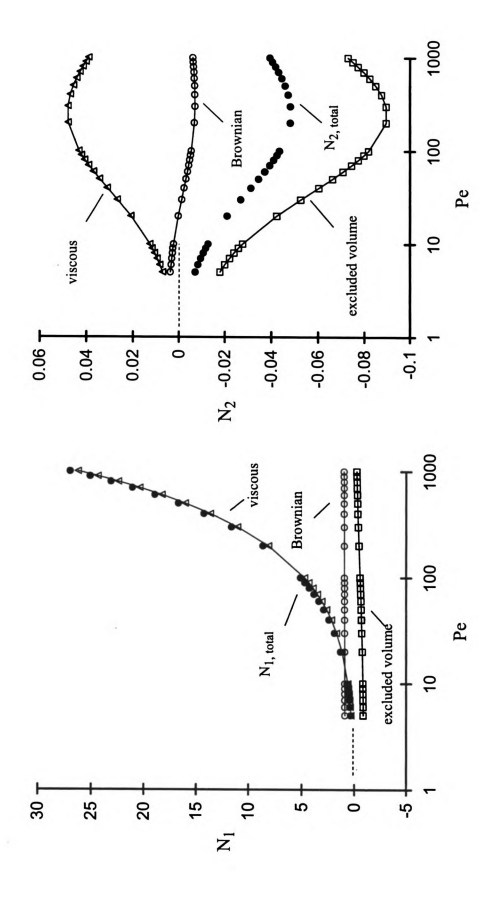


Figure 9.7 The Contributions of Stress on the Time Averaged Normal Stress Differences (FSQ-model;  $F_{TD} = 1$ ;  $\lambda = 1$ ; U = 27).

## 9.3 Rheological Properties: L/d $\approx$ 12

### Shear Viscosity

Figure 9.8 shows the effect of the tumbling parameter  $\lambda$  on  $\eta - \eta_S$  for U = 0. This rigid rod contribution to the viscosity for  $\lambda = 0.987$  (L/d  $\cong 12$ ) is the same as  $\lambda = 1$  for Pe <100. However, for Pe > 100, a Newtonian plateau occurs for  $\lambda = 0.987$  and the shear thinning region continues for  $\lambda = 1$ . Because Pe is high (see Eq. (4.1)), the diffusive flux becomes negligible, but it still makes a relatively significant contribution because the convective flux (hydrodynamic interaction part) is mitigated by  $\lambda$ . For example, Table 8.1 shows that the invariants of the structure tensor are nearly constant with  $\lambda = 0.987$  at high value of Pe. Hypothetically, if the microstructure could be forced to align more for  $\lambda = 0.987$ , another shear thinning state may appear for larger Pe (Region III) (see Larson, 1999 p. 509 – 511; Walker and Wagner, 1994; Walker et al., 1995).

In the tumbling region (high U and low Pe), the shear viscosity has a periodic behavior because the microstructure does (see CHAPTER 8). Figure 9.9 shows an example of the instantaneous viscosity for director tumbling ( $\lambda = 0.987$ , U = 27, Pe = 10, and  $F_{TD} = 1$ ). The dimensionless frequency of the dynamic viscosity tumbling is 0.21. Note that it has two local maximums and one local minimum per period. The shear viscosity shows instantaneous thickening when the director is not aligned with the flow direction. A period of shear thinning follows when the director rotates towards the cross flow direction (i.e.,  $\underline{u} \times \underline{w}$ ), but the flow and rigid rod resistance is not significant. The resistance to director rotation becomes significant when the director passes through the

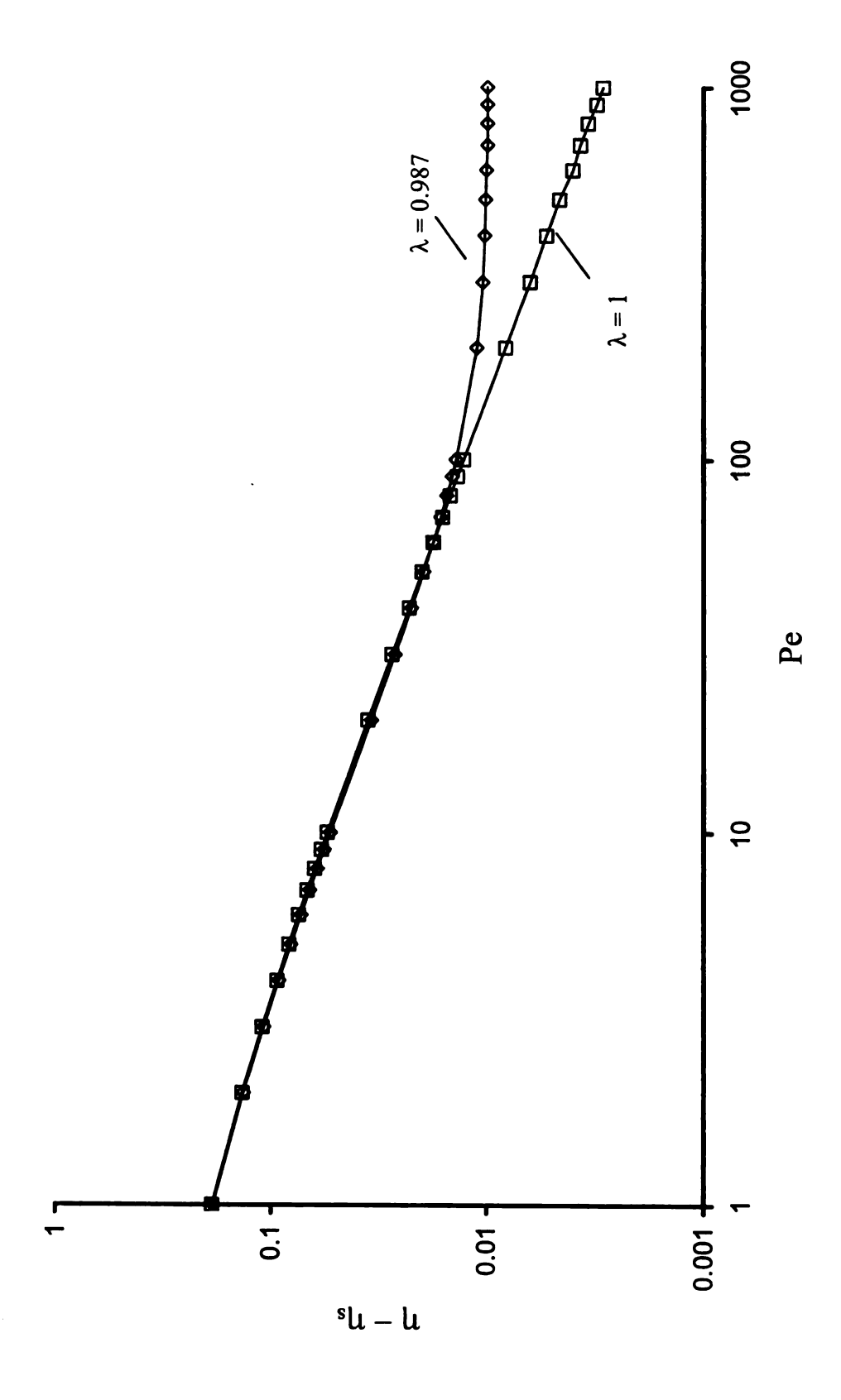


Figure 9.8 The Effect of Tumbling Parameter on the Shear Viscosity for U=0(FSQ-model;  $F_{TD} = 1$ ).

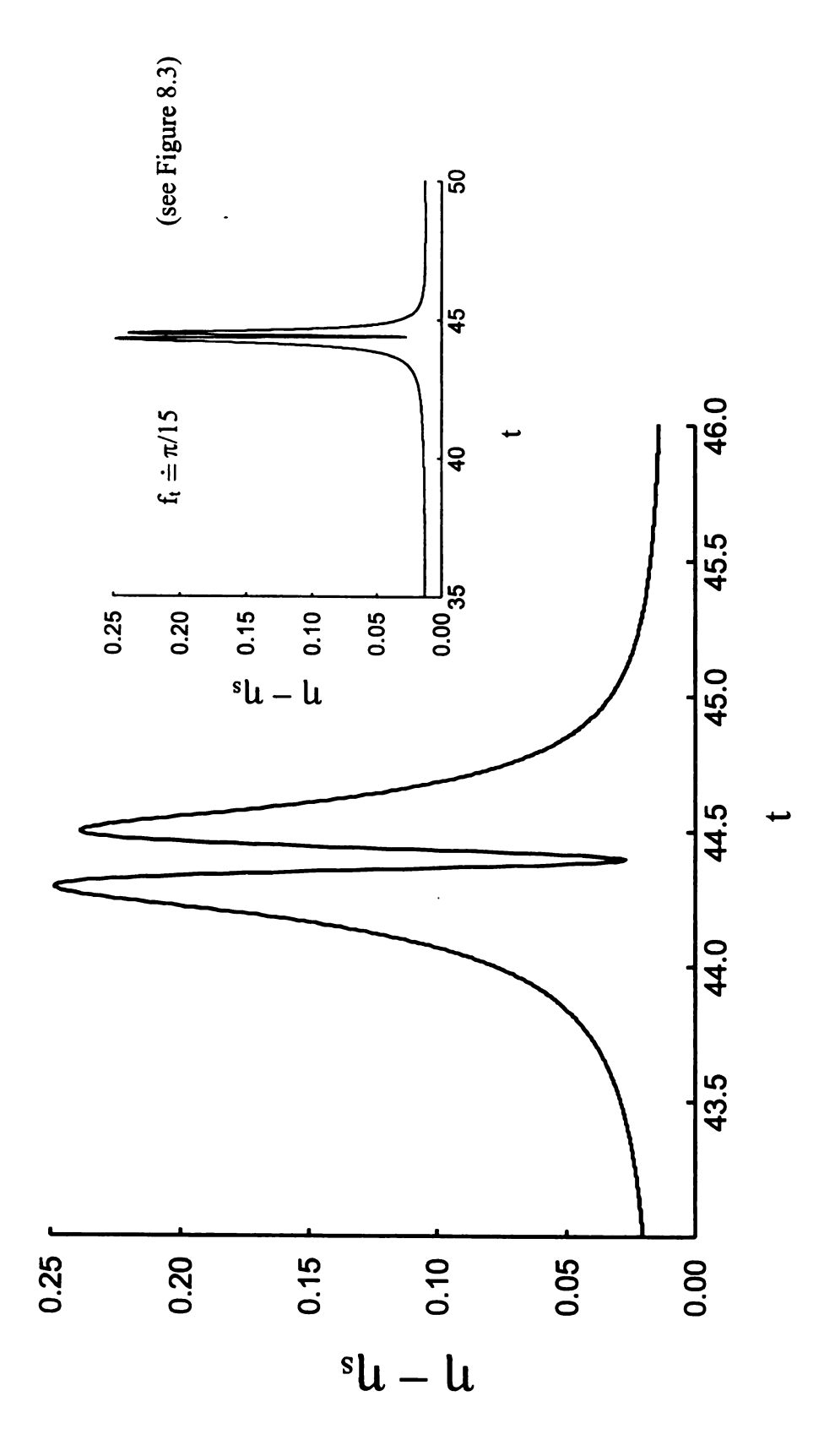


Figure 9.9 The Instantaneous Shear Viscosity for Director Tumbling (FSQ-model;  $F_{TD} = 1$ ;  $\lambda = 0.987$ ; U = 27, Pe = 10).

cross-flow/vorticity plane, which trigger another shear thickening episode occurs (see Figure 8.3). As the director rotates away from the cross flow direction, another shear thinning episode occurs. It is noteworthy that this prediction agrees qualitatively with experimental results reported by Gu and Jamieson for thermotropic liquid crystals, 8CP at 36.6 °C (see p.465 in Larson 1999; Chaubal and Leal, 1999).

The time averaged shear viscosity can be obtained by averaging the instantaneous shear viscosity over several time periods. Figure 9.10 shows the effect of U and Pe on the time averaged shear viscosity for  $\lambda = 0.987$ . As U increases, the Newtonian plateau region is extended to higher values of Pe because the tumbling region is extended for  $\lambda = 0.987$  (see Figure 8.9). Shear thinning occurs in the wagging region. In the steady alignment region (high values of Pe), the shear viscosity is independent of Pe. In addition, shear viscosity becomes independent of U and Pe for  $\lambda = 0.987$  at high Pe because the orientation state becomes nearly constant (see Table 8.1).

For some LCP experimental studies, the shear viscosity shows a shear thinning phenomenon at low strain rates (Region I), a Newtonian plateau region at medium strain rates (Region II), and a shear thinning region at high strain rates (Region III) (Walker and Wagner 1994, Walker et al. 1995, and see Larson 1999 p. 509 – 511). Region I may be due to layers of different orientation states (texture affect) in LCP solutions (Marrucci, 1991), Region II is due to the director tumbling phenomenon, and Region III is due to the shear aligning phenomenon (see Larson 1999, p. 509 – 511). Figure 9.10 shows that Region II coincides with director tumbling and Region III with the director wagging region (see Figure 8.9). Note, however, that additional Newtonia plateau occurs in the

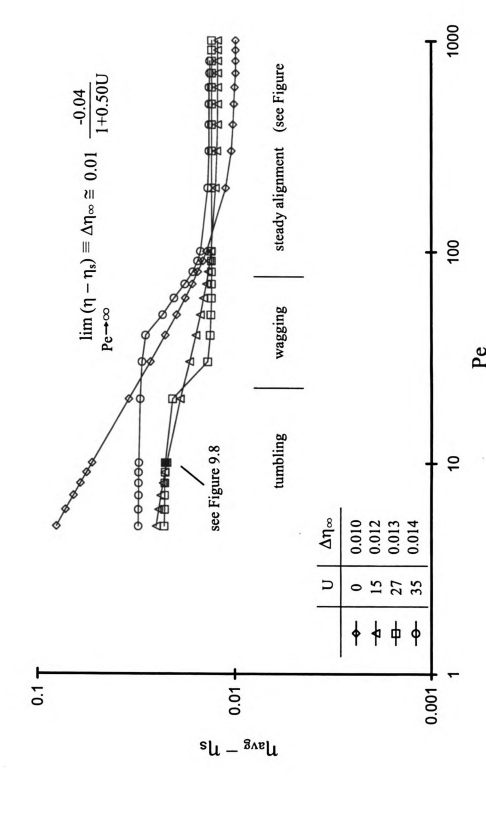


Figure 9.10 The Effect of U and Pe on the Time Averaged Shear Viscosity for  $L/d \cong 12$ (FSQ-model;  $F_{TD} = 1$ ;  $\lambda = 0.987$ ).

steady alignment region at high Péclet numbers (see CHAPTER 11 for further discussion). For U = 27, Figure 9.11 shows that the elastic contribution to the shear viscosity is relatively small for all Péclet number. Indeed, the elastic contribution to the rigid rod suspension stress is almost negligible for Pe > 20, and the viscous contribution becomes independent of Pe (see Table 9.2). This shows that the Newtonian plateau region at high Pe is determined by the viscous contribution of the stress and that the local microstructure is insensitive to further increases in Pe.

### Normal Stress Differences

Figure 9.12 shows the instantaneous first normal stress difference  $(N_1)$  for director tumbling. The frequency of tumbling is approximately  $6\,D_R^o\,\pi/15$  when U=27, Pe=10,  $\lambda=0.987$ , and  $F_{TD}=1$ . When the director tumbles,  $N_1$  changes sign.  $N_1$  increases when the initial director is off-aligned from the flow direction ( $t\cong44.3$ ), and decreases when the director rotates towards the cross-flow direction (compare with Figure 8.3).  $N_1$  increases again when the director completes the rotation from the cross-flow direction to the flow direction. In a cone-and-plate viscometer, the plate is pushed apart when the director rotates away from flow direction because this causes an increase in  $N_1$ . On the other hand, when the director aligns with the flow direction the plates push back on the fluid.

Figure 9.13 shows the effect of U and Pe on the time averaged first normal stress difference for  $\lambda = 0.987$  and  $F_{TD} = 1$ . When U is relatively small (steady alignment

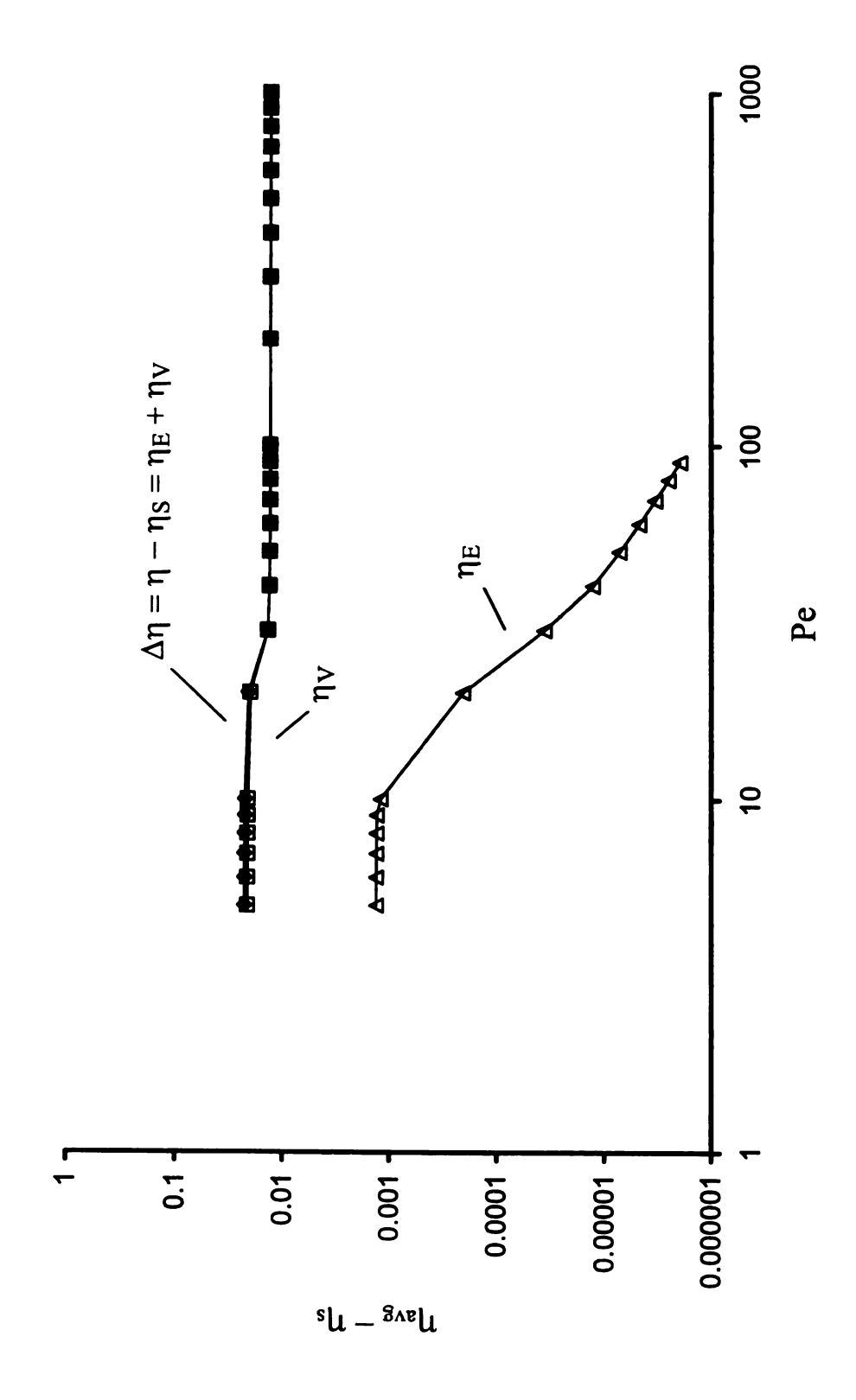


Figure 9.11 The Contributions of Viscous and Elastic Stresses on the Time Averaged Shear Viscosity for L/d  $\approx$  12 (FSQ-model;  $F_{TD} = 1$ ;  $\lambda = 0.987$ ; U = 27).

Table 9.2 Viscous and Elastic Contributions to the Shear Viscosity and the First and Second Normal Stress Differences at Selected Values of U and Pe for L/d ≅ 12

Property	Pe	U	Total	Viscous	Elastic		
					Total	Brownian	Excluded Volume
η-η <sub>s</sub>	5	0	0.0809	0.0560	0.0249	0.0249	0
		15	0.0251	0.0238	0.0011	0.0126	-0.0115
		27	0.0228	0.0214	0.0014	-0.0004	0.0018
	1,000	0	0.0099	0.0099	0.0000+	0.0000+	0
		15	0.0123	0.0123	0.0000+	0.0000+	0.0000+
		27	0.0132	0.0132	0.0000+	0.0000+	0.0000+
N <sub>1</sub>	5	0	0.8728	0.3813	0.4915	0.4915	0
		15	0.3586	0.2803	0.0190	0.8223	-0.8033
		27	-0.0128	-0.0111	-0.0017	0.8699	-0.8716
	1,000	0	5.5053	4.6326	0.8727	0.8727	0
		15	0.2563	1.9266	0.3297	0.8952	-0.5655
		27	-0.3244	-0.2789	-0.0455	0.9046	-0.9501
N <sub>2</sub>	5	0	-0.0470	0.0399	-0.0869	-0.0869	0
		15	-0.0140	0.0102	-0.0242	-0.0245	0.0003
		27	0.0003	-0.0001	0.0004	0.0196	-0.0192
	1,000	0	-0.0579	-0.0074	-0.0505	-0.0505	0
		15	-0.0537	0.0275	-0.0813	-0.0135	-0.0678
		27	0.0094	-0.0056	0.0150	0.0014	0.0136

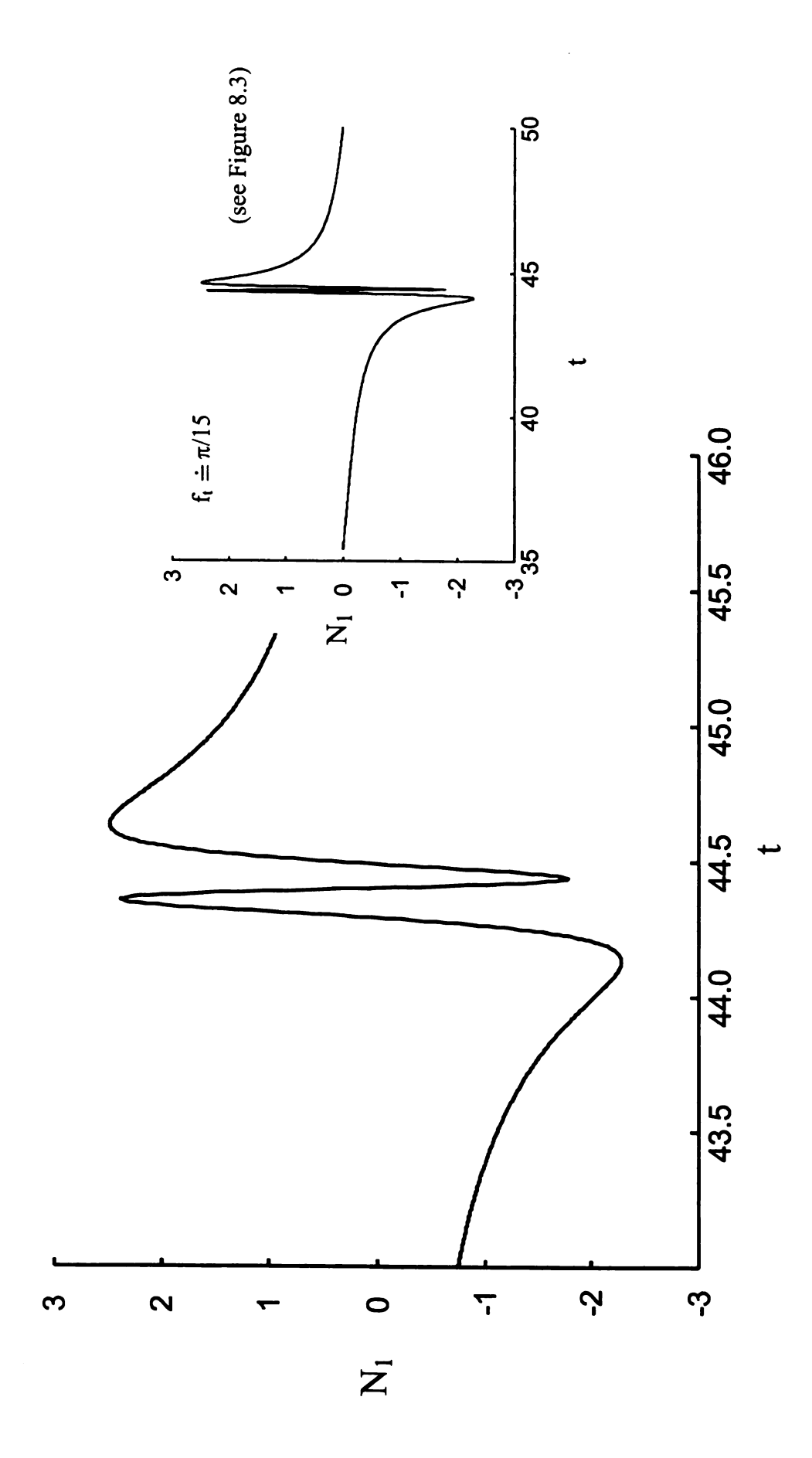


Figure 9.12 The Instantaneous First Normal Stress Difference for Director Tumbling (FSQ-model;  $F_{TD} = 1$ ;  $\lambda = 0.987$ ; U = 27, Pe = 10).

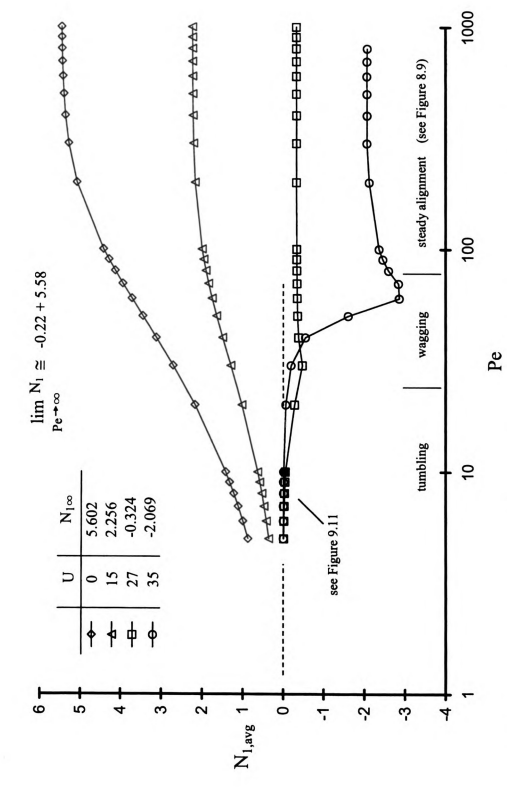


Figure 9.13 The Effect of U and Pe on the Time Averaged First Normal Stress Difference for L/d  $\approx 12$  (FSQ-model; F<sub>TD</sub> = 1;  $\lambda = 0.987$ ).

region),  $N_1$  is always positive. However,  $N_1$  is negative in the tumbling region and remains negative for higher values of Pe. Figure 8.7 shows that the director angle for high U and Pe is negative. The negative angle indicates that the director is pointing downward so that the plate is pushed towards the local microstate. Larson (1999) explains that  $N_1$  is positive when the director is tumbling, and becomes negative when it is wagging. He suggests that the negative  $N_1$  in both the computational results and experimental results supports the idea of director tumbling for LCPs. Both results also show increase in  $N_1$  at high strain rates. Figure 9.13, however, shows that  $N_{1,avg}$  predicted by the Doi stress is independent of Pe at high values of Pe. However,  $N_{1,avg}$  still depends on U.  $N_1$  remains negative as long as the director tumbles. A dependence of Pe only occurs when  $\lambda = 1$  (see Figure 9.1). As mentioned previously, a negative  $N_1$ , which is independent of Pe, is caused by a constant orientation state.

Figure 9.14 shows the instantaneous second normal stress difference  $(N_2)$  for director tumbling. The dimensionless frequency of tumbling is 0.21 when U = 27, Pe = 10, and  $F_{TD} = 1$ . Analogous to the instantaneous  $N_1$  analysis, the sign of  $N_2$  can be related to the microstructure of the rigid rod suspension.  $N_2$  decreases to negative values when the director is close to the cross flow direction. However, when the director passes the cross flow direction ( $t \cong 44.3$ ), it changes to positive values. Then,  $N_2$  slowly decreases to zero as the director approaches the flow direction (see Figure 8.3).

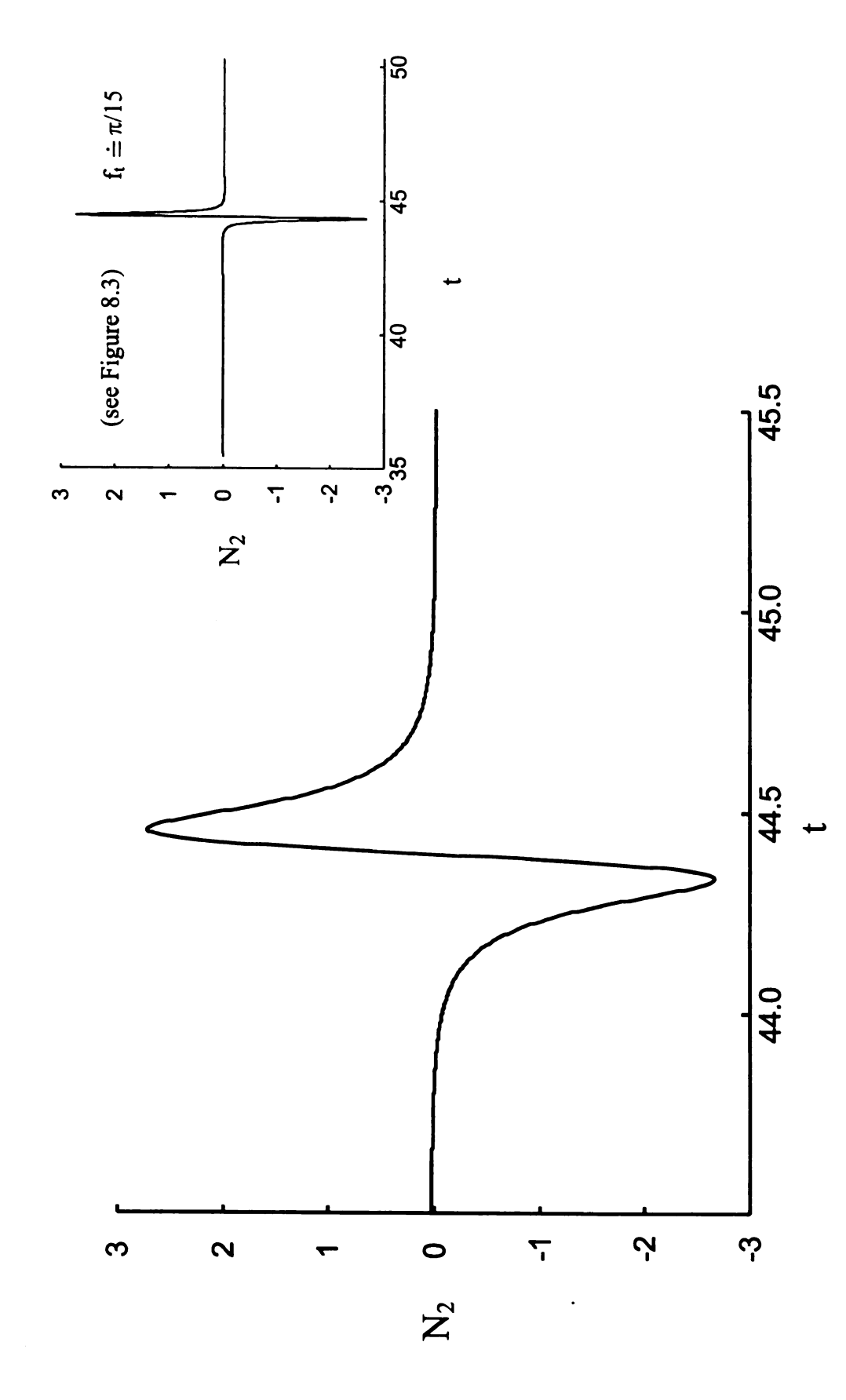


Figure 9.14 The Instantaneous Second Normal Stress Difference for Director Tumbling with L/d  $\approx 12$  (FSQ-model;  $F_{TD} = 1$ ;  $\lambda = 0.987$ ; U = 27, Pe = 10).

Figure 9.15 shows the effect of U and Pe on the time averaged  $N_2$ . When U is relatively small (steady alignment region),  $N_2$  is always negative. For U > 27 (where the director tumbles),  $N_2$  is always positive. At the high value of Pe,  $N_2$  becomes independent of Pe, but depends on U. As previously noted by Beak and Magda (1993), Beak et al. (1993), and Larson (see p.534, 1999), the results summarized by Figure 9.15 show that 1)  $N_1$  and  $N_2$  have opposite signs; 2)  $N_2$  has a local minimum where  $N_1$  has a local maximum; and,  $N_2 \le |N_1|/20$  (see Table 9.2).

## 9.4 Rheological Properties: $0 \le L/d < \infty$

Figure 9.16 shows the effect of the tumbling parameter  $\lambda$  on the shear viscosity with  $F_{TD}=1$ . In this research, the tumbling parameter is related to the aspect ratio of a rigid rod by Eq. (2.3), which shows that  $\lambda \to 1$  as  $L/d \to \infty$ ; and,  $\lambda \to -1$  as  $L/d \to 0$ . If L/d=1, then  $\lambda=0$ . The suspension viscosity  $\eta_{avg}-\eta_S \equiv \Delta \eta_{avg}$  has a maximum at  $\lambda=0$ . On the corresponds to L/d=1.106. Note that the shear viscosity is not symmetric about  $\lambda=0$ . As  $|\lambda|\to 0$ , the frequency of tumbling increases, which causes the viscosity to increase (see Table 8.2).

Figure 9.17 shows the effect of  $\lambda$  on the first normal stress difference with  $F_{TD}=1$ . There are two local positive maxima: one at  $\lambda=0.750$  and  $N_1=0.1084$ ; and, another at  $\lambda=-0.965$  and  $N_1=-0.0168$ . A local minimum is located at  $\lambda=-0.600$  and

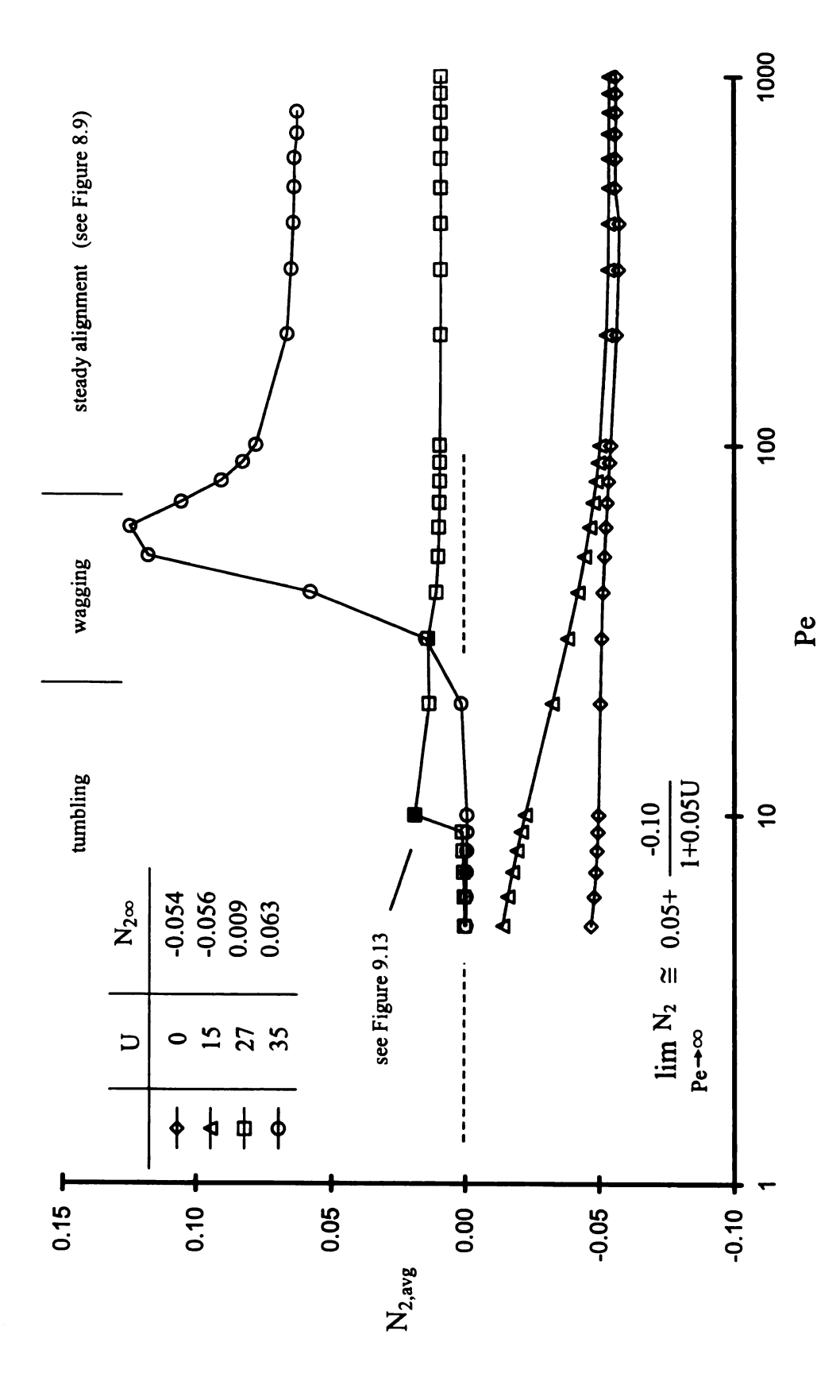


Figure 9.15 The Effect of U and Pe on the Time Averaged Second Normal Stress Difference for L/d  $\approx$  12 (FSQ-model;  $F_{TD} = 1$ ;  $\lambda = 0.987$ ).

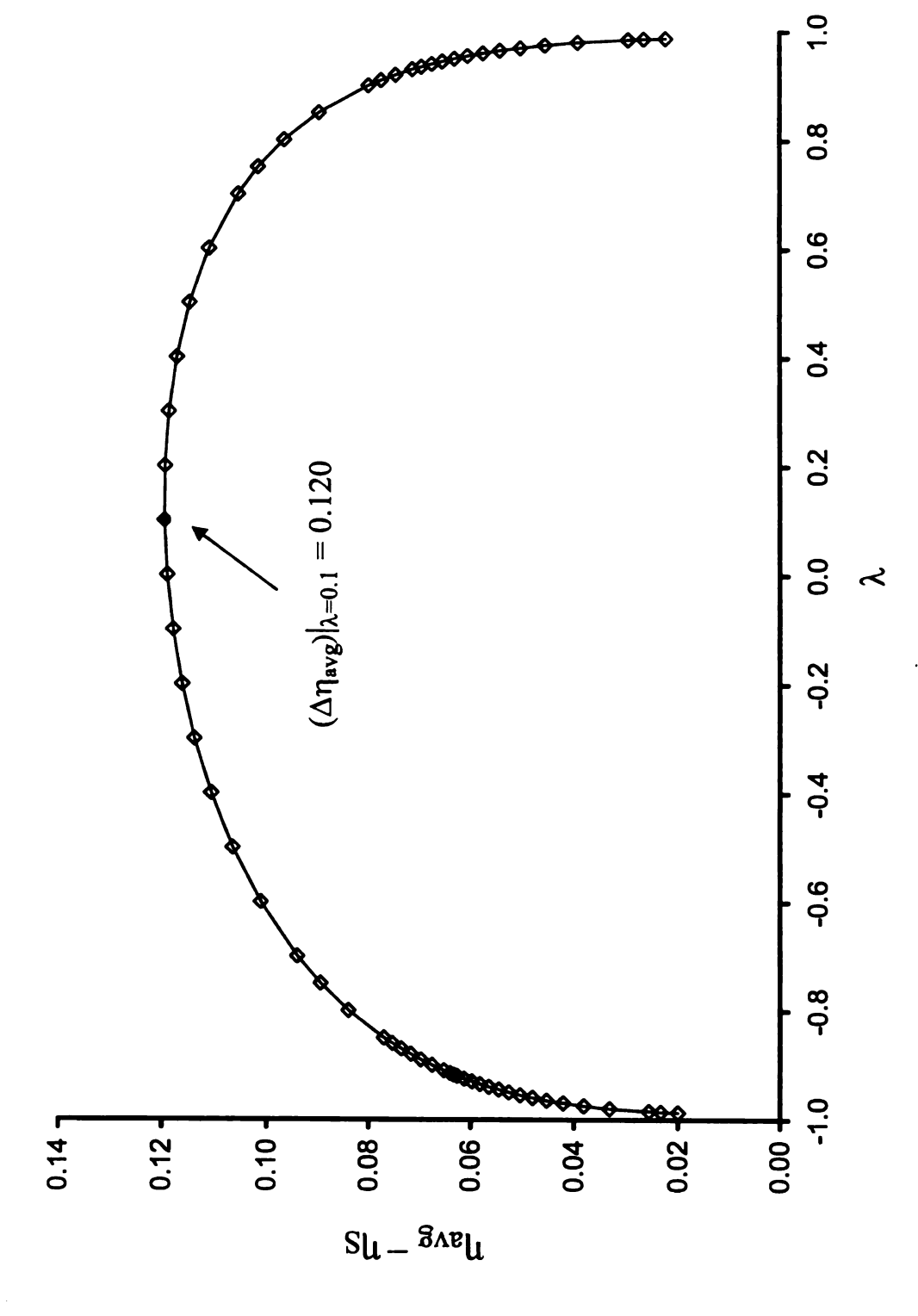


Figure 9.16 The Effect of Tumbling Parameter on the Time Averaged Shear Viscosity (FSQ-model;  $F_{TD} = 1$ ; U = 27, Pe = 10).

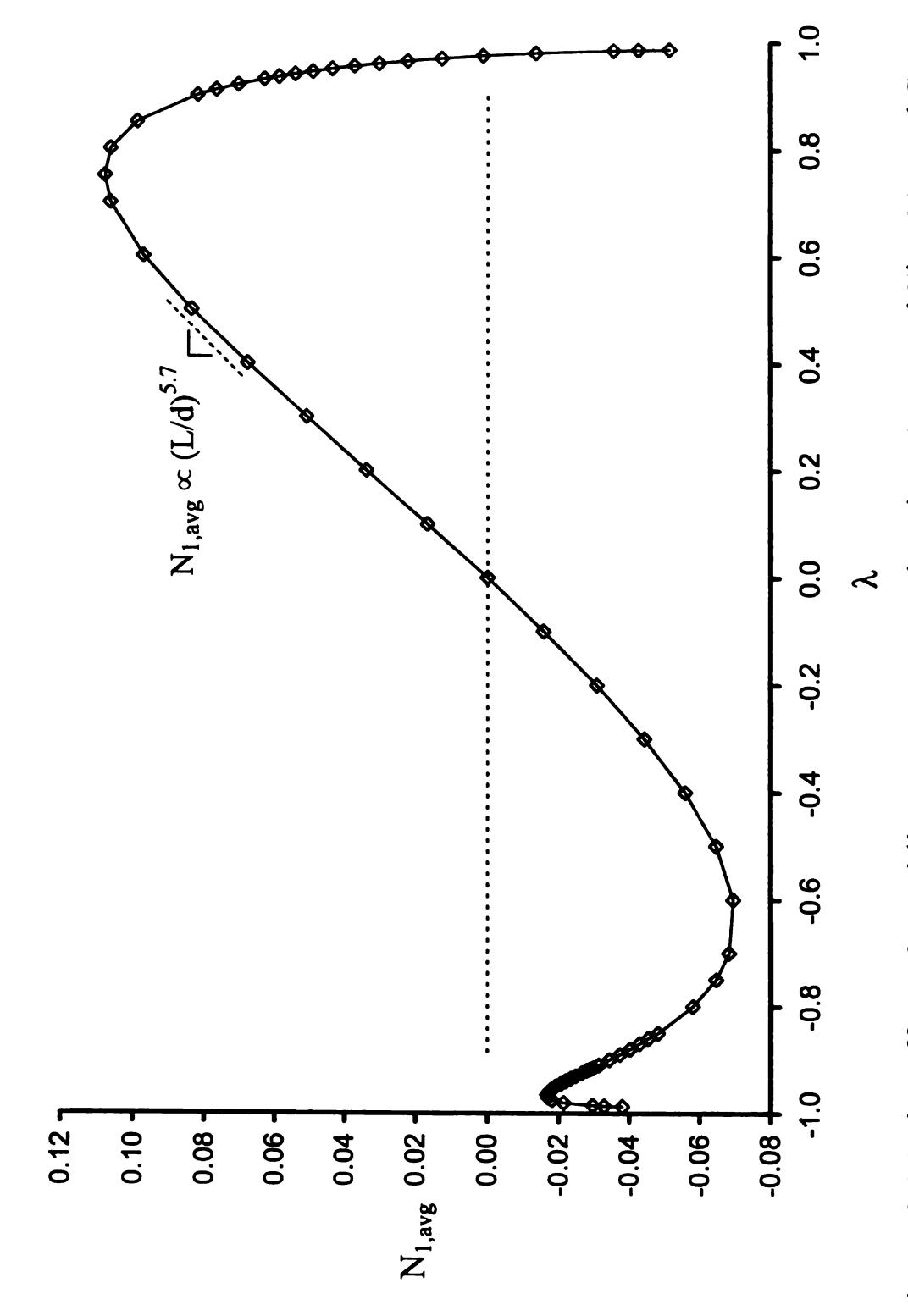


Figure 9.17 The Effect of Tumbling Parameter on the Time Averaged First Normal Stress Difference (FSQ-model;  $F_{TD} = 1$ ; U = 27, Pe = 10).

 $N_1 = -0.070$ .  $N_1$  is negative for both positive and negative values of  $\lambda$ . However,  $N_1$  is positive for  $\lambda = \pm 1$  ( $\lambda = 1$ ,  $N_1 = 0.699$ ; and,  $\lambda = -1$ ,  $N_1 = 0.531$ ). According to Larson (1999 p. 294),  $N_1 \propto (L/d)^2 \ln(L/d)$  for rigid rods ( $\lambda > 0$ ). This relationship can be approximated by power law relationship,  $N_1 \propto (L/d)^{7.4}$ . Figure 9.17 shows qualitative agreement with this theory until  $\lambda \cong 0.7$ .  $N_1$  decreases with the tumbling parameter as  $\lambda \to 1$ .

Figure 9.18 shows the effect of  $\lambda$  on the second normal stress difference with  $F_{TD}=1$ . Notice that there are two local minima:  $\lambda=0.700$ ,  $N_2=-0.025$ ; and,  $\lambda=-0.920$ ,  $N_2=-0.007$ . A local maximum occurs at  $\lambda=-0.500$  ( $N_2=0.012$ ).  $N_2$  increases to positive values as  $\lambda\to\pm1$ ; however,  $N_2$  is negative for  $\lambda=\pm1$  ( $\lambda=1$ ,  $N_2=-0.0127$ ; and,  $\lambda=-1$ ,  $N_2=-0.5688$ ). The sign of  $N_2$  is always opposite  $N_1$ , but the magnitude varies with  $\lambda$ .

# 9.5 Rheological Properties: Effect of Tube Dilation

## **Shear Viscosity**

In this section, the effect of tube dilation on the rheological properties will be examined. This phenomenon directly impacts the rotary diffusion coefficient in Eqs.(4.1) and (4.6). The tube dilation coefficient  $F_{TD}$  depends on the local microstructure through the second invariant of the structure tensor:  $F_{TD}^{Doi} = \left(1 - \frac{3}{2}II_b\right)^{-2}$ . Table 9.3 defines how

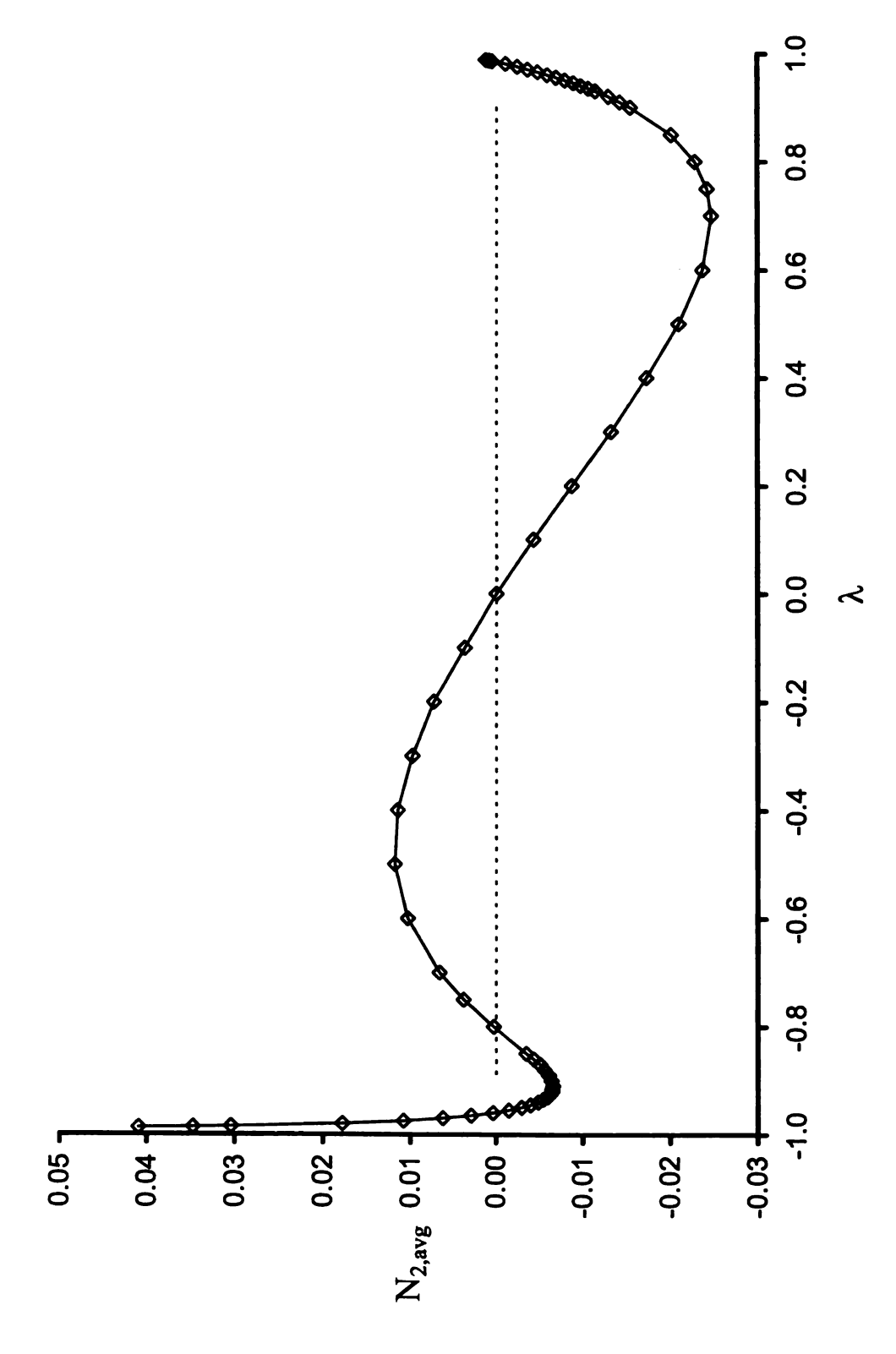


Figure 9.18 The Effect of Tumbling Parameter on the Time Averaged Second Normal Stress Difference (FSQ-model;  $F_{TD} = 1$ ; U = 27, Pe = 10).

Table 9.3 Legend for Figures 9.19 – 9.23

$F_{TD}^{Doi} = \left(1 - \frac{3}{2}II_b\right)^{-2}$ , Eq.(2.8)						
legend	Eq.(4.1)	Eq.(4.6)				
-8-	No	No				
	Yes	No				
-	Yes	Yes				

the F<sub>TD</sub>-factor is applied in the results presented hereinafter. If no tube dilation is considered, then this is designated as "No" in the table. If tube dilation is included, then the affected equations are identified as "Yes." Figure 9.19 shows the effect of tube dilation on the time averaged shear viscosity for  $\lambda = 0.987$  and U = 27. With tube dilation, the tumbling region is extended to larger values of Pe (cf. Figures 8.9 and 8.17). Tube dilation enhances the diffusive flux in the moment equation so the director has more freedom to rotate. Because of director tumbling, the Newtonian plateau is also extended. When the tube dilation is included in Eq.(4.1) and Eq.(4.6), shear thickening occurs near the tumbling and wagging transition region. Larson notes that shear thickening occurs because the increase in interparticle spacing makes it harder for the solution to deform (see p.273, Larson, 1999). In Figure 9.19, the shear thickening phenomenon may be explained as an interparticle spacing effect. However, Larson also mentions that there is no known direct relationship between tube dilation and shear thickening. Figure 9.20 shows the contribution of stress components on the time averaged shear viscosity when  $F_{TD} = F_{TD}^{Doi}$  in Eq. (4.1) and Eq.(4.6). Shear viscosity is nearly identical with the viscous contribution of the stress, which is consistent with  $\lambda = 1$  and  $\lambda = 0.987$  study without tube dilation.

#### Normal Stress Differences

Figure 9.21 shows the effect of tube dilation on the time averaged of the first normal stress difference with  $\lambda=0.987$  and U=27. Note that  $N_1$  is independent of Pe

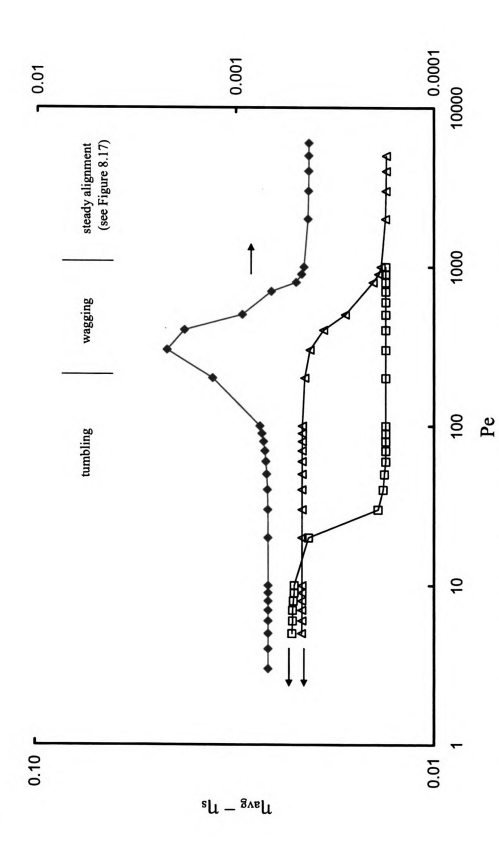


Figure 9.19 The Effect of Tube Dilation on the Time Averaged Shear Viscosity (FSQ-model;  $\lambda = 0.987$ ; U = 27 see Table 9.3 for legend)

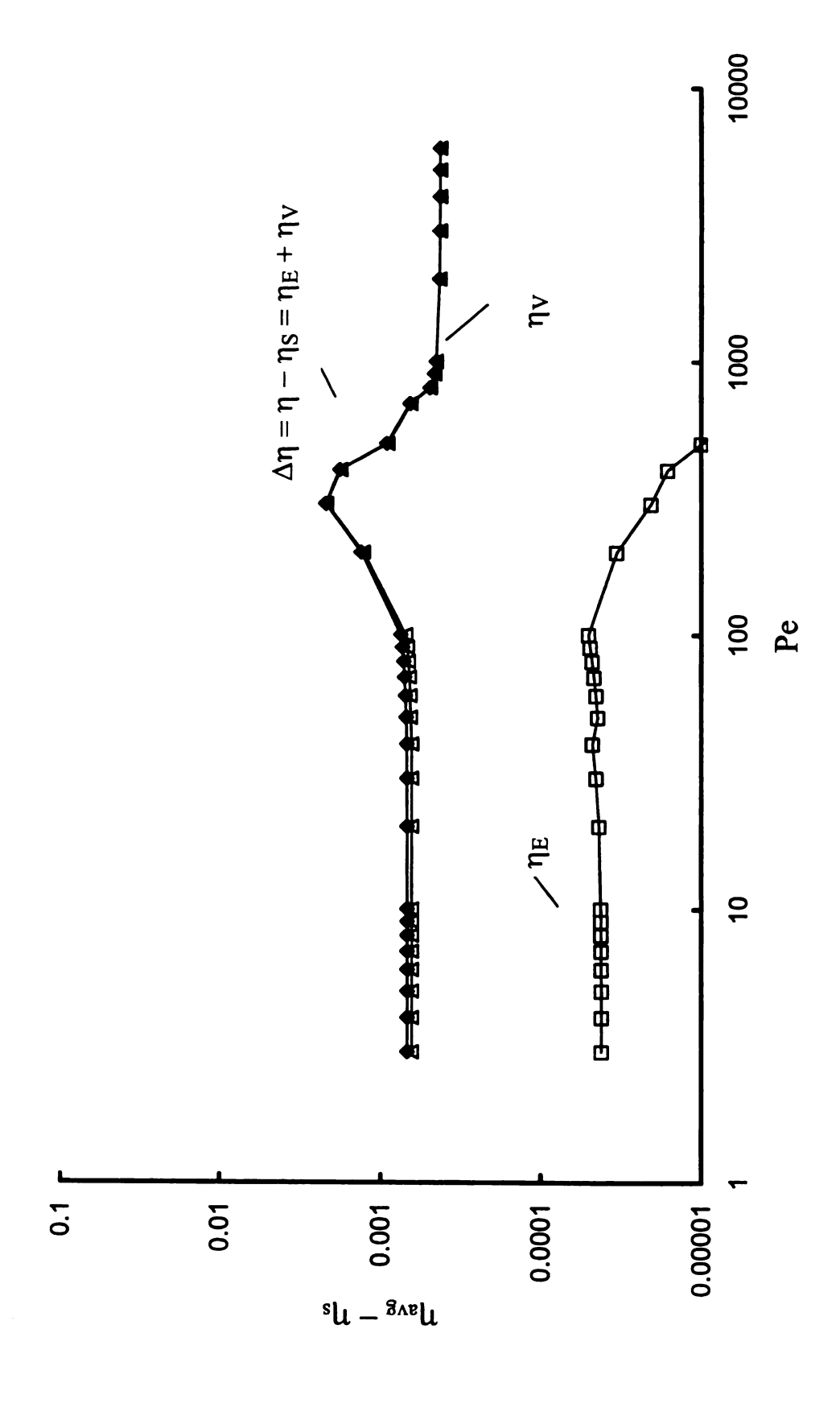


Figure 9.20 The Contribution of Stress on the Time Averaged Shear Viscosity (FSQ-model;  $F_{TD}^{Doi}$  in Eqs. (4.1) and (4.6);  $\lambda = 0.987$ ; U = 27)

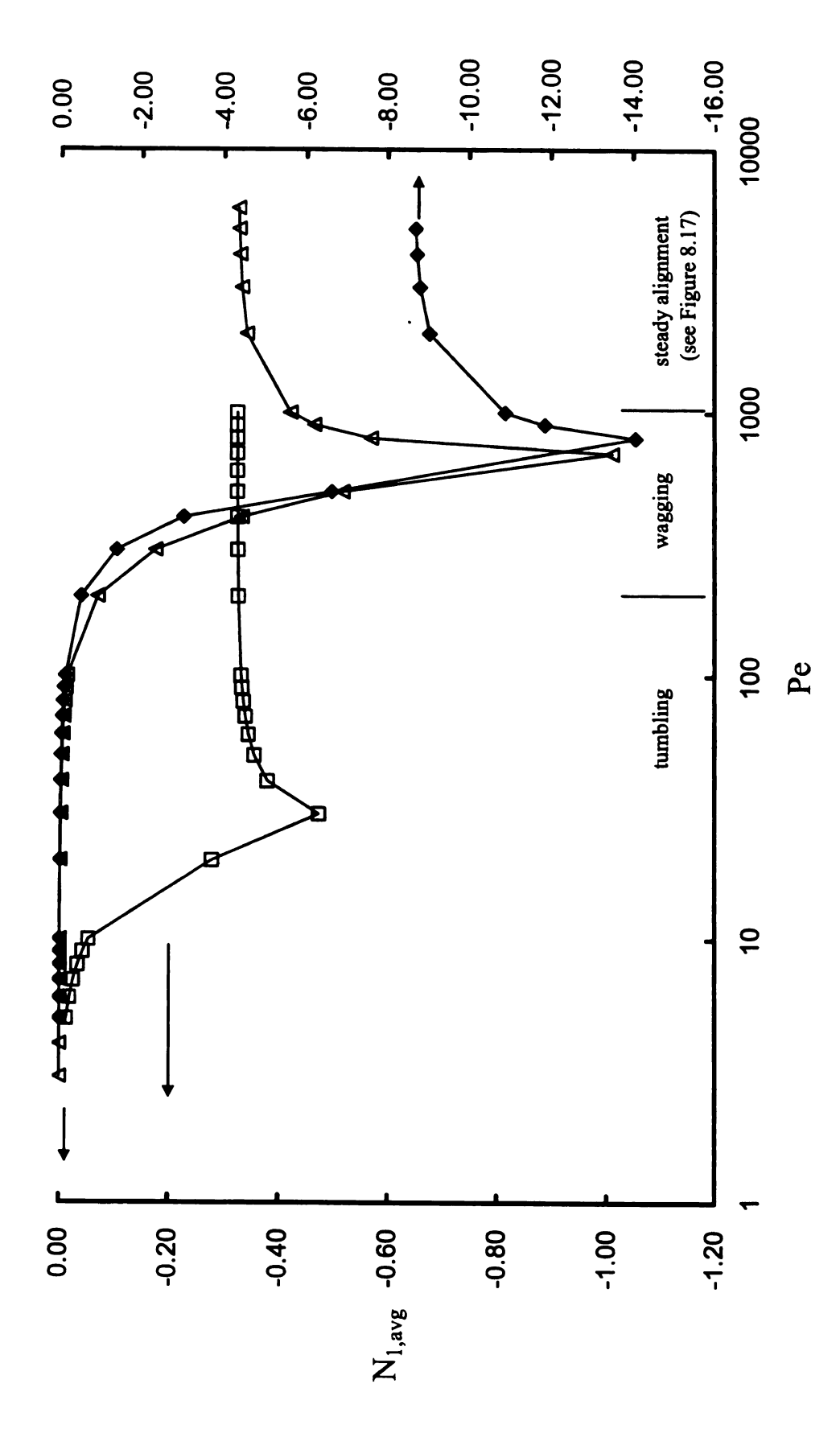


Figure 9.21 The Effect of Tube Dilation on the Time Averaged First Normal Stress Difference (FSQ-model;  $\lambda = 0.987$ ; U = 27 see Table 9.3 for legend)

for Pe >> 2,000. In addition, N<sub>1</sub> with and without tube dilation have similar trends in the tumbling, wagging, and steady alignment regions. The inclusion of tube dilation in Eq.(4.1) causes the tumbling at high value of Pe. This influences prediction of the minimum of  $N_1$  and its magnitude of  $N_1$ . If tube dilation is included in Eq.(4.1) and Eq.(4.6), N<sub>1</sub> has a local minimum in the wagging region. Tube dilation affects the magnitude of  $N_1$  at the local minimum significantly. Figure 9.22 shows the effect of tube dilation on the time averaged second normal stress difference with  $\lambda = 0.987$  and U = 27. Though N2 values are independent of large Pe value for all tube dilation cases (see Table 9.3), they have different trends related to tumbling, wagging, and steady alignment. With the tube dilation effect, signs of  $N_2$  values are not always opposite to  $N_1$ . When  $F_{TD}^{Doi}$  is only applied to Eq.(4.1), N2 is negative for low value of Pe. In the director wagging region, N<sub>2</sub> changes from negative to positive. In the steady alignment region, N<sub>2</sub> remains positive and becomes independent of Pe. When F<sub>TD</sub><sup>Doi</sup> is applied to both Eq.(4.1) and Eq.(4.6), N<sub>2</sub> is positive for low value of Pe and decreases to negative in the wagging region. In the steady alignment region, N<sub>2</sub> remains negative and becomes independent of Pe. None of these results have been observed experimentally.

Figure 9.23 shows the contribution of stress on the time averaged normal stress differences with  $F_{TD}^{Doi}$  only in Eq.(4.1),  $\lambda = 0.987$ , and U = 27. The viscous contribution

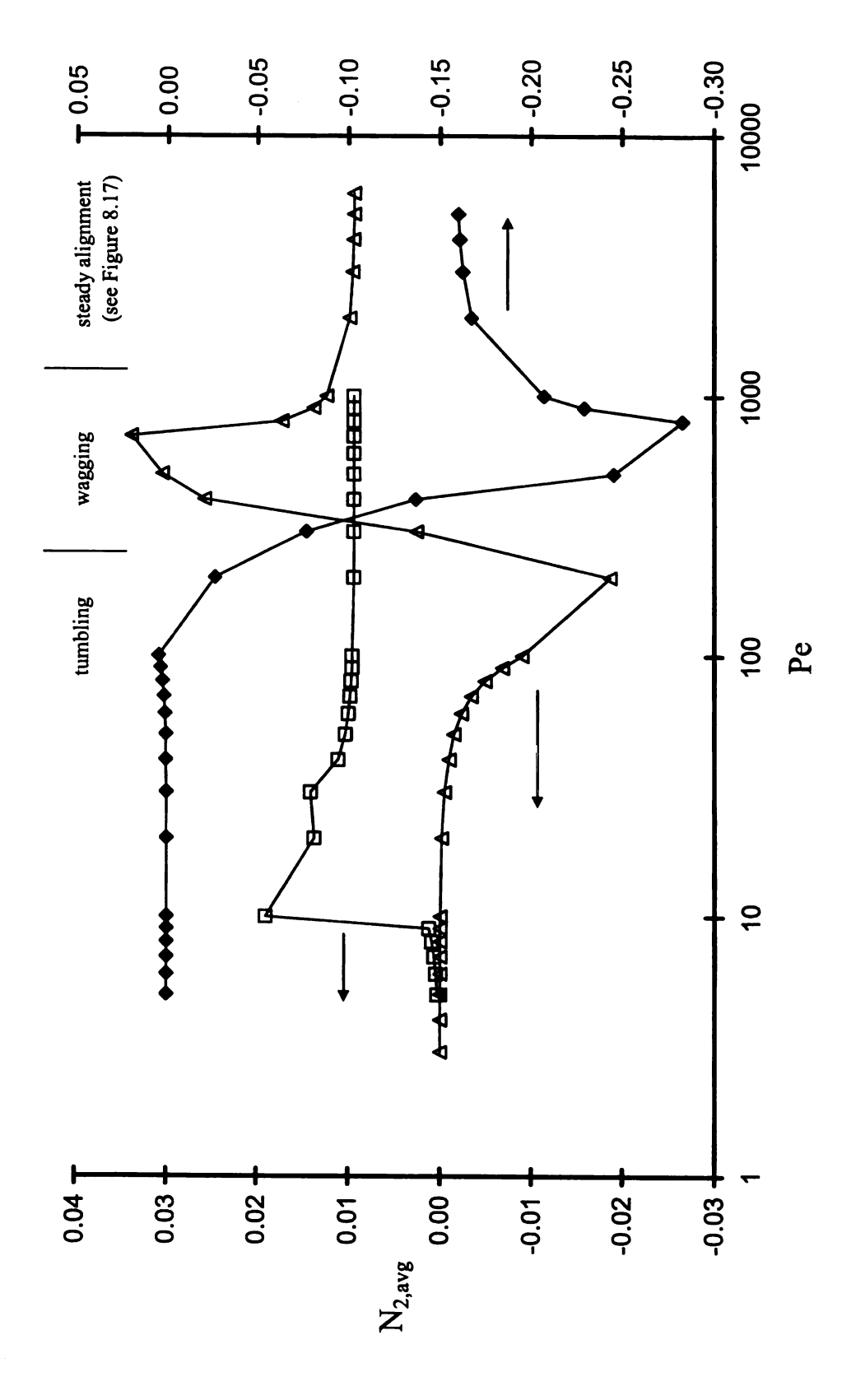


Figure 9.22 The Effect of Tube Dilation on the Time Averaged Second Normal Stress Difference (FSQ-model;  $\lambda = 0.987$ ; U = 27 see Table 9.3 for legend)

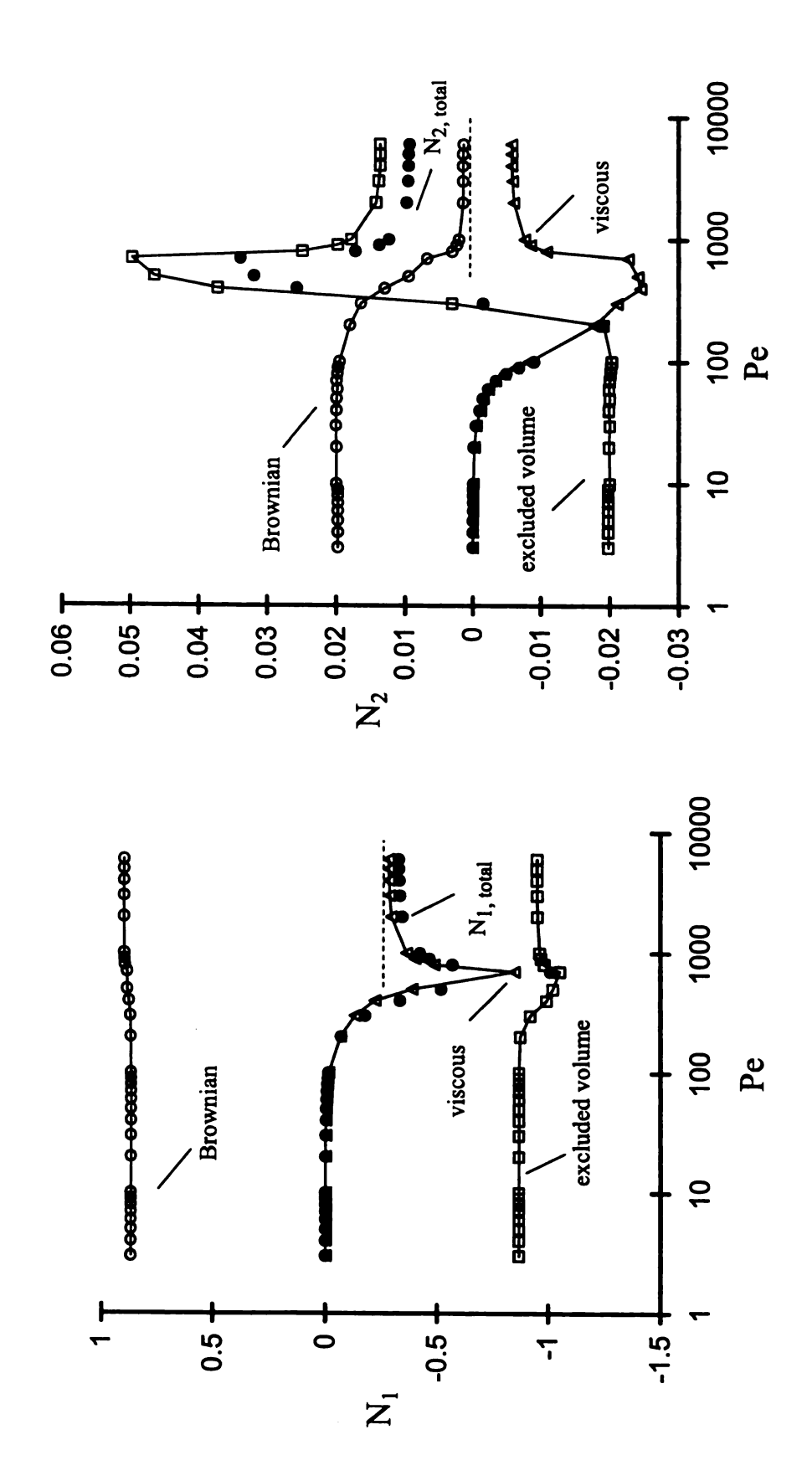


Figure 9.23 The Contributions of Stress on the Time Averaged Normal Stress Differences (FSQ-model; F  $_{\text{TD}}^{\text{Doi}}$ ;  $\lambda = 0.987$ ; U = 27).

to  $N_1$  determines the total  $N_1$ , while the sum of Brownian and the excluded volume contribution to the elastic component of  $N_1$  are very small.

## 9.6 Discussion

Predictions of rheological properties,  $N_1$ ,  $N_2$ , and  $\Delta \eta$  are coupled with the microstructure of the orientation states. These orientation states can be categorized by a tumbling parameter  $\lambda$ . For  $\lambda=1$ , all solutions are steady state.  $\Delta \eta$  has a Newtonian plateau and a shear thinning region,  $N_1$  is always positive, and  $N_2$  is always negative (see Figures 9.1, 9.5, and 9.6).

For  $\lambda \cong 0.987$ , a steady alignment region at small values of U (U < 27) is predicted.  $\Delta \eta$ ,  $N_1$ , and  $N_2$  have similar trends as the case with  $\lambda = 1$ , until the orientation state becomes independent of Pe at large values of Pe. Based on previous experimental and theoretical studies, negative  $N_1$  is caused by tumbling phenomenon, which is predicted by this research. For  $\lambda \cong 0.987$ ,  $N_1$  becomes independent of Pe for large values of Pe.

The effect of tube dilation in the moment equation adds additional diffusive flux in the orientation state, which gives an extended tumbling region. This phenomenon broadens the Newtonian plateau region. When the tube dilation effect is included in the moment equation and in the viscous contribution of the stress, shear thickening occurs near the tumbling/wagging transition region. Moreover, the magnitudes of the normal stress differences are increased significantly.

In general,  $\Delta\eta$  and  $N_1$  are mainly determined by the viscous contribution to the stress, while the elastic contribution, which includes rotary Brownian motion and the excluded volume effect, is very small. The second normal stress difference, however, is determined mainly by the excluded volume contribution. These results offer useful insights on how to modify the stress model.

## CHAPTER 10

#### CONCLUSIONS

In this research, the Smoluchowski equation (S-equation) for the orientation density function was used to study the self-alignment and the flow-induced alignment of semi-dilute and concentrated suspensions of ellipsoidal particles. A Maier-Saupe excluded volume potential and Jeffery's model for rotary convection in a homogeneous shear field were used to close the S-equation. Doi's model for the rotary diffusion coefficient accounts for the influence of tube dilation on highly aligned suspensions.

Low-order moments of the orientation density function were used to quantify the relaxation of the microstructure from initial anisotropic states. An unclosed moment equation for the orientation dyad  $\langle \underline{p}\underline{p} \rangle$  was derived from the S-equation. An algebraic closure for the orientation tetrad  $\langle \underline{p}\underline{p}\underline{p}\underline{p} \rangle$ , which appears in the moment equation for  $\langle \underline{p}\underline{p} \rangle$ , was developed based on the hypothesis that all *planar anisotropic states* are attracted by three dimensional anisotropic states.

The objective of this chapter is to summarize the salient conclusions of this research. The following four complementary topics, which relate to the self-alignment and the flow-induced alignment of rigid rod suspensions, will be addressed: 1) closure for the orientation tetrad; 2) equilibrium states; 3) non-equilibrium states; and, 4) rheology of rigid-rod suspensions.

## Closure for the Orientation Tetrad

This research has developed a new algebraic closure approximation (FSQ-closure) for the orientation tetrad  $\langle \underline{p}\underline{p}\underline{p}\underline{p}\rangle$  in terms of the orientation dyad  $\langle \underline{p}\underline{p}\rangle$  with the following three characteristics:

- the closure retains the six-fold symmetry properties of the exact orientation tetrad;
- the closure retains the six-fold contraction properties of the exact orientation tetrad; and,
- the second-order FSQ-closure coefficient, defined by

$$C_2 = \frac{8 + 45 \text{ III}_b}{18(1 + 9 \text{ III}_b)}$$
,  $-\frac{1}{36} \le \text{III}_b \le \frac{8}{36}$  (10.1a)

$$III_{\mathbf{b}} \equiv \operatorname{tr}[\underline{\mathbf{b}} \cdot \underline{\mathbf{b}} \cdot \underline{\mathbf{b}}] \tag{10.1b}$$

$$\underline{\underline{b}} \equiv \langle \underline{p}\underline{p} \rangle - \frac{1}{3}\underline{\underline{I}} \qquad , \tag{10.1c}$$

has the feature that all planar anisotropic states are attracted by three dimensional anisotropic states (see Figure 1.1).

The FSQ-closure for < pppp > is

$$= [1 - C_2(III_b)] \Im_1() + C_2(III_b) \Im_2().$$
 (10.2)

The tetradic operators  $\mathfrak{I}_1(\cdot)$  and  $\mathfrak{I}_2(\cdot)$  are defined by Eqs.(5.5) and (5.6), respectively. Eqs.(10.1a) and (10.2) are significant discoveries that will have an immediate impact on the further development and understanding of the flow (and light scattering) properties of suspensions, liquid crystalline polymers, and other fluids with microstructure.

Figure 10.1 compares the steady state solutions of the moment equation (see Eq.(4.1)) with statistical properties calculated from solutions of the S-equation developed

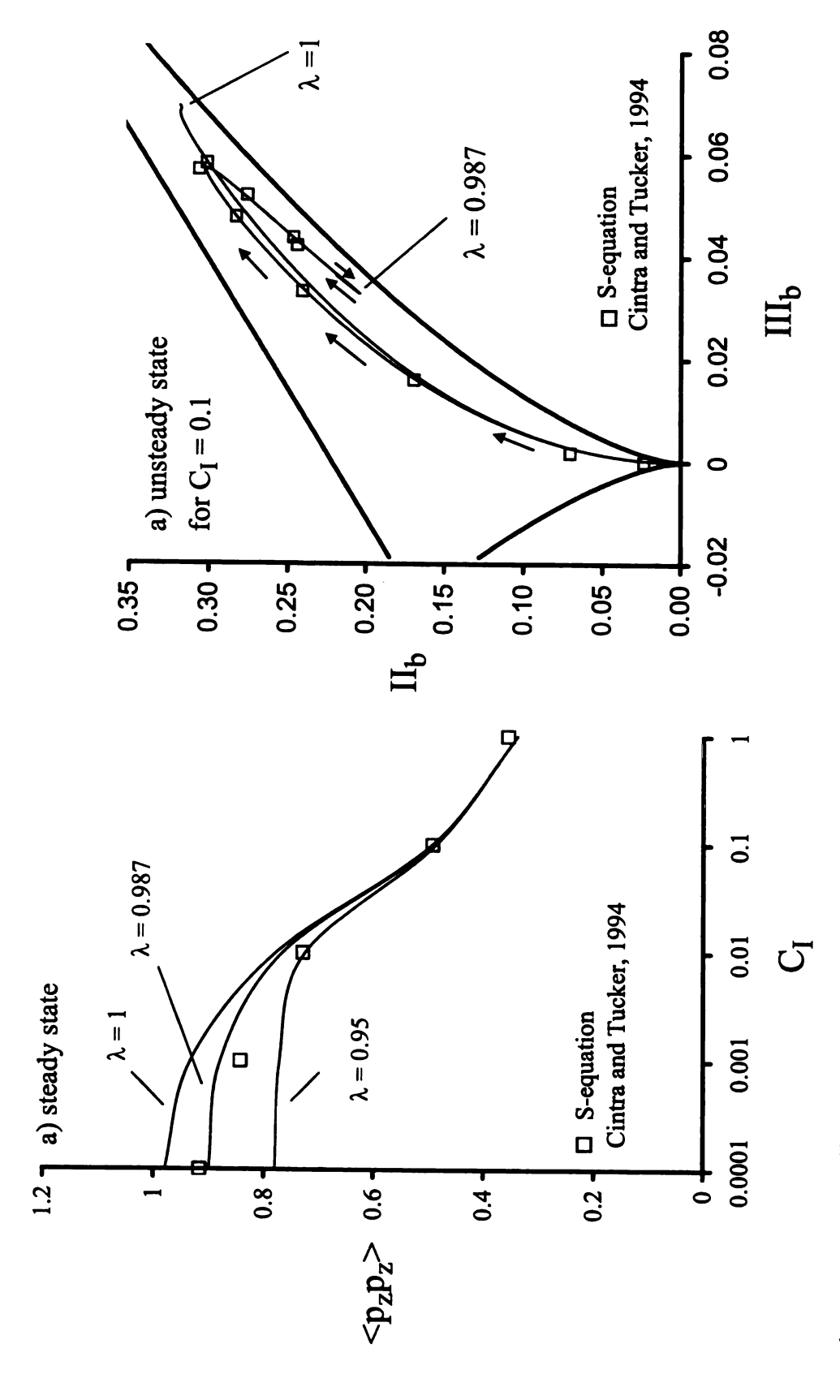


Figure 10.1 Validation of the FSQ-closure

by Cintra and Tucker (1994). Cintra and Tucker solved Eq.(2.14) numerically subject to a uniform initial condition (isotropic) with  $\lambda = 1$ , U = 0,  $F_{TD}/Pe = 9C_I$ , and  $t^* = tPe$ . The orientation dyad was calculated directly from the orientation density function. No closure approximation was required for <pppp>. It is noteworthy that solutions to Eq.(4.1) with the realizable FSQ-closure for < pppp > predicts qualitatively the same steady states as the direct numerical simulation for a wide variation in the dimensionless diffusion coefficient C<sub>I</sub>. Figure 10.1a shows a comparison of the FSQ-closure predictions of  $\langle pp \rangle : \underline{e}_z \underline{e}_z$  with the results of Cintra and Tucker (1994). Figure 10.1b compares the relaxation of the microstructure (i.e., IIb and IIIb) for the two approaches. The results show that the FSQ-closure with C<sub>2</sub>(III<sub>b</sub>) defined by Eq.(6.28) provides a qualitatively consistent prediction of the exact statistical properties. Note that for  $C_I \rightarrow 0$ , the steady state approaches the nematic state (see Point A on Figure 1.1); and, as  $C_I \rightarrow \infty$ , the steady state approaches the isotropic state. Earlier application of the FSQclosure with C<sub>2</sub>(III<sub>b</sub>) = constant (see Parks et al., 1999; Nguyen et al., 2001; Kini et al., 2003) predicted unrealizable behavior for small values of  $C_1$ . For example, if  $C_2 = 1/3$ , unrealizable steady states occur for  $C_I < 0.01$ . Clearly, the discovery of the closure coefficient C<sub>2</sub>(III<sub>b</sub>) defined by Eq.(6.28) is a major accomplishment of this research.

### Equilibrium States

The steady state (equilibrium) solutions to Eq.(4.1) with Pe = 0 are either isotropic, prolate anisotropic, or oblate anisotropic. All initial planar anisotropic microstructures are attracted (relax) to the prolate anisotropic boundary of Figure 1.1. If the initial state is oblate anisotropic, then the equilibrium state is oblate anisotropic. However, if an infinitesimal disturbance produces a microstructure within the invariant domain (see Figure 1.1) near the oblate line, the relaxed equilibrium state will be prolate anisotropic, not oblate. Thus, oblate equilibrium states are stable to disturbance that are oblate; however, they are unstable to arbitrary realizable disturbance.

Figure 7.2 shows how the steady state order parameter  $\alpha$  ( $\equiv$  (3/2II<sub>b</sub>)<sup>1/2</sup>) depends on the excluded volume coefficient U. The isotropic state ( $\alpha$  = 0) is a solution to Eq.(4.1) for all U,  $0 \le U < \infty$ . For  $U < U_1$ ,  $\alpha$  = 0 is the only steady state solution.

For  $U_1 < U < U_2$ , three equilibrium solutions exist: two are stable (isotropic and prolate anisotropic) and one is unstable (prolate anisotropic). The existence of this so-called biphasic region has been confirmed by experiments and by other theories (see CHAPTER 1).

For  $U > U_2 = 5$ , Eq.(4.1) still predicts the existence of three equilibrium states for the same value of U: 1) a stable prolate anisotropic state; 2) an unstable isotropic state; and, 3) a conditionally stable oblate state. For  $U \to \infty$ , the prolate state approaches the nematic state (Point A on Figure 1.1) and the oblate state approaches the planar isotropic state (Point C on Figure 1.1)

### Non-equilibrium States

The class of transient solutions to Eq.(4.1) with the FSQ-closure is sensitive to the tumbling parameter  $\lambda$  and to the initial conditions for  $\langle \underline{p}\,\underline{p} \rangle$  (0). For  $\lambda=1$ , Pe > 0, and U > 0, all planar anisotropic states with the initial director in the flow/cross-flow plane (see Figure 8.8) relax to three-dimensional anisotropic states. None of these states are on the prolate boundary. Figure 8.2 shows the distribution of the steady state invariants. The locus of steady states (II<sub>b</sub>, III<sub>b</sub>)<sub>SS</sub> is parameterized by U and Pe. For fixed Pe, the steady states approach the prolate boundary as U increases. Also, for fixed U, the steady states approach the nematic state as Pe increases. Increases in U and Pe have qualitatively similar effect on director alignment. Thus, Figure 8.1 suggests that an initially isotropic material could be processed to attain the same three-dimensional anisotropic microstructure by following different paths in the plane variations in U and Pe.

For  $\lambda < 1$ , Pe > 0, and U > 0, the asymptotic solutions to Eq.(4.1) with the FSQ-closure may be either steady or periodic. Periodic solutions require a relatively large value of the excluded volume coefficient (e.g., U > 27). If the initial director is in the flow/cross-flow plane and if U > 27, then the theory predicts *director tumbling* for Pe < 20 and *director wagging* as Pe increases. For large Pe and U > 27, the director relaxes to a steady state alignment relative to the flow direction. Figure 8.9 summarizes the physical nature of the asymptotic states for different combinations of U and Pe. This phase diagram or microstructure map, provides the insight needed to attain (or to avoid) specific microstructures.

Table 8.1 summarizes an unanticipated result related to the alignment

phenomenon for large values of Pe. Note that for  $\lambda < 1$ , the steady state invariants approach a highly aligned state independent of Pe; whereas, for  $\lambda = 1$ , the steady state invariants continue to approach the nematic state (see Point A on Figure 1.1). Apparently, the rotational torque due to the vorticity ( $\sim$  Pe) is unable to counter the strong rotational torque due to diffusion because the complementary rotational torque due to the strain rate ( $\sim \lambda$ Pe) is weaker with  $\lambda < 1$ .

For high Péclet numbers (Pe > 90) and for high excluded volume coefficients (U > 27), the asymptotic response of the director for  $\lambda < 1$  depends on the initial condition  $\langle pp \rangle$  (0). For example, if the initial director is in the flow/cross-flow plane, then the director relaxes to a steady state, which has a *negative* offset from the flow direction (see Figure 8.7;  $\lambda = 0.987$ ; U = 27; Pe = 95). However, if the initial director is in the vorticity/flow plane, *director log-rolling* occurs (see Figure 8.10;  $\lambda = 0.987$ ; U = 27; Pe = 95) with a positive offset from the flow direction. On the other hand, if the initial director is in the vorticity/flow plane and the initial condition of  $\langle pp \rangle$  (0) has an off-diagonal component, then *director kayaking* occurs (see Figure 8.13;  $\lambda = 0.987$ ; U = 27; Pe = 95) with a negative offset from the flow direction. This type of behavior has been reported by others based on direct simulations of the S-equation, but the comprehensive set of results given in CHAPTER 8 has not been previously developed using low-order moments to the S-equation primarily because a realizable theory for  $\langle pp \rangle$  was unavailable heretofore.

### Rheology of Rigid Rod Suspensions

The microstructure of a rigid rod suspension has a significant impact on the viscous and elastic components of the deviatoric stress (see Eqs.(4.5) and (4.8)) inasmuch as

$$\hat{\underline{\tau}}^{V} \propto \langle pppp \rangle : \hat{\underline{S}} . \tag{10.3}$$

$$\underline{\hat{\underline{\tau}}}^{E} \propto \left[ (\langle \underline{p}\underline{p} \rangle - \frac{1}{3}\underline{\underline{I}}) - U(\langle \underline{p}\underline{p} \rangle \cdot \langle \underline{p}\underline{p} \rangle - \langle \underline{p}\underline{p}\underline{p}\underline{p} \rangle : \langle \underline{p}\underline{p} \rangle) \right]. \tag{10.4}$$

The tumbling parameter  $\lambda$ , which controls the behavior of  $\langle \underline{p}\underline{p} \rangle$  and, thereby,  $\langle \underline{p}\underline{p}\underline{p}\underline{p} \rangle$ , also impacts the rheology of the suspensions. For  $\lambda=1$ , the shear viscosity has a Newtonian-like behavior for low Pe and a shear thinning behavior at high Pe (see Figure 9.1). As indicated by Figure 9.2, the viscous component of the suspension viscosity determines the shear thinning behavior at high Pe. At low Pe, the elastic and viscous components are equally important.

Figure 9.4 shows how U and Pe influence the shear component of the elastic stress for  $\lambda=1$  (see Eq.(10.4) above; and, Eq.(4.8)). It is not surprising that for Pe > 1, the contribution of the elastic stress decreases inasmuch as the excluded volume contribution to  $\tau_{yz}^E$  diminishes as the director aligns with the flow. Note that the stress model (Eq.(4.7)) with the FSQ-closure for  $\langle pppp \rangle$  (see Figure 9.4) predicts that  $\tau_{yz}^V \propto Pe^{1/3}$  for U = 0 and Pe > 10. However, for U = 5 and 0.2 < Pe < 2,  $\tau_{yz}^E \propto Pe^{1/3}$  also. Thus, in a flow/stop experiment for which  $\hat{\tau}_{yz}^E$  can be measured (see Smyth et al., 1995), it is important to cover a wide range of U ( $\propto$  c) and Pe ( $\propto$   $\dot{\gamma}$ ) to compare with appropriate

theoretical models. For 0.05 wt% xanthan gum in a fructose solution, Smyth et al. (1995) observed that  $\hat{\tau}_{yz}^{E} \propto \dot{\gamma}^{1/3}$  for 1 s<sup>-1</sup> <  $\dot{\gamma}$  < 20 s<sup>-1</sup>. A comparison of this experimental result with the microstructure theory developed herein indicates that  $D_R^o \sim 1.3 \text{ s}^{-1}$  if  $U \cong 5$ . This estimate is consistent with the rotary diffusion coefficients for PBLG solutions (Baek and Magda, 1993; also see Figure 9.4).

As anticipated by the microstructure results in Table 8.1, the shear viscosity predicted for  $\lambda < 1$  has a Newtonian plateau for Pe  $\rightarrow \infty$  (i.e.,  $\lambda = 0.987$ , U = 0, and Pe > 500). Once again, this phenomenon implies that shear thinning is limited by the weaker rotational torque due to particle coupling with the strain rate.

Finally, Figure 9.19 shows that tube dilation causes shear thickening. This unanticipated result occurs provided tube dilation affects rotational diffusion in the moment equation and hydrodynamic drag in the viscous stress equation. This interesting (and perhaps doubtful) result requires additional research (see p.337 Doi and Edwards 1986).

## CHAPTER 11

## RECOMMENDATIONS

The FSQ-closure for the orientation tetrad needs additional development and validation to become a practical closure for Eq.(4.1). Although the traditional models for the *rotary convective flux* and the *rotary diffusive flux* used to close the Smoluchowski equation could be improved, the purpose of this chapter is to identify specific problems that would support the use of Eqs.(4.1) and (4.4).

#### Suspension Theory

In the approach adopted in this research, the tumbling parameter  $\lambda$  (see Eq.(2.5)), the excluded volume coefficient U (see Eq.(2.12)), and the Péclet number Pe (see Eq.(2.15)) were treated as independent dimensionless groups. In general,  $\lambda$ , U,  $\langle D_R \rangle$ , and  $\zeta_R$  depend on the aspect ratio L/d, the volume fraction of the dispersed phase  $\alpha_v$ , and the local microstructure (II<sub>b</sub> and III<sub>b</sub>):

$$\lambda = F_{\lambda}(\frac{L}{d}, \alpha_{v}, II_{b}, III_{b})$$

$$U = F_U(\frac{L}{d}, \alpha_v, II_b, III_b)$$

$$\frac{\langle D_R \rangle}{D_R^o} = F_U(\frac{L}{d}, \alpha_v, II_b, III_b)$$

$$\frac{D_R^0 \zeta_R}{k_B T} = F_\zeta(\frac{L}{d}, \alpha_V, II_b, III_b).$$

A systematic parametric study of Eq.(4.1) and (4.4) with the FSQ-closure should be developed for suspensions of prolate ellipsoids for which  $1 \le L/d < \infty$ . An explicit dependence of L/d and  $\alpha_v$  on the above groups should be used in the parametric study.

The *tube dilation* model of Doi was used in this research to determine the effect of the microstructure on  $<D_R>/D_R^o$  and  $D_R^o\zeta_R/k_BT$ . Shear thickening occurs because tube dilation was included in both factors. The influence of *tube dilation* on the tumbling parameter  $\lambda$  should also be developed, if appropriate. An explicit dependence of L/d on the tumbling parameter was used in this research to study oblate and prolate ellipsoidal suspensions. However, the effect of L/d on  $<D_R>$  and  $\zeta_R$  were not studied. Figure 11.1 shows the variation of the rotary drag coefficient with L/d for prolate ellipsoidal suspensions (see p.292, Doi and Edwards, 1986; and Jeffery, 1922). This theory, and its generalization to oblate ellipsoidal suspensions, should be used in the proposed parametric study of Eqs.(4.1) and (4.4).

#### FSQ-closure coefficient

The FSQ-closure was developed based on the Cayley-Hamilton theorem, which led to the representation of  $\langle \underline{p}\,\underline{p}\,\underline{p}\,\underline{p}\rangle$  given by Eq.(5.7). The second order closure coefficient was selected so that planar anisotropic states are attracted by three-dimensional anisotropic states for all values of  $\lambda$ , U, and Pe. The results in CHAPTER 7, 8, and 9 validated that this approach produces realizable orientation states for simple shear flows. However, the *universality* of C<sub>2</sub>(III<sub>b</sub>) as a second-order closure coefficient

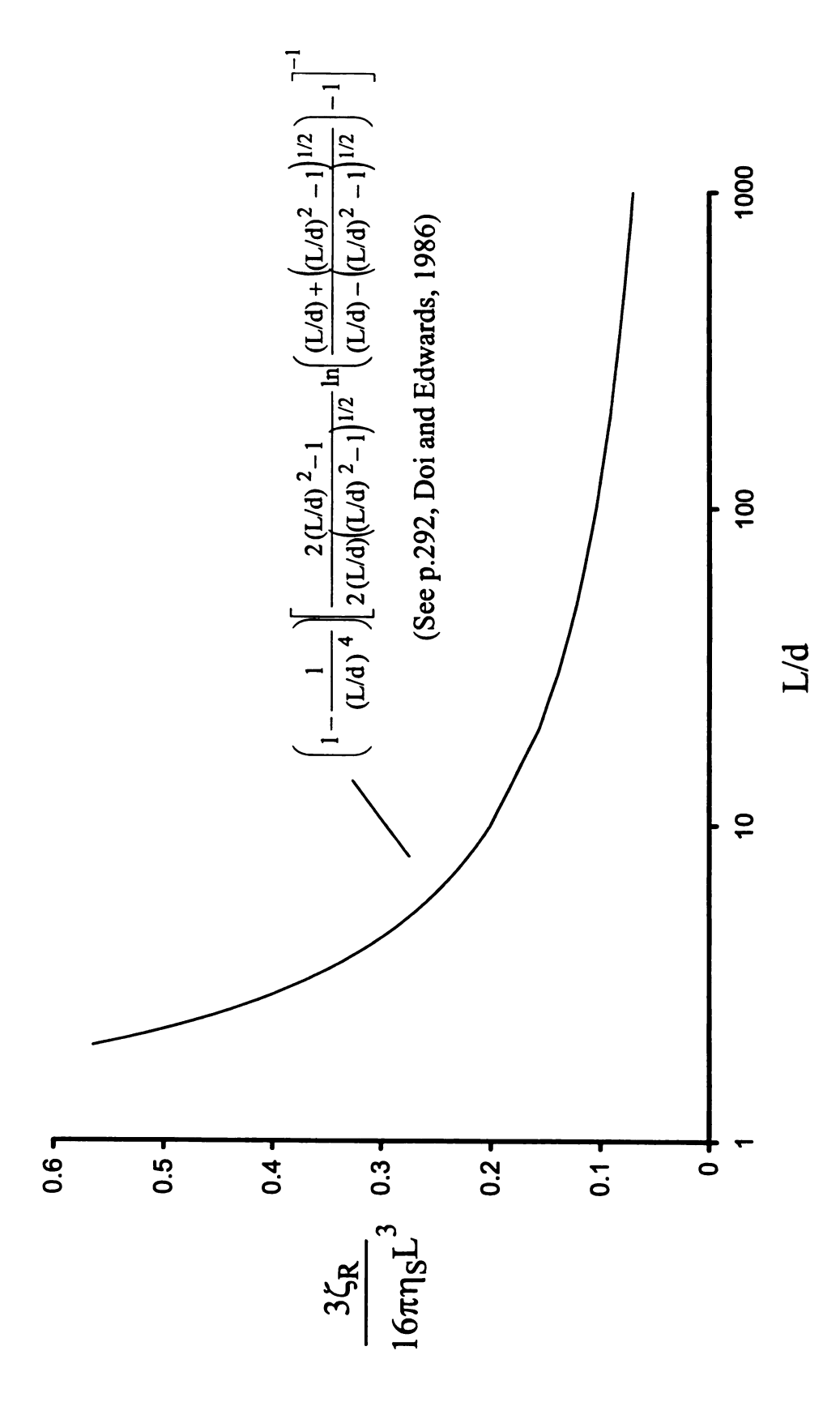


Figure 11.1 The Effect of Particle Aspect Ratio on the Dimensionless Friction Coefficient

needs to be tested for other flows. C<sub>2</sub>(III<sub>b</sub>) also needs to be validated experimentally for simple shear flows.

As demonstrated in CHAPTER 7 as well as in CHAPTER 8, the relaxation of the microstructure to an anisotropic state has a dynamic *signature* that is sensitive to the closure model for  $\langle \underline{p}\,\underline{p}\,\underline{p}\,\underline{p}\rangle$ . For example, the initial trajectory from a planar anisotropic state depends on the closure assumption and could be tested directly (see Figure 7.4). Stress relaxation experiments and/or optical experiments that directly measure the relaxation of the director could be designed to test the *ad hoc* assumption of replacing Ineq.(6.27) with Eq.(6.28).

#### Texture (Pe > 0)

Figure 11.2 shows that Eq.(4.1) with an FSQ-closure has multiple steady states for the same parameter set ( $\lambda$ , U, Pe). Note that for  $\lambda$  = 0.987, U = 27, and Pe = 95, two stable steady state solutions to Eq.(4.1) occur with distinct microstructures: ( $\Pi_b$ ,  $\Pi_b$ )<sub>1</sub> = (0.4923, 0.1381) and ( $\Pi_b$ ,  $\Pi_b$ )<sub>2</sub> = (0.5463, 0.1648). This result was discovered serendipitously by numerically integrating Eq.(4.1) from two different initial conditions (see Figure. 11.2). The first microstructure was obtained by the relaxation of an initial director in the flow/vorticity plane, whereas the second microstructure resulted from the relaxation of an initial director in the flow/cross-flow plane. The existence of multiple steady states for Pe = 0 has been known for many years (see *biphasic* region in CHAPTER 7). The existence of multiple steady states for Pe > 0 have not been systematically studied or discussed in the literature. Larson (p.515, 1999) and Marrucci

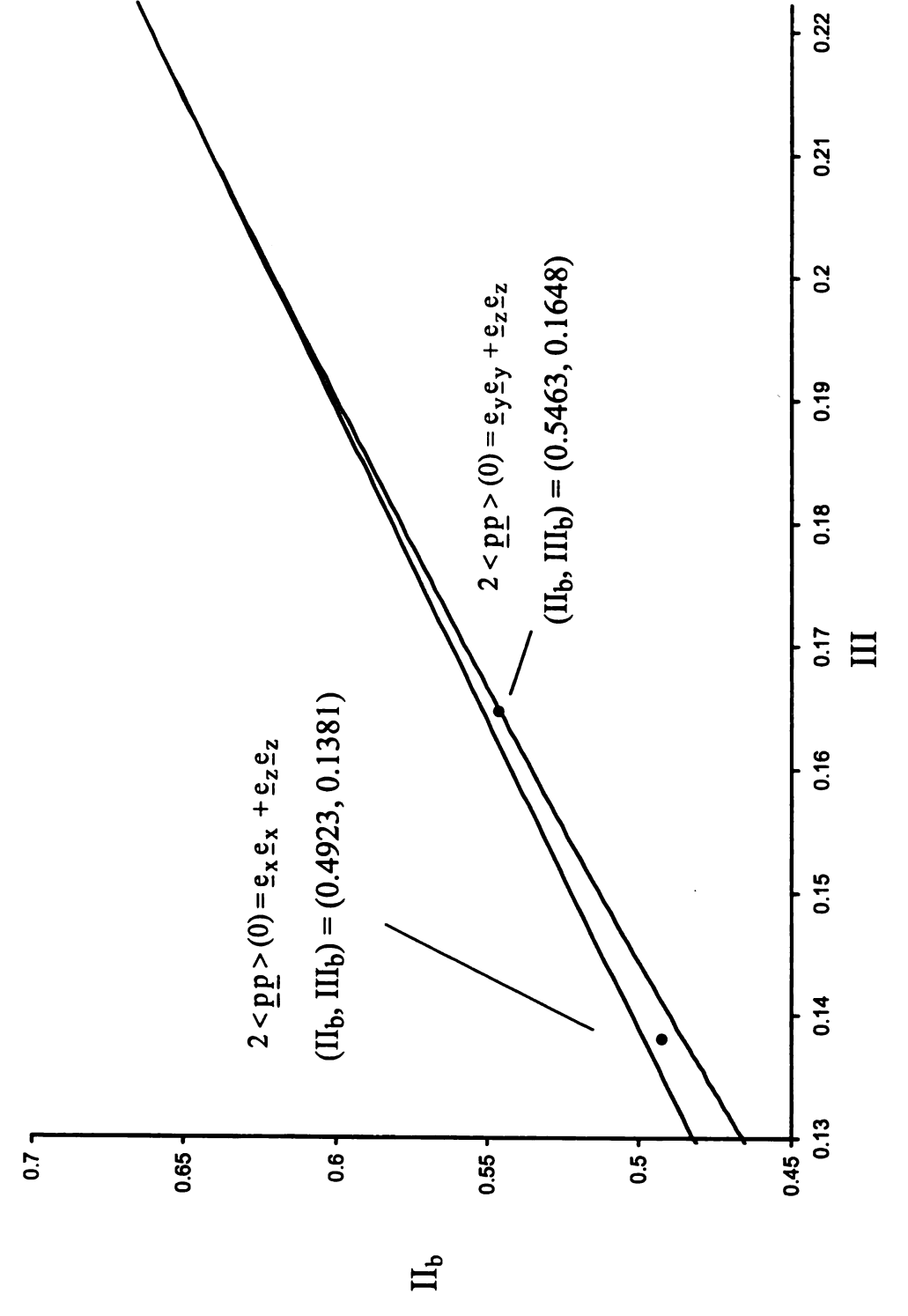


Figure 11.2 Multiple Stable Steady States for Various Initial Orientation Dyads  $(U = 27, Pe = 95, \lambda = 0.987)$ 

(1999) have previously suggested that multiple steady state phenomenon may be the underlying cause for the existence of small strains associated with defects in the microstructure (texture). For very small strain rates, the viscosity would be high, but would decrease significantly for marginal increases in the strain rate inasmuch as the multiple steady states would be eliminated. Marrucci has hypothesized that this phenomenon may explain the *Region I* behavior observed for some liquid crystalline polymers. Thus, the results illustrated by Figure 11.2 together with the possibility that multiple steady states for Pe > 0 may relate to *Region I* behavior supports the suggestion that a comprehensive study of the possible multiple steady state solutions to Eq.(4.1) with the FSQ-closure should be conducted for  $0 < U < \infty$  and  $0 < Pe < \infty$ . This could provide significant new insights and understanding on the origins of *texture* and other phenomena associated with structured fluids.

**APPENDICES** 

### APPENDIX A

Derivation of Moment Equations with Structure Tensor

The objective of APPENDIX A is to find the moment equation in terms of the structure tensor  $\underline{b}$ . From Eq.(4.1), the derivative of dynamic equation with the structure tensor  $\underline{b}$  for  $F_{TD} = 1$  is starting from:

$$\frac{\delta < \underline{p}\underline{p}>}{\delta t} = -\underline{\underline{b}} + U(<\underline{p}\underline{p}> \cdot <\underline{p}\underline{p}> - <\underline{p}\underline{p}>\underline{p}\underline{p}\underline{p}>)$$

$$+ \lambda Pe(\underline{S} \cdot < \underline{p}\underline{p}> + < \underline{p}\underline{p}> \cdot \underline{S} - 2 < \underline{p}\underline{p}\underline{p}>\underline{S})$$
(A.1)

Where

$$\underline{\underline{b}} = <\underline{p}\,\underline{p}> -\frac{1}{3}\,\underline{\underline{I}}\,,$$

$$\langle \underline{p}\,\underline{p} \rangle Pe \equiv \frac{\dot{\gamma}}{6D_R}, \quad \dot{\gamma} \equiv \sqrt{2\underline{\hat{\underline{S}}} : \underline{\hat{\underline{S}}}},$$

$$\underline{\underline{S}} = \frac{1}{\dot{\gamma}} \underline{\hat{S}}, \quad \underline{\hat{S}} = \frac{\nabla u + \nabla u^{T}}{2},$$

and

$$\frac{\delta < \underline{p}\,\underline{p} >}{\delta\,t} = \frac{1}{6D_{R}} \left( \left( \frac{\partial}{\partial\,\hat{t}} + \underline{\hat{u}} \cdot \hat{\nabla} \right) < \underline{p}\,\underline{p} > + \underline{\hat{W}} \cdot < \underline{p}\,\underline{p} > + < \underline{p}\,\underline{p} > \cdot \underline{\hat{W}}^{T} \right)$$
(A.2)

Once the orientation dyad  $\langle \underline{p} \underline{p} \rangle$  is substituted with  $\underline{\underline{b}}$  from left hand side of Eq.(A.1) becomes:

$$\underline{\underline{\hat{W}}} < \underline{p}\,\underline{p} > + < \underline{p}\,\underline{p} > \underline{\hat{W}}^{T} = \underline{\underline{\hat{W}}} \cdot \left(\frac{1}{3}\,\underline{\underline{I}} + \underline{\underline{b}}\right) + \left(\frac{1}{3}\,\underline{\underline{I}} + \underline{\underline{b}}\right) \cdot \underline{\underline{\hat{W}}}^{T} = \underline{\underline{\hat{W}}} \cdot \underline{\underline{b}} + \underline{\underline{b}} \cdot \underline{\underline{\hat{W}}}^{T},$$
where 
$$\underline{\hat{W}} \cdot \underline{\underline{I}} = \underline{\underline{I}} \cdot \underline{\hat{W}}^{T} = 0$$
(A.3)

Once the orientation dyad  $\langle \underline{p} \underline{p} \rangle$  is substituted with  $\underline{b}$ , right hand side of the first line in Eq.(A.1) becomes:

$$\langle \underline{p}\underline{p} \rangle \cdot \langle \underline{p}\underline{p} \rangle - \langle \underline{p}\underline{p} \rangle = \left(\frac{1}{3}\underline{\underline{I}} + \underline{\underline{b}}\right) \cdot \left(\frac{1}{3}\underline{\underline{I}} + \underline{\underline{b}}\right) - \left(\frac{1}{3}\underline{\underline{I}} + \underline{\underline{b}}\right) : \langle \underline{p}\underline{p}\underline{p}\underline{p} \rangle$$

$$= \frac{1}{9}\underline{\underline{I}} + \frac{2}{3}\underline{\underline{b}} + \underline{\underline{b}} \cdot \underline{\underline{b}} - \frac{1}{3} \cdot \langle \underline{p} \cdot \underline{p} \rangle \underline{p}\underline{p} \rangle - \underline{\underline{b}} : \langle \underline{p}\underline{p}\underline{p}\underline{p} \rangle \rangle$$

$$= \frac{1}{9}\underline{\underline{I}} + \frac{2}{3}\underline{\underline{b}} + \underline{\underline{b}} \cdot \underline{\underline{b}} - \frac{1}{9}\underline{\underline{I}} - \frac{1}{3}\underline{\underline{b}} - \underline{\underline{b}} : \langle \underline{p}\underline{p}\underline{p}\underline{p} \rangle \rangle$$

$$= \frac{1}{3}\underline{\underline{b}} + \underline{\underline{b}} \cdot \underline{\underline{b}} - \underline{\underline{b}} : \langle \underline{p}\underline{p}\underline{p}\underline{p} \rangle \rangle$$

$$= \frac{1}{3}\underline{\underline{b}} + \underline{\underline{b}} \cdot \underline{\underline{b}} - \underline{\underline{b}} : \langle \underline{p}\underline{p}\underline{p}\underline{p} \rangle \rangle$$

, and the second line is:

$$\underline{\underline{S}} \cdot \langle \underline{p}\underline{p} \rangle + \langle \underline{p}\underline{p} \rangle \cdot \underline{\underline{S}} - 2 \langle \underline{p}\underline{p}\underline{p}\underline{p} \rangle : \underline{\underline{S}} = \underline{\underline{S}} \cdot \left(\frac{1}{3}\underline{\underline{I}} + \underline{\underline{b}}\right) + \left(\frac{1}{3}\underline{\underline{I}} + \underline{\underline{b}}\right) \cdot \underline{\underline{S}} - 2 \langle \underline{p}\underline{p}\underline{p}\underline{p} \rangle : \underline{\underline{S}}$$

$$= \frac{2}{3}\underline{\underline{S}} + \underline{\underline{S}} \cdot \underline{\underline{b}} + \underline{\underline{b}} \cdot \underline{\underline{S}} - 2 \langle \underline{p}\underline{p}\underline{p}\underline{p} \rangle : \underline{\underline{S}}$$
(A.5)

Combining Eqs.(A.4) and (A.5),

$$\frac{\delta b}{\delta t} = -b + U(\frac{1}{3}b + b \cdot b - b : \langle \underline{p}\underline{p}\underline{p}\underline{p} \rangle) + \lambda Pe(\frac{2}{3}S + S \cdot b + b \cdot S - 2 \langle \underline{p}\underline{p}\underline{p}\underline{p} \rangle : S)$$
 (A.6)

Note1:

$$\operatorname{tr}\left(\frac{\delta \, \underline{b}}{\delta \, t}\right) = \frac{1}{6D_{R}} \operatorname{tr}\left(\frac{D \, \underline{b}}{D \, t}\right) + \frac{1}{6D_{R}} \left(\underline{\underline{\hat{W}}} : \langle \, \underline{p} \, \underline{p} \, \rangle + \langle \, \underline{p} \, \underline{p} \, \rangle : \underline{\underline{\hat{W}}}^{T}\right)$$

$$= \frac{1}{6D_{R}} \operatorname{tr}\left(\frac{D \, \underline{b}}{D \, t}\right) = \frac{1}{6D_{R}} \frac{D}{D \, t} \left(\operatorname{tr}\underline{b}\right), \tag{A.7}$$

since  $\underline{\hat{\mathbf{W}}} : \langle \underline{\mathbf{p}} \, \underline{\mathbf{p}} \rangle = \langle \underline{\mathbf{p}} \, \underline{\mathbf{p}} \rangle : \underline{\hat{\mathbf{W}}}^{\mathrm{T}} = 0$ 

And

$$tr\left(\frac{\delta \underline{b}}{\delta t}\right) = -tr(\underline{b}) + U(\langle \underline{p}\underline{p} \rangle : \langle \underline{p}\underline{p} \rangle - \langle \underline{p}\underline{p} \rangle : \langle \underline{p}\underline{p} (\underline{p} \cdot \underline{p}) \rangle)$$

$$+ \lambda Pe(\underline{S} : \langle \underline{p}\underline{p} \rangle + \langle \underline{p}\underline{p} \rangle : \underline{S} - 2 \langle (\underline{p} \cdot \underline{p}) \underline{p}\underline{p} \rangle : \underline{S})$$

$$= -tr(\underline{b})$$
(A.8)

Therefore, t = 0,  $tr(\underline{b}) = 0$  and t > 0,  $tr(\underline{b}) = 0$ .

Note2:

$$\left(\frac{\delta \, \underline{b}}{\delta \, t}\right)^{T} = \frac{1}{6D_{R}} \left(\left(\frac{\partial \, \underline{b}}{\partial \, t}\right)^{T} + \langle \, \underline{p} \, \underline{p} \, \rangle^{T} : \underline{\hat{W}}^{T} + \underline{\hat{W}} : \langle \, \underline{p} \, \underline{p} \, \rangle^{T}\right) 
= \frac{1}{6D_{R}} \left(\frac{\partial}{\partial \, t} \, \underline{b}^{T} + \langle \, \underline{p} \, \underline{p} \, \rangle^{T} : \underline{\hat{W}}^{T} + \underline{\hat{W}} : \langle \, \underline{p} \, \underline{p} \, \rangle^{T}\right) 
= \frac{\mathcal{D}}{\mathcal{D} \, t} \, \underline{b}^{T} = U(\langle \, \underline{p} \, \underline{p} \, \rangle^{T} : \langle \, \underline{p} \, \underline{p} \, \rangle^{T} - \langle \, \underline{p} \, \underline{p} \, \rangle^{T}) 
+ \lambda Pe(\langle \, \underline{p} \, \underline{p} \, \rangle^{T} : \underline{S}^{T} + \underline{S}^{T} : \langle \, \underline{p} \, \underline{p} \, \rangle^{T} - 2 \langle \, \overline{p} \, \underline{p} \, \underline{p} \, \underline{p} \, \rangle)$$
(A.9)

And

$$\underline{\underline{b}}^{T} = \underline{\underline{b}}, \quad tr(\underline{\underline{b}}) = 0$$
 $\underline{\underline{S}}^{T} = \underline{\underline{S}}, \quad tr(\underline{\underline{S}}) = 0$ 

 $\underline{b}^T$  satisfies the same equation as  $\underline{b}$ . If  $\underline{b}^T = \underline{b}$  at t = 0, then  $\underline{b}^T = \underline{b}$  for t > 0.

Therefore,  $tr(\underline{b})$  and the symmetry of  $\underline{b}$  are "conserved."

## APPENDIX B

Derivation of Moment Equations in the Invariant Form

The objective of APPENDIX B is to find the moment equations in terms of the invariants  $II_b$  and  $III_b$  of the structure tensor  $\underline{b}$ .

General Second Invariant Dynamic Equation

The second invariant dynamic equation is derived by taking trace of the dot product of the structure tensor from Eq.(A.6):

$$\frac{d}{dt} (\underline{b} \cdot \underline{b}) = \frac{d \underline{b}}{dt} \cdot \underline{b} + \underline{b} \cdot \frac{d \underline{b}}{dt}$$

$$= \left[ -(\underline{W} \cdot \underline{b} + \underline{b} \cdot \underline{W}^{T}) - \underline{b} + U\underline{J} + \lambda Pe\underline{K} \right] \cdot \underline{b}$$

$$+ \underline{b} \cdot \left[ -(\underline{W} \cdot \underline{b} + \underline{b} \cdot \underline{W}^{T}) - \underline{b} + U\underline{J} + \lambda Pe\underline{K} \right]$$

$$= -2\underline{b} \cdot \underline{b} + U[\underline{J} \cdot \underline{b} + \underline{b} \cdot \underline{J}] + \lambda Pe[\underline{K} \cdot \underline{b} + \underline{b} \cdot \underline{K}]$$

$$-(\underline{W} \cdot \underline{b} + \underline{b} \cdot \underline{W}^{T}) \cdot \underline{b} + \underline{b} \cdot (\underline{W} \cdot \underline{b} + \underline{b} \cdot \underline{W}^{T})$$
(B.1)

, where 
$$\underline{\underline{J}} = \frac{1}{3}\underline{\underline{b}} + \underline{\underline{b}} \cdot \underline{\underline{b}} - \underline{\underline{b}} : \langle \underline{p} \ \underline{p} \ \underline{p} \ \underline{p} \rangle \text{ and } \underline{\underline{K}} = \frac{2}{3}\underline{\underline{S}} + \underline{\underline{S}} \cdot \underline{\underline{b}} + \underline{\underline{b}} \cdot \underline{\underline{S}} - 2 \langle \underline{p} \ \underline{p} \ \underline{p} \ \underline{p} \rangle : \underline{\underline{S}} .$$

The trace of the ordinary derivative is:

$$tr\left[\frac{d}{dt}\left(\underline{b}\cdot\underline{b}\right)\right] = \frac{d}{dt}\left[tr\left(\underline{b}\cdot\underline{b}\right)\right] = \frac{d\Pi_{b}}{dt}$$

$$= -2\Pi_{b} + 2U\left[\underline{J}:\underline{b}\right] + 2\lambda Pe\left[\underline{K}:\underline{b}\right]$$

$$-\left[\left(\underline{W}\cdot\underline{b} + \underline{b}\cdot\underline{W}^{T}\right):\underline{b} + \underline{b}:\left(\underline{W}\cdot\underline{b} + \underline{b}\cdot\underline{W}^{T}\right)\right]$$
(B.2)

Note that

$$(\underline{\mathbf{W}} \cdot \underline{\mathbf{b}}) : \underline{\mathbf{b}} = \underline{\mathbf{W}} : (\underline{\mathbf{b}} \cdot \underline{\mathbf{b}}) \equiv \mathbf{0}$$

because b is traceless tensor.

Since  $\underline{\underline{W}}^T = -\underline{\underline{W}}$ ,  $(\underline{\underline{b}} \cdot \underline{\underline{W}}^T)$ :  $\underline{\underline{b}} = -(\underline{\underline{b}} \cdot \underline{\underline{W}})$ :  $\underline{\underline{b}} = -(\underline{\underline{b}} \cdot \underline{\underline{b}})$ :  $\underline{\underline{W}} = 0$ . Therefore, the vorticity does not influence dynamic equation of second invariant. The second and third terms in the second line of Eq. (B.2) is

$$\underline{J} : \underline{b} = \frac{1}{3}\underline{b} : \underline{b} + (\underline{b} \cdot \underline{b}) : \underline{b} - \underline{b} : \langle \underline{p} \, \underline{p} \, \underline{p} \, \underline{p} \, \underline{p} \rangle : \underline{b}$$

$$= \frac{1}{3} \Pi_b + \Pi_b - \underline{b} : \langle \underline{p} \, \underline{p} \, \underline{p} \, \underline{p} \, \underline{p} \rangle : \underline{b}$$
(B.3)

and

$$\underline{K} : \underline{b} = \frac{2}{3} \underline{S} : \underline{b} + (\underline{S} \cdot \underline{b}) : \underline{b} + (\underline{b} \cdot \underline{S}) : \underline{b} - 2\underline{b} : \langle \underline{p} \, \underline{p} \, \underline{p} \, \underline{p} \, \underline{p} \rangle : \underline{S}$$

$$= \frac{2}{3} \underline{S} : \underline{b} + \underline{S} : (\underline{b} \cdot \underline{b}) + \underline{S} : (\underline{b} \cdot \underline{b}) - 2\underline{S} : \langle \underline{p} \, \underline{p} \, \underline{p} \, \underline{p} \rangle : \underline{b}$$

$$= 2\underline{S} : \left[ \frac{1}{3} \underline{b} + \underline{b} \cdot \underline{b} - \underline{b} : \langle \underline{p} \, \underline{p} \, \underline{p} \, \underline{p} \rangle \right] = 2\underline{S} : \underline{J}$$
(B.4)

Combining Eqs.(B.3) and (B.4) into Eq.(B.2), the dynamic equation for the second invariant becomes:

$$\frac{d \Pi_{b}}{d t} = -2\Pi_{b} + 2U\left[\underline{\underline{J}} : \underline{\underline{b}}\right] + 2\lambda Pe\left[\underline{\underline{K}} : \underline{\underline{b}}\right]$$

$$= -2\Pi_{b} + 2U\left[\frac{1}{3}\Pi_{b} + \Pi_{b} - \underline{\underline{b}} : \langle \underline{\underline{p}} \, \underline{\underline{p}} \, \underline{\underline{p}} \, \underline{\underline{p}} \, \rangle : \underline{\underline{b}}\right] + 4\lambda Pe\left[\underline{\underline{S}} : \underline{\underline{J}}\right]$$
(B.5)

General Third Invariant Dynamic Equation

The third invariant dynamic equation is derived by taking trace of another dot product from Eq.(B.1):

$$\frac{d}{dt}(\underline{b} \cdot \underline{b} \cdot \underline{b}) = \frac{d\underline{b}}{dt} \cdot \underline{b} \cdot \underline{b} + \underline{b} \cdot \frac{d\underline{b}}{dt} \cdot \underline{b} + \underline{b} \cdot \underline{b} \cdot \underline{d} \cdot \underline{b}$$

$$= -3\underline{b} \cdot \underline{b} \cdot \underline{b} + U[\underline{J} \cdot \underline{b} \cdot \underline{b} + \underline{b} \cdot \underline{J} \cdot \underline{b} + \underline{b} \cdot \underline{b} \cdot \underline{J}] + \lambda Pe[\underline{K} \cdot \underline{b} \cdot \underline{b} + \underline{b} \cdot \underline{K} \cdot \underline{b} + \underline{b} \cdot \underline{b} \cdot \underline{K}]$$

$$- [(\underline{W} \cdot \underline{b} + \underline{b} \cdot \underline{W}^T) \cdot \underline{b} \cdot \underline{b} + \underline{b} \cdot (\underline{W} \cdot \underline{b} + \underline{b} \cdot \underline{W}^T) \cdot \underline{b} + \underline{b} \cdot \underline{b} \cdot (\underline{W} \cdot \underline{b} + \underline{b} \cdot \underline{W}^T)]$$
(B.6)

, where 
$$\underline{\underline{J}} = \frac{1}{3}\underline{\underline{b}} + \underline{\underline{b}} \cdot \underline{\underline{b}} - \underline{\underline{b}} : \langle \underline{p} \, \underline{p} \, \underline{p} \, \underline{p} \rangle \text{ and } \underline{\underline{K}} = \frac{2}{3}\underline{\underline{S}} + \underline{\underline{S}} \cdot \underline{\underline{b}} + \underline{\underline{b}} \cdot \underline{\underline{S}} - 2 \langle \underline{p} \, \underline{p} \, \underline{p} \, \underline{p} \rangle : \underline{\underline{S}}.$$

Note that

$$(\underline{\underline{\mathbf{W}}} \cdot \underline{\underline{\mathbf{b}}}) : (\underline{\underline{\mathbf{b}}} \cdot \underline{\underline{\mathbf{b}}}) = \underline{\underline{\mathbf{W}}} : (\underline{\underline{\mathbf{b}}} \cdot \underline{\underline{\mathbf{b}}} \cdot \underline{\underline{\mathbf{b}}}) \equiv 0.$$

And since 
$$\underline{\underline{W}}^T = -\underline{\underline{W}}$$
,  $(\underline{\underline{b}} \cdot \underline{\underline{W}}^T) : (\underline{\underline{b}} \cdot \underline{\underline{b}}) = -(\underline{\underline{b}} \cdot \underline{\underline{W}}) : (\underline{\underline{b}} \cdot \underline{\underline{b}}) = -(\underline{\underline{b}} \cdot \underline{\underline{b}} \cdot \underline{\underline{b}}) : \underline{\underline{W}} \equiv 0$ .

Therefore, the vorticity does not influence dynamic equation of second invariant. The second and third terms in the second line of Eq. (B.6)

$$\operatorname{tr}\left[\frac{\mathrm{d}}{\mathrm{d}\,t}\left(\underline{\mathbf{b}}\cdot\underline{\mathbf{b}}\cdot\underline{\mathbf{b}}\right)\right] = \frac{\mathrm{d}}{\mathrm{d}\,t}\left[\operatorname{tr}\left(\underline{\mathbf{b}}\cdot\underline{\mathbf{b}}\cdot\underline{\mathbf{b}}\right)\right] = \frac{\mathrm{d}\,\mathrm{III}_{\mathbf{b}}}{\mathrm{d}\,t}$$

$$= -3\mathrm{III}_{\mathbf{b}} + 3\mathrm{U}\left[\underline{\mathbf{J}}:\left(\underline{\mathbf{b}}\cdot\underline{\mathbf{b}}\right)\right] + 3\lambda\mathrm{Pe}\left[\underline{\mathbf{K}}:\left(\underline{\mathbf{b}}\cdot\underline{\mathbf{b}}\right)\right]$$
(B.7)

The second and third terms in the second line of Eq. (B.7)

$$\underline{J}: (\underline{b} \cdot \underline{b}) = \frac{1}{3} \operatorname{tr} (\underline{b} \cdot \underline{b} \cdot \underline{b}) + \operatorname{tr} (\underline{b} \cdot \underline{b} \cdot \underline{b} \cdot \underline{b}) - \underline{b}: \langle \underline{p} \, \underline{p} \, \underline{p} \, \underline{p} \, \underline{p} \, \underline{p} \rangle : (\underline{b} \cdot \underline{b})$$

$$= \frac{1}{3} \Pi I_b + \frac{1}{2} \Pi_b^2 - \underline{b}: \langle \underline{p} \, \underline{p} \, \underline{p} \, \underline{p} \, \underline{p} \rangle : (\underline{b} \cdot \underline{b})$$
(B.8)

and

$$\underline{\underline{K}} : (\underline{b} \cdot \underline{b}) = \frac{2}{3} \underline{\underline{S}} : (\underline{b} \cdot \underline{b}) + \underline{\underline{S}} : (\underline{b} \cdot \underline{b} \cdot \underline{b}) + \underline{\underline{S}} : (\underline{b} \cdot \underline{b} \cdot \underline{b}) - 2\underline{\underline{S}} : (\underline{p} \, \underline{p} \, \underline{p} \, \underline{p} \, \underline{p}) > : (\underline{b} \cdot \underline{b})$$

$$= 2\underline{\underline{S}} : \left[ \frac{1}{3} \underline{\underline{b}} \cdot \underline{\underline{b}} + \underline{\underline{b}} \cdot \underline{\underline{b}} - \langle \underline{p} \, \underline{p} \, \underline{p} \, \underline{p} \, \underline{p} \rangle : (\underline{\underline{b}} \cdot \underline{\underline{b}}) \right]$$
(B.9)

Notice that  $tr(\underline{b} \cdot \underline{b} \cdot \underline{b} \cdot \underline{b}) = \frac{1}{2}II_b^2$  by using Caley-Hamilton theorem.

Combining Eqs.(B.8) and (B.9) into Eq.(B.6), the dynamic equation for the second invariant becomes:

$$\frac{d \operatorname{III}_{b}}{d t} = -3 \operatorname{III}_{b} + 3 \operatorname{U} \left[ \frac{1}{3} \operatorname{III}_{b} + \frac{1}{2} \operatorname{II}_{b}^{2} - \underline{b} : \langle \underline{p} \, \underline{p} \, \underline{p} \, \underline{p} \rangle : (\underline{b} \cdot \underline{b}) \right] 
+ 6 \lambda \operatorname{Pe} \underline{S} : \left[ \frac{1}{3} \underline{b} \cdot \underline{b} + \underline{b} \cdot \underline{b} \cdot \underline{b} - \langle \underline{p} \, \underline{p} \, \underline{p} \, \underline{p} \rangle : (\underline{b} \cdot \underline{b}) \right]$$
(B.10)

# APPENDIX C

Normal Vectors in the Invariant Diagram

The objective of APPENDIX C is to find the outward pointing normal vectors in the boundary of the invariant diagram. Normal vector  $\underline{\mathbf{n}}$  of the invariant diagram is defined as:

$$\underline{\mathbf{n}} = \underline{\mathbf{n}}_{\mathrm{II}} \underline{\mathbf{e}}_{\mathrm{II}} + \underline{\mathbf{n}}_{\mathrm{III}} \underline{\mathbf{e}}_{\mathrm{III}} \tag{C.1}$$

In order to be realizable for the orientation state, the dot product of invariant dynamic equations (dII<sub>b</sub>/dt and dIII<sub>b</sub>/dt) and the normal vector must be less than zero:

$$\underline{\mathbf{n}} \cdot \frac{\mathbf{d}\underline{\mathbf{f}}}{\mathbf{d} \mathbf{t}} \le 0 \quad \text{or } \underline{\mathbf{n}} \cdot \underline{\mathbf{h}} \le 0 \tag{C.2a}$$

where 
$$\frac{d\underline{f}}{dt} = \frac{dII_b}{dt} \underline{e}_{II} + \frac{dIII_b}{dt} \underline{e}_{III}$$
,  $\underline{h} = \frac{d\underline{f}/dt}{\sqrt{(d\underline{f}/dt)\cdot(d\underline{f}/dt)}}$  (C.2b)

Normal vector on the planar anisotropic line

The relationship of IIb and IIIb is

$$II_b = 2 III_b + 2/9$$
 (C.3)

Therefore slope on the planar anisotropic line is 2.

Based on Eq.(C.3) the normalized vector of the planar anisotropic line is:

$$\underline{\mathbf{u}} = \frac{2}{\sqrt{5}} \underline{\mathbf{e}}_{\mathrm{II}} + \frac{1}{\sqrt{5}} \underline{\mathbf{e}}_{\mathrm{III}} \tag{C.4}$$

Then, the normal vector becomes

$$\underline{\mathbf{n}}_{\text{planar anisotropic}} = \frac{1}{\sqrt{5}} \underline{\mathbf{e}}_{\text{II}} - \frac{2}{\sqrt{5}} \underline{\mathbf{e}}_{\text{III}}$$
 (C.5)

Normal vector on the prolate line

From Eq.(3.18), the slope of the prolate line is

$$(4/6)(6/III_b)^{1/3}$$
 (C.6)

Then, normalized base vector becomes:

$$\underline{\mathbf{u}}_{\text{prolate}} = \frac{(4/6)(6/\text{III}_{\text{b}})^{1/3}}{\sqrt{1 + (4/9)(6/\text{III}_{\text{b}})^{2/3}}} \underline{\mathbf{e}}_{\text{II}} + \frac{1}{\sqrt{1 + (4/9)(6/\text{III}_{\text{b}})^{2/3}}} \underline{\mathbf{e}}_{\text{III}}$$
(C.7)

Therefore, the normal vector on the prolate line becomes:

$$\underline{\mathbf{n}}_{\text{prolate}} = \frac{-1}{\sqrt{1 + (4/9)(6/III_b)^{2/3}}} \underline{\mathbf{e}}_{\text{II}} + \frac{(4/6)(6/III_b)^{1/3}}{\sqrt{1 + (4/9)(6/III_b)^{2/3}}} \underline{\mathbf{e}}_{\text{III}}$$
(C.8)

Normal vector at oblate line

From Eq.(3.17), the normalized base vector becomes:

$$\underline{\mathbf{u}}_{\text{oblate}} = \frac{(4/6)(-6/\Pi_b)^{1/3}}{\sqrt{1+(4/9)(-6/\Pi_b)^{2/3}}} \underline{\mathbf{e}}_{\text{II}} + \frac{-1}{\sqrt{1+(4/9)(-6/\Pi_b)^{2/3}}} \underline{\mathbf{e}}_{\text{III}}$$
(C.9)

Therefore, the normal vector becomes:

$$\underline{\mathbf{n}}_{\text{oblate}} = \frac{-1}{\sqrt{1 + (4/9)(-6/\Pi_b)^{2/3}}} \underline{\mathbf{e}}_{\text{II}} + \frac{-(4/6)(-6/\Pi_b)^{1/3}}{\sqrt{1 + (4/9)(-6/\Pi_b)^{2/3}}} \underline{\mathbf{e}}_{\text{III}}$$
(C.10)

### APPENDIX D

Derivation of Various Closure Analysis in the Invariant Form

The objective of APPENDIX D is to find the moment equations in terms of the invariants  $II_b$  and  $III_b$  of the structure tensor  $\underline{b}$  for various closure approximations. With the invariants of moment equations, the realizability of orientation dyad  $\langle \underline{p} \, \underline{p} \rangle$  is determined.

#### Realizability of Decoupling Closure

Decoupling approximation provides realizable orientation dyad without the external field (Pe = 0). The moment equation can be represented with invariants of  $\underline{\underline{b}}$ , then the moment equation can be represented with scalar value of  $II_b$  and  $III_b$ .

The invariant form of decoupling closure double dot with dyad  $\underline{\underline{b}}$  from Eq.(A.6) is:

$$\underline{\underline{b}}: \langle \underline{p}\,\underline{p}\,\underline{p}\,\underline{p} \rangle = \underline{\underline{b}}: \langle \underline{p}\,\underline{p} \rangle \langle \underline{p}\,\underline{p} \rangle \tag{D.1}$$

Based on general the invariant dynamic equations (see Eq. (B.5) and Eq. (B.10)), each the double dot product of decoupling closure becomes:

$$\underline{\underline{b}}: \langle \underline{p}\,\underline{p} \rangle \langle \underline{p}\,\underline{p} \rangle: \underline{\underline{b}}. \tag{D.2}$$

$$\underline{\underline{b}}: <\underline{p}\,\underline{p}> <\underline{p}\,\underline{p}>: \left(\,\underline{\underline{b}}\cdot\underline{\underline{b}}\,\right)$$

Since 
$$\langle \underline{p} \ \underline{p} \rangle : \underline{\underline{b}} = \left(\underline{\underline{b}} + \frac{1}{3}\underline{\underline{I}}\right) : \underline{\underline{b}} = \underline{\underline{b}} : \underline{\underline{b}} = \underline{II}_{\underline{b}}$$
 (D.3a)

and 
$$\langle \underline{p} \ \underline{p} \rangle : (\underline{\underline{b}} \cdot \underline{\underline{b}}) = (\underline{\underline{b}} + \frac{1}{3}\underline{\underline{I}}) : (\underline{\underline{b}} \cdot \underline{\underline{b}}) = tr(\underline{\underline{b}} \cdot \underline{\underline{b}}) + \frac{1}{3}tr(\underline{\underline{b}} \cdot \underline{\underline{b}}) = III_b + \frac{1}{3}II_b$$
, (D.3b)

the invariant form from Eq.(D.2) becomes:

$$\underline{\mathbf{b}} : \langle \mathbf{p} \, \mathbf{p} \rangle \langle \mathbf{p} \, \mathbf{p} \rangle : \underline{\mathbf{b}} = \mathrm{II}_{\mathbf{b}}^{2} \tag{D.4a}$$

and

$$\underline{\underline{b}} : \langle \underline{p} \, \underline{p} \rangle \langle \underline{p} \, \underline{p} \rangle : \left(\underline{\underline{b}} \cdot \underline{\underline{b}}\right) = \Pi_b \Pi_b + \frac{1}{3} \Pi_b^2 \tag{D.4b}$$

Therefore, the invariant forms of moment equations for the decoupling closure, when Pe = 0 are:

$$\frac{d II_b}{d t} = -2II_b + 2U \left[ \frac{1}{3}II_b + III_b - II_b^2 \right]$$
 (D.5a)

and

$$\frac{d \Pi I_b}{d t} = -3\Pi I_b + 3U \left[ \frac{1}{3} \Pi I_b + \frac{1}{6} \Pi_b^2 - \Pi I_b \Pi_b \right]$$
 (D.5b)

Realizability at planar anisotropic line

Substituting  $II_b$  and  $III_b$  relationship at planar anisotropic line ( $II_b = 2III_b + 2/9$ ) into Eq.(D.5a) and Eq.(D.5b), the invariant form of moment equations become:

$$\frac{d \Pi_b}{d t} = -4 \Pi_b - \frac{4}{9} + U \left[ -8 \Pi_b^2 + \frac{14}{9} \Pi_b + \frac{4}{81} \right]$$
 (D.6a)

$$\frac{d III_b}{d t} = -3III_b + U \left[ -4III_b^2 + \frac{7}{9}III_b + \frac{2}{81} \right].$$
 (D.6b)

Using normal vector analysis (see Eq.(C.2)),

$$\underline{\mathbf{n}} \cdot \frac{d\underline{\mathbf{f}}}{dt} = \underline{\mathbf{n}} \cdot \left( \frac{dII_b}{dt} \underline{\mathbf{e}}_{II} + \frac{dIII_b}{dt} \underline{\mathbf{e}}_{III} \right) \le 0 \tag{D.7}$$

Therefore dot product becomes:

$$\underline{\mathbf{n}} \cdot \frac{d\underline{\mathbf{f}}}{d t} = \frac{1}{\sqrt{5}} \frac{dII_b}{d t} + -\frac{2}{\sqrt{5}} \frac{dIII_b}{d t}$$

$$= \frac{2(-2 + 9III_b)}{9\sqrt{5}}$$
(D.8)

Since the maximum  $III_b$  value is 2/9, the dot product is always negative.

Realizability prolate and oblate line

Using the same method from Eq.(D.6), the invariant form of moment equations on the prolate line become:

$$\frac{d II_b}{d t} = -12 \left(\frac{III_b}{6}\right)^{\frac{2}{3}} + 2U \left[2 \left(\frac{III_b}{6}\right)^{\frac{2}{3}} + III_b - 36 \left(\frac{III_b}{6}\right)^{\frac{4}{3}}\right]$$
 (D.9a)

$$\frac{d III_b}{d t} = -3III_b + 3U \left[ \frac{1}{3}III_b + 6\left(\frac{III_b}{6}\right)^{\frac{4}{3}} - 6III_b \left(\frac{III_b}{6}\right)^{\frac{2}{3}} \right]$$
 (D.9b)

After taking dot product with normal vector from Eq.(C.10) to Eq.(D.9a) and Eq.(D.9b), Eq.(D.7) is zero. Analogous to the prolate line, the oblate line provides the same result. Therefore, decoupling closure in prolate line and oblate line are realizable.

#### Realizability of Hand's Closure

From section 6.2 mention, Hand's closure provides realizable orientation dyad on the prolate and the oblate line. Based on general the invariant moment equations (see Eq. (B.5) and Eq. (B.10)), each the double dot products of Hand's closure are:

$$\underline{\underline{b}} :< p_{i}p_{j}p_{k}p_{l} >_{Hand} : \underline{\underline{b}} = b_{ij} \left[ -\frac{1}{35} \left( I_{ij}I_{kl} + I_{ik}I_{jl} + I_{il}I_{jk} \right) + \frac{1}{7} \left( p_{i}p_{j}I_{kl} + p_{i}p_{k}I_{jl} + p_{i}p_{l}I_{jk} + I_{ij}p_{k}p_{l} + I_{ik}p_{j}p_{l} + I_{il}p_{j}p_{k} \right) \right] b_{ij}$$
(D.10)

$$\underline{\underline{b}} :< p_{i}p_{j}p_{k}p_{l} >_{Hand}: (\underline{\underline{b}} \cdot \underline{\underline{b}}) = b_{ij} \left[ -\frac{1}{35} \left( I_{ij}I_{kl} + I_{ik}I_{ji} + I_{il}I_{jk} \right) + \frac{1}{7} \left( p_{i}p_{j}I_{kl} + p_{i}p_{k}I_{jl} + p_{i}p_{l}I_{jk} + I_{ij}p_{k}p_{l} + I_{ik}p_{j}p_{l} + I_{il}p_{j}p_{k} \right) \right] (b_{i\gamma}b_{j\gamma})$$
(D.11)

The right hand side from Eq. (D.11) becomes

$$\frac{2}{15}II_b + \frac{4}{7}III_b \tag{D.12}$$

Substituting Eq.(D.12) into Eq. (B.5), the second invariant moment equation becomes:

$$\frac{d II_b}{d t} = -2F_{TD}II_b + 2F_{TD}U \left[ \frac{7}{35}II_b + \frac{6}{7}III_b \right]$$
 (D.13)

The right hand side from Eq. (D.11) becomes

$$\frac{3}{7}\Pi_{b}^{2} + \frac{2}{15}\Pi_{b} \tag{D.14}$$

Substituting Eq.(D.14) into Eq. (B.10), the third invariant moment equation becomes:

$$\frac{d III_b}{d t} = -3F_{TD}III_b + 3F_{TD}U \left[ \frac{1}{5}III_b + \frac{1}{14}II_b^2 \right]$$
 (D.15)

Realizability at planar anisotropic line

Substituting  $II_b$  and  $III_b$  relationship at planar anisotropic line ( $II_b = 2III_b + 2/9$ ) into Eq.(D.13) and Eq.(D.15), the invariant form of moment equations become:

$$\frac{d \Pi_b}{d t} = -4 \Pi_b - \frac{4}{9} + U \left[ \frac{2}{9} + \frac{29}{7} \Pi_b \right]$$
 (D.16)

$$\frac{d III_b}{d t} = -3III_b + U \left[ -6III_b^2 + \frac{83}{15}III_b + \frac{2}{27} \right]$$
 (D.17)

Using normal vector analysis (see Eq.(C.2)),

$$\underline{\mathbf{n}} \cdot \frac{\mathbf{d}\underline{\mathbf{f}}}{\mathbf{d}\,\mathbf{t}} = \underline{\mathbf{n}} \cdot \left( \frac{\mathbf{d}\Pi_{\mathbf{b}}}{\mathbf{d}\,\mathbf{t}} \underline{\mathbf{e}}_{\mathbf{II}} + \frac{\mathbf{d}\Pi\Pi_{\mathbf{b}}}{\mathbf{d}\,\mathbf{t}} \underline{\mathbf{e}}_{\mathbf{III}} \right) \le 0 \tag{D.18}$$

Therefore dot product becomes:

$$\underline{\mathbf{n}} \cdot \frac{d\underline{\mathbf{f}}}{dt} = -\frac{2(-2 + 9III_b)(-105 + 2(8 + 45III_b)U)}{945\sqrt{5}}$$
(D.18b)

Therefore, Hand's closure is not realizable at a certain U and  $III_b$  (where  $2(8+45III_b)U$  is more than 105).

Realizability prolate and oblate line

The invariant forms of moment equation of Hand's closure on the prolate line become:

$$\frac{d II_b}{d t} = -12 \left( \frac{III_b}{6} \right)^{\frac{2}{3}} + 2U \left[ \frac{6}{5} \left( \frac{III_b}{6} \right)^{\frac{2}{3}} + \frac{6}{7} III_b \right]$$
 (D.19)

$$\frac{d III_b}{d t} = -3III_b + 3U \left[ \frac{1}{5}III_b + \frac{18}{7} \left( \frac{III_b}{6} \right)^{\frac{4}{3}} \right]$$
 (D.20)

Multiplying Eq.(D.19) and .Eq. (D.20) with 
$$-\frac{2}{3} \left( \frac{-6}{\text{III}_b} \right)^{1/3}$$
 (see Eq.(C.10)), Eq.(D.7)

becomes zero. Therefore,  $n \cdot \frac{d\underline{f}}{dt} = 0$  at the prolate line. Analogous to the prolate line, the oblate line provides the same result. Therefore, Hand's closure on the prolate line and the oblate line are realizable.

#### Realizability of HL1 Closure

HL1 closure provides realizable orientation dyad on the prolate and the oblate line for Pe = 0. Based on general the invariant moment equations (see Eq. (B.5) and Eq. (B.10)), each the double dot products of in HL1 closure are:

$$\underline{\underline{b}} : \langle \underline{p} \, \underline{p} \, \underline{p} \, \underline{p} \rangle : \underline{\underline{b}} = \frac{1}{5} \, \underline{\underline{b}} : (6 \langle \underline{p} \, \underline{p} \rangle \cdot \underline{\underline{b}} \langle \underline{p} \, \underline{p} \rangle - \langle \underline{p} \, \underline{p} \rangle \cdot \underline{\underline{b}} ) : \underline{\underline{b}} 
+ 2\underline{\underline{I}} \langle \underline{p} \, \underline{p} \rangle : \underline{\underline{b}} - 2\underline{\underline{I}} \langle \underline{p} \, \underline{p} \rangle \cdot \langle \underline{p} \, \underline{p} \rangle : \underline{\underline{b}}) : \underline{\underline{b}}$$
(D.21)

$$\underline{\underline{b}} : < \underline{p} \, \underline{p} \, \underline{p} \, \underline{p} > : (\underline{\underline{b}} \cdot \underline{\underline{b}}) = \frac{1}{5} \, \underline{\underline{b}} : (6 < \underline{p} \, \underline{p} > : \underline{\underline{b}} \cdot < \underline{p} \, \underline{p} > - < \underline{p} \, \underline{p} > : \underline{\underline{b}} ) : (\underline{\underline{b}} \cdot \underline{\underline{b}}) = \underline{\underline{b}} : (2\underline{\underline{I}} < \underline{p} \, \underline{p} > - < \underline{p} \, \underline{p} > : \underline{\underline{b}} ) : (\underline{\underline{b}} \cdot \underline{\underline{b}}) : (\underline{\underline{b}}$$

Eq. (D.21) becomes

$$\frac{1}{5}(4III_b + \frac{2}{3}II_b + 2II_b^2)$$
 (D.23)

Substituting Eq.(D.22) into Eq. (B.5), the second invariant moment equation becomes:

$$\frac{d II_b}{d t} = -2F_{TD}II_b + 2F_{TD}U \left[ \frac{1}{5}III_b + \frac{1}{5}II_b - \frac{2}{5}II_b^2 \right]$$
 (D.24)

Eq.(D.22) becomes

$$\frac{1}{5} \left( \frac{2}{3} III_b + 2II_b III_b + \frac{7}{3} II_b^2 \right)$$
 (D.25)

Substituting Eq.(D.25) into Eq. (B.10), the third invariant moment equation becomes:

$$\frac{d \, \Pi I_b}{d \, t} = -3F_{TD} \Pi I_b + 3F_{TD} U \left[ \frac{1}{5} \Pi I_b - \frac{2}{5} \Pi_b \Pi I_b + \frac{1}{30} \Pi_b^2 \right]$$
 (D.26)

Realizability at planar anisotropic line

Substituting  $II_b$  and  $III_b$  relationship at planar anisotropic line ( $II_b = 2III_b + 2/9$ ) into Eq.(D.24) and Eq.(D.26), the invariant form of moment equations become:

$$\frac{d\Pi_b}{dt} = -4\Pi I_b - \frac{4}{9} + U \frac{3}{405} [(-2 + 9\Pi I_b)(5 + 72\Pi I_b)]$$
 (D.27)

$$\frac{d \text{ III}_b}{d t} = -3 \text{III}_b + \text{U}[(-2 + 9 \text{III}_b)(1 + 90 \text{III}_b)]. \tag{D.28}$$

Using normal vector analysis (see Eq.(C.2)),

$$\underline{\mathbf{n}} \cdot \frac{\mathrm{d}\underline{\mathbf{f}}}{\mathrm{d}\,\mathbf{t}} = \underline{\mathbf{n}} \cdot \left( \frac{\mathrm{d}\Pi_{\mathbf{b}}}{\mathrm{d}\,\mathbf{t}} \underline{\mathbf{e}}_{\mathbf{III}} + \frac{\mathrm{d}\Pi_{\mathbf{b}}}{\mathrm{d}\,\mathbf{t}} \underline{\mathbf{e}}_{\mathbf{III}} \right) \le 0 \quad . \tag{D.29a}$$

Therefore dot product becomes:

$$\underline{\mathbf{n}} \cdot \frac{d\underline{\mathbf{f}}}{dt} = \frac{2(-2 + 9III_b)(45 + 2(-2 + 9III_b)U)}{405\sqrt{5}}$$
(D.30b)

Therefore, HL1 closure is not realizable at a certain U and  $III_b$  (where  $2(-2+9III_b)$ U is more than 105).

#### Realizability prolate line

The invariant forms of moment equation of HL1 on the prolate line become:

$$\frac{d \Pi_b}{d t} = -12 \left( \frac{III_b}{6} \right)^{\frac{2}{3}} + 2U \left[ \frac{6}{5} \left( \frac{III_b}{6} \right)^{\frac{2}{3}} + \frac{1}{5} III_b - \frac{72}{5} \left( \frac{III_b}{6} \right)^{\frac{4}{3}} \right]$$
 (D.31)

$$\frac{d III_b}{d t} = -3III_b + 3U \left[ \frac{1}{5}III_b + \frac{6}{5} \left( \frac{III_b}{6} \right)^{\frac{4}{3}} - \frac{72}{5} \left( \frac{III_b}{6} \right)^{\frac{5}{3}} \right]$$
 (D.32)

Multiplying Eq.(D.31) and .Eq. (D.32) with 
$$-\frac{2}{3} \left(\frac{-6}{III_b}\right)^{1/3}$$
 (see Eq.(C.10)), Eq.(D.7)

becomes zero. Therefore,  $n \cdot \frac{d\underline{f}}{dt} = 0$  at prolate line. Analogous to the prolate line, the oblate line provides the same result. Therefore, decoupling closure on the prolate line and the oblate line are realizable.

#### Realizability of FSQ Closure

FSQ-model provides realizable orientation dyad on the planar anisotropic line if  $C_2 \ge \frac{8+45\Pi I_b}{18(1+9\Pi I_b)}$ . In addition, FSQ-model provides realizable orientation dyad on the prolate and the oblate line, regardless of  $C_2$  without the external field. The first term of FSQ-model is Hand's closure and it is already proven in Eq. (D.18), Eq. (D.19), and (D.20). Based on general the invariant moment equations (see Eq. (B.5) and Eq. (B.10)), each the double dot products of in second term of FSQ closure are:

$$\underline{b}: \Im_{2}(\langle \underline{p} \, \underline{p} \rangle): \underline{b} = C_{2}(II_{b}, III_{b}) \, b_{ij} \left[ \frac{2}{35} \langle p_{\alpha} p_{\beta} \rangle \langle p_{\alpha} p_{\beta} \rangle \langle I_{ij} I_{kl} + I_{ik} I_{jl} + I_{il} I_{jk} \rangle \right] \\
+ \left( \langle p_{i} p_{j} \rangle \langle p_{k} p_{l} \rangle + \langle p_{i} p_{k} \rangle \langle p_{j} p_{l} \rangle + \langle p_{i} p_{l} \rangle \langle p_{j} p_{k} \rangle \right) \\
- \frac{2}{7} \left( \langle p_{i} p_{\gamma} \rangle \langle p_{\gamma} p_{j} \rangle I_{kl} + \langle p_{i} p_{\gamma} \rangle \langle p_{\gamma} p_{k} \rangle I_{jl} + \langle p_{i} p_{\gamma} \rangle \langle p_{\gamma} p_{l} \rangle I_{jk} \\
+ I_{ij} \langle p_{k} p_{\gamma} \rangle \langle p_{\gamma} p_{l} \rangle + I_{ik} \langle p_{j} p_{\gamma} \rangle \langle p_{\gamma} p_{l} \rangle + I_{il} \langle p_{j} p_{\gamma} \rangle \langle p_{\gamma} p_{k} \rangle \right] b_{ij} \tag{D.33}$$

$$\underline{b}: \Im_{2}(\langle \underline{p} \, \underline{p} \rangle): (\underline{b} \cdot \underline{b}) \\
= C_{2}(II_{b}, III_{b}) b_{ij} \left[ \frac{2}{35} \langle p_{\alpha} p_{\beta} \rangle \langle p_{\alpha} p_{\beta} \rangle (I_{ij} I_{kl} + I_{ik} I_{jl} + I_{il} I_{jk}) \\
+ (\langle p_{i} p_{j} \rangle \langle p_{k} p_{l} \rangle + \langle p_{i} p_{k} \rangle \langle p_{j} p_{l} \rangle + \langle p_{i} p_{l} \rangle \langle p_{j} p_{k} \rangle) \\
- \frac{2}{7} (\langle p_{i} p_{\gamma} \rangle \langle p_{\gamma} p_{j} \rangle I_{kl} + \langle p_{i} p_{\gamma} \rangle \langle p_{\gamma} p_{k} \rangle I_{jl} + \langle p_{i} p_{\gamma} \rangle \langle p_{\gamma} p_{l} \rangle I_{jk} \\
+ I_{ij} \langle p_{k} p_{\gamma} \rangle \langle p_{\gamma} p_{l} \rangle + I_{ik} \langle p_{j} p_{\gamma} \rangle \langle p_{\gamma} p_{l} \rangle + I_{il} \langle p_{j} p_{\gamma} \rangle \langle p_{\gamma} p_{k} \rangle) (b_{i\gamma} b_{j\gamma})$$
(D.34)

Eq. (D.33) becomes

$$\left[\frac{4}{35}\left(\Pi_b + \frac{1}{3}\right) + \frac{2}{21}\right]\Pi_b + \frac{10}{7}\Pi_b^2 + \frac{4}{7}\Pi_b^2 + \frac{4}{7}\Pi_b = \frac{2}{105}\left(7\Pi_b + 8\Pi_b^2 + 30\Pi_b\right)$$
 (D.35)

Substituting Eq.(D.35) into Eq. (B.5), the second invariant moment equation becomes:

$$\frac{d \Pi_b}{d t} = -2F_{TD}\Pi_b + 2F_{TD}U \left[ \frac{7}{35}\Pi_b + \frac{3}{7}\Pi_b - \frac{54}{35}\Pi_b^2C_2 \right]$$
 (D.36)

Eq. (D.34) becomes

$$\left[\frac{4}{35}\left(\Pi_{b} + \frac{1}{3}\right) + \frac{2}{21}\right]\Pi_{b} + \frac{3}{7}\Pi_{b}^{2} + \frac{10}{7}\Pi_{b}\Pi_{b} = \frac{3}{7}\Pi_{b}^{2} + \frac{2}{15}\Pi_{b} + \frac{54}{35}\Pi_{b}\Pi_{b}$$
 (D.37)

Substituting Eq.(D.37) into Eq. (B.5), the third invariant moment equation becomes:

$$\frac{d III_b}{d t} = -3F_{TD}III_b + 3F_{TD}U \left[ \frac{7}{35}III_b + \frac{1}{14}II_b^2 - \frac{54}{35}II_bIII_bC_2 \right]$$
 (D.38)

#### Realizability prolate line

The invariant forms of dynamic equation of FSQ-model on the prolate line become:

$$\frac{d \Pi_b}{d t} = -12 \left( \frac{III_b}{6} \right)^{\frac{2}{3}} + 2U \left[ \frac{6}{5} \left( \frac{III_b}{6} \right)^{\frac{2}{3}} + \frac{3}{7} III_b - \frac{1944}{35} \left( \frac{III_b}{6} \right)^{\frac{4}{3}} C_2 \right]$$
 (D.39)

$$\frac{d \, III_b}{d \, t} = -3III_b + 3U \left[ \frac{1}{5} III_b + \frac{18}{7} \left( \frac{III_b}{6} \right)^{\frac{4}{3}} - \frac{1944}{35} \left( \frac{III_b}{6} \right)^{\frac{5}{3}} C_2 \right]$$
 (D.40)

Multiplying Eq.(D.39) and .Eq. (D.40) with 
$$-\frac{2}{3} \left( \frac{-6}{\text{III}_b} \right)^{1/3}$$
 (see Eq.(C.10)), Eq.(D.7)

becomes zero. Therefore,  $n \cdot \frac{d\underline{f}}{dt} = 0$  at prolate line. Analogous to the prolate line, the oblate line provides the same result. Therefore, FSQ-model closure on the prolate line and the oblate line are realizable.

## APPENDIX E

Eigenvalues and Eigenvectors of the Orientation Dyad

The objective of APPENDIX E is to find the eigenvalues and eigenvectors when the dyadic valued operator has zero components in  $p_xp_y$ ,  $p_xp_z$ ,  $p_yp_x$ , and  $p_zp_x$ . Thus, the eigenvalues and the eigenvectors can be solved algebraically. If the dyadic valued operator is given as:

$$\langle pp \rangle \cdot \underline{x}_i = \lambda_i \underline{x}_i$$
 (E.1)

, then it can be expanded to:

$$\begin{pmatrix}
p_{\mathbf{x}}p_{\mathbf{x}} & 0 & 0 \\
0 & p_{\mathbf{y}}p_{\mathbf{y}} & p_{\mathbf{y}}p_{\mathbf{z}} \\
0 & p_{\mathbf{z}}p_{\mathbf{y}} & p_{\mathbf{z}}p_{\mathbf{z}}
\end{pmatrix}
\begin{pmatrix}
x_{ix} \\
x_{iy} \\
x_{iz}
\end{pmatrix} = \lambda_{i} \begin{pmatrix}
x_{ix} \\
x_{iy} \\
x_{iz}
\end{pmatrix}, 
(E.2)$$

where  $\underline{x}_i$  is the eigenvector, related to the eigenvalues  $\lambda_i$ 

Therefore,

$$p_{x}p_{x} x_{ix} = \lambda_{i} x_{ix}$$
 (E.3a)

$$p_y p_y x_{iy} + p_y p_z x_{iy} = \lambda_i x_{iy}$$
 (E.3b)

$$p_z p_y x_{iz} + p_z p_z x_{iz} = \lambda_i x_{iz}$$
 (E.3c)

Based on Eqs.(E.3b) and (E.3c),  $x_{1x}$ ,  $x_{2y}$ ,  $x_{2z}$ ,  $x_{3y}$ , and  $x_{3z}$  are only non-zero component of eigenvector if all of non-zero components of the dyad from Eq.(E.2) and all of the eigenvalues are different each other.

Using Eqs.(E.3b) and (E.3c),

$$\left[ \left( p_z p_z - \lambda_i \right) \left( p_y p_y - \lambda_i \right) - p_z p_y p_y p_z \right] x_{iz} = 0$$
 (E.4)

For i = 1, Eq.(E.3a) becomes:

$$p_x p_x x_{1x} = \lambda_1 x_{1x} \tag{E.5}$$

Therefore,  $\lambda_1$  is the same as  $p_x p_x$ .

The first eigenvector related to  $\lambda_1$  becomes:

$$\underline{\mathbf{x}}_{1} = \mathbf{x}_{1\mathbf{x}} \begin{pmatrix} 1 \\ 0 \\ 0 \end{pmatrix} \tag{E.6}$$

For i = 2, Eqs.(E.3a) and (E.4) becomes:

$$x_{2y} = -\frac{p_y p_z x_{2z}}{(p_y p_y - \lambda_2)}$$
 (E.7a)

$$[(p_{z}p_{z} - \lambda_{2})(p_{y}p_{y} - \lambda_{2}) - p_{z}p_{y} p_{y}p_{z}]x_{3y} = 0$$
 (E.7b)

Since  $x_{32}$  is non-zero component, the inside bracket in Eq.(E.7b) can be solved using quadratic equation.

$$\lambda_{2} = \frac{(p_{y}p_{y} + p_{z}p_{z}) - \sqrt{(p_{y}p_{y} + p_{z}p_{z})^{2} - 4(p_{y}p_{y} p_{z}p_{z} - p_{y}p_{z} p_{z}p_{y})}}{2}$$
(E.8)

From Eq.(E.7a), the second eigenvector related to  $\lambda_2$  becomes:

$$\underline{\mathbf{x}}_{2} = \begin{pmatrix} 0 \\ -\frac{\mathbf{p}_{y}\mathbf{p}_{z}}{(\mathbf{p}_{y}\mathbf{p}_{y} - \lambda_{2})} \end{pmatrix} \mathbf{x}_{3y}$$
 (E.9)

For i = 3, Eqs.(E.3b) and (E.4) becomes:

$$x_{zz} = -\frac{p_z p_y x_{2z}}{(p_z p_z - \lambda_3)}$$
 (E.10a)

$$[(p_z p_z - \lambda_3)(p_y p_y - \lambda_3) - p_z p_y p_y p_z] x_{3z} = 0$$
 (E.10b)

Since  $x_{3z}$  is non-zero component, the inside bracket in Eq.(E.10b) can be solved using quadratic equation.

$$\lambda_3 = \frac{(p_y p_y + p_z p_z) + \sqrt{(p_y p_y + p_z p_z)^2 - 4(p_y p_y p_z p_z - p_y p_z p_z p_y)}}{2}$$
(E.11)

From Eq.(E.7a), the third eigenvector related to  $\lambda_3$  becomes:

$$\underline{\mathbf{x}}_{3} = \begin{pmatrix} 0 \\ 1 \\ -\frac{\mathbf{p}_{z}\mathbf{p}_{y}}{(\mathbf{p}_{z}\mathbf{p}_{z} - \lambda_{3})} \end{pmatrix} \mathbf{x}_{2z}$$
 (E.12)

The eigenvectors are orthogonal to each other, the dot product of each eigenvector itself becomes:

$$\underline{\mathbf{x}}_1 \cdot \underline{\mathbf{x}}_1 = \underline{\mathbf{x}}_2 \cdot \underline{\mathbf{x}}_2 = \underline{\mathbf{x}}_3 \cdot \underline{\mathbf{x}}_3 = 1 \tag{E.13}$$

Therefore,

$$\mathbf{x}_{1\mathbf{x}} = 1 \tag{E.14a}$$

$$\underline{\mathbf{x}}_{2} \cdot \underline{\mathbf{x}}_{2} = \left[ 1 + \left( \frac{\mathbf{p}_{y} \mathbf{p}_{z}}{\mathbf{p}_{y} \mathbf{p}_{y} - \lambda_{2}} \right)^{2} \right] \mathbf{x}_{3y}^{2} = 1$$
 (E.14b)

$$\underline{\mathbf{x}}_{3} \cdot \underline{\mathbf{x}}_{3} = \left[ 1 + \left( \frac{\mathbf{p}_{z} \mathbf{p}_{y}}{\mathbf{p}_{z} \mathbf{p}_{z} - \lambda_{3}} \right)^{2} \right] \mathbf{x}_{2z}^{2} = 1$$
 (E.14c)

Solving Eqs.(E.14b) and (E.14c),

$$x_{3y} = \frac{1}{\sqrt{1 + \left(\frac{p_y p_z}{p_y p_y - \lambda_2}\right)^2}}$$
 (E.15a)

and

$$x_{2z} = \frac{1}{\sqrt{1 + \left(\frac{p_z p_y}{p_z p_z - \lambda_3}\right)^2}}$$
 (E.15b)

Therefore, the eigenvectors are becomes:

$$\underline{\mathbf{x}}_1 = \begin{pmatrix} 1 \\ 0 \\ 0 \end{pmatrix} \tag{E.16a}$$

$$\underline{\mathbf{x}}_{2} = \begin{pmatrix} 0 \\ -\frac{\mathbf{p}_{y}\mathbf{p}_{z}}{(\mathbf{p}_{y}\mathbf{p}_{y} - \lambda_{2})} \end{pmatrix} \frac{1}{\sqrt{1 + \left(\frac{\mathbf{p}_{y}\mathbf{p}_{z}}{\mathbf{p}_{y}\mathbf{p}_{y} - \lambda_{2}}\right)^{2}}}$$
 (E.16b)

$$\underline{\mathbf{x}}_{3} = \begin{pmatrix} 0 \\ 1 \\ -\frac{\mathbf{p}_{z}\mathbf{p}_{y}}{(\mathbf{p}_{z}\mathbf{p}_{z} - \lambda_{3})} \end{pmatrix} \frac{1}{\sqrt{1 + \left(\frac{\mathbf{p}_{z}\mathbf{p}_{y}}{\mathbf{p}_{z}\mathbf{p}_{z} - \lambda_{3}}\right)^{2}}}$$
 (E.16c)

# APPENDIX F

Realizability in the Planar Anisotropic Line

The objective of APPENDIX F is to derive the inequality equation in Ineq.(6.27). In order to find the closure coefficient  $C_2$ , Ineq.(6.1) is applied to the planar anisotropic line. The outward pointing normal vectors in the prolate line are

$$n_{II}^{pa} = \frac{1}{\sqrt{5}} \tag{F.1}$$

$$n_{III}^{pa} = -\frac{2}{\sqrt{5}} \tag{F.2}$$

In the planar anisotropic line Eqs.(6.2b) and (6.2c) become

$$\frac{d II_b}{d t} = -\frac{4}{9} - 4III_b + U \left[ \frac{4}{45} + \frac{58}{35} III_b - (\frac{16}{105} + \frac{96}{35} III_b + \frac{423}{35} III_b^2) C_2 \right]$$
 (F.3)

$$\frac{d III_b}{d t} = -3III_b + U \left[ \frac{2}{189} + \frac{83}{105} III_b + \frac{6}{7} III_b^2 - (\frac{36}{35} III_b - \frac{324}{35} III_b^2) C_2 \right]$$
 (F.4)

Multiplying Eq.(F.1) with Eq.(F.3) and Eq.(F.2) with Eq.(F.4), Ineq.(6.1) becomes

$$\underline{\mathbf{n}} \cdot \frac{d\underline{\mathbf{F}}}{dt} = -\frac{4}{9\sqrt{5}} + \frac{2}{\sqrt{5}} III_{\mathbf{b}} \\
+ U \left[ \frac{64}{945\sqrt{5}} + \frac{8}{105\sqrt{5}} III_{\mathbf{b}} - \frac{12}{7\sqrt{5}} III_{\mathbf{b}}^{2} \right] \\
- \left( \frac{16}{105\sqrt{5}} + \frac{24}{35\sqrt{5}} III_{\mathbf{b}} - \frac{216}{35\sqrt{5}} III_{\mathbf{b}}^{2} \right) C_{2} \le 0 \quad .$$
(F.5)

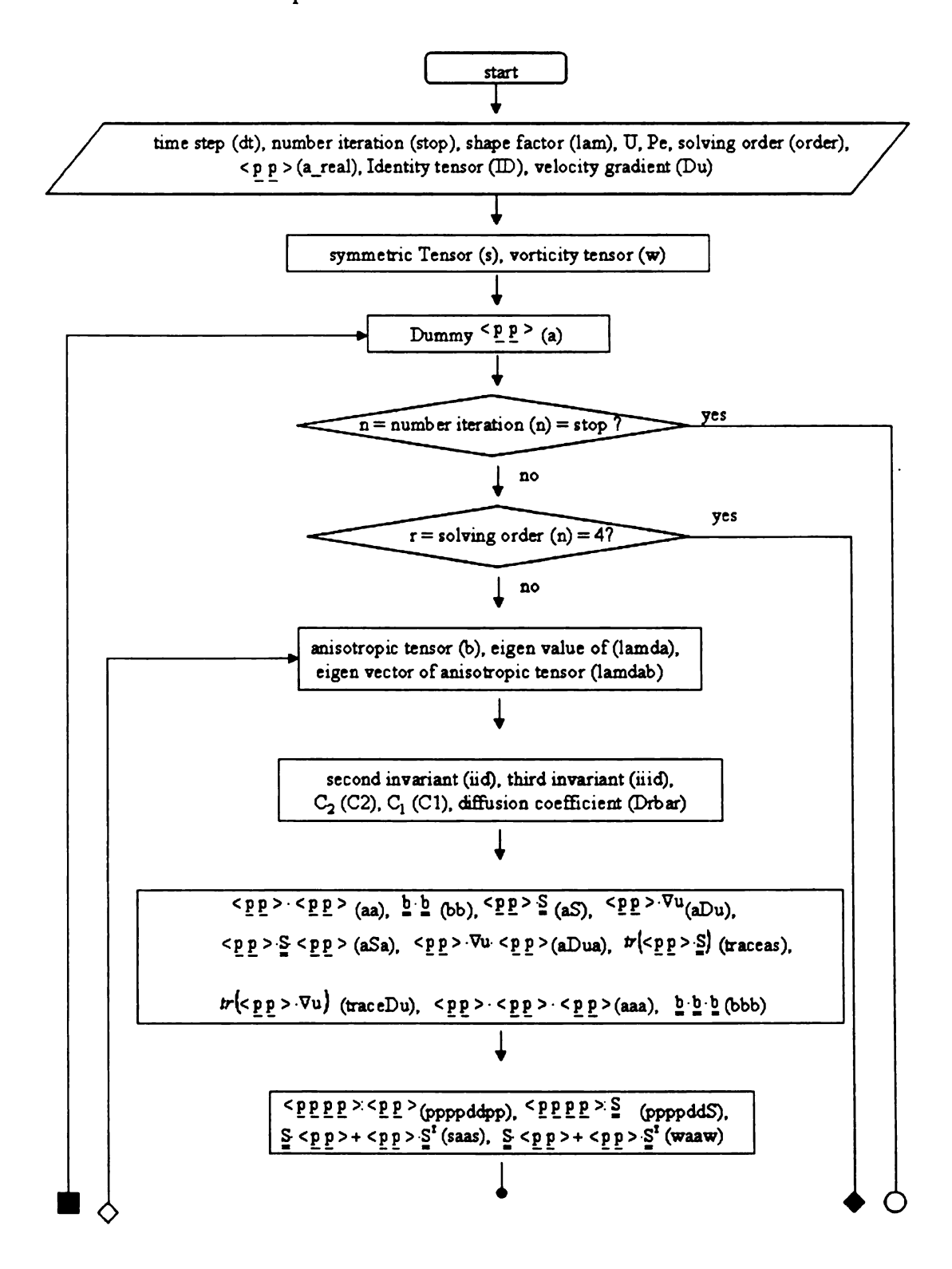
After arrange Eq.(F.5) the inequality becomes

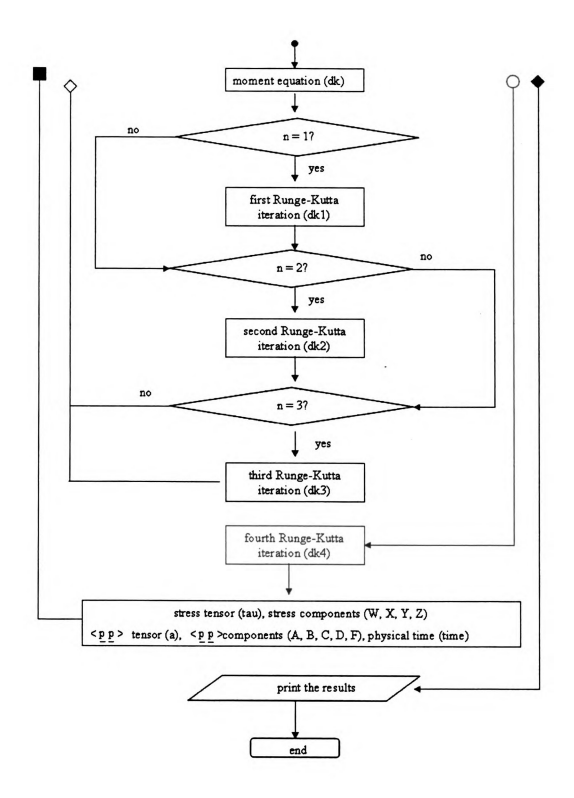
$$= \frac{2(-2+9III_b)\{105+2U[-8-45III_b+18C_2(1+III_b)]\}}{945\sqrt{5}} \le 0$$
 (F.6)

## APPENDIX G

Computational Code for Transient Calculations

The objective of APPENDIX G is to demonstrate the computation scheme using flow chart and list the computational code for MATLAB 12.





```
%clf
clear all
%time step
dt=0.003;
%number of time step
stop=20000;
%tumbling parameter
lam=0.987;
%nematic potential
U=27:
%Péclet number
Pe=30;
%1st order Euler order=1
%2nd order R-K order=2
%4th order R-K order=4
order=1:
%Constant Diffusion Coefficient Dr=1
%Doi Tube Dilation Dr=2
Dr=1;
dbar=1;
%Decoupling approximation closure=1
%Hybrid approximation closure=2
%FSQ approximation closure=3
closure=3:
%Doi stress st=1
%Ottinger stress st=2
st=1:
%Constant C2 const=1
%function of IIIb const=2
const=2;
c2const=1/3;
%Initial Condition
a real(1,1)=0; a real(1,2)=0; a real(1,3)=0;
a real(2,1)=0; a real(2,2)=1/3; a real(2,3)=0;
a real(3,1)=0;a real(3,2)=0;a real(3,3)=2/3;
%Unit tensor;
ID(1,1)=1;ID(1,2)=0;ID(1,3)=0;
ID(2,1)=0; ID(2,2)=1; ID(2,3)=0;
ID(3,1)=0; ID(3,2)=0; ID(3,3)=1;
%Velocity gradient for simple shear flow;
```

```
Du(1,1)=0; Du(1,2)=0; Du(1,3)=0;
Du(2,1)=0; Du(2,2)=0; Du(2,3)=1;
Du(3,1)=0; Du(3,2)=0; Du(3,3)=0;
for i=1:3
    for j=1:3
        s(i,j)=.5*(Du(i,j)+Du(j,i));
        w(i,j) = .5*(Du(i,j)-Du(j,i));
    end
end
a_test=a_real;
a=a real;
for n=1:stop
    for r=1:order
        b=a-1/3*ID;
        %Determine eigenvalues;
        lamda1=a(1,1);
        lamda2 = (a(2,2) + a(3,3) - ((a(2,2) + a(3,3))^2 -
4*(a(2,2)*a(3,3)-a(2,3)*a(3,2)))^(1/2))/2;
        lamda3= (a(2,2)+a(3,3)+((a(2,2)+a(3,3))^2-
4*(a(2,2)*a(3,3)-a(2,3)*a(3,2)))^(1/2))/2;
        lamdab1=lamda1-1/3;
        lamdab2=lamda2-1/3;
        lamdab3=lamda3-1/3;
        %determine C2
        iiid=lamdab1^3+lamdab2^3+lamdab3^3;
        iid=lamdab1^2+lamdab2^2+lamdab3^2;
        if const==1
            C2=c2const;
        end
        if const==2
            C2=(8+45*iiid)/(18*(1+9*iiid));
        end
        C1=1-C2;
        C3=0;
        C4=1-C1-C2-C3;
        c2(n) = C2;
     %Tube Dilation
        if Dr==1
            Drbar=dbar;
        end
        if Dr==2
```

```
Drbar=(1-3/2*iid)^(-2);
            end
            if st==2
                Drbar=(1-3/2*iid)^(-1);
            end
        end
        %Determine S[I(a*a)];
        aa=a*a;
        bb=(a-ID/3)*(a-ID/3);
        aS=a*s:
        aDu=a*Du;
        aSa=aS*a;
        aDua=aDu*a;
        traceas=trace(aS);
        traceaDu=trace(aDu);
        aaa=aa*a;
        bbb=bb*(a-ID/3);
        %Determine a:a (IIa) and alpha(2,1);
        IIa=aa(1,1)+aa(2,2)+aa(3,3);
        IIb=bb(1,1)+bb(2,2)+bb(3,3);
        %Determine alpha(3,1);
        IIIa=aaa(1,1)+aaa(2,2)+aaa(3,3);
        IIIb=bbb(1,1)+bbb(2,2)+bbb(3,3);
        if closure==1
            %Decoupling
            ppppddpp=IIa*a;
            ppppddS=traceas*a;
        end
        if closure==2
            %Hybrid
            ppppddpp=(1-27*det(a))*IIa*a+27*det(a)*((-
1/35+1/7*IIa)*ID+3/35*a+4/7*aa);
            ppppddS=(1-27*det(a))*traceas*a+27*det(a)*(-
2/35*s+1/7*(2*a*s+2*s*a+traceas*ID));
        end
        if closure==3
           %<pppp>:<pp>
            ppppddpp=C1*((-
1/35+1/7*IIa)*ID+3/35*a+4/7*aa)+C2*(2/35*IIa*ID-
2/7*IIIa*ID+6/7*aaa-2/7*aa+39/35*IIa*a);
```

if st==1

```
%<pppp>:S
            ppppddS=C1*(-
2/35*s+1/7*(2*a*s+2*s*a+traceas*ID))+C2*(4/35*s*IIa+a*traceas+2*a
Sa-2/7*(trace(aa*s)*ID+2*aa*s+2*s*aa));
            ppppddDu=C1*(-
2/35*Du+1/7*(2*a*Du+2*Du*a+traceaDu*ID))+C2*(4/35*Du*IIa+a*tracea
Du+2*aDua-2/7*(trace(aa*Du)*ID+2*aa*Du+2*Du*aa));
            ppppddSC2=(4/35*s*IIa+a*traceas+2*aSa-
2/7*(trace(aa*s)*ID+2*aa*s+2*s*aa));
      end
        saas=s*a+a*s;
        waaw=w*a+a*(w');
        if st==1
            ot=1;
        end
        if st==2
            ot=(6*(1-3/2*iid))^(-1/2);
        end
     %Moment Equation
        dk=Drbar*((ID/3-a)+ot*(U*(aa-ppppddpp)))+lam*Pe*(saas-
2*ppppddS)-Pe*waaw;
     % 1st order Eular
        if order==1
            a=a+dk*dt;
        end
     %4th order Runge-Kuttar
        if order==4
            if r==1
                dk1=dk;
                a=a real+dk1*dt*0.5;
            end
            if r==2
                dk2=dk;
                a=a real+dk2*dt*0.5;
            end
            if r==3
                dk3=dk;
                a=a real+dk3*dt;
            end
            if r==4
                dk4=dk:
                a=a real+(1/6)*(dk1+2*dk2+2*dk3+dk4)*dt;
            end
        end
```

```
%Second order Runge-Kuttar
         if order==2
             if r==1
                  dk1(i,j) = dk(i,j);
                  a(i,j)=a real(i,j)+dkl(i,j)*dt;
             end
             if r==2
                  dk2(i,j)=dk(i,j);
                  a(i,j)=a real(i,j)+(1/2)*(dk1(i,j)+dk2(i,j))*dt;
             end
         end
    end
%Decomposition of Moment Equation
    test1(n)=U* (aa(2,3) - ppppddpp(2,3));
    test2(n)=U^*(aa(2,2)-ppppddpp(2,2));
    test3(n) = U^* (aa (3, 3) -ppppddpp (3, 3));
    test4(n) = Pe* (saas (2, 3) - 2*ppppddS(2, 3) - waaw(2, 3));
    test5(n) = Pe^* (saas (2, 2) - 2*ppppddS(2, 2) - waaw(2, 2));
    test6(n) = Pe*(saas(3,3)-2*ppppddS(3,3)-waaw(3,3));
    test7(n)=ID(2,3)/3-a(2,3);
    test8(n)=ID(2,2)/3-a(2,2);
    test9(n)=ID(3,3)/3-a(3,3);
    test10(n)=dk(2,3);
    test11(n) = dk(2,2);
    test12(n)=dk(3,3);
    test13(n) = Pe* (saas (2,3) - 2*ppppddS(2,3));
    test14(n) = Pe^* (saas (2, 2) - 2*ppppddS(2, 2));
    tets15(n)=Pe*(saas(3,3)-2*ppppddS(3,3));
    test16(n) = -Pe*waaw(2,3);
    test17(n) = -Pe*waaw(2,2);
    test18(n) = -Pe*waaw(3,3);
    test19(n) = (dk(2,2) - (ID(2,2)/3 - a(2,2)) - (U*(aa(2,2) - a(2,2)))
ppppddpp(2,2)) - (-Pe*waaw(2,2))) / (Pe*(saas(2,2)-2*ppppddS(2,2)));
    test20(n) = (dk(3,3) - (ID(3,3)/3-a(3,3)) - (U*(aa(3,3)-a(3,3)))
ppppddpp(3,3)))-(-Pe*waaw(3,3)))/(Pe*(saas(3,3)-2*ppppddS(3,3)));
    test21 (n) = (dk(2,3) - (ID(2,3)/3 - a(2,3)) - (U*(aa(2,3) - a(2,3)))
ppppddpp(2,3)) - (-Pe*waaw(2,3))) / (Pe*(saas(2,3)-2*ppppddS(2,3)));
    if st==1
         tau=b-U*(aa-ppppddpp)+Pe*ppppddS/Drbar;
    end
    if st==2
         tau=b-U/((1-IIa)^{(1/2)})/3*(aa-ppppddpp)+Pe*ppppddS/Drbar;
    end
%Decomposition of Stress
    N1btest (n) = b(3,3) - b(2,2);
    N1ntest (n) = -U^* (aa (3, 3) -ppppddpp (3, 3)) +U^* (aa (2, 2) -
ppppddpp(2,2));
    N1htest(n)=Pe*ppppddS(3,3)/Drbar-Pe*ppppddS(2,2)/Drbar;
    N2btest(n) = b(2,2) - b(1,1);
```

```
N2ntest(n) = -U*(aa(2,2) - ppppddpp(2,2)) + U*(aa(1,1) - Ppppddpp(2,2))
ppppddpp(1,1));
    N2htest(n)=Pe*ppppddS(2,2)/Drbar-Pe*ppppddS(1,1)/Drbar;
    shearb(n)=b(2,3)/Pe;
    shearn (n) = -U^* (aa (2, 3) -ppppddpp (2, 3)) / Pe;
    shearh(n) = Pe*ppppddS(2,3) / Drbar/Pe;
    A11(n) = a11;
    A22(n)=a22;
    A33(n) = a33;
    A23(n) = a23;
    a real=a;
%Components of <pp> and Stress
    W(n) = tau(2,3);
    X(n) = tau(2,2);
    Y(n) = tau(1,1);
    Z(n) = tau(3,3);
    A(n) = a(1,1);
    B(n) = a(2,2);
    C(n) = a(3,3);
    D(n) = a(2,3);
    F(n) = a(3,2);
      %Time step
    time (n) = (n-1) * dt;
      %First Normal Stress
    N1=Z-X;
      %Second Normal Stress
    N2=X-Y;
end
%Eigenvalue and Eigenvector
eigenvalue 1=A11;
eigenvalue 2=(A22+A33-sqrt((A22+A33).^2-4.*(A22.*A33-A23.^2)))/2;
eigenvalue 3=(A22+A33+sqrt((A22+A33).^2-4.*(A22.*A33-A23.^2)))/2;
eigenvector 32=1./sqrt(1+(A23./(B-eigenvalue 2)).^2);
eigenvector 23=1./sqrt(1+(A23./(A33-eigenvalue 3)).^2);
eigenvector 33=(-A23./(A33-eigenvalue 3))./sqrt(1+(A23./(A33-
eigenvalue \overline{3}).^2);
eigenvector 22=(-A23./(A22-eigenvalue 2))./sqrt(1+(A23./(A22-
eigenvalue 2)).^2);
eigenvalueb 1=eigenvalue 1-1/3;
eigenvalueb 2=eigenvalue 2-1/3;
eigenvalueb 3=eigenvalue 3-1/3;
%Shear Viscosity
shear=W/Pe;
```

```
%Invariants
II=eigenvalueb_1.^2+eigenvalueb_2.^2+eigenvalueb_3.^2;
III=eigenvalueb_1.^3+eigenvalueb_2.^3+eigenvalueb_3.^3;

%Invariant Domain
xIII=[-1/36:0.0001:2/9];
yII=2/9+2*xIII;

yyII=[0:0.0001:1/6];
xxIII=-6*(yyII/6).^(3/2);

yyyII=[0:0.0001:2/3];
xxxIII=6*(yyyII/6).^(3/2);

plot(xIII,yII,xxIII,yyII,xxxIII,yyyII,III,II,'+')
```

## LIST OF REFERENCES

- Abe, A. and T. Yamazaki, 1989, "Deuterium NMR Analysis of Poly(γ-benzyl L-glutamate) in the Lyotropic Liquid-Crystalline State: Orientational Order of the α-Helical Backbone and Conformation of the Predant Side Chain," *Macromolecule*, 22, 2138 2145.
- Abe, A. and T. Yamazaki, 1989, "Orientational Order of the  $\alpha$ -Helical Poly( $\gamma$ -benzyl L-glutamate) in the Lyotropic Liquid-Crystalline State Comparison of Theory with Experiments," *Macromolecule*, 22, 2145 2149.
- Advani, S.G. and C.L. Tucker III, 1987, "The Use of Tensors to Describe and Predict Fiber Orientation in Short Fiber Composites," J. Rheol., 31 (8), 751 784.
- Advani, S.G., and C.L. Tucker III, 1990, "Closure Approximations for Three-Dimensional Structure Tensors," J. Rheol., 34 (3), 367 386.
- Advani, S.G., 1994, Editor, Flow and Rheology in Polymer Composites Manufacturing, Volume 10, Composite Materials Series, Elsevier Publishers, Amsterdam.
- Anczurowski, E. and S. G. Mason, 1967, "The Kinetics of Flowing Dispersions III. Equilibrium Orientations of Rods and Discs (Experimental)," J. Colloid and Interface Science, 23, 533 546.
- Asada, T., T. Tanaka and S. Onogi, 1985, "Rheology of Liquid Crystalline Solution of α-helix Polypeptides," J Appl Polym Sci Appl Polym Symp 41 229.
- Batchelor, G. K., 1976, "Brownian Diffusion of Particles with Hydrodynamic Interaction", J. Fluid Mechanics, 74,1 29.
- Batchelor, G. K., 1982, "Sedimentation in a Dilute Polydisperse System of Interacting Spheres, Part I: General Theory", J. Fluid Mechanics, 119, 379 408.
- Baek, Seong-Gi, J.J. Magda and S. Cementwala, 1993, "Normal stress differences in liquid crystalline hydroxypropylcellulose solutions," J. Rheol., 37, 935 945.
- Baek, S.-G. and J. J. Magda, 1993, "Rheological differences among liquid-crystalline polymers. I. The first and second normal stress differences of PBG solutions," J. Rheol., 37, 1201 1224.
- Baek, S.-G. and J. J. Magda, 1994, "Rheological differences among liquid-crystalline polymers. II. Disappearance of negative N<sub>1</sub> in densely packed lyotropes and thermotropes," J. Rheol., 38, 1473 1503.

- Bedford, B. and W. R. Burghardt, 1996, "Molecular Orientation of a Liquid-Crystalline Polymer Solution in Mixed Shear-Extensional Flows," *Journal of Rheology*, **40** (2), 235 257.
- Becraft, M. L. and A. B. Metzner, 1992, "The Rheology, Fiber Orientation, and Processing Behavior of Fiber-Fiber Fluids," J. Rheol., 36 (1), 143-174.
- Bénard, A., Mandal, D. K., S. M. Parks, and C. A. Petty, 2002, "A Closure Model for Fluids with Microstructure", Poster Session 3.3, WCCM V Fifth World Congress on Computational Mechanics, Vienna, Austria, July 7-12.
- Bhave, A. V., R. K. Menon., R. C. Armstrong and R. A. Brown, 1993, "A Constitutive Equation for Liquid-Crystalline Polymer Solutions," J. Rheol., 37 (3), 413 441.
- Bibbo, M.A. and R.C. Armstrong, 1988, "Rheology of Semi-Concentrated Fiber Suspensions in Newtonian and Non-Newtonian Fluids," p.105 in *Manufacturing International '88*, the Manufacturing Science of Composites, Editor: T.G. Gutowski, Vol. IV, ASME.
- Bibbo, M. A., S. M. Dinh and R. C. Armstrong, 1985, "Shear Flow Properties of Semiconcentrated Fiber Suspensions," J. Rheol., 29 (6), 905 929.
- Bird, R.B., R.C. Armstrong and O. Hassager, 1987, Dynamics of Polymeric Liquids: Volume 1, Fluid Mechanics, Second Edition, Wiley-Interscience, New York.
- Bird, R.B., C.F. Curtiss, R.C. Armstrong and O. Hassager, 1987, *Dynamics of Polymeric Liquids: Volume 2, Kinetic Theory*, Second Edition, Wiley-Interscience, New York.
- Brenner H, 1974, "Rheology of a dilute suspension of axisymmetric Brownian particles," *International Journal of Multiphase Flow*, 1 (2), 195 341.
- Bretherton, F. P., 1962, "The Motion of Rigid Particles in a Shear Flow at Low Reynolds Number," J. Fluid Mech., 14, 284 304.
- Burghardt, W. R. and G. G. Fuller, 1990, "Transient Shear Flow of Nematic Liquid Crystals: Manifestations of Director Tumbling," *Journal of Rheology*, 34, 959 992.
- Burghardt, W. R. and G. G. Fuller, 1991, "Role of Director Tumbling in the Rheology of Polymer Liquid Crystal Solutions," *Macromolecules*, 24, 2546 2555.
- Carlsson, T., 1982, "The Possibility of the Existence of a Positive Leslie Viscosity α<sub>2</sub>. Proposed Flow Behavior of Disk Like Nematic Liquid Crystals," Molecular Crystals and Liquid Crystals, 89, 57-66.

- Carlsson, T. and K. Skarp, 1986, "Observation of the tumbling instability in torsional shear flow of a nematic liquid crystal with  $\alpha_3 > 0$ ," Liquid Crystals, 1, 455 471.
- Chandrasekhar, S., 1943, "Stochastic Problems in Physics and Astronomy, Review of Modern Physics," 15 (1), p.1 89. Reproduced in Selected Papers on Noise and Stochastic Processes, Editor: N. Wax, Dover Publications, New York.
- Chaubal, C. V., 1997, Theoretical Models for the Dynamics of Liquid Crystalline Polymers, Ph.D. Thesis, University of California, Santa Barbara.
- Chaubal, C. V., G. Leal and G. H. Fredrickson, 1995, "A Comparison of Closure Approximations for the Doi Theory of LCPs," J. Rheol., 39 (1), 73 103.
- Chaubal, C. V. and G. Leal, 1998, "A Closure Approximation for Liquid-Crystalline Polymer Models Based on Parametric Density Estimation," J. Rheol., 42(1), 177 201.
- Chaubal C. V, and L. G. Leal, 1997, "Smoothed particle hydrodynamics technique for the solution of kinetic theory problems. Part 1. Method," J. Non-Newtonian Fluid Mech., 70, 125 154.
- Chaubal C. V, and L. G. Leal, 1999, "Smoothed particle hydrodynamics technique for the solution of kinetic theory problems. Part 2. The effect of flow perturbations on the simply shear behavior of LCPs," J. Non-Newtonian Fluid Mech., 82, 25 55.
- Chono, S., T. Tsuji and A. Taniguchi, 1996, "Numerical Analysis of the Rheology of Polymeric Liquid Crystals (1<sup>st</sup> Report, Shear Flow Behavior)," *Transactions of the Japan Society of Mechanical Engineers, Part B*, **62**, 600-607.
- Cintra, J.S. and C.L. Tucker III, 1995, "Orthotropic Closure Approximations for Flow-Induced Fiber Orientation," J. Rheol., 39 (6), 1095 1122.
- Cladis, P. E. and S. Torza, 1975, "Stability of Nematic Liquid Crystals in Couette Flow," *Physical Review Letters*, **35**, 1283 1286.
- Clark, M. G., F. C. Saunders, I. A. Shanks, and F. M. Leslie, 1981, "A Study of Flow Alignment Instability During Rectilinear Oscillatory Shear of Nematic," *Molecular Crystals and Liquid Crystals*, 79, 195 22.
- Clarke, A. R., N. C. Davidson and G. Archenhold, 1997, "Mesostructural Characteristics of Aligned Fiber Composites," p.230 292 in *Flow Induced Alignment in Composite Materials*, Editor: T.D. Papathanasian and D.C. Guell, Woodhead Publishing Ltd., Cambridge, England.

- Collyer 1992, Liquid Crystal Polymers: From Structures to Applications., Elsevier Applied Science, London.
- Currie, P.K., 1982, "Constitutive Equations for Polymer Melts Predicted by the Doi-Edwards and Curtiss-Bird Kinetic Theory Models," J. Non-Newtonian Fluid Mech. 11, 53 – 68.
- De, S. K. and J.R. White, 1996, Editors, Short fibre-polymer composites, Woodhead Publishing Ltd., Cambridge.
- de Gennes, P. G., 1974, The Physics of Liquid Crystals, Oxford University Press, London.
- Dinh, S.M. and R.C. Armstrong, 1984, "A Rheological Equation of State for Semiconcentrated Fiber Suspensions," J. Rheol., 28 (3), 207 227.
- Doi, M. and S. F. Edwards, 1978, "Dynamics of Rod-like Macromolecules in Concentrated Solution, Part 1," J. Chem. Soc. Faraday Trans. II, 74, 560 570.
- Doi, M. and S. F. Edwards, 1978, "Dynamics of Rod-like Macromolecules in Concentrated Solution, Part 12," J. Chem. Soc. Faraday Trans. II, 74, 918 932.
- Doi, M., 1981, "Molecular Dynamics and Rheological Properties of Concentrated Solutions of Rodlike Polymers in Isotropic and Liquid Crystalline Phases," *Journal of Polymer Science*, 19, 229 243.
- Doi, M. and S.F. Edwards, 1986, *Theory of Polymer Dynamics*, Oxford University Press, London.
- Donald, A. M., A. H. Windle, 1992, *Liquid Crystalline Polymers*, Cambridge University Press, New York.
- Doraiswamy, D. and A. B. Metzner, 1986, "The rheology of polymeric liquid crystals," *Rheologica Acta*, 25, 580 587
- Edwards, B.J. and A.N. Beris, 1989, "Flow Induced Orientation in Monodomain Systems of Polymeric Liquid Crystals," J. Rheol., 33 (3), 537 557.
- Edwards, B.J. and H. C. Öttinger, 1997, "Time-Invariance Criteria for Closure Approximations," *Physical Review E*, **56** (4), 4097 4103.
- Faraoni, V., M. Grosso, S. Crescitelli, P. L. Maffettone, 1999, "The rigid-rod model for nematic polymers: An analysis of the shear flow problem," J. Rheol., 43 (3), 829 843.

- Farhoudi, Y. and A.D. Rey, 1993, "Shear Flows of Nematic Polymers. I. Orienting Models, Bifurcations, and Steady State Rheological Predictions," J. Rheol., 37 (2), 289-314.
- Feng, J. and L.G. Leal, 1997, "Simulating Complex Flows of Liquid-Crystalline Polymers Using the Doi Theory," J. Rheol., 41(6), 1317-1335.
- Feng, J., C. V. Chaubal and L.G. Leal, 1998, "Closure Approximations for the Doi Theory: Which to Use in Simulating Complex Flows of Liquid-Crystalline Polymers?," J. Rheol., 42(5), 1095-1119.
- Folgar, F. and C.L. Tucker III, 1984, "Orientation Behavior of Fibers in Concentrated Suspensions," J. Reinf. Plast. Compos., 98-119.
- Frattini, P. L. and G. G. Fuller, 1986, "Rheo-Optical Studies of the Effect of Weak Brownian Rotations in Sheared Suspensions," J. Fluid Mech., 168, 119 150.
- Frazer, R.A., W.J. Duncan and A.R. Collar, 1960, Elementary Matrices and Some Applications to Dynamics and Differential Equations, Cambridge.
- Goettler, L.A., 1970, "Controlling Flow Orientation in Molding of Short-Fiber Compounds," *Modern Plastics*, 47, 1–140.
- Guell, D.C. and A. Benard, 1997, "Flow-Induced Alignment in Composite Materials: Current Applications and Future Prospects," p.1 42, in *Flow Induced Alignment in Composite Materials*, Editor: T.D. Papathanasian and D.C. Guell, Woodhead Publishing Ltd., Cambridge, England.
- Gähwiller, CH., 1973, "Direct Determination of the Five Independent Viscosity Coefficients of Nematic Liquid Crystals," *Molecular Crystals and Liquid Crystals*, 20, 301-318.
- Han, C. D., and S. S. Kim, 1993, "Transient rheological behavior of a thermotropic liquid-crystalline polymer. I. The start-up of shear flow," J. Rheol., 37, 847 866.
- Hand, G.L., 1962, "A Theory of Anisotropic Fluids," J. Fluid Mech., 13, 33 46.
- Happel, J. and H. Brenner, 1965, Low Reynolds Number Hydrodynamics with Special Applications to Particulate Media, Prentice-Hall, Englewood Cliffs, N.J.
- Harlen, O.G. and D.L. Koch, 1992, "Extensional Flow of a Suspension of Fibers in a Dilute Polymer Solution," *Phys. Fluids*, 4(5), 1070 1072.
- Harlen, O.G. and D.L. Koch, 1993, "Simple Shear Flow of a Suspension of Fibres in a Dilute Polymer Solution at High Deborah Number," J. Fluid Mech., 252, 187 207.

- Herczynski, R. and I. Pienkowska, 1980, "Toward a Statistical Theory of Suspensions," Ann. Rev. Fluid Mech., 12, 237 269.
- Hinch, E. J. and L. G. Leal, 1972, "The effect of Brownian motion on the rheological properties of a suspension of non-spherical particles," Fluid Mech., 52, 683 712.
- Hinch, E.J. and L.G. Leal, 1975, "Constitutive Equations in Suspension Mechanics. Part 1. General Formulation," J. Fluid Mech., 71, Part 3, 481 495.
- Hinch, E. J. and L. G. Leal, 1976, "Constitutive Equation in Suspension Mechanics. Part 2. Approximate forms for a suspension of rigid particles affected by Brownian Rotations," J. Fluid Mech., 76, 187 208.
- Holmström, S. and S. T. Lagerwall, 1977, "Shear Flow in the Presence of Elastic Fields," *Molecular Crystals and Liquid Crystals*, 38, 141 153.
- Imhoff, A., 2000, Diplomarbeit: Validation of Closure Models for Fiber Induced Alignment of Fibers, Mechanical Engineering, Michigan State University and University of Aachen, 2000.
- Imhoff, A., S. Parks, C. Petty, and A. Bénard, 2000, "Validation of a New Closure Model for Flow-Induced Alignment of Fibers", in Proceedings of the International Mechanical Engineering Conference and Exhibit, Symposium on CAE and Related Innovations for Polymer Processing, IMECE '00, Orlando, Florida, November 5-10.
- Ilg, P., I. V. Karlin and H. C. Öttinger, 1999, "Generating moment equation in the Doi model of liquid-crystalline polymers," *Physical Review E*, **60**(5), 5783 5787.
- Iso, Y., D.L. Koch and C. Cohen, 1996a, "Orientation in Simple Shear Flow of Semi-Dilute Fiber Suspensions 1. Weakly Elastic Fluids," J. Non-Newtonian Fluid Mech.,
  62, 115 134.
- Iso, Y., C. Cohen and D.L. Koch, 1996b, "Orientation in Simple Shear Flow of Semi-Dilute Fiber Suspensions 2. Highly Elastic Fluids," J. Non-Newtonian Fluid Mech.,
  62, 135 153.
- Jeffery, G.B., 1922, "The Motion of Ellipsoidal Particles Immersed in Viscous Fluid," *Proc. R. Soc. Lond. A*, 102, 161 179.
- Jansson, J. F., 1992, "Applications of LCP Materials," Liquid Crystal Polymers: From Structures to Applications, edited by A. A. Collyer, Elsevier, London.
- Kacir, L., M. Narkis and O. Ishai, 1975, "Orientation Short Glass-Fiber Composites. I Preparation and Statistical Analysis of Aligned Fiber Mats," *Polymer Engineering Science*, 15, 525.

- Kacir, L., M. Narkis and O. Ishai, 1975, "Orientation Short Glass-Fiber Composites. II Analysis of Parameters Controlling the Fiber/Glycerine Orientation Process," *Polymer Engineering Science*, 15, 532.
- Kacir, L., M. Narkis and O. Ishai, 1977, "Orientation Short Glass-Fiber Composites. III. Structure and Mechanical Properties of Molded Sheets," *Polymer Engineering Science*, 17, 234.
- Kamal, M.R. and A. T. Mutel, 1989, "The Prediction of Flow and Orientation Behavior of Short Fiber Reinforced Melts in Simple Flow Systems," *Polymer Composites*, 10(5), 337.
- Kennedy, P., 1995, "Flow Analysis of Injection Molds," Hanser Publishers, New York, NY.
- Kim, S.S. and C. D. Han, 1993, "Effect of molecular weight on the rheological behavior of thermotropic liquid-crystalline polymer," *Macromolecules*, **26**(24), 6633 6642.
- Kim, S. and S. J. Karrila, 1991, Microhydrodynamics: Principles and Selected Applications, Butterworth-Heineman, New York.
- Kim, Y-C, C. T. Nguyen, S. M. Parks, C. A. Petty, D. Mandal and A. Bénard, 2001, "Rheological and Alignment Properties of Liquid Crystalline Polymers", Poster Session on Fluid Mechanics, Annual AIChE Meeting, Reno Hilton, Reno, NV, November 4-9.
- Kim, Y-C, C. T. Nguyen, S. M. Parks, D. Mandal, A. Bénard, and C. A. Petty, 2002, "Microstructure of Liquid Crystalline Polymers Induced by Simple Shear", Symposium on Manipulation of Nanophases by External Fields, Annual AIChE Meeting, Indianapolis Convention Center, Indianapolis, November 3 8.
- Kim, Y-C, H. Kini, D. Mandal, A. Bénard, and C. Petty, 2003, "Realizable Closure for the Orientation Tetrad for Rigid Rod Suspensions", Symposium on Suspensions, 56th Annual Meeting, American Physical Society: Division of Fluid Dynamics, 2003, East Rutherford, NJ, November 23-25.
- Kim, Y-C, C.A. Petty, and A. Bénard, 2004, "Equilibrium Microstructure of Complex Fluids", Symposium on Self-Assembly in Solutions I, AIChE Annual Meeting, Austin, 7-12 November 7-12.
- Kim, Y-C, C.A. Petty, and A. Bénard, 2005, "Microstructure of Multiphase Fluids in Homogeneous Shear Flows", Symposium 144:Poster Session in Fluid Mechanics, Exhibit Hall A, Cincinnati Convention Center, AIChE Annual Meeting, October 31.

- Kini, H., Y-C Kim, S. M. Parks, C. A. Petty, D. Mandal and A. Bénard, 2002, "Flow Induced Microstructure of Composite Materials with Clay Fillers", Symposium on Particle Technology, Poster Session, Annual AIChE Meeting, Indianapolis Convention Center, November 3 8.
- Kini, H. K. 2003, Equilibrium Microstructure for Liquid Crystalline Polymers, Master of Science Thesis, Michigan State University.
- Kini, H., Y.C. Kim, C. T. Nguyen, A. Bénard, and C. A. Petty, 2003, "Flow Induced Microstructure in Composite Materials", *Proceedings of 14<sup>th</sup> International Conference on Composite Materials*, ICCM14, CD-ROM, San Diego, July 14-18.
- Kiss, G. and R. S. Porter, 1980, "Rheo-Optical Studies of Liquid Crystalline Solutions of Helical Polypeptides," *Molecular Crystals and Liquid Crystals*, **60**, 267-280.
- Koch, D. L., 1995, "A Model for Orientational Diffusion in Fiber Suspensions," *Phys. Fluids*, 7(8), 2086-2088.
- Kubo, K. and K. Ogino, 1979, "Comparison of Osmotic Pressure for the Poly(γ-benzyl-L-glutamate) Solutions with the Theories for a System of Hard Spherocylinders," *Mol. Cryst. Liq. Crsyt.*, 53, 207 228.
- Kuzuu, N. and M. Doi, 1983, "Constitutive Equation for Nematic Liquid Crystals under Weak Velocity Gradient Derived from a Molecular Kinetic Equation," *Journal of the Physical Society of Japan*, 52(10), 3486-3494.
- Kuzuu, N. and M. Doi, 1984, "Constitutive Equation for Nematic Liquid Crystals Under Weak Velocity Gradient Derived from a Molecular Kinetic Equation. II. -Leslie Coefficients for Rodlike Polymers-," Journal of the Physical Society of Japan, 53(3), 1031-1040.
- Lamb, H., 1932, Hydrodynamics, Dover Publications, New York.
- Larson, R. G., 1990, "Arrested Tumbling in Shearing Flows of Liquid Crystal Polymers," *Macromolecules*, 23, 3983 3992.
- Larson, R. G. and H. C. Öttinger, 1991, "Effect of Molecular Elasticity on Out-of-Plane Orientations in Shearing Flows of Liquid-Crystalline Polymers," *Macromolecules*, 24, 6270 6282.
- Larson, R. G., 1988, Constitutive Equations for Polymer Melts and Solutions, Butterworths, Boston.
- Larson, R. G., 1999, *The Structure of Complex Fluids*, Oxford University Press, New York.

- Leal, L.G., 1980, "Particle Motions in Viscous Fluid," Ann. Rev. Fluid Mech., 12, 435 476.
- Leighton, D. T. and A. Acrivos, 1987, "The Shear-induced migration of particles in concentrated suspension," J. Fluid Mech. 181, 415-439.
- Lipscomb II, G.G., M.M. Denn, D.U. Hur and D.V. Bogar, 1988, "The Flow of Fiber Suspensions in Complex Geometries," J. Non-Newtonian Fluid Mech., 26, 297-325.
- Magda, J. J., S-G Baek, K. L. DeVries and R. G. Larson, 1991, "Shear Flows of Liquid Crystal Polymers: Measurements of the Second Normal Stress Difference and the Doi Molecular Theory," *Macromolecules*, 24, 4460-4468.
- Maier, W. and A. Saupe, 1959, "Eine einfache molecular-statistische Theorie der nematischen kristallinflüssigen Phase," Z. Naturforsch, 13A, 564-566.
- Mandal, D, S. M. Parks, C. A. Petty, and A. Bénard, 2001, "Discussion of a Closure Model for Fiber Orientation", *Proceedings of the Seventh Annual Meeting of the Polymer Processing Society*, Montreal, Canada, May 21-24.
- Mandal, D., Bénard, A., Petty, C.A., 2004, "Modeling Flow-Induced Orientation of Fibers Using a New Closure Model", International Conference on Flow Processes in Composite Materials, Newark, DE, July 7-9.
- Mandal, D. K. 2004, Simulation of Flow-Induced Fiber Orientation with a New Closure Model Using the Finite Element Method, Ph.D. Dissertation, Michigan State University.
- Marrucci, G. and P. L. Maffettone, 1990, "Nematic Phase of Rodlike Polymers I. Prediction of Transient Behavior at High Shear Rates," J. Rheol., 34, 1217-1230.
- Marrucci, G., 1991, "Tumbling Regime of Liquid-Crystalline Polymers," *Macromolecules*, 24, 4176-4182.
- Marrucci, G., 1996, "Theoretical aspect of the flow of liquid crystal polymers," p.31 48, in *Rheology and Processing of Liquid Crystal Polymers*, Editor: D. Acierno and A. Collyer, Chapman & Hall, London.
- Milliken, W.J. and R.L. Powell, 1994, "Short-Fiber Suspensions," p.53 83, in *Flow and Rheology in Polymer Composites Manufacturing*, 10, Composite Materials Series, Editor: S.G. Advani, Elsevier Publishers, Amsterdam.
- Mondy, L. A., H. Brenner, S. A. Altobelli, J. R. Abbott and A. L. Grahman, 1994, "Shear-Induced Particle Migration in Suspensions of Rods," *J. Rheol.*, 38(2), 444 452.

- Murthy, S. N., J. R. Knox, and E. T. Samulski, 1976, "Order Parameter Measurement in Polypeptide Liquid Crystals," *Journal of Chemical Physics*, 19, 4823 4839.
- Nguyen, C. T. 2001, Microstructure of Liquid Crystalline Polymers in Simple Shear Flows, Master of Science Thesis, Michigan State University.
- Nguyen, C. T., S. M. Parks, A. Bénard and C. A. Petty, 2001a, "Prediction of Low-Order Orientation Statistics for Alignment of Liquid Crystalline Polymers in Homogeneous Shear," *Proceedings of 13th International Conference on Composite Materials*, ICCM13 CD-ROM, Beijing, June 25-29
- Nguyen, C. T., Y-C Kim, S. M. Parks, C. A. Petty, D. Mandal, and A. Benard, 2001b, "Flow-Induced Alignment of Liquid Crystalline Polymers", Symposium on *Polymer Processing and Rheology III*, Annual AIChE Meeting, Reno Hilton, Reno, NV, November 4-9.
- Odijk, T., 1986, "Theory of Lyotropic Polymer Liquid Crystals," *Macromolecules*, 19, 2313 2329.
- Orwoll, R. D. and R. L. Vold, 1971, "Molecular Order in Liquid Crystalline Solutions of Poly (γ-Benzyl-L-Glutamate) in Dichloromethane," J. Am. Chem. Soc., 93, 5335 5338.
- Onsager, L., 1949, "The Effect of Shape on the Interaction of Colloidal Particles," Ann. N. Y. Acad. Sci., 51, 627 659.
- Papathanasiou, T.D., 1996, "Microstructure Evolution During Molding of Particulate Reinforced Thermoplastic Composites," *International Polymer Processing*, 11(3), 275 283.
- Papathanasiou, T.D., 1997, "Flow-Induced Alignment in Injection Molding of Fiber-Reinforced Polymer Composites," p.112 165, in *Flow-Induced Alignment in Composite Materials*, Editors: T. D. Papathanasiou and D.C. Guell, Woodhead Publishing Ltd., Cambridge, England.
- Papathanasiou, T. D. and D.C. Guell, 1997, Flow-Induced Alignment in Composite Materials, Woodhead Publishing Ltd., Cambridge, England.
- Parks, S. M. 1997, Relaxation Model for Homogeneous Turbulent Flows, Ph.D. Dissertation, Michigan State University.
- Parks, S.M., K. Weispfennig, C. A. Petty, 1998, "An Algebraic Preclosure Theory for the Reynolds Stress", *Physics of Fluids*, 10(13), 645 653.

- Parks, S. M. and C. A. Petty, 1999, "Prediction of Low-Order Orientation Statistics for Flow-Induced Alignment of Fibers and Platelets", Fundamental Research in Fluid Mechanics: Particulate and Multiphase Flow I, AIChE Annual Meeting, Dallas, TX, October 31- November 5.
- Parks, S. M., C. A. Petty, and S. M. Shao, 1999, "Flow Induced Alignment of Fibers," in Proceedings of 12<sup>th</sup> International Conference on Composite Materials, ICCM12/TCA, Paris, July 5-9.
- Petty, C. A., S. M. Parks, and M. Shafer, 1999, Flow-Induced Alignment of Fibers in the Absence of Fiber-Fiber Interactions, paper presentation, *Symposium on Suspensions*, APS/DFD, New Orleans, LA, November 21-23.
- Phan-Thien, N., 1995, "Constitutive Equation for Concentrated Suspensions in Newtonian Liquids," J. Rheol., 39 (4), 679 695.
- Phan-Thien, N. and R. Zheng, 1997, "Macroscopic Modelling of the Evolution of Fibre Orientation During Flow," p.77 111, in *Flow Induced Alignment in Composite Materials*, Editors: T.D. Papathanasian and D.C. Guell, Woodhead Publishing Ltd., Cambridge, England.
- Picken, S. J., J. Aerts, H. L. Doppert, A. J. Reuvers, and M. G. Northolt, 1991 "Structure and rheology of aramid solutions: transient rheological and rheooptical measurements," macromolecules, 24(6), 1366 1375.
- Pieranski, P. and E. Guyon, 1974, "Two Shear-Flow Regimes in Nematic p-n-Hexyloxybenzilidene-p'-aminobenzonitrile," *Physical Review Letters*, 32, 924 926.
- Rahnama, M., D.L. Koch and E.S.G. Shaqfeh, 1995, "The Effect of Hydrodynamic Interactions on the Orientation Distribution in a Fiber Suspension Subject to Simple Shear Flow," *Phys. Fluids*, 7 (3), 487-506.
- Rahnama, M., D.L. Koch and C. Cohen, 1995, "Observations of Fiber Orientation in Suspensions Subjected to Planar Extensional Flows," *Phys. Fluids*, 7(8), 1811 1817.
- Ranganathan, S. and S.G. Advani, 1997, "Fiber-Fiber and Fiber-Wall Interactions During the Flow of Non-Dilute Suspensions," p.43 76, in *Flow Induced Alignment in Composite Materials*, Editors: T.D. Papathanasian and D.C. Guell, Woodhead Publishing Ltd., Cambridge, England.
- Rey, A.D., 1997, "Theory and Simulation of Shear Flow-Induced Microstructure in Liquid Crystalline Polymers," p.203 229, in *Flow Induced Alignment in Composite Materials*, Editors: T.D. Papathanasian and D.C. Guell, Woodhead Publishing Ltd., Cambridge, England.

- Rey, A.D. and M.M. Denn, 2002, "Dynamical Phenomena in Liquid-Crystalline Materials," *Annual Review of Fluid Mechanics*, 34, 233 266.
- Robinson, C., 1966, "The Cholesteric Phase in Polypeptide Solutions and Biological Structure," Mol. Cryst., 1, 467 494.
- Russo, P.S., 2001, "Diffusion of Tabacco Mosaic Virus Through Solutions of Dextran," see web site <a href="https://www.chem.lsu.edu/web/faculty/bios/prs.html">www.chem.lsu.edu/web/faculty/bios/prs.html</a>.
- Sartirana, M. L., M. Marsano, E. Bianchi, 1987, "Order Parameter in Polymer Liquid Crystal 2. Poly(γ-Benzyl-L-Glutamate) in Dioxane," *Mol. Cryst. Liq. Cryst.*, **144**, 263 274.
- Servais, C. A., J. E. Manson and S. Toll, 1999, "Fiber-Fiber Interaction in Concentrated Suspensions: Dispersed Fibers," J. Rheol., 43(4), 991 1004.
- Servais, C., A. Luciani and J. E. Manson, 1999, "Fiber-Fiber Interaction in Concentrated Suspensions: Dispersed Fiber Bundles," J. Rheol., 43(4), 1005 1018.
- Shaqfeh, E. S. G. and D. L. Koch, 1990, "Orientational Dispersion of Fibers in Extensional Flows," *Phys. Fluids A*, 2(7), 1077 1093.
- Skarp, K and T. Carlsson, 1978, "Influence of an Electric Field on the Flow Alignment Angle in Shear Flow of Nematic Liquid Crystals," *Molecular Crystals and Liquid Crystals*, 49, 75 82.
- Skarp, K., S. Carlson, T. Lagerwall, and B. Stebler, 1981, "Flow Properties of Nematic 8CB: An Example of Diverging and Vanishing α<sub>3</sub>," Molecular Crystals and Liquid Crystals, 66, 199 208.
- Soize, C., 1995, The Fokker-Planck Equation for Stochastic Dynamical Systems and Its Explicit Steady State Solutions, World Scientific, River Edge, NJ.
- Srinivasarao, M. and G. C. Barry, 1991, "Rheo-optical Studies on Aligned Nemactic Solutions of a Rodlike Polymer," *Journal of Rheology*, 35(3), 379 397.
- Stover, C.A., D.L. Koch and C. Cohen, 1992, "Observations of Fibre Orientation in Simple Shear Flow of Semi-Dilute Suspensions," J. Fluid Mech., 238, 277-296.
- Szeri, A. J. and L. G. Leal, 1993, "Microstructure suspended in three-dimensional flows," J. Fluid Mech., 250, 143 – 167.
- Smyth, S. F. and M. E. Mackay, 1994, "The viscous stress contribution to lyotropic hydroxypropylcellulose solutions in the biphasic and liquid-crystalline regions," J. Rheol., 38(5), 1549 1558.

- Smyth, S. F., C. Liang, M. E. Mackay, and G. G. Fuller, 1995, "The stress jump of a semirigid macromolecule after shear: Comparison of the elastic stress to the birefringence," J. Rheol., 39(4), 659 672.
- Tetlow, N., A. L. Graham, M. S. Ingber, S. R. Subia, L. A. Mondy and S. A. Altobelli, 1998, "Particle Migration in a Couette Apparatus: Experiment and Modelling," *J. Rheol.*, 42(2), 307 327.
- Trevelyn, B. J., and S. G. Mason, 1951, "Particle motions in sheared suspensions. I. Rotations," *J Colloid Science*, 6, 354 367.
- Tucker, C.L., 1988, "Predicting Fiber Orientations in Short Fiber Composites," p.95 in *Proc. Manufacturing Int'l*, AMSE Publication, New York..
- Tucker, C.L., 1991, "Flow Regimes for Fiber Suspensions in Narrow Gaps," *Journal of Non-Newtonian Fluid Mechanics*, 39(3), 239 268.
- Tucker III, C.L. and S.G. Advani, 1994, "Processing of Short-Fiber Systems," p.147 –202, in *Flow and Rheology in Polymer Composites Manufacturing*, 10, Composite Materials Series, Editor: S.G. Advani, Elsevier Publishers, Amsterdam.
- Tucker, C. L. and P. Moldenaers, 2002, "Microstructural Evolution in Polymer Blends," *Annual Reviews of Fluid Mechanics*, 34, 177 210.
- Vermant, J., P. Moldenaers, S. J. Picken, J. Mewis, 1994, "A comparison between texture and rheological behavior of lyotropic liquid crystalline polymers during flow," *J Non-Newtonian Fluid Mech*, 53, 1 23.
- Wahl, J. and F. Ficher, 1973, "Elastic and Viscosity Constants of Nematic Liquid Crystals from a New Optical Method," *Liquid Crystals*, 1, 455 471.
- Walker, L. M. and N. J. Wagner, 1994, "Rheology of region I flow in a lyotropic liquid crystal polymer: The effects of defect texture," *Journal of Rheology*, 38, 1525 1547.
- Walker, L. M., N. J. Wagner, R. G. Larson, P. A. Mirau and P. Moldenaers, 1995, "The rheology of highly concentrated PBLG solutions," *Journal of Rheology*, 39, 925 952.
- Weispfennig, K., S. M. Parks, and C. A. Petty, 1999, "Isotropic Prestress for Fully Developed Channel Flows", *Physics of Fluids*, 11(5), 1262-1271.
- Williams, M., 1975, "Molecular Rheology of Polymer Solutions: Interpretation and Utility," AlChE *Journal* 21, 1-25.

Yousefi, H., G. Wiberg, M.-L. Skytt, J.J. Magda and U.W. Gedde, 2003, "Development and relaxation of orientation in sheared concentrated lyotropic solutions of hydroxypropylcellulose in m-cresol," *Polymer*, 44, 1203–1210.